DESIGN AND DEVELOPMENT OF AN ON-LINE SEDIMENTATION ANALYSER

A thesis submitted to the University of London for the degree of Doctor of Philosophy

by

Dick Kamugasha

Department of Chemical Engineering
University College London
Torrington Place
London WC1E 7JE
December 1998

ABSTRACT

This thesis describes the design and development of a multiple vibrating reed analyser for the routine on-line procurement of sedimentation kinetic data in two phase media.

Briefly, each reed system comprises a stainless steel rod pinned at an intermediate point along its length. One end is exposed to the settling suspension whilst the other is driven into transverse vibration at resonance using an alternating current electromagnet.

The principle of operation of the device relies on the fact that the resonance frequency of a stiff reed performing simple harmonic motion in a fluid medium is directly related to the fluid bulk density. In the case of a settling solid/liquid suspension, or a two-phase liquid dispersion containing a heavier phase, the fluid bulk density and hence the hydrodynamic head decreases with time as the heavier phase settles. Sedimentation kinetic data including settling velocities and flux profiles are in turn obtained by continuous monitoring of the resonance frequencies of a number of reeds positioned at set levels along a settling tank.

The feasibility of operation of the analyser has been successfully verified in conjunction with a variety of model and industrially relevant systems. The former include mono and polydisperse glass ballotini / water mixtures with solids particle size and concentration ranges 55 - 200 μm and 1.75 - 2.81 % v/v respectively. Measured settling velocities are in excellent accord (ca. ± 0.1 %) with those obtained from direct visual observation of suspension-clear liquid interfaces. The industrially relevant systems include kaolin/water suspensions with solids concentrations as high as 20 % v/v and oil / water emulsions with light phase concentrations in the range 30 - 50 % v/v.

The performance of a number of empirical models including those proposed by Richardson and Zaki (1954), Garside and Al-Dibouni (1977), Barnea and Mizrahi (1973), Reed and Anderson (1980), Batchelor (1972) and Happel (1958) has been evaluated by comparing predicted settling velocities with those obtained using the analyser. We find that the model

proposed by Richardson and Zaki produces the best agreement (ca ± 1.3 %) whilst Happel's model (1958) produces the worst results (ca ± 24 %).

For polydisperse systems we observe that measured interface velocities correspond to Stokes (1851) particle sizes which are in reasonable agreement (ca. ± 6 %) with the experimentally determined smallest significant particle size in the sample distribution. Also, as the initial solids concentration increases, the Stokes diameter decreases indicating a greater tendency for particles to segregate resulting in more diffuse interfaces. Therefore, the behaviour of such systems is characterised by differential rather than hindered settling.

By measuring the time delay between the onset of sedimentation and that resulting in a change in reed resonance frequencies at various locations along the settling tank we have been able to obtain estimates of propagation wave velocities marking the transition between steady and unsteady state behaviour. For the systems tested we find that the wave propagation velocity is, in general, independent of solids concentration but increases with the mean particle size.

To Patience

for your love and all you

have made possible

"Industry must make measurements of unprecedented accuracy before it can manufacture new products"

John Battle.

Minister for Science, Energy & Industry

4th November 1997, Birmingham

ACKNOWLEDGEMENTS

A special thank you to my supervisor Dr. Haroun Mahgerefteh for his constant support, guidance and inestimable encouragement throughout this work.

Many thanks also to Dr. Stefaan Simons for the many useful discussions which have contributed to the successful completion of this work.

I would also like to extend my sincere gratitude to my family for being supportive and understanding especially in what were at times, very difficult situations.

I wish to express my appreciation for my colleagues for their moral support, kindness and the many useful discussions we have shared throughout this work.

Finally, I wish to express my utmost gratitude to the technical staff of the Chemical Engineering mechanical and electronic workshops, particularly Mr Martin Town and Miss Sarah Bailey for their invaluable help and support during the construction of the experimental apparatus.

LIST OF CONTENTS

ABSTRACT.....1

ACKNOWLEGEMENTS.....5

CHAPTER 1: INTRODUCTION.....10

CHAPTER 2:LITERATURE SURVEY: SOLID-LIQUID SEPARATION BY SEDIMENTATION

2.0 Introduction.....18

2.1 Applications in Process Industries.....19

2.2 Industrial Design Procedures for Sedimentation Equipment.....20

2.2.1 Operational Characteristics.....22

2.2.2 Types of Sedimentation Tanks.....23

2.2.2.1 Horizontal Flow Tanks.....23

2.2.2.2 Radial Flow Tanks.....25

2.2.2.3 Vertical Flow Tanks.....25

2.2.2.4 High-Rate Settlers.....26

2.3 Conclusion.....26

CHAPTER 3: FLUID-PARTICLE HYDRODYNAMIC INTERACTIONS

3.0 Introduction.....29

3.1 The Effect of Drag on a Single Settling Particle.....30

3.1.1 Spherical Particles.....32

3.1.2 Non-Spherical Particles.....36

3.1.3 Wall Effects.....38

3.1.3.1 Single Particle Case.....38

3.1.3.2 Mulitple Particle Case.....42

3.1.3.2.1 Dilute Suspensions.....42

3.1.3.2.2 Concentrated Suspensions....44
3.2 Monodisperse Suspensions....44
3.3 Polydisperse Suspensions....45
3.4 Channelling Effects....45
3.5 Flow in Inclined Channels....46
3.6 Conclusion....48

CHAPTER 4: THEORETICAL MODELLING OF SEDIMENTATION

4.0 Introduction....49
4.1 Stokes' Law and the Hindered Settling Function....51
4.2 Hydrodynamic, Empirical and Semi-Theoretical Models....52
4.3 Hydrodynamic Simulation Models....62
4.4 Stochastic Simulation Models....66
4.5 Conclusion....68

CHAPTER 5: A REVIEW OF SEDIMENTATION MEASUREMENT TECHNIQUES

5.0 Introduction....70
5.1 Direct Sampling....71
5.2 Optical Methods....73
5.3 Ultrasonic Sensing....74
5.4 Penetrative Radiation Techniques....75
5.5 Transducers....75
5.5.1 Electrical Transducers....76
5.5.1.1 Capacitance Transducers....78
5.5.1.2 Resistance Transducers....80
5.5.1.3 Inductance Transducers....83
5.5.1.4 Impedance Transducers....83
5.6 Pressure Sensors....84
5.7 Conclusion....85

CHAPTER 6: EXPERIMENTAL: DESIGN AND DEVELOPMENT OF THE VIBRATING REED SEDIMENTATION ANALYSER

6.0 Introduction....88
6.1 The Remote Drive Arrangement....89
6.1.1 The Electronic Drive and Detection System....89
6.1.2 Modelling of the Vibration Mechanics and Optimal Design Criteria....93
6.2 Design of the Bench-Top Analyser....95
6.2.1 Design Optimisation Studies....100
6.2.1.1 Optimisation of Reed Length....100
6.2.1.2 Optimisation of Reed Diameter....105
6.3 Design of the Optimised Unit for Sedimentation Analysis....109
6.4 On-Line Multiple Reed System and the Associated Sedimentation Rig....118
6.4.1 Ancillary Electronics and a Computerised Data Acquisition System....124
6.4.1.1 System Power Regulators....124
6.4.1.2 The Photo-Transistor Detectors....124
6.4.1.3 The Variable Bandpass Filter....125
6.4.1.4 Pulsed Power Amplifier....125
6.4.1.5 The Computer Data Logging Interface....126

CHAPTER 7: EXPERIMENTAL PROCEDURES

7.0 Introduction....128
7.1 Particulate Specification and Preparation....128
7.2 Preparation of Two-Phase Solid/Liquid Suspensions....137
7.3 Study of the Performance Characteristics of the Vibrating Reed System....138
7.3.1 Effect of Amplitude of Vibration....138
7.3.2 Effect of Fluid Viscosity and Temperature....143
7.3.3 Effect of Fluid Hydrodynamic Head....147
7.4 Calibration of System Response....149

CHAPTER 8: RESULTS AND DISCUSSION

8.0 Introduction....163
8.1 Resonance Frequency/Time Profiles....164
8.2 The Effect of Particle Size....174
8.3 Sedimentation Kinetic Data....187
8.4 Solids Flux Profiles....193
8.5 Solids Mass Balance Calculations....207
8.6 Comparison of Experimental Data with Theoretical Models....228
8.6.1 Estimation of Propagation Wave Velocities....231
8.6.2 Interface Velocity Measurements....233
8.7 Real Systems....243
8.7.1 Sedimentation of Flocculated Kaolin/Water Suspensions....243
8.7.2 Two-Phase Liquid/Liquid Emulsions....257

CHAPTER 9: CONCLUSION AND FUTURE WORK

9.0 Summary....261
9.1 Conclusions....264
9.2 Further Work....265
9.2.1 Monitoring of Colloidal Stability and Dispersion Structure....265
9.2.2 Concentrated Systems: De-coupling the Effects of Bulk Density and Viscosity....266

NOMENCLATURE....269

REFERENCES....274

APPENDIX A....285

APPENDIX B....295

CHAPTER 1

INTRODUCTION

The separation of solid/liquid suspensions by gravity sedimentation is a common process in several industries ranging from mineral processing to environmental pollution mitigation operations such as waste water treatment where stringent effluent quality standards are in effect. Of particular current interest is the on-line monitoring and characterisation of waste water treatment plant. The estimated investment required in order to meet the recent EC Urban Waste Water Directive is of the order £107 billion (Wright, 1992). This has focused attention on issues of economics and the need for process design optimisation in waste water treatment plants, the majority of which are based on the separation of the dispersed solids phase from water via gravity sedimentation. Accordingly, understanding the kinetics of sedimentation is of primary importance since this governs the handling characteristics of such dispersions, and hence provides information on the optimal design specification of the appropriate sedimentation equipment.

The ability to obtain direct measurements to characterise dispersions is an obvious prerequisite to any quantitative description of their behaviour under different process conditions. In addition, what is particularly desirable is to do this in a model-independent manner (i.e. without recourse to a model based on prior knowledge of the system under investigation), thereby allowing such a technique to be used on-line or in-situ without the need for calibration to specific dispersions.

Another application in which an understanding of sedimentation kinetics is important are Colloidal dispersions. These can be defined as two phase systems where the dispersion medium is in most cases a liquid and the dispersed phase exists as particulates (either solid particles, gas bubbles or liquid drops) in the colloidal size range. Although colloids themselves are normally regarded as being in the size range 1nm to 1 μm, these limits are rather arbitrary, since dispersions containing larger particles can exhibit colloidal behaviour. Therefore, the dispersions which are typical in chemical processes, containing high

particulate volume fractions (> 0.2) of size range (e.g. 1 to 100 microns) can also be regarded as colloidal dispersions, although they have been defined (Williams and Simons, 1992) more accurately as mixed-colloidal-non-colloidal systems.

Colloidal dispersions occur in a wide range of chemical processes and products, such as paints, pharmaceuticals and foodstuffs (particularly dairy products) and in the solid-liquid dispersions encountered in crystallisation, minerals processing and waste water treatment.

Most industrially important colloidal dispersions are polydisperse in nature, in terms of both size and density of the particulate species. The behaviour of such systems lies between the surface-dominated interactions of conventional colloidal dispersions (d_p < 1 micron) and the hydrodynamic interactions of coarse particles (> 10 microns) and, as a consequence, it is difficult to model their behaviour from first principles in a systematic way. Many judicious assumptions are often made (e.g. rigid spheres, uniform size and shape, neglecting non-hydrodynamic interactions), particularly when extending theories to high solids volume fraction systems. For instance, one assumption often made is that all particles settle at the same velocity. In practice, however, there is a good deal of experimental evidence (see, for instance, Williams et al, 1991) that points to the segregation of particles, whether by size or density (or a combination of both) during settling of even high solids concentration dispersions. This is known as hindered settling and implies that the conventional approach of determining solids flux (defined as the mass or volume of solids settling per unit area unit time) by the velocity of the suspension-supernatant interface is inadequate for most industrially relevant systems, leading to underestimates of the true value. In many cases, this limitation is addressed by the use of design correction factors particularly when sizing industrial scale thickeners and clarifiers. However, this practice adversely affects capital and operating costs since settling tanks can be oversized by up to 40% for a given duty. Good reviews of the development of sedimentation models can be found in (Williams et al, 1991) and (Barnes and Holbrook, 1993) for systems of high solids concentration and in (Tadros, 1992) and (Russel et al., 1989) for low solids concentration.

An additional complication to the monitoring and modelling of sedimentation in industrial applications is that very often particles will aggregate, whether intentional or otherwise to the process, to form flocs. These flocs will have different structures

depending on the process conditions and, therefore, will have different settling behaviours. For instance, they may have either loose, open structures, containing a high proportion of the liquid phase, or dense, closed structures consisting mostly of the solid phase. In practice, at least five types of mixed-colloidal-non-colloidal and colloidal dispersions can be identified. These involve stable, strongly flocculated, strongly coagulated, weakly flocculated or weakly coagulated systems (where the use of the term flocculation implies the use of polymeric species, and coagulation represents aggregation via electrostatic and van der Waals mechanisms). In addition there are other composite cases. Some quantitative investigations and simulations on stable and strongly flocculated colloidal systems have been reported (for a review, see Williams et al. 1992). In addition, sedimentation is a dynamic process in the sense that it is quite likely that flocculated particles may form larger aggregates and on reaching a critical size (for a given locality where a certain fluid velocity is experienced in the separation vessel) may break up into smaller aggregates. Recent advances in computational techniques have led to the development of stochastic models to simulate such behaviour, but these are limited in the finite number of particles that can be incorporated into the models (hundreds instead of the many millions encountered in practice) and the lack of fundamental understanding of the effects of multi-particle interactions, both hydrostatic and electrostatic. It is evident that there remains a need to describe such complex phenomena by empirical modelling based on the acquisition of comprehensive experimental data.

In recent years, several sedimentation measurement techniques which attempt to address the above requirements have been developed. The majority rely on monitoring the variation of some property (e.g. hydrostatic pressure, electrical resistance/capacitance) over a defined sensing volume. Unfortunately, this approach is often associated with a need for calibration to specific dispersions. Most are not suitable for continuous on-line operation.

The objective of this research is to design and develop a novel technique based on a multiple vibrating reed system for the on-line monitoring of the behaviour of settling suspensions, independent of the physico-chemical properties of the constituent phases.

Each reed system comprises a stainless steel rod pinned at an intermediate point along its length. One end (the 'remote side') is exposed to the settling suspension whilst the other (the 'drive side') is driven into transverse vibration at resonance by an alternating current electromagnet. With length ratios of the drive to the remote spans of the reed of less than 0.4, the resonance frequency of the reed becomes predominantly sensitive to changes occurring on the remote side only (Mahgerefteh et al., 1990).

The principle of operation of the device is simple and relies on the fact that the resonance of a stiff reed performing simple harmonic motion in a fluid medium is directly related to the fluid hydrodynamic head. We make use of the fact that in the case of a settling suspension, the fluid bulk density and hence the hydrodynamic head decreases with time as solids settle out of suspension. Particle settling velocities and solids flux profiles may in turn be easily obtained by continuous monitoring of the resonance frequencies of a number of reeds positioned at set levels along a settling tank.

The thesis is presented in nine chapters.

In Chapter 2, different types of gravity sedimentation equipment for the recovery of solids from suspensions are reviewed. In particular, it is shown that the process of sedimentation is often complicated by the interaction of several inherently complex phenomena. The associated need for a better understanding of the theory of sedimentation with respect to the influence of the various underlying physico-chemical processes which govern the settling rate of suspended particles is examined. The latter requirement emerges from a critical review of the limitations of traditional methods (Kynch, 1952; Coe and Clevenger, 1916) of analysing suspensions the majority of which rely on the assumption of a visible and sharp suspension-clear liquid interface as well as several other often unrealistic assumptions. The chapter concludes by addressing the need for a more accurate mathematical representation of sedimentation.

In chapter 3, the hydrodynamic effect of a viscous fluid on the settling rate of suspended particles is discussed. In particular, the application of Stokes' (1851) law for the determination of the terminal settling velocity of a single spherical particle falling through an unbounded fluid is reviewed. The use of subsequent empirical correlations which take into account the influence of particle shape, the presence of multiple particles in the fluid medium, wall effects and the particle concentration is also considered. The chapter also describes the nature of particle-particle hydrodynamic interactions for both monodisperse and polydisperse systems and concludes by highlighting the need for more rigorous theoretical models which take into account the influence of electrostatic and dispersion forces on the stability of suspensions.

Chapter 4 reviews various predictive hydrodynamic and semi-theoretical correlations for the estimation of settling velocities in multi-particle systems such as glass ballotini/water suspensions. It is shown that such correlations work on the basis of incorporating a hindered settling function calculated from the suspended solids volume fraction, ϕ_s and in some cases, the particle Reynolds number, Re_p. The chapter also reviews a number of hydrodynamic and stochastic simulation models which have been developed over the years by extension of the aforementioned hydrodynamic correlations in conjunction with appropriate experimental data. Such models attempt to compute particle settling velocities in complex polydisperse systems whilst at the same time simulating the effect of hydrodynamic and/or electrostatic forces. The chapter concludes by emphasising the role of extensive experimental data in the development and validation of existing correlations and simulation models. The associated need for reliable experimental techniques of analysing suspensions is also briefly discussed.

In Chapter 5, the reliability of several sedimentation measurement techniques which have been developed in recent years is critically evaluated. The extent to which such techniques address the limitations of existing models by providing direct measurements of particle settling velocities, the solids concentration and the solids flux is discussed in detail. In particular, it is shown that in order to fully characterise the behaviour of the dispersed phase the majority of existing analysers rely on monitoring the variation of some property over a defined sensing volume. This is the important prerequisite for the

quantitative assessment of the sedimentation process since all real effects must be taken into account. The latter can be achieved via in-situ measurements obtained in a model-independent manner that does not require prior knowledge of the suspension characteristics. The chapter concludes by highlighting the considerable incentive to develop such techniques since most of the analysers reviewed require calibration to specific dispersions.

Chapter 6 describes the design and development of a resonating vibrating reed sedimentation analyser which addresses most of the limitations of existing techniques. The development of a bench-top unit utilising a single reed is described first. This system is used in conjunction with theoretical modelling (Mahgerefteh and Al-Khoory, 1991(a)) to determine the optimal design and operational characteristics required for the multiple reed system. The resulting performance data relating to the system sensitivity, stability and mass resolution are also presented in chapter 6. This is followed by a description of the disposition of the multiple reed system and the design of the associated sedimentation rig. The chapter concludes by describing specially developed ancillary electronics and a computerised data acquisition system with a capability to provide frequency measurements at a rate of ca. 10^{-3} s per channel.

The results of a series of experiments elucidating the performance characteristics of the multiple reed system are presented in chapter 7. In the main, these demonstrate the effects of the reed amplitude of vibration, the suspension bulk viscosity as well as its temperature on the system's response. This work is then followed by a number of further studies the results of which form the basis for establishing the feasibility and reliability of the vibrating reed system in providing particle settling velocities and the solids flux. The chapter also deals with the methods and equipment used to prepare and characterise test samples as well as the manner in which test suspensions are prepared and monitored. The accuracy of experimental settling velocity measurements obtained in conjunction with nominally monodisperse 200 - 212 μm glass ballotini (solid volume concentrations 1.75 - 2.81 %)/water suspensions is verified by comparison with data obtained from direct visual observation of the rate of descent of the suspension-clear liquid interface. The former are obtained directly from the

breakthrough times of resonance frequency versus time profiles. In conclusion, the calibration of the system's rate of change of resonance frequency to the solids flux is presented. It is shown that the system calibration plots can be applied to other test suspensions in order to obtain solids flux profiles from direct measurements of the rate of change of resonance frequency.

The main body of experimental settling velocity and solids flux data is presented in chapter 8. The chapter deals with the utilisation of the aforementioned calibration plots to characterise the settling behaviour of various polydisperse glass ballotini (density 2550 kgm^{-3})/water suspensions. This is achieved by taking the first derivative of resonance frequency versus time profiles. The resulting rate of change of resonance frequency data is then used in conjunction with the system calibration plots to produce solids flux ($kgm^{-2}s^{-1}$) versus time profiles the accuracy of which is validated by direct mass balance. Such data is then compared with the corresponding volume-based estimate of the solids mass throughput calculated from the known initial solids concentration (kgm^{-3}) and the suspension volume above each reed.

Chapter 8 also discusses the comparison of experimental settling velocity measurements with theoretical data generated from some of the important predictive models presented in chapter 4. This analysis is limited to the monodisperse 200 - 212 μm glass ballotini/water suspensions for which the correlations are appropriate. The reliability of measurements obtained in conjunction with the various polydisperse suspensions on the other hand, is deduced from the aforementioned direct mass balance approach rather than by comparison with theoretical models. This is primarily due to a lack of reliable models capable of simulating the behaviour of very dilute (solids concentrations < 5 % v/v) polydisperse suspensions.

Preliminary data on the effects of solids concentration and mean particle size on the propagation wave velocity following the transition from steady (prior to sedimentation) to unsteady operation are also given.

The chapter concludes by presenting preliminary data on the sedimentation of flocculated kaolin/water slurries which demonstrates the capability of the current multiple reed system in providing useful information on the settling behaviour of an industrially relevant system. In addition, the feasibility of extending the application of the current measurement technique to monitoring the stability of two-phase liquid/liquid emulsions is briefly discussed by reference to preliminary data obtained in conjunction with oil/water emulsions.

Chapter 9 is a general conclusion of the main findings of the thesis as well as suggestions for future work.

CHAPTER 2

LITERATURE SURVEY

SOLID-LIQUID SEPARATION BY SEDIMENTATION

2.0 Introduction

Although sedimentation is a superficially simple process which occurs in nature, for instance in geological solid-liquid separation processes and the accumulation of mud on river beds, the underlying physico-chemical activities that govern the rate of solids removal are not trivial. Thus, sedimentation is not as simple as it might first appear and careful design and operation of practical equipment which exploits this process is essential. It is therefore important to understand the theory of sedimentation in order to be able to relate the influence of various phenomena on practical systems.

The handling and separation of solid-liquid suspensions is a common process in several industries ranging from mineral processing to environmental pollution mitigation operations such as waste water treatment. In both of these cases operators are concerned with recovering solids from slurries, often in the form of a thickened product and the primary objective is, therefore, to maximise the rate of settling of the solid phase. This in turn requires a detailed understanding of sedimentation kinetics, in particular, the principle factors that influence the settling behaviour of suspended particles. The important parameters with respect to process monitoring and control include particle settling velocities, particle concentration and the solids flux (mass settling per unit area per unit time) which is essential for the design of industrial unit operations such as conventional thickeners and clarifiers.

This chapter is a literature review of the practical application of gravity sedimentation to the recovery of solids from suspensions. The importance of achieving an accurate understanding of the process kinetics is discussed and the influence of the various phenomena which govern the handling characteristics of settling suspensions is

presented. The traditional jar test method (Kynch, 1952) which relies on observing the settling rate of the suspension-supernatant interface and the subsequent application of momentum-balance theory to infer sedimentation kinetic data is also reviewed. This approach incorporates several unrealistic assumptions which often lead to erroneous predictions of the handling capacity of sedimentation equipment.

This chapter also presents a review of existing practical sedimentation equipment. In particular, the various conventional thickener and clarifier configurations used in process industries are described. In addition, a brief account of the use of more sophisticated high-rate settlers is presented.

2.1 Applications in Process Industries

In recent years the investment required in order to meet the EC Urban Waste Water Directive has been estimated to be of the order £107 billion per annum (Wright, 1992). This has focused significant attention on issues of economics and the need for process design optimisation in waste water treatment plants the majority of which rely on gravity sedimentation as the primary means of removing suspended solids. Accordingly, the acquisition of accurate process kinetic data is essential for the optimal design and specification of the appropriate sedimentation equipment. Unfortunately, very little kinetic data is available for waste water sedimentation because the main attention and focus until recent times, has been on the final effluent quality. The little data that exists has very often been derived from infrequent spot samples of influent and effluent streams. This approach is retrospective and evidently non-representative as the composition of both streams varies with time. Consequently, the optimal hydraulic retention time of the treatment works can not be reliably predicted. This limitation is often addressed by incorporating large design safety factors when sizing clarifiers resulting in unnecessarily high capital and operating costs.

In contrast to processes which rely on separation by gravity sedimentation, there are several systems which require the minimisation of the rate of separation of the dispersed phase. These include food processing, the processing of clay (kaolin/water)

suspensions and the handling of emulsions where phase separation must be avoided in order to maintain uniform dispersions. In such systems it is important to have a good understanding of the stability of the dispersion as a function of time. This can also be achieved by monitoring factors such as particle concentration and settling velocities.

2.2 Industrial Design Procedures for Sedimentation Equipment

The conventional approach applied to the study of settling suspensions involves carrying out laboratory jar tests in order to observe the rate of descent of the suspension-supernatant interface as a function of time and where applicable, the rate of growth of the sediment-suspension interface. One of the most notable attempts of the application of this method is reported by Kynch (1952) who used momentum-balance theory arguments to arrive at a simple mathematical representation of sedimentation. Talmage and Fitch (1955) and Shannon et al.(1964) employed the Kynch approach to derive more useful expressions for the characterisation of the sedimentation process.

This approach is based on the assumption that interfaces are readily discernible and representative of the bulk settling behaviour of suspensions. However, very often complications arise from the action of inherently complex processes and the rate of descent of the interface may not represent the true behaviour of suspended particles. Thus, if the product of the interface velocity and the initial solids concentration is used to estimate the solids flux (kg m^{-2} s^{-1}) the rate of settling may be seriously underestimated. This is because the true settling velocity may be much higher than that inferred from the interface. In addition, suspensions are assumed to be monodisperse with respect to particle size and/or density. In contrast, there are many cases where suspensions contain a wide range of particle sizes and densities. For such systems there exists a range of settling velocities within the bulk of the suspension each corresponding to a discrete particle size range. For instance Amarasinghe (1990) reports that the suspension-supernatant interface velocity corresponds to the settling velocity of the smallest particles present in a suspension. Accordingly, the rate of descent of the interface does not represent the average settling rate of particles and the design of a clarifier or thickener on the basis of such data would be inappropriate. It is

noteworthy that even for nominally monodisperse systems effects such as aggregation can induce a particle size distribution thereby inducing similar errors in the predicted flux.

When handling concentrated suspensions hindered settling effects dominate the settling behaviour of particles. The nature of particle-particle hydrodynamic interactions in such systems is such that particles tend to settle at the same minimum rate irrespective of the particle size distribution. This effect is often validated by the observation of sharp suspension-supernatant interfaces and formulates the basis for the classic work of Coe and Clevenger (1916). These workers used the assumption of a uniform settling rate to relate the interface velocity to the average settling rate of a suspension and their theoretical predictions are still widely applied to the design of conventional thickeners. Coe and Clevenger concluded that a "critical sedimentation point" is reached at the end of the settling process such that all particles are confined to a clearly defined sediment. Beyond this point the level of the supernatant is assumed to be constant except for the case where the sediment can be dewatered by compression. On this basis they define a working solid flux, G_w for a thickener which is given by the expression:

$$G_w = \frac{u_s}{\left(\frac{1}{C_T} - \frac{1}{C_u}\right)} \qquad (2.1)$$

where, u_s is the apparent (suspension-supernatant) settling velocity, C_T is the concentration of solids in the settling vessel and C_u is the concentration of solids in the underflow product. The solids concentration is expressed as the ratio of the solids mass to the fluid mass and the procedure involves determining corresponding values of u_s and C_T between the feed composition, C_f and the desired underflow composition, C_u.

The required thickener settling area is then estimated by conducting a simple mass balance.

Coe and Clevenger (1916) studied suspensions of discrete fast settling particles for which sediment compaction effects are almost negligible. In contrast, the suspensions handled in many practical applications contain a range of particles which may settle as aggregates. The interstices between particles in these aggregates may contain significant amounts of fluid which is released during sediment compression. Thus, as the aggregates collapse under the weight above them a sediment with a range of levels of compaction is formed. For instance, Micheals and Bolger (1962) used the jar test method to study the settling behaviour of flocculated (aggregation by electrostatic forces) clay suspensions and observed that the compaction rate is strongly dependent on the initial solids concentration. Therefore, for such systems the assumption of Coe and Clevenger can lead to a serious overestimation of the solid flux which may in turn lead to underestimation of the predicted thickener area. Shannon and Tory (1966) suggested the use of a raking arrangement which induces shear and breaks up aggregates to produce a compact sediment.

Fitch (1979) gives a review of various models which can be applied to the design of thickeners and suggests alternative design methods. Although prone to several limitations, the traditional jar test method offers preliminary data which can be used for design purposes albeit with the customary inclusion of "correction factors" which attempt to account for some of the above mentioned effects (Merta and Ziolo, 1986).

2.2.1 Operational Characteristics

Whilst thickening and clarification are essentially similar operations fundamental distinctions can be drawn between the two processes on the basis of their respective primary objectives. Thickeners are designed to produce concentrated solid products and the bulk settling rate of solids tends to be dominated by hindered settling effects (Dick, 1972). In contrast, clarifiers are usually designed to remove relatively small amounts of suspended solids and produce a clear liquid as an overflow product. Typically, the process of clarification is characterised by quiescent settling conditions and minimal hydrodynamic interactions between settling particles. However, this is strictly only true for dilute systems and the bulk settling rate of particles can be

determined by direct sampling of the overflow effluent at different time intervals followed by analysis to determine the suspended solids content.

The mechanical design of thickeners and clarifiers usually consists of; a settling tank, a system of feeding pipes with an associated feedwell, an overflow withdrawal/ collection mechanism and an underflow withdrawal/collection mechanism. A raking mechanism similar to the one described by Shannon and Tory (1966) is often used when handling concentrated suspensions or high viscosity non-Newtonian suspensions. These are usually large rotating structures with sophisticated drive and lifting mechanisms.

2.2.2 Types of Sedimentation Tanks

One of the earliest types of sedimentation tanks is the rectangular fill and draw vessel which is operated on a semi-continuous basis. Whilst this type of unit provides free-settling conditions in the bulk suspension it is difficult to desludge and is costly to construct and operate (Tebbutt, 1992). Consequently, rectangular flow units are now rare except in small scale industrial applications where their relative simplicity compensates for these disadvantages. In contrast, the majority of modern sedimentation vessels are operated on a continuous basis and the sediment is removed at regular intervals without recourse to stopping the inflowing feed.

2.2.2.1 Horizontal Flow Tanks

Rectangular horizontal flow settling tanks have the advantage of allowing for the efficient use of area and are therefore suited to applications where the minimisation of floor space is a primary objective (Tebbutt, 1992; Hall and Hyde, 1992). Figure 2.1(a) shows a schematic representation of a horizontal flow tank. A reciprocating scraper mechanism is required in order to deliver the sediment to a withdrawal hopper. This particular type of raking mechanism can be costly and is prone to mechanical failure. For this configuration a single-end weir is used to discharge the overflow product,

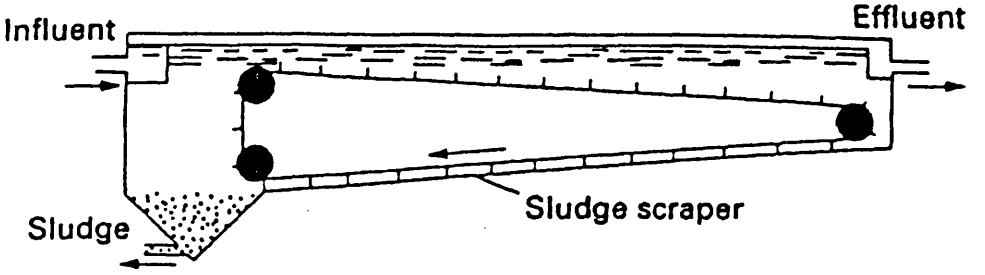

a) Horizontal flow

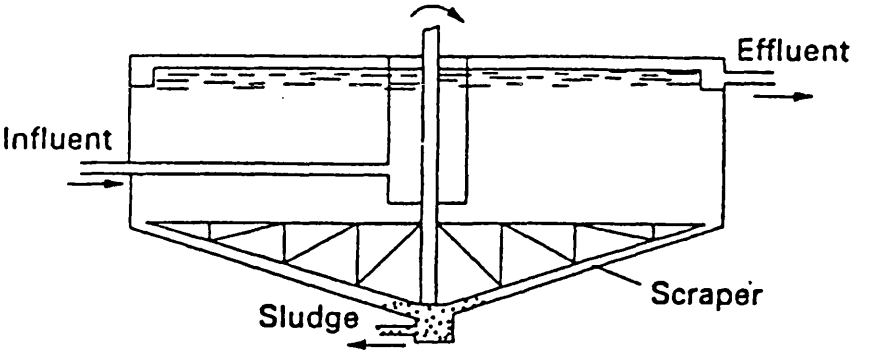

b) Radial flow

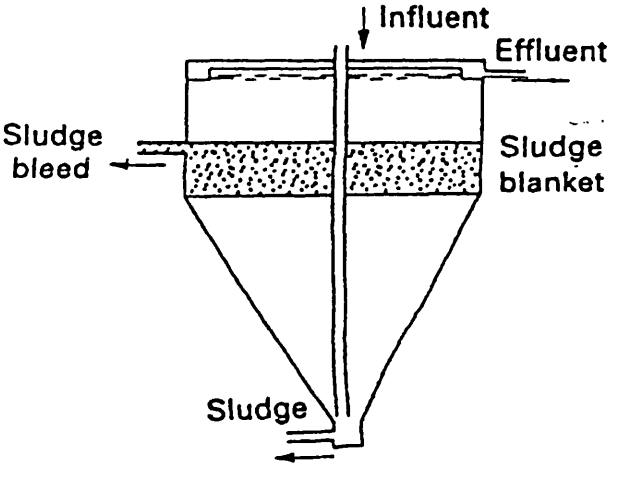

c) Vertical flow

Figure 2.1 Common types of gravity sedimentation tank; a) horizontal flow tank b) radial flow tank and c) vertical flow tank (Tebbutt, 1992).

however, this tends to generate high local velocities. The latter effect can be detrimental to the separation efficiency of the unit since some suspended solids may be convected upwards near the outlet. This effect can be minimised by the use of inset or double-sided weirs.

2.2.2.2 Radial Flow Tanks

These units are circular and have the hydraulic advantage of even flow distribution across the entire vessel. Figure 2.1(b) shows a schematic representation of a radial flow tank. Compared to rectangular tanks, these units tend to have low indices of short circuiting (i.e. there are few dead spaces). In addition, a circumferential overflow collection arrangement allows for ample weir length in order to ensure low velocities in the vicinity of the outlet. An appropriate circular scraper mechanism such as the one shown in figure 2.1(b) is usually used to remove the sediment on a continuous basis. This is more reliable than the reciprocating mechanism used in rectangular tanks. However, circular tanks tend to require significantly more floor space for a given duty and are more difficult to construct. Circular tanks are particularly suited for the handling of suspensions with a high suspended solids content.

2.2.2.3 Vertical Flow Tanks

These units are commonly used in small scale wastewater treatment plants often as potable devices. Figure 2.1(c) shows a schematic representation of a vertical flow tank. These units are conceptually simple and can be very efficient provided they are not overloaded (Montgomery, 1985). However, because of their depth and overall configuration they can be costly to construct. The application of vertical flow settlers to wastewater treatment is particularly attractive since flocculation and sedimentation processes can be carried out simultaneously (Tebbutt, 1979). In such arrangements flocculation occurs within a separate inner zone whilst sedimentation takes place in outer zones. This effect can also be achieved in circular units.

2.2.2.4 High-Rate Settlers

These are generally inclined units which provide large effective surface areas for sedimentation (Davis and Acrivos, 1985). Compared to conventional settlers they are characteristically small and occupy small floor spaces. Typical examples include lamella and inclined-plate settlers which consist of several closely packed inclined plates. Figure 2.2(a) shows a diagram of a typical lamella thickener. In such systems, the plates are typically 1 to 3 m in length and 1.2 m wide and the spacing between them usually varies between 25 mm and 100 mm. A suitable system configuration is selected such that the flow distribution to each plate results in maximum efficiency (see figures 2.2(b) and 2.2(c)). The separation of solids from the fluid relies on solids settling onto the inclined plates and then sliding downwards where they are collected in a hopper. These units are therefore, not suitable for handling fouling slurries such as thixotropic slimes or operation under turbulent conditions. In the latter case resuspension of settled solids can occur (Schaflinger et al., 1990) thereby reducing the separation efficiency as discussed later in chapter 3.

2.3 Conclusion

In this chapter, the practical application of gravity sedimentation to the recovery of solids from suspensions has been discussed. In particular, it has been shown that the process of sedimentation is not as trivial as it might first appear due to complications which arise from the interaction of several inherently complex processes. Accordingly, the need to understand the theoretical basis of sedimentation in relation to the influence of various phenomena is important. For instance the limitations of the traditional jar test method of Kynch (1952) which is commonly used to provide preliminary estimates of suspension settling rates has been shown to incorporate several unrealistic assumptions. These include the suspension-supernatant interface velocity being equated to the average settling rate of particles which can lead to overestimation of the solids flux and therefore, underestimation of settler area. The approach of Coe and Clevenger (1916) is also flawed since it fails to take sediment compression effects into account. Thus, the assumption that multiple critical zones of compaction do not occur

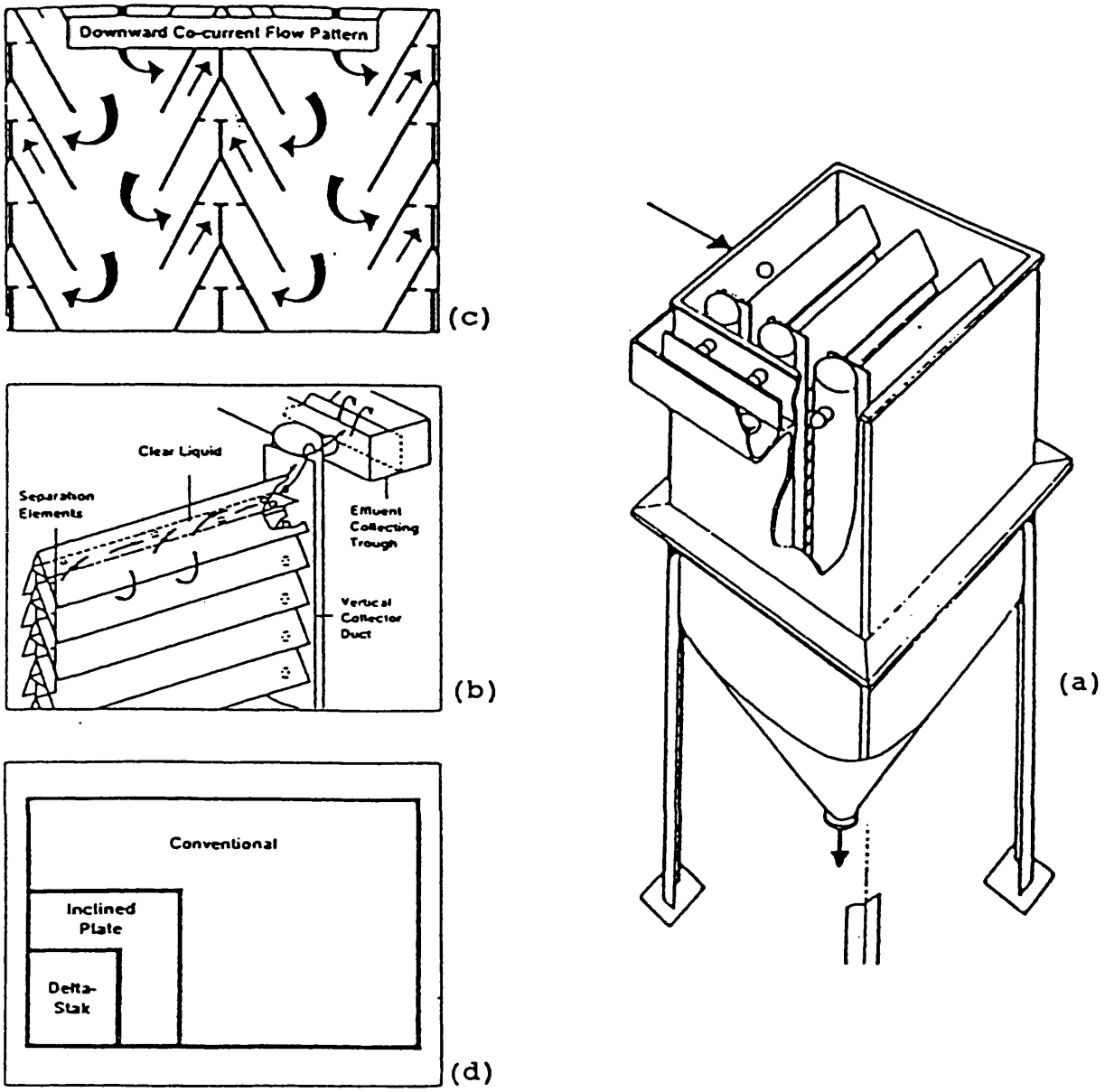

Figure 2.2 Design of Delta Stak (lamella) thickener a) general view of equipment; b) detail of the flow pattern across a single element; c) details of the downward co-current flow patterns within the device and d) the floor space saving as compared with other lamella and conventional thickener equipment (courtesy, BH Process Equipment, Europe).

at the end to the sedimentation process can lead to erroneous predictions of the handling capacity of settlers especially for systems where aggregation effects dominate.

The limitations of the jar test method are highlighted by the frequent use of large design correction factors to compensate for the seemingly intractable phenomena which occur in real systems. This represents a problem and calls for a better understanding of settling phenomena and the development of more accurate mathematical representations of the sedimentation process. Further more, the primary method of determining the settling rate of suspended solids in conventional settlers is direct sampling of influent and effluent samples. This approach is retrospective and evidently non-representative of the dynamic performance of real systems.

CHAPTER 3

FLUID-PARTICLE HYDRODYNAMIC INTERACTIONS

3.0 Introduction

The settling behaviour of suspensions of fine particles, typically in the size range 1 - 100 μm is very often dominated by the effect of electrostatic forces. In particular, sedimentation systems in the colloidal range can be greatly influenced by forces of repulsion or attraction depending on the nature of the surface charge carried by the particulate phase. For such systems hydrodynamic forces may have a negligible impact on the settling rate of particles. In contrast, there are several practical applications where coarse particles settle through viscous fluids. The settling rate of particles in these systems tends to be governed by hydrodynamic forces such as viscous drag rather than electrostatic interactions.

The hydrodynamic force acting on a single particle falling through a viscous fluid is well understood and can be determined directly from experimental observations in conjunction with established theory. In the case of a suspension, however, several particles settle through a fluid simultaneously, and multi-body effects lead to a complicated array of momentum balance equations and it becomes difficult to determine the net hydrodynamic force.

This chapter describes the hydrodynamic effects of a viscous fluid on the settling rate of single spherical and irregular particles taking into account wall effects. It also represents a review of the important work carried out on monodisperse and polydisperse dilute as well as concentrated suspensions. The appropriate theoretical modelling for sedimentation kinetics of such systems is given in chapter 4.

3.1 The Effect of Drag on a Single Settling Particle

A single particle settling through a fluid medium displaces and at the same time redirects the flow of the fluid around it. This represents a disturbance of the fluid and results in a local velocity gradient along the surface of the particle. If the fluid is incompressible and non-viscous then there is no net force exerted on the particle by the fluid due to the absence of skin friction (also known as viscous drag). Referring to figure 3.1, the sum of kinetic energy and pressure energy is constant at all points on the surface of the particle. This is because the pressure decreases from A to B and from A to C whilst pressure increases from B to D and from C to D. The kinetic energy of the fluid on the other hand attains a maximum value at B and C and is zero at points A and D. This means that for this two-dimensional model an infinite velocity exists at the surface of the particle.

In the case of a viscous fluid, a boundary layer forms on the surface of the particle thereby retarding the flow of the displaced fluid. Since pressure energy decreases from A to B and from A to C the boundary layer is thin and therefore, the retarding effect of the particle on the surrounding fluid is insignificant as in the case for a non-viscous fluid. However, since pressure rises from B to D and from C to D the thickness of the boundary layer increases and may well separate from the surface of the particle creating a wake of eddies. These eddies dissipate energy and are associated with an additional force commonly referred to as form drag. Therefore, the net drag force exerted on a particle falling through a viscous fluid is the sum of viscous and form drag components the relative magnitudes of which depend on the settling rate of the particle. If the settling velocity of the particle relative to the fluid is small the formation of eddies is suppressed and the form drag component is negligible. However, if the relative velocity of the particle is high large eddies are generated and the form drag component dominates the drag force.

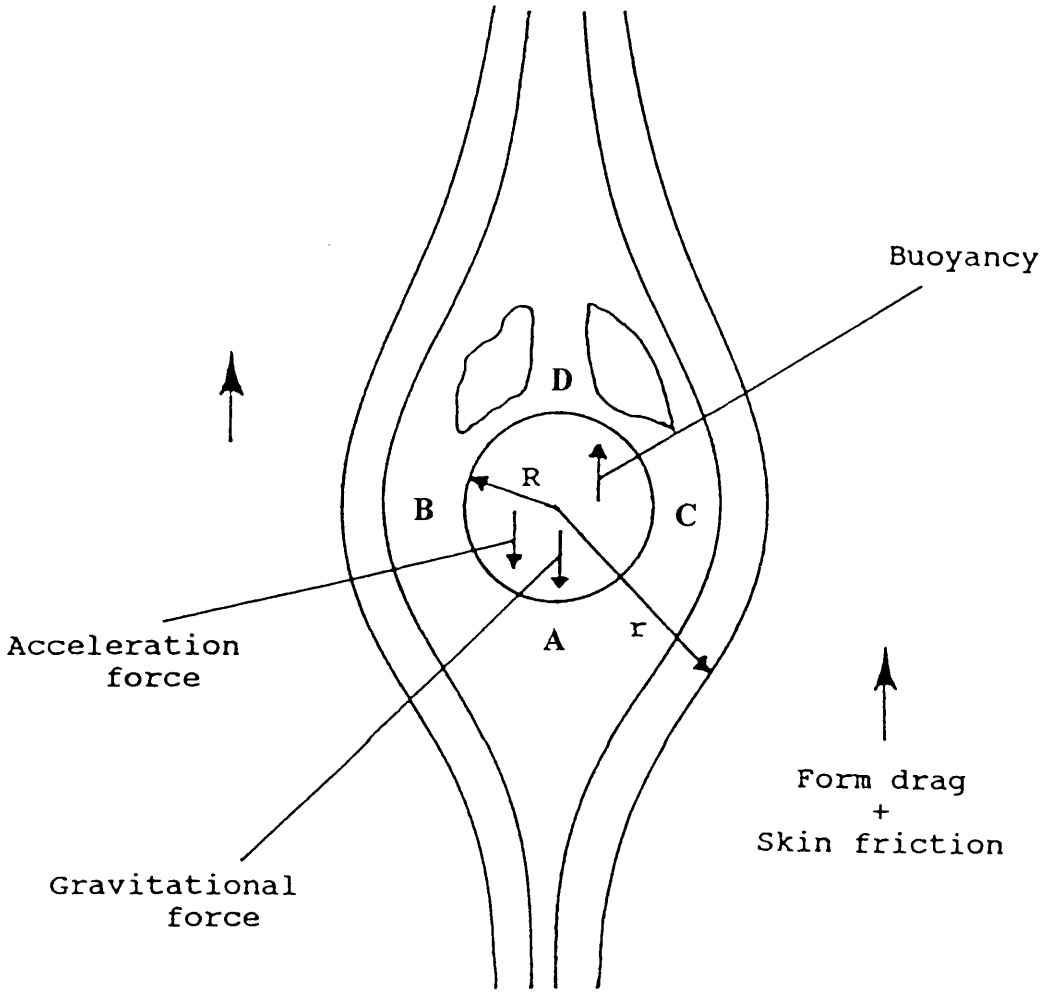

Figure 3.1 Flow around a spherical particle in an unbounded fluid.

3.1.1 Spherical Particles

The drag force exerted on a spherical particle falling through a viscous fluid is given by:

$$F_D = F_{\text{friction drag}} + F_{\text{form drag}} \tag{3.1}$$

The ratio of the total drag force, F_D to the inertial forces acting on a particle is known as the drag coefficient, C_D (Lappel and Shepherd, 1940) and for a spherical particle is given by:

$$C_D = \frac{F_D}{\frac{\pi}{8}\rho_f u_\phi^2 d_p^2} \tag{3.2}$$

where, u_ϕ is the particle velocity relative to the fluid, ρ_f is the fluid density and d_p is the particle diameter. The drag coefficient, C_D is a very useful dimensionless group since in this form the drag force acting on a spherical particle can be presented in the form of a standard curve showing the variation of C_D with the Reynolds number, Re. Figure 3.2 shows a typical drag curve. For $Re < 0.2$ viscous drag dominates the drag force whilst for $Re > 500$ form drag dominates. For the intermediate range of Reynolds numbers both components of the drag force become significant.

Referring to figure 3.2 the fitting equation for each part of the curve corresponds to a drag coefficient correlation for that range of Reynolds numbers. There are several correlations of this type in the open literature all of which apply to a limited range of Reynolds number (Clift et al., 1978). For the laminar flow regime ($Re < 0.1$) the drag coefficient can be estimated from the equation:

$$C_D = \frac{24}{Re} \tag{3.3}$$

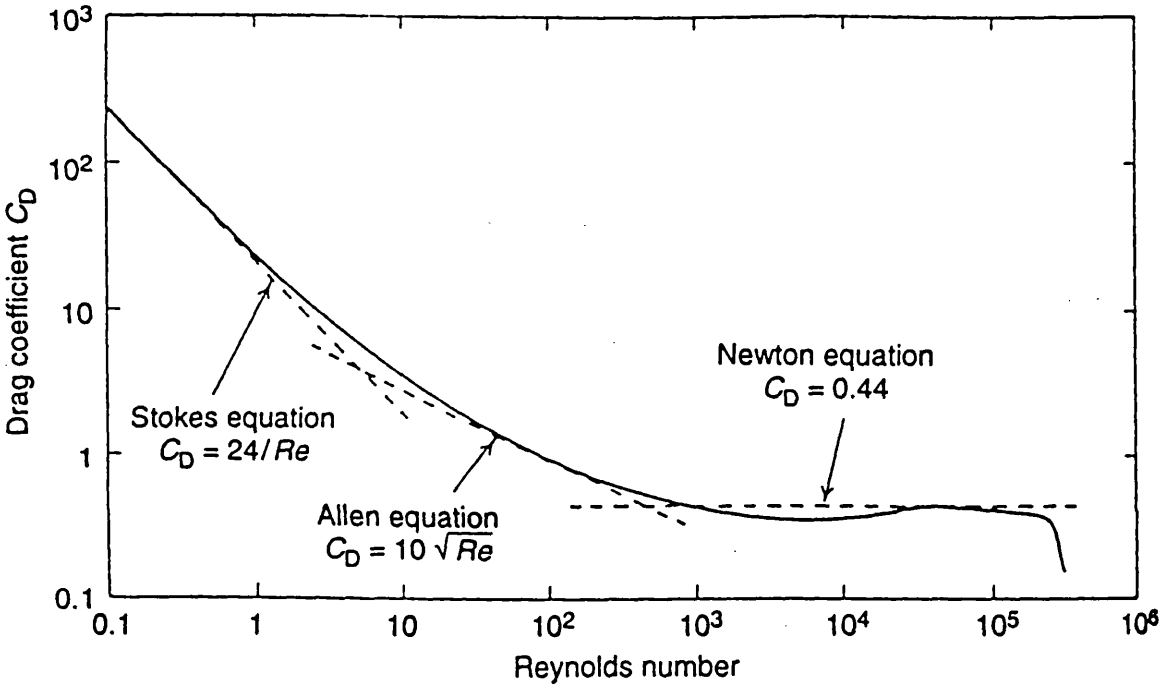

Figure 3.2 Standard drag curve showing a comparison of experimental and calculated values of the drag coefficient, C_D (Arai, 1996).

For the turbulent flow regime ($750 < Re < 3.5 \times 10^5$) C_D is approximately constant at a value of ca. 0.44 whilst for transition flow C_D is given by:

$$C_D = \frac{18.5}{Re^{0.6}} \tag{3.4}$$

Several workers have attempted to develop correlations for the drag coefficient for as wide a range of Reynolds numbers as possible. For instance the correlation of Concha and Almendra (1979a):

$$C_D = 0.28\left[1 + \frac{9.06}{Re^{1/2}}\right]^2 \tag{3.5}$$

which is widely accepted is valid for $Re >> 1$. Dallavalle (1948) reports a similar generalised correlation:

$$C_D = \left[0.6 + \frac{4.8}{Re^{1/2}}\right]^2 \tag{3.6}$$

which has been extensively tested and shown to be valid for a wide range of Reynolds numbers.

Considering the force balance for the case of a spherical particle falling through a viscous fluid, the effect of gravity is such that the velocity of the particle initially increases as it accelerates. The particle continues to accelerate until the retarding drag force causes it to settle at a constant rate known as the terminal velocity, u_o. The gravitational force acting on the particle is given by:

$$F_g = \frac{\pi}{6} d_p^3 (\rho_s - \rho_f) g \tag{3.7}$$

where, $\pi/6$ is a rationalising factor for spherical geometry, g is the universal gravitational constant and ρ_s is the particle density.

For the laminar flow regime:

$$\frac{24}{Re} = \frac{8F_D}{\pi \rho_f u_o^2 d_p^2} \tag{3.8}$$

Hence, substituting for the Reynolds number gives:

$$F_D = 3\pi \mu_f d_p u_o \tag{3.9}$$

where, μ_f is the fluid viscosity.

Therefore, for the equilibrium condition where the magnitude of the drag force is equal to the gravitational force and equating equations 3.7 and 3.9 gives:

$$3\pi \mu_f d_p u_o = \frac{\pi}{6} d_p^3 (\rho_s - \rho_f) g \tag{3.10}$$

and:

$$u_o = \frac{d_p^2 g(\rho_s - \rho_f)}{18\mu_f} \tag{3.11}$$

Equation 3.11 can be used to determine the terminal velocity of a single spherical particle and is known as Stoke's Law (1851) which is based on the assumption of a no-slip condition at the interface between the surface of the particle and the fluid. Other important underlying assumptions in this analysis include; free settling of the particle through an unbounded fluid, negligible wall effects and fluid incompressibility.

For the turbulent flow regime:

$$F_D = \frac{0.44\pi}{8} \rho_f u_o^2 d_p^2 = 0.055\pi d_p^2 \rho_f u_o^2 \qquad (3.12)$$

Therefore, for the equilibrium condition:

$$0.055\pi d_p^2 \rho_f u_o^2 = \frac{\pi}{6} d_p^3 (\rho_s - \rho_f) g \qquad (3.13)$$

and:

$$u_o = \left[\frac{3 d_p g (\rho_s - \rho_f)}{\rho_f} \right]^{1/2} \qquad (3.14)$$

Equation 3.14 is known as Newton's Law (Newton, 1687).

3.1.2 Non-Spherical Particles

The majority of particles found in real suspensions are irregular. Accordingly, their settling behaviour can be quite different from that of spherical particles and in some cases Stokes' law may not apply even at low Reynolds numbers. This is due to the fact that irregular particles tend to have a rotational component to their motion in addition to their downward flow and consequently, may not fall vertically. This means that the drag force acting on an irregular particle is not necessarily parallel to the direction of flow. Furthermore, at higher particle Reynolds numbers the boundary layer between the particle and the viscous fluid may separate prematurely compared to the case for a spherical particle of equivalent characteristic dimensions.

It is, therefore, evident that in order to estimate the drag force acting on an irregular particle it is necessary to first identify its orientation relative to the fluid. This problem is very often resolved by determining the projected area, A_p of the particle in the vertical plane. This is then used to calculate the projected area diameter which is

equivalent to the diameter of a circle of the same area. However, since the orientation of the particle may vary with time as well as particle shape it is convenient to apply a mean value based on the plane of greatest stability. Heywood (1948) used this approach and reports the projected area diameter, d_p' to be given by:

$$d_p' = 2\sqrt{\frac{A_p}{\pi}} \tag{3.15}$$

Heywood defines a shape factor based on the volume of an irregular particle as:

$$k' = \frac{\text{particle volume}}{\left(d_p'\right)^3} \tag{3.16}$$

and the corresponding correlation for the terminal velocity is:

$$u_o' = K_p\, u_o \tag{3.17}$$

where K_p is an empirical correction factor which accounts for the particle shape and volume:

$$K_p = f(k') \tag{3.18}$$

The shape factor, k' can be expressed in terms of characteristic particle dimensions as follows:

$$k' = k_e \frac{t_p}{\sqrt{b_p\, l_p}} \tag{3.19}$$

where, l_p is particle length in the plane of greatest stability. b_p and t_p are, respectively, the particle breadth and thickness normal the plane of greatest stability. Clift et al. (1978) carried out extensive experiments with various particle shapes and report different values for the empirical constant k_e for different geometries.

It is noteworthy that this treatment of the settling behaviour of irregular particles is not valid at high Reynolds numbers since the rotational component of the particle motion is large and it is not possible to make simplifying assumptions about particle orientation.

3.1.3 Wall Effects

Since suspended particles settle in containers of finite dimensions wall effects may contribute an additional retarding force which affects the motion of the particles as well as the fluid. The extent to which the motion of particles is hindered by this effect depends on the ratio of the particle size, d_p to the diameter of the container, D.

3.1.3.1 Single Particle Case

For a single particle falling through a viscous fluid, the hindering effect of the container wall can be theoretically determined and expressed as a function of the diameter ratio d_p/D. This case has been extensively studied by several workers over the years and there are several correlations, both theoretical and empirical, which relate the terminal velocity of a particle settling in a bounded fluid.

For a Newtonian fluid in laminar flow, Lali et al. (1989) report wall effects to be significant for $d_p/D > 0.05$ and suggest use of the correlation:

$$\frac{u_t}{u_o} = 1 - 2.105\frac{d_p}{D} + 2.087\left(\frac{d_p}{D}\right)^3 - 0.95\left(\frac{d_p}{D}\right)^5 \qquad (3.20)$$

where u_t is the terminal settling velocity of the particle in the bounded fluid. Similarly, Garside and Al-Dibouni (1977) suggest the expression:

$$\frac{u_o}{u_t} = 1 + 2.35\left(\frac{d_p}{D}\right) \qquad (3.21)$$

which is valid for Reynolds numbers in the range $3 < Re < 1200$. Another useful correlation is the empirical equation developed by Francis (1933):

$$\frac{u_t}{u_o} = \left[\frac{1 - \frac{d_p}{D}}{1 - 0.475 \frac{d_p}{D}} \right]^4 \qquad (3.22)$$

According to Clift et al. (1978) and Iwaoka and Ishii (1979) equation 3.22 predicts terminal velocities which are in very good accord with the more rigorous theoretical model of Haberman and Sayre (1958).

The theoretical representation of settling at Reynolds numbers outside the laminar flow regime is difficult since there is very little pertinent experimental data for this case. However, it has been shown that wall effects become less important as the Reynolds number increases (Fidleris and Whitmore, 1961) and the empirical correlation of Munroe (1988) best represents experimental data:

$$\frac{u_t}{u_o} = 1 - \left(\frac{d_p}{D} \right)^{1.5} \qquad (3.23)$$

However, there still remains a great deal of uncertainty with regard to the influence of wall effects on the settling behaviour of particles in the transition flow regime. In order to address this difficulty, Di Felice (1996(a)) developed a fluid dynamic analogy model based on geometric equivalence between a single sphere settling in a cylindrical vessel and a multi-particle suspension and found that suspension voidage, ε is related to the diameter ratio d_p/D by the expression:

$$\varepsilon = \left[\frac{1 - \frac{d_p}{D}}{1 - 0.33 \frac{d_p}{D}} \right] \qquad (3.24)$$

The author defines a function $f(d_p/D)$ to take wall effects into account as well as a voidage function $g(\varepsilon)$ which represents multi-particle effects. The two functions are related by the equation:

$$f\left(\frac{d_p}{D}\right) C_{Dt} = g(\varepsilon) C_{Dt}^{*} \varepsilon^2 \qquad (3.25)$$

where, C_{Dt} is the drag coefficient for a single particle settling in a confined vessel whilst C_{Dt}^{*} is the drag coefficient for the multi-particle system. The relationship between particle settling velocities for the two cases is given by:

$$u_t^{*} = u_t \varepsilon \qquad (3.26)$$

The drag force acting on the single particle is given by:

$$F_{Dt} = f\left(\frac{d_p}{D}\right) k C_{Dt} Re_t^{\,2} \qquad (3.27)$$

compared to the expression for the same particle settling in an unbounded fluid:

$$F_{Do} = k\, C_{Do}\, Re_o^2 \qquad (3.28)$$

Since the particle settles at its terminal settling velocity in both cases equations 3.27 and 3.28 are equal. Therefore, the terminal settling velocity of the particle can be expressed in terms of the function $f(d_p/D)$:

$$\frac{u_t}{u_o} = \left(\frac{C_{Do}}{f\left(\frac{d_p}{D}\right) C_{Dt}} \right)^{0.5} \qquad (3.29)$$

and the introduction of the fluid dynamic analogy gives an expression in terms of the suspension voidage:

$$\frac{u_t}{u_o} = \left(\frac{C_{Do}}{g(\varepsilon) C_{Dt}^{*} \varepsilon^2} \right)^{0.5} \tag{3.30}$$

Equation 3.3 is most convenient since all terms on the right hand side can be easily determined for any flow regime. For instance the voidage function g(ε) can be obtained from experiments in which the behaviour of a fluidised bed is observed over a wide range of Reynolds numbers (Di Felice, 1996(b))

For a non-Newtonian fluid shear thinning may cause a reduction in fluid viscosity thereby reducing the influence of wall effects on the settling behaviour of particles. Lali et al. (1989) report a correlation in which fluid viscosity is taken into account by incorporating a term for the modified Reynolds number, Re_o':

$$\frac{u_t}{u_o} = \left(1 - \frac{d_p}{D} \right)^{2.1} \left(Re_o' \right)^{-0.02} \tag{3.31}$$

and:

$$Re_o' = \frac{d_p^n u_o^{(n-2)} \rho_f}{K_v} \tag{3.32}$$

In the equation 3.32, K_v is the fluid consistency factor which is related to the apparent fluid viscosity, μ_a by the expression:

$$\mu_a = K_v \left(\frac{u_o}{d_p} \right)^{n-1} \tag{3.33}$$

where, n is a flow index whose value depends on the rheological behaviour of the fluid.

3.1.3.2 Multiple Particle Case

The extension of the treatment for a single particle to real suspensions is not trivial and relies on experimental validation. This is due to the fact that particle-wall hydrodynamic interactions are influenced by the volume concentration of particles.

3.1.3.2.1 Dilute Suspensions

For very dilute suspensions it may well be that particle-particle and particle-wall hydrodynamic interactions are comparable. Unfortunately, there are very few accounts in the open literature dedicated to the estimation of the influence of wall effects on the settling velocity of very dilute suspensions. This is largely due to the practical difficulties encountered during the measurement of particle settling rates on the basis of visual observations of the suspension-supernatant interface. Thus, diffuse interfaces make it difficult to distinguish between the suspension and the clear liquid thereby producing discrepancies in experimental data (Davis and Hassen, 1988; Famularo and Happel, 1965).

Al-Naffa and Selim (1992) employed an experimental technique based on light transmission to obtain more reliable measurements which are well represented by the theoretical correlation of Batchelor (1972):

$$\frac{u_t}{u_o} = 1 - n\,(1-\varepsilon) \qquad (3.34)$$

where, ε is the suspension voidage

For dilute monodisperse suspensions, the value of the coefficient n is approximately 6.55 compared to a value of 5.5 for slightly polydisperse systems (Batchelor and Wen 1982). More recently, Di Felice and Parodi (1995) carried out experiments in which

the settling behaviour of dilute suspensions ($\varepsilon > 0.95$) was observed for various container diameters. In this work the authors measured the settling velocities of individual particles as well as the interface velocity under controlled conditions and conclude that the value of the coefficient n is a strong function of the diameter ratio, d_p/D. They report a marked decrease in n as d_p/D increases thus contradicting the trend predicted by Richardson and Zaki (1954) and suggest the following correlation for dilute suspensions in the laminar flow regime:

$$\frac{u_t}{u_o} = \varepsilon^n \tag{3.35}$$

The analogous form for the empirical correlation of Richardson and Zaki (1954) is given by:

$$\frac{u_t}{u_o} = k\varepsilon^n \tag{3.36}$$

where k is an empirical constant. Richardson and Zaki (1954) also report a correlation for n as a function of d_p/D for particles settling in the laminar flow regime:

$$n = 4.65 + 19.5\frac{d_p}{D} \tag{3.37}$$

It is noteworthy that the study of the influence of wall effects was not of primary importance in the experimental work of Richardson and Zaki.

According to Di Felice and Parodi (1995) wall effects are negligible for dilute suspensions provided the ratio d_p/D is small.

3.1.3.2.2 Concentrated Suspensions

In contrast to the case for a dilute suspension, the Richardson and Zaki (1954) equation has been extensively validated by experimental data for concentrated systems. This is probably because particle-particle interactions tend to be dominant in such systems and, therefore, particle-wall interactions have little effect on the sedimentation velocity. Thus, for concentrated suspensions values for the empirical parameters n and k can be independent of the diameter ratio d_p/D (Di Felice and Parodi, 1995).

3.2 Monodisperse Suspensions

A monodisperse suspension can be described as a system in which all particles present are uniform with respect to size, density and shape. For this special case, particle-particle hydrodynamic interactions are negligible and, therefore, particles settle at the same rate provided the influence of electrostatic and dispersion forces is not important. Accordingly, the settling behaviour of such systems is relatively easy to model since the settling velocity of particles can be determined on the same basis as for the case of a single particle. Thus, Stokes' law can be applied to the mathematical representation of nominally monodisperse suspensions albeit with the appropriate modifications to account for the volume concentration of particles.

Unfortunately, the reliability of theoretical predictions tends to be hampered by the fact that the concentration of particles can also affect the stability of the suspension. In the case of a dilute suspension (solid volume fraction, $\phi_s < 0.05$) hydrodynamic forces may result in the formation of aggregates or clusters thereby inducing a settling velocity distribution. This effect is characterised by aggregates settling at much higher velocities than individual particles (Taweel et al., 1989). Taweel et al. postulated that the driving force for the formation of hydrodynamic aggregates is the acquisition of an energy state which minimises the dissipation of energy within the suspension. Typically, the aggregates formed by this mechanism are weaker than those created by the action of electrostatic forces and are easily disrupted when subjected to shear forces.

Kaye and Boardman (1962) showed that the formation of hydrodynamic aggregates in concentrated suspensions ($\phi_s > 0.4$) is suppressed by hindered settling effects which dominate the settling behaviour of particles. This is because the fluid displaced by settling particles in a concentrated system is associated with hydrodynamic shear forces sufficient to cause the break-up of the relatively weak aggregates. This effect is responsible for the sharp suspension-supernatant interfaces observed in highly concentrated suspensions since particles settle at a hindered but constant rate.

3.3 Polydisperse Suspensions

These are suspensions in which particles of different sizes or densities settle through a fluid at different rates. Thus, large/high density particles settle fast whilst small/low density particles settle slowly or, in some cases, are displaced upwards by the back-flowing fluid. This behaviour is known as differential settling and is characterised by the occurrence of diffuse interfaces. In the absence of a clear suspension-supernatant interface it becomes difficult to determine suspension settling velocities solely on the basis of visual observations. This is in contrast to hindered settling where particles settle at the same rate and in theory, as many distinct zones of settling as there are particle sizes/densities may occur within the suspension (Mizra and Richardson, 1979; Selim et al., 1983). In practice the number of discernible zones of settling depends on the particle size or density distribution of the suspended particles.

For dilute polydisperse suspensions, the formation of hydrodynamic aggregates in the manner described for the monodisperse case is still possible. However, these tend to be less stable and are much easier to disrupt (Kaye and Boardman, 1962).

3.4 Channelling Effects

This is the lateral segregation of suspended particles induced by differences in particle density or size. This phenomenon can be observed in suspensions containing a mixture of heavy and neutrally buoyant particles and is characterised by the formation of what are commonly referred to as "fingers" (Whitmore, 1955). In effect the flow of the

solid phase through the fluid is stratified and distinct regions containing neutrally buoyant particles are formed and convected upwards whilst at the same time regions containing heavy particles are created and settle under gravity. It has been reported that the settling rate of heavy particles in such systems can be a great deal faster than for the case where buoyant particles are absent. Weiland and McPherson (1979) developed a technique which exploits channelling effects to enhance sedimentation. They studied systems that did not contain neutrally buoyant particles and concluded that provided there are at least two species of distinct density or size channelling may occur.

Although channelling effects are capable of improving the settling rate of heavy particles the overall hydraulic retention time is not always reduced since convection effects may cause rapid stratification and the zones of heavy particles formed may be associated with particle concentrations much higher than for the case where stratification does not occur. Thus, hindered settling effects may be far more significant thereby retarding the flow of the suspension. It is noteworthy that in accordance with Kolmogoroff's (1962) concept of spectral energy transfer there must be sufficient particle-particle hydrodynamic interaction in order to destabilise the uniform suspension and cause stratification. Therefore, in practical applications there exists a minimum solids concentration (typically, $\phi_s < 0.1$) below which stratification cannot occur and particles of different densities settle together at their respective velocities.

3.5 Flow in Inclined Channels

So far the settling behaviour of suspended particles has been described on the assumption of sedimentation in a vertical vessel. For this case settling rates are only affected by the vessel if particle-wall interactions are significant. In contrast, suspensions settling in inclined vessels settle much faster than in conventional systems on account of increased surface area for sedimentation (Davis and Acrivos, 1985; Boycott, 1920). This consideration is the basis for the design of commercial inclined settling vessels such as Lamella and Deltasak settlers which are associated with

considerably shorter hydraulic retention times compared to equivalent conventional settlers.

For a typical system in which dynamic effects do not occur, three distinct settling zones can be observed. A layer of sediment is formed along the bottom surface of the vessel, the original suspension occupies a region immediately above the sediment and a supernatant appears near the top of the channel (Miskin et al., 1996). The three layers are maintained separate by kinematic shocks. However, convection and diffusion effects very often result in the disappearance of the intermediate layer and instead, a bottom layer of varying composition is formed. This is due to the fact that the suspension experiences shear and particle migration (also known as shear-induced diffusion) occurs in addition to sedimentation and convection phenomena (Leighton and Acrivos, 1987; Phillips et al, 1992). This effect is caused by irreversible hydrodynamic interactions between adjacent particles and is not to be confused with Brownian diffusion which is induced by motion at a molecular level.

The improvement in settling rate that can be achieved in an inclined channel is critically dependent on the ability to maintain laminar flow conditions. Otherwise the upward shear-induced particle flux may exceed the downward particle flux due to sedimentation resulting in the formation waves which travel upwards thereby reducing the separation efficiency (Schaflinger et al., 1990). This unstable condition can even bring about resuspension of the sediment especially for cases where polydisperse suspensions settle in inclined channels at high Reynolds numbers (Schaflinger et al., 1985). The extent to which the separation efficiency is reduced by this effect also depends on the angle of inclination of the vessel. Although resuspension effects are usually associated with turbulence and high Reynolds numbers they have also been observed in the laminar flow regime (Gadala-Maria, 1979). This phenomenon is known as "viscous resuspension" and can be predicted on the basis of force balance arguments (Leighton and Acrivos, 1986).

3.6 Conclusion

In this chapter the hydrodynamic effect of a viscous fluid on the settling behaviour of particles has been presented. In particular, the application of Stokes' law for the theoretical determination of the terminal settling velocity of a single spherical particle falling through an unbounded fluid has been discussed. The use of subsequent derivations which attempt to take into account the effects of particle shape, the presence of multiple particles in the fluid medium and the particle concentration has also been described in detail. In addition, since sedimentation takes place in containers of finite dimensions, the influence of wall effects which may contribute an additional retarding force to settling particles has been reviewed.

The sedimentation of monodisperse suspensions for which particle-particle hydrodynamic interactions are frequently assumed to be negligible in order to derive settling velocity correlations on the basis of the single particle model has also been reviewed. The limitations of this approach have been discussed. These include the extent to which the influence of electrostatic and dispersion forces are important as well as the effect of particle concentration on suspension stability. In addition, it was noted that in practice hydrodynamic forces can result in the formation of aggregates thereby inducing settling velocity distributions. In the case of polydisperse suspensions, it is difficult to determine particle settling velocities by visual observation due to the occurrence of diffuse interfaces and channelling effects.

In view of the above, it is evident that the accurate theoretical representation of the settling behaviour of particles requires the application of more rigorous models which take into account the effects of the above mentioned phenomena.

CHAPTER 4

THEORETICAL MODELLING OF SEDIMENTATION

4.0 Introduction

The extent to which kinetic parameters such as particle settling velocities and concentration can be used to reliably assess the behaviour of suspensions depends on the ability to understand the interaction between the physical and chemical properties of a given system. The physical properties of interest include characteristic particle size, particle density and the viscosity of the fluid all of which must be clearly defined. The evaluation of more complex properties such as particle shape and particle size distribution may also be required. The important chemical properties of a suspension include the surface charge and reactivity of particles both of which can greatly affect the stability of suspensions. The stability of a suspension of fine (colloidal) particles (< 1 μm) usually depends on the nature of the electrostatic charge carried by the particulate phase (Stern, 1924). The surface charge of such particles is often inferred from experimental zeta potential measurements which exploit electrokinetic phenomena. The technique most commonly used to determine particle surface charge is known as electrophoresis and works on the basis of determining the distance moved by a charged particle through a fluid as a result of applying an electric field (Smoluchowski, 1903; Huckel, 1924). The migration velocity of the particle is then used to calculate the zeta potential, ζ. The collective charge of all particles in a given system can result in either, a net repulsive force which prevents the aggregation of particles thereby resulting in a stable suspension macrostructure or, conversely, a net attractive force which encourages particles to adhere resulting in a less stable system. In the context of sedimentation the latter effect can be beneficial provided the aggregates formed have higher settling velocities than the original individual particles. If the aggregates have a high voidage they may contain amounts of entrapped fluid sufficient to cause a net reduction in the overall settling rate. In contrast, for coarse

particles such as those handled in this study (typically > 60 μm) particle-particle hydrodynamic interactions are likely to dominate the settling behaviour of particles with a negligible contribution from electrostatic forces.

The prediction of the settling behaviour of coarse particles (>10 μm) is relatively simple for suspensions which are monodisperse with respect to size, density and shape. For this ideal case, all particles settle at the same rate provided electrostatic interactions between individual particles are negligible. Consequently, the settling behaviour of suspensions of monodisperse spherical particles has been extensively studied and several correlations have been developed for the prediction of particle settling velocities as a function of suspended solids concentration. These correlations can generally be categorised as empirical equations, semi-theoretical correlations or hydrodynamic models although there is a fair amount of overlap in the theory. The majority of established settling velocity correlations are hydrodynamic expressions which have been validated by experimental data. More recently, improvements in computation time have led to the development of hydrodynamic simulation and stochastic simulation models capable of taking several physical and chemical suspension properties into account. For instance some models are capable of taking the effect of electrostatic forces on the settling behaviour of particles into account whilst others can predict spatial variations in particle size distribution for initially well mixed polydisperse suspensions. However, as mentioned in chapter 3, the settling behaviour of polydisperse suspensions is inherently complex due to the nature of physical interactions between particles of different sizes.

The purpose of this chapter is to review the various predictive settling velocity correlations and simulation models cited in the open literature. We first describe the application of Stokes' (1851) law for the determination of the terminal settling velocity of a single particle falling through an infinite fluid medium. This is followed by a review of several subsequent derivations which attempt to account for the presence of multiple particles in the fluid medium by incorporating a hindered settling function. The latter is calculated from the solids volume fraction and in some cases the particle Reynolds

number. The majority of such correlations are hydrodynamic-based whilst others are empirical or semi-theoretical.

This chapter also describes a number of hydrodynamic and stochastic simulation models which take some of the above mentioned complex phenomena into account. For example, some models attempt to compute particle settling velocities, particle size distributions and concentrations in polydisperse systems. In addition, the influence of particle-particle hydrodynamic and electrostatic forces on the settling behaviour of such systems is incorporated into some of these models.

4.1 Stokes' Law and the Hindered Settling Function

Most of the settling velocity correlations reported in the open literature are modified versions of Stokes' law (1851) which describes the settling behaviour of a single spherical particle in an 'infinite' fluid medium. The modification of Stokes' law to account for the presence of multiple particles in the fluid comes in the guise of a hindered settling function. This is introduced to account for particle-particle and particle-vessel interactions and in general, is an expression involving the volume fraction of suspended solids. The average settling velocity of particles of a single size is calculated as the product of the Stokes terminal settling velocity, u_o for a single particle falling through an infinite fluid medium and a hindered settling function, $f(\phi_s)$. Thus:

$$u_s = u_o f(\phi_s) \tag{4.1}$$

and:

$$u_o = \frac{d_p^2(\rho_p - \rho_f)g}{18\mu} \tag{4.2}$$

where u_s is the suspension settling velocity, μ is the viscosity of the fluid, d_p is the particle diameter, g is acceleration due to gravity and ϕ_s is the suspended solids volume

fraction. ρ_p and ρ_f are the particle density and the fluid density respectively. For cases where Stokes' law is not valid, for example when handling large or high density particles, u_o must be determined experimentally.

In order to account for the presence of multiple particles in suspension, some modified versions of Stokes' law use suspension viscosity, μ_s instead of the fluid viscosity and the suspension(mixture) density, ρ_m instead of the fluid density to determine suspension settling velocity, u_s.

4.2 Hydrodynamic, Empirical and Semi-Theoretical Models

Robinson (1926) developed the following hydrodynamic correlation:

$$u_s = \frac{K\, d_p^2 \left(\rho_p - \rho_m\right)}{\mu_s} \qquad (4.3)$$

where K is a constant for a given suspension.

Suspension viscosity can either be experimentally determined or estimated from an empirical correlation (Einstein, 1906). Einstein's viscosity correlation only applies to dilute suspensions and is given by;

$$\mu_s = \mu\left(1 + k\phi_s\right) \qquad (4.4)$$

where the constant k has a value of approximately 2.5 for settling hard spheres.

Similarly, the expression:

$$u_\phi = \frac{(\rho_p - \rho_m) d_p^2 \; g.10^{-1.82\,(1-\varepsilon)}}{18\mu} \qquad (4.5)$$

where $\varepsilon = (1-\phi_s)$ is the suspension voidage and u_ϕ is the velocity of particles relative to the fluid was obtained by Steinour (1944) who investigated both theoretically and experimentally, the effect of concentration on the settling rate of suspensions of well-dispersed (non-flocculated) spherical particles.

Hawksley (1950) analysed Steinour's data and found it to be well represented by the equation:

$$u_\phi = \frac{(\rho_p - \rho_m) d_p^2 \ g}{18\mu_s} \qquad (4.6)$$

It is important to note that the correlations considered so far, are only valid in the laminar flow regime. Furthermore, the interactions between suspended particles are not taken into account and therefore, these correlations are only valid for dilute suspensions of monodisperse particles where hindered settling effects and electrostatic forces are ignored.

In a subsequent study, Hawksley (1950) developed another settling correlation for spherical particles:

$$u_{\phi_s} = \left[\frac{(\rho_p - \rho_f) g d_p^2 (1-\phi_s)^2}{18\mu}\right] \exp -\left[\frac{k\phi_s}{(1-Q\phi_s)}\right] \qquad (4.7)$$

where, $u_{\phi s}$ is the settling rate of a suspension of volume ratio ϕ_s, k is Einstein's viscosity constant (Einstein, 1906) and Q is Vand's interaction constant for spheres (Vand, 1948).

The above correlation is based on a combination of the theoretical work of Burgers (1941, 1942) on the sedimentation of dilute suspensions and Vand's research on the

viscosity of suspensions. This correlation attempts to take particle-particle interactions into account.

In developing the above correlation, Hawksley (1950) discovered that some of the particles used in Steinour's experiments had marked deviations from spherical geometry and argued that this affected settling velocities in an unknown manner.

Richardson and Zaki (1954) developed an empirical correlation that has since been shown to be valid for all flow regimes and particles between 5 μm and 6 mm in diameter. The Richardson and Zaki equation given by;

$$u_s = u_o (1-\phi_s)^n \qquad (4.8)$$

is perhaps the best known and most useful settling velocity correlation. The index 'n' is principally a function of the particle Reynolds number, Re_p and the ratio of particle diameter to settling vessel diameter, d_p/D. Very often, for small values of d_p/D, n is taken to be 4.65. However, for suspensions of large particles, n has to be calculated directly from the particle Reynolds number, Re_p. Thus:

$$n = f(Re_p) \qquad (4.9)$$

Whitmore (1955) demonstrated that the Richardson and Zaki correlation could be applied to irregular particles if n is multiplied by a shape factor, $1.1K^{0.165}$ where K is the volume coefficient for the particles. The results of Whitmore's work have been validated for particle Reynolds numbers in the range ($Re_p > 500$).

Garside and Al-Dibouni (1977) carried out velocity-voidage studies and used the logistic curve approach to determine the value of the flow index, n. They determined the velocity of particles relative to the fluid, u_ϕ as a function of the Reynolds number and found that a value of n equal to 5.1 most accurately represented their settling

velocity data at low Reynolds numbers. The empirical correlation of Garside and Al-Dibouni is given by:

$$\frac{u_\phi - A(\varepsilon)}{B(\varepsilon) - u_\phi} = 0.06\,\mathrm{Re}^{(\varepsilon+0.2)} \qquad (4.10)$$

where $A(\varepsilon)$ and $B(\varepsilon)$ are functions of the suspension voidage.

In both the Garside and Al-Dibouni and the Richardson and Zaki correlations, the term $(1-\phi_s)^n$ is the hindered settling function, $f(\phi_s)$.

Also reported in the literature is the hydrodynamic correlation of Barnea and Mizrahi (1973):

$$u_s = u_o \left[\frac{(1-\phi_s)^2}{(1+\phi_s^{1/3}) \exp\left(\frac{5\phi_s}{3(1-\phi_s)}\right)} \right] \qquad (4.11)$$

In this correlation the term in ϕ_s is the hindered settling function whilst the group $(1+\phi_s^{1/3})$ is a correction factor for wall effects.

Batchelor (1972) presents a hydrodynamic model for the analysis of monodisperse colloidal suspensions in which pair-wise hydrodynamic interactions between particles are taken into account using :

$$u_\phi = u_o(1-6.55\phi_s) \qquad (4.12)$$

However, this correlation is limited by the occurrence of non-convergent integrals. These arise from attempting to calculate global averages of particle interactions from

several discrete particle pairings and the correlation is only valid for dilute systems in which Re < 0.2. In a later publication, Batchelor (1976) resolved the problem of non-convergent integrals to provide an improved model. Reed and Anderson (1980) used a similar approach to develop a hydrodynamic model in which the influence of electrostatic forces between particles is also considered. They note that electrostatic forces can substantially reduce particle settling velocities by changing their trajectories. The expression of Reed and Anderson is given by:

$$u_\phi = u_o\left(\frac{1-1.88\phi_s}{1+4.0\phi_s}\right) \qquad (4.13)$$

According to Batchelor (1976) hydrodynamic interactions between two spheres can be calculated exactly. However, the accuracy of such numerical evaluations can be difficult to assess and few exact numerical solutions exist all of which apply to specific systems.

Concha and Almendra (1979b) developed a semi-theoretical correlation which is valid for spherical particles for the full range of Reynolds numbers:

$$u_s = \frac{20.52}{d_p}\left[\left(1+0.0921 d_p^{3/2} f_2\left(\phi_S\right)^{1/2}\right) - 1\right]^2 f_1(\phi_s) \qquad (4.14)$$

This correlation is in good accord with the experimental data of Lappel and Shepherd (1940) and utilises the drag coefficient-Reynolds number expression of Dallavalle (1948) which is:

$$C_D = 0.28\left[1+\frac{9.06}{Re^{1/2}}\right]^2 \qquad (4.15)$$

where, C_D is the drag coefficient.

Dallavalle's expression is based on the analysis of Wadell's (1934) experimental data and its solution involves determining values of the derived dimensionless terms $C_D Re^2$ and C_D/Re. Graphical, tabular or iterative methods can then be used to determine particle terminal velocities provided the particle diameter is known. Dallavalle's equation is only suitable for predicting the drag coefficient of spherical particles. However, several workers (see for example Ganser, 1993; Thompson and Clark, 1991; Haider and Levenspiel, 1989; Leith, 1987; Pettyjohn and Christiansen, 1948) have developed correlations that use shape descriptors (factors) for the analytical determination of the drag coefficient. For instance Haider and Levenspiel (1989) suggested a correlation that can be used to predict drag coefficients for both spherical and non-spherical shapes in the laminar flow regime. Differences in particle shape are quantified in terms of a parameter known as sphericity. This is defined as the ratio of the surface area of a sphere of equivalent volume to the actual surface area of the particle. Thus, the drag coefficient, C_D is a function of the Reynolds number, Re as well as sphericity. Since in this case C_D is a function of two variables the resulting correlation for C_D is more complicated:

$$C_D = \frac{24}{Re}\left[1+A\,Re^B\right] + \frac{C}{\left[1+\frac{D}{Re}\right]} \qquad (4.16)$$

where, the coefficients A, B, C and D are functions of particle sphericity, ϕ and are given by:

$$A = \exp(2.3288 - 6.4581\phi + 2.4486\phi^2) \qquad (4.17)$$

$$B = 0.0964 + 0.5565\phi \qquad (4.18)$$

$$C = \exp(4.9050 - 13.8944\phi + 18.4222\,\phi^2 - 10.2599\,\phi^3) \qquad (4.19)$$

$$D = \exp(1.4681 - 12.2584\phi - 20.7322\phi^2 + 15.8855\,\phi^3) \qquad (4.20)$$

In practice it is very difficult to determine ϕ for irregular(non-isometric) particle shapes. This problem has been addressed by Thompson and Clark (1991) who proposed a quantitative method of distinguishing particle shapes. The method is such that it is applicable to all particles. This approach relies on the premise that all particles experience a Newtonian flow regime when settling. Newton's shape factor, K_2 and Re are used to calculate C_D (Thompson and Clark, 1991). Thus, C_D is a function of both K_2 and Re:

$$C_D = f(Re, K_2) \tag{4.21}$$

K_2 is defined as the ratio of the drag coefficient of a particle, C_D to the drag coefficient of an equivalent sphere, C_{DS} settling in Newton's regime. Both coefficients are determined at a Reynolds number of 10^4 and:

$$K_2 = \frac{C_D}{C_{DS}} \tag{4.22}$$

Pettyjohn and Christiansen (1948) describe an empirically defined shape factor, K_1 that can be used to determine the drag on a non-spherical particle settling in Stokes' regime. K_1 is known as Stokes' shape factor (Stokes, 1851) and is given by:

$$K_1 = K_{10} - m\frac{d_v}{D} \tag{4.23}$$

where, K_{10} is the limiting value of K_1 as $d_v \rightarrow 0$, m is a constant of proportionality, d_v is the diameter of a sphere with a volume equivalent to that of the particle and D is the coefficient in the correlation of Haider and Levenspiel (1989).

From this analysis C_D is found to be:

$$C_D = \frac{4 d_v g(\rho_p - \rho_f)}{3 v^2 \rho_f} = \frac{24}{Re K_1} \qquad (4.24)$$

where, v is the particle settling velocity. In determining K_1, a shape factor based on the projected area of a given particle is included to account for orientation relative to the direction of flow (Leith, 1987). Strictly, the projected area in the direction of motion is an instantaneous quantity. Thus, the area presented to the flow by a particle varies with time. However, in the mean, there is a "dominant" projected area corresponding to the plane of greatest stability provided Stokes' regime prevails.

Ganser (1993) concluded that any further improvement in C_D estimation must involve the Reynolds number and at least two shape factors such as K_1 and K_2 described above.

Ganser's work is based on dimensional analysis and similarity arguments. This treatment leads to the conclusion that knowledge of K_1 and K_2 are sufficient for the accurate determination of C_D over a wide range of Re values and a generalised Reynolds number ($Re\ K_1K_2$) is used to give the following expression for the drag coefficient:

$$\frac{C_D}{K_2} = \frac{24}{Re K_1 K_2}\left[1 + 0.1118(Re K_1 K_2)^{0.6567}\right] + \frac{0.4305}{\left[1 + \frac{3305}{Re K_1 K_2}\right]} \qquad (4.25)$$

According to Ganser this correlation is valid for $Re\ K_1K_2$ values less than or equal to 10^5.

The sedimentation models considered so far, are strictly only applicable to dilute suspensions of monodisperse spherical particles in which the effect of particle-particle

interactions on the settling rate of the dispersed phase can often be neglected. In contrast, suspensions of polydisperse particles tend to be characterised by complex multi-body interactions which make it difficult to determine the appropriate form of the hindered settling function. These effects complicate the theoretical treatment of polydisperse suspensions and include hindered settling which can be caused by a combination of particle-particle electrostatic, steric and hydrodynamic forces all of which may be present in a given system to varying degrees. In addition, differential settling effects prevalent in dilute polydisperse systems induce spatial variations in particle size distribution and, therefore, particle settling velocities, concentrations and the solids flux. Thus, a range of settling rates may exist within the suspension as illustrated by the occurrence of diffuse suspension-supernatant interfaces (Davis and Hassen, 1988). This effect is often coupled with the upward convection of fine particles due to the back flow of fluid displaced by coarse particles.

Despite the above mentioned complications there have been several attempts at the theoretical representation of the settling behaviour of polydisperse suspensions. Masliyah (1979) developed an empirical-hydrodynamic solution for the settling velocity of a polydisperse suspension based on a one-dimensional momentum equation:

$$u_s = \frac{d_p^2 \varepsilon (\rho_p - \rho_m) g F(\varepsilon)}{18\mu} \qquad (4.26)$$

where $F(\varepsilon)$ is a suspension voidage function which can be determined from established equations such as (4.8) and (4.11). At low Reynolds numbers $F(\varepsilon)$ derived from (4.8) is given by the expression:

$$F(\varepsilon) = \varepsilon^{2.7} \qquad (4.27)$$

Similarly, from equation (4.11):

$$F(\varepsilon) = \left[1+(1-\varepsilon)^{1/3}\exp\left(\frac{5(1-\varepsilon)}{3\varepsilon}\right)\right]^{-1} \qquad (4.28)$$

It is also possible to determine F(ε) by carrying out velocity-voidage studies and developing an appropriate model for a given system.

Smith (1967) presents the following "theoretical cell" model for the sedimentation of polydisperse particles:

$$u_i + F_1(\phi_i)\sum u_i\,\phi_i + F_2(\phi_i) + u_{\phi_i}F_3(\phi_i) = 0 \qquad (4.29)$$

where, u_i is the settling velocity of the i^{th} size fraction and $u_{\phi i}$ is the relative velocity of the i^{th} size fraction relative to the fluid. This hydrodynamic model is an extension of the "theoretical cell" model originally proposed by Happel (1958) for polydisperse suspensions:

$$u_\phi = \frac{u_o}{1+1.5\phi^{1/3}} \qquad (4.30)$$

In a cell model, each particle in the suspension is considered as being surrounded by a fluid envelope in such a way that the ratio of particle volume to fluid volume is equal to the overall solids volume fraction in a vessel. Computations are then done on this basis to determine settling velocities. Smith's model predicts, with reasonable success, trends in particle settling velocities at different solids concentrations. However, individual particle settling velocities are consistently underestimated. Subsequently, Patwardhan and Tien (1985) developed a more useful empirical-hydrodynamic model which is an extension of Masliyah's (equation (4.26)) correlation:

$$\frac{u_{\phi i}}{u_o} = \varepsilon_i^{(n-2)}\left(\frac{\rho_{pi}-\rho_m}{\rho_{pi}-\rho_f}\right) \qquad (4.31)$$

4.3 Hydrodynamic Simulation Models

Hydrodynamic simulation models are computational and can be used to simulate the behaviour of particles in nominally polydisperse suspensions. Unlike the relatively simple mathematical correlations considered so far these models involve a more rigorous assessment of particle settling rates and take the influence of effects such as electrostatic forces into account. In principle, these models are sets of diffusion-type matrix equations which are programmed into computers to simulate the settling behaviour of polydisperse suspensions. Continuity and momentum balance equations are solved simultaneously by applying the appropriate boundary conditions and the models attempt to account for particle-particle hydrodynamic interactions during sedimentation. Typically, the results obtained from such simulations are predictions of spatial variations of particle settling velocities, concentrations, size distributions and the solid flux.

Mirza and Richardson (1979) extended a semi-empirical model originally developed for binary particle mixtures by Lockett and Al-Habbooby (1974) to the sedimentation of polydisperse suspensions. This empirical-hydrodynamic simulation model is reported to consistently predict particle settling velocities that are greater than those found experimentally. An empirical correction factor, $(1-\phi_s)^{0.4}$ is introduced to overcome this inconsistency.

Selim et al. (1983) conducted experiments with polydisperse suspensions of equi-density particles and concluded that the terminal settling velocity of particles of a given size can be calculated. In their approach, the density of the fluid phase is replaced with the average density of a suspension consisting of particles with a cut size equal the particle size of interest. This method is ad hoc and neglects the hydrodynamic influence of particles larger than the size range considered. Despite this obvious limitation, Selim et al. report good agreement between their model and experimental results for particle volume fractions in the range $0.12 < \phi_s < 0.45$. This observation has been validated by Hin-Sum Law et al. (1987) who compared the performance of several models for polydisperse systems with their own experimental data obtained in conjunction with

bidisperse suspensions of mono-sized polymethyl methacrylate (PMMA) (density, 1186 kgm^{-3}; average particle diameter, 241 μm) and polystyrene (PS) (density, 1050 kgm^{-3}; average particle diameter, 237 μm) particles settling in aqueous solutions of sodium chloride (density, 1120 kgm^{-3}; viscosity, 0.0141 Pas). The authors found the correlations of Masliyah (1979), Patwardhan and Tien (1985) and Selim et al. (1983) to be among the most reliable. Table 4.1 shows a summary of the performance of various predictive models as compared to the experimental results of Hin-Sum Law et al. (1987).

Williams and Amarasinghe (1989) developed a hydrodynamic simulation model capable of predicting the settling behaviour of concentrated polydisperse suspensions. The first stage of this model involves calculating the local settling velocities of particles for a discrete time interval from the onset of sedimentation (time, t = 0) for an initially well mixed suspension. In this computation a set of simultaneous linear equations is solved to provide estimates of settling velocities for discrete size fractions over the selected time interval. These velocities are then used in conjunction with a number of simplifying assumptions to predict the new location of all particles. In the second stage a dynamic simulation of the settling process is carried out in the space domain by repeating the procedure for the entire height of the sedimentation vessel. Thus, the calculation is repeated until all particles are assigned to the sediment. Williams and Amarasinghe conducted parallel experiments to validate their model. In this separate study they used a specially designed settling vessel with a facility to divide the settling zone into a number of sections. Suspensions of known concentrations were then allowed to settle for selected time intervals following which the settling process was suddenly terminated by sealing off each section and determining the mass of particles and the particle size distribution in each isolated volume. The procedure was then repeated for different settling times. Figure 4.1 shows simulated concentration profiles for different sedimentation processes as a function of time for two levels of initial solids volume concentration (5 and 20 % v/v). The authors report that although experimentally determined solids fluxes were found to be significantly higher than those predicted by the model the predicted trends were correct. However, it is noteworthy that the experimental study was carried out at constant zeta-potential so as

Table 4. Experimental results of bidisperse suspensions (H = 28.3 cm)

Bidisperse suspensions	$u_{s,l,b}$ (cm/s)	$u_{s,h,b}$ (cm/s)	t_c (s)	$H - z_c$ (cm)
8% PS–8% PMMA	−0.075	0.075	188.8	14.1
4% PS–8% PMMA	−0.086	0.077	171.6	15.1
8% PS–4% PMMA	−0.079	0.083	176.4	13.9

Table 5. Predictions from models using eq. (1) for $u_{s,l,m}$ and $u_{s,h,m}$. Shown in parentheses are the absolute per cent deviations of predicted with experimental values

(a) Bidisperse suspension of 8% PS–8% PMMA
Experimental results : $u_{s,l,b}$ = −0.075 cm/s, $u_{s,h,b}$ = 0.075 cm/s.

	$F(\varepsilon)$					
	Richardson and Zaki:		Barnea and Mizrahi:		Garside and Al-Dibouni:	
Models	$u_{s,l,b}$ (cm/s)	$u_{s,h,b}$ (cm/s)	$u_{s,l,b}$ (cm/s)	$u_{s,h,b}$ (cm/s)	$u_{s,l,b}$ (cm/s)	$u_{s,h,b}$ (cm/s)
Lockett and Al-Habbooby	−0.0623 (16.8%)	0.0582 (22.4%)	−0.0644 (14.0%)	0.0602 (19.7%)	−0.0663 (11.5%)	0.0618 (17.6%)
Mirza and Richardson	−0.0581 (22.4%)	0.0542 (27.7%)	−0.0601 (19.8%)	0.0561 (25.2%)	−0.0618 (17.5%)	0.0577 (23.1%)
Masliyah	−0.0739 (1.3%)	0.0695 (7.3%)	−0.0764 (2.0%)	0.0719 (4.1%)	−0.0786 (4.9%)	0.0739 (1.5%)
Selim *et al.*	−0.0674 (10.0%)	0.0634 (15.5%)	−0.0695 (7.2%)	0.0655 (12.7%)	−0.0716 (4.4%)	0.0674 (10.1%)
Patwardhan and Tien	−0.0735 (1.9%)	0.0699 (6.8%)	−0.0762 (1.7%)	0.0721 (3.9%)	−0.0783 (4.5%)	0.0742 (1.1%)

(b) Bidisperse suspension of 4% PS–8% PMMA
Experimental results: $u_{s,l,b}$ = 0.086 cm/s, $u_{s,h,b}$ = 0.077 cm/s.

	$F(\varepsilon)$					
	Richardson and Zaki:		Barnea and Mizrahi:		Garside and Al-Dibouni:	
Models	$u_{s,l,b}$ (cm/s)	$u_{s,h,b}$ (cm/s)	$u_{s,l,b}$ (cm/s)	$u_{s,h,b}$ (cm/s)	$u_{s,l,b}$ (cm/s)	$u_{s,h,b}$ (cm/s)
Lockett and Al-Habbooby	−0.0795 (7.7%)	0.0683 (11.0%)	−0.0757 (12.1%)	0.0650 (15.3%)	−0.0832 (3.4%)	0.0714 (6.9%)
Mirza and Richardson	−0.0755 (12.3%)	0.0649 (15.4%)	−0.0719 (16.5%)	0.0618 (19.4%)	−0.0791 (8.1%)	0.0678 (11.6%)
Masliyah	−0.0930 (8.0%)	0.0749 (2.3%)	−0.0886 (2.9%)	0.0714 (6.9%)	−0.0974 (13.1%)	0.0783 (2.1%)
Selim *et al.*	−0.0854 (0.8%)	0.0714 (6.9%)	−0.0812 (5.7%)	0.0680 (11.3%)	−0.0893 (3.7%)	0.0747 (2.6%)
Patwardhan and Tien	−0.0925 (7.4%)	0.0751 (2.1%)	−0.0884 (2.7%)	0.0715 (6.8%)	−0.0969 (12.5%)	0.0785 (2.3%)

(c) Bidisperse suspension of 8% PS–4% PMMA
Experimental results: $u_{s,l,b}$ = −0.079 cm/s, $u_{s,h,b}$ = 0.083 cm/s.

	$F(\varepsilon)$					
	Richardson and Zaki:		Barnea and Mizrahi:		Garside and Al-Dibouni:	
	$u_{s,l,b}$ (cm/s)	$u_{s,h,b}$ (cm/s)	$u_{s,l,b}$ (cm/s)	$u_{s,h,b}$ (cm/s)	$u_{s,l,b}$ (cm/s)	$u_{s,h,b}$ (cm/s)
Lockett and Al-Habbooby	−0.0736 (6.4%)	0.0742 (10.1%)	−0.0701 (10.8%)	0.0707 (14.3%)	−0.0770 (2.0%)	0.0776 (5.9%)
Mirza and Richardson	−0.0699 (11.1%)	0.0705 (14.5%)	−0.0666 (15.3%)	0.0671 (18.7%)	−0.0732 (6.9%)	0.0737 (10.7%)
Masliyah	−0.0803 (2.2%)	0.0875 (6.1%)	−0.0765 (2.7%)	0.0833 (1.0%)	−0.0841 (7.0%)	0.0915 (10.9%)
Selim *et al.*	−0.0766 (2.5%)	0.0803 (2.7%)	−0.0730 (7.1%)	0.0764 (7.4%)	−0.0802 (2.0%)	0.0840 (1.8%)
Patwardhan and Tien	−0.0801 (1.9%)	0.0880 (6.7%)	−0.0764 (2.8%)	0.0835 (1.2%)	−0.0839 (6.7%)	0.0919 (11.4%)

Table 4.1 Summary of the performance of various predictive models as compared to experimental results (Hin-Sum Law et al., 1987).

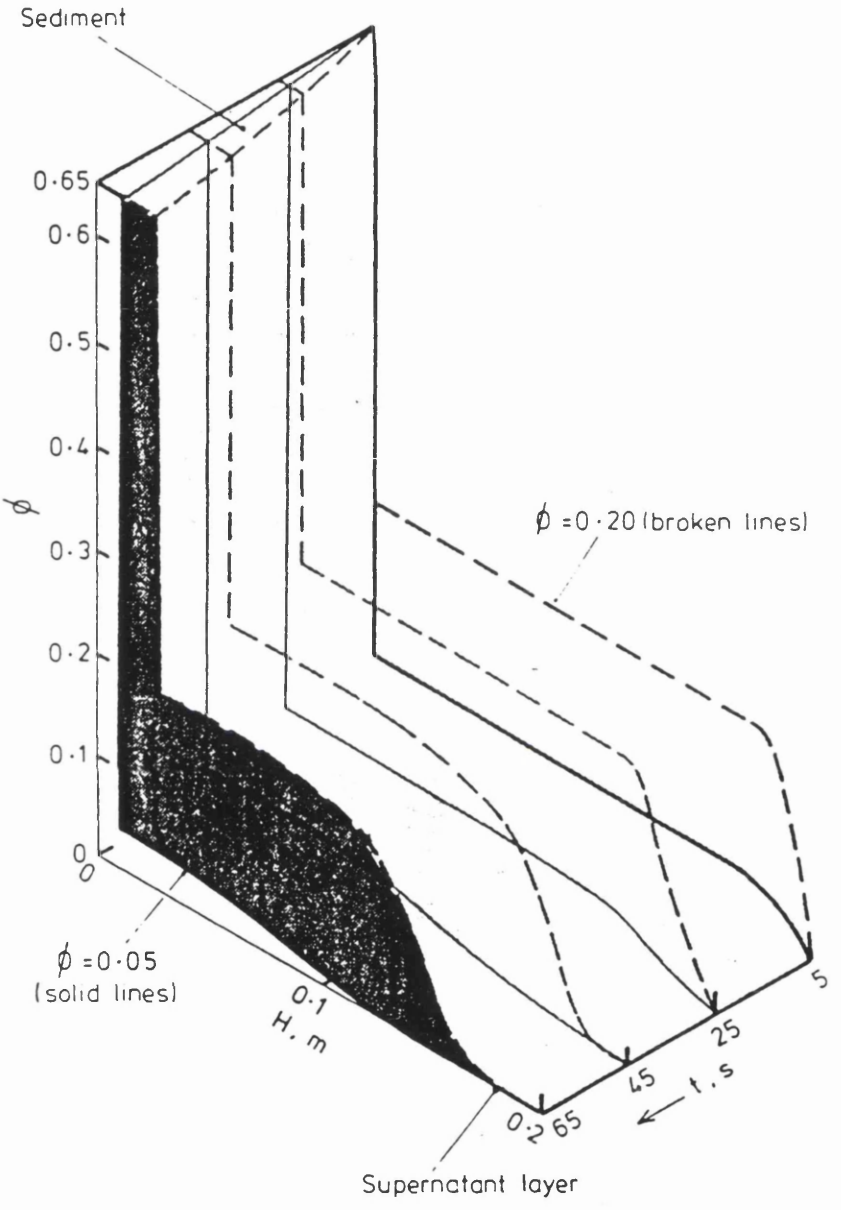

Figure 4.1 Simulated concentration profiles for different sedimentation processes as a function of time for two levels of initial solids volume concentration: ϕ, 0.05 and 0.2 % (Williams and Amarasinghe, 1989).

to eliminate the influence of electrostatic forces which are not taken into account in the model.

Glendinning and Russel (1982) report a statistical-mechanical simulation model based on the pair-wise additivity approach of Batchelor (1972). This model employs two-body interaction theory to predict the settling velocities of particles. Thus, the probability of finding the centres of pairs of particles at particular locations within the suspension is computed. The resulting data is then used to evaluate settling velocities. The results obtained on this basis apply to arbitrary solids concentrations and interaction potentials, the latter being governed by particle centre-to-centre separations within the suspension. Unfortunately, coefficients in the pair-wise additive model become negative at high solids concentrations (Glendinning and Russel, 1982). This represents a failure to model hindered settling effects which cause light particles to be convected upwards along with the fluid by heavier particles. Furthermore, the model assumes elastic hard sphere interactions for which particles immediately regain their terminal velocities after they collide and, therefore, is not applicable to soft solid dispersions. This is also one of the assumptions made in the model of Williams and Amarasinghe (1989).

4.4 Stochastic Simulation Models

Stochastic models rely on the use of probability theory to predict the likelihood of particles of a given size colliding and flowing collectively. Two types of particle movement are considered; particles settling individually and particles settling collectively as "clusters" formed by collision induced aggregation. These models use the distribution functions of particles falling on their own and particles falling as aggregates to compute the spatial distribution of particle settling velocities at different times from the onset of the sedimentation process. Some models involve the solution of particle population balances in which appropriate terms are included to account for the formation and disruption of clusters. The terminology 'aggregates' and 'clusters' is used in the context of particles moving together momentarily as a consequence of the system hydrodynamics. This is not to be confused with phenomena such as

coagulation and flocculation where the aggregates formed by the action of electrostatic and/or steric forces are permanent. Thus, the formation and destruction of clusters in this sense is a highly dynamic process.

Tory and Pickard (1977) developed a three-parameter Markov simulation model to estimate the movement of particles in a suspension as a function of particle concentration. They report that the configuration of the system as a whole dictates particle translational and rotational velocities and the model takes into account the variance and mean values of probability density functions. This information allows for the analysis of the seemingly random motion of particles. Thus, the Markov model takes into account the fact that for any given suspension concentration, there is a distribution of particle settling velocities. However, the mean of the steady-state probability density function of this distribution is taken to be dependent on the solids concentration only.

An important criterion in the Markov model is that the velocity of a particle in one short interval of time is highly correlated with the velocity in the next interval. This idea is exploited when computing particle settling velocities. The longer the duration of incremental time steps in the model, the lower the probability of collective flow while the probability of individual settling increases. Thus, in the mean, particles settle individually in which case, Stokes' law and related correlations can be applied to estimate settling velocities. The authors report a difficulty to reach a comprehensive simulation model that takes into account all multi-particle interactions on account of the large amount of data required for accurate parameter optimisation. In addition, there is no direct experimental proof regarding the validity of some of the assumptions made during the development of the Markov model. For instance, it is assumed that when two particles interact they gain the same minimum velocity. This is a prodigious assumption made on the basis of observations of macroscopic hindered settling effects which cause particles to settle at the same rate during sedimentation. Consequently, this assumption only holds true for concentrated suspensions for which hindered settling dominates particle-particle interactions. Another disadvantage is that the

motion of particles is related even at large separations through long range hydrodynamic interactions. No account is made of this in the Markov model.

Furthermore, the model also includes a coefficient of variation which is used to compute expected values of particle settling velocities. This coefficient is assumed to be constant for a given system. However, the value of this coefficient itself alters expected values of velocities during iteration and, therefore, predictions can become increasingly less accurate. The Markov model is also only applicable to systems with low particle Reynolds numbers and is therefore, only suitable for dispersions of small particles, for example the colloidal sub-range, or suspensions with high fluid viscosities.

Iordache and Corbu (1986) also describe a stochastic simulation model which uses kinetic theory to predict particle velocity distribution functions from which the settling behaviour of particles can be estimated for polydisperse suspensions. The authors also define two distinct modes of flow; singular flow for individual particles and regular flow for particles in contact.

As in the case for hydrodynamic simulation models, care must be taken when using stochastic models to ensure that all underlying assumptions and constraints are satisfied. Since the accuracy and validity of the models developed so far is not easy to assess there is a need for more robust models which incorporate a parametric dependency on probability density functions for individual systems (Tory and Kamel, 1992).

4.5 Conclusion

In this Chapter, it has been shown that despite the practical importance of polydisperse suspensions very few systematic investigations have been carried out. This is probably due to the fact that the behaviour of real systems lies between surface-dominated interactions such as those prevalent in colloidal systems ($d_p < 1$ μm) and hydrodynamic interactions for suspensions of coarse particles ($d_p > 10$ μm). Consequently, many of

the correlations developed to describe sedimentation phenomena are restricted to dilute monodisperse suspensions of rigid spherical particles. The majority of the empirical, hydrodynamics and simulation based models considered incorporate a large number of often unrealistic assumptions in their development. For instance there are several references in the open literature where models originally developed for dilute monodisperse suspensions of non-interacting spheres are extended to systems with higher solids concentrations and/or polydisperse suspensions. In particular, several models assume that interacting particles settle at the same rate whereas in practice there is sufficient experimental evidence to show that segregation occurs during sedimentation. The segregation of particles occurs due to differences in size and/or density and may happen even in concentrated suspensions where it is usually assumed that hindered settling effects give rise to uniform settling rates. Accordingly, the application of theoretical models to the determination of the flux of solids (mass settling per unit area per unit time) can yield erroneous results. In many cases, such limitations are addressed by the use of large design correction factors particularly when sizing large scale industrial thickeners and clarifiers. However, this practice adversely affects capital and operating costs since settling tanks can be oversized by up to 40% for a given duty (Williams et al. 1992).

An additional complication encountered during the modelling of sedimentation is that particles tend to aggregate to form flocs thereby altering the structure of the suspension and, therefore, its settling behaviour. There are very few satisfactory models capable of the quantitative analysis and simulation of such systems. For instance some models assume flocs to be spherical contrary to the results of microscopic studies (Micheals and Bolger, 1962). Furthermore, many simulation models are limited to a finite number of particles several orders of magnitude less than encountered in real systems. It is also worth noting that there is a fundamental lack of knowledge on the complex phenomenon of the combined effect of hydrodynamic and electrostatic forces. It is evident that extensive experimental data is required for use in conjunction with theoretical modelling in order to develop a more clear understanding of such effects. This in turn calls for the development of more reliable experimental techniques for the analysis of settling suspensions.

CHAPTER 5

A REVIEW OF SEDIMENTATION MEASUREMENT TECHNIQUES

5.0 Introduction

In recent years, several experimental techniques have been developed that attempt to address the limitations of existing theoretical sedimentation models by providing direct kinetic data such as particle settling velocities and concentrations. These techniques include light extinction methods (Davis and Birdsell, 1988), ultrasonic sensing (Howe and Robins, 1990; Wedlock et al., 1990), radiation imaging (Williams et al., 1990), pressure sensing (Raffle, 1976) and the use of a variety electrical transducers (Shi et al., 1993). In each case, a specific measurement principle which exploits some physical or chemical property of the suspension is used to provide information pertaining to the solids flux (mass of solids settling per unit area per unit time) during sedimentation. This is the data required for the design of practical separation equipment such as thickeners and clarifiers.

Of particular interest in this study, is the capability to monitor settling suspensions from direct measurements which can in turn be used to fully characterise the behaviour of the dispersed phase. This is the important prerequisite for the quantitative assessment of the sedimentation process since all real effects must be taken into account. Accordingly, the acquisition of such data should be on a model-independent basis since it is only for this case that a prior knowledge of suspension characteristics is not required. Therefore, for this special case calibration becomes unnecessary and measurements can be carried out in-situ for any suspension.

The relative merits of various techniques which have been widely applied to the interrogation of settling suspensions has been the subject of a previous survey

(Williams et al., 1990). This chapter reviews and critically evaluates the reliability of some of the important techniques.

5.1 Direct Sampling

One of the earliest methods of sedimentation analysis utilising direct sampling is that based on the jar test method reported by Kynch (1952). In this case, pilot scale laboratory tests are carried out in simple sedimentation columns (typically, 1.5 - 3 m tall) in order to provide preliminary estimates of the settling rates of suspensions. The analysis of the suspension is done on the basis of withdrawing samples from the column via a series of ports for subsequent analysis. This procedure is repeated at known time intervals and the suspended solids content is determined as a function of time. In principle, a sample collected at time, t_1 at a depth, d_1 below the surface of the suspension is assumed to contain suspended solids with a settling velocity less than or equal to d_1/t_1. Such data can then be expressed as a "cumulative percentage with a velocity less than a stated value" in order to plot a settling characteristic curve (Tebbutt, 1992). Figure 5.1 shows a typical characteristic curve which can be used to predict, by integration, the rate of settling for discrete particle size fractions. Thus, the proportion of particles of arbitrary settling velocity, v_s removed from the settling column is given by:

$$(100 - p_o) + \int_o^{p_o} \left(\frac{v_s}{v_o}\right) dp \qquad (5.1)$$

where, v_o is the critical settling velocity corresponding to particles leaving the sedimentation column at a given flowrate, Q and p_o is the percentage of particles with settling velocities $\leq v_o$.

Unfortunately, the extraction of samples during sedimentation is evidently invasive since this process interferes with the hydrodynamics of the system. Nasr-el-din et al. (1987) describe sampling efficiency studies in which the effect of various parameters such as probe design, particle size and sample take-off rate are considered for flow in

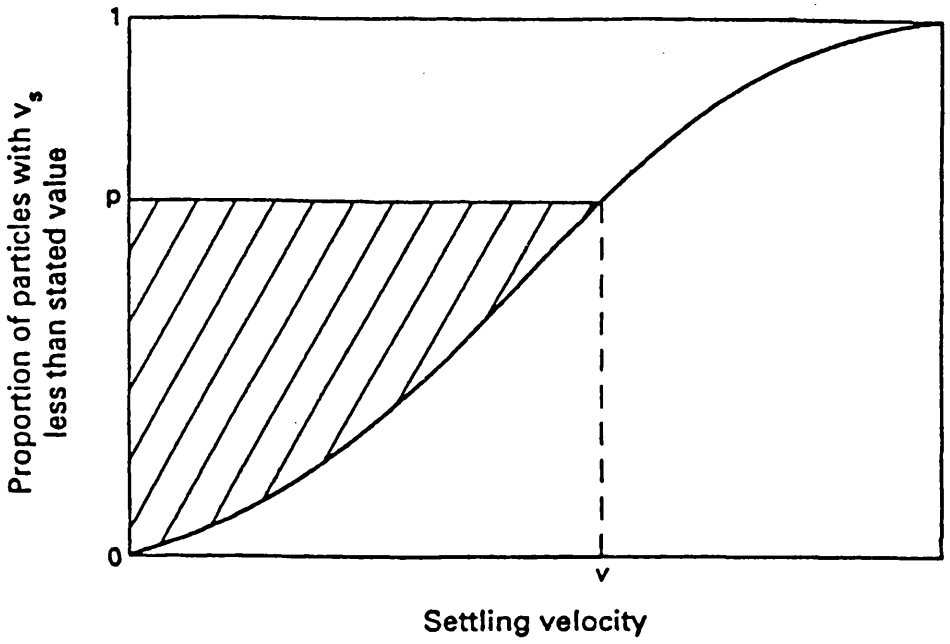

Figure 5.1 A typical settling velocity characteristic curve (Tebbutt, 1992).

pipelines. They report that in order for direct sampling to be representative the velocity at the sampling point must be related to the upstream velocity where quiescent settling conditions exist. This is because the velocity near sampling ports can be much higher than the bulk flow thereby inducing changes in the local solids concentration. In addition, since measurements are taken ex-situ errors can occur during subsequent analytical stages in which the suspended solids content is determined. This approach is clearly laborious and does not provide on-line measurements.

Williams and Amarasinghe (1990), also report a direct measurement technique in which the sedimentation process is "frozen" instantaneously. In this approach a specially designed settling vessel with a facility to divide the settling zone into a number of sections is used to isolate discrete suspension volumes. These can then be collected for subsequent analysis. This procedure has the obvious disadvantage of terminating the entire settling process and therefore, a dynamic approximation of the settling process can only be reached by repeating the procedure for a number of distinct settling times. However, this procedure has been shown to provide reproducible data since there is minimal interference of the suspension hydrodynamics.

5.2 Optical Methods

The use of optical methods to determine the rate of sedimentation is also possible, however, these techniques tend to be restricted to suspensions of low solids volume concentration (typically, $\phi_s < 0.4$). At much higher solids concentrations, suspensions effectively become optically opaque and, therefore, are no longer amenable to examination by this method.

Davis and Birdsell (1988) describe the use of an optical technique based on the principle of light-extinction to measure the rate of descent of suspension-supernatant interfaces. They report an experimental arrangement in which two narrow horizontal slits of light are produced by passing a laser beam through a set of cylindrical lenses. The light transmitted through the suspension is then focused onto a photo-diode detector which emits a pulse with a voltage signal proportional to the intensity of the

light beam. This signal is then recorded as a function of time in order to follow the sedimentation process. As sedimentation occurs, there is a continuous change in light absorbance in the region immediately above the lateral plane separating the suspension from the supernatant. This change is detected by each light slit and for dilute suspensions light absorbance can be directly related to the solids volume concentration. However, at high solids concentrations it becomes difficult to relate these two quantities directly due to changes in the refractive indices of the suspension. This method is apparently more reliable than simple visual observations of the interface, however, the difficulties that arise from the occurrence of diffuse interfaces in dilute suspensions still remain unresolved.

5.3 Ultrasonic Sensing

There are several ultrasonic sensing methods for the determination of the solids flux, solids volume concentration and in some cases, the extent of sediment consolidation. Some of the techniques reported in the open literature include the works of Blaachandran and Beck (1980), Bonnet and Tavlarides (1987), Howe et al. (1987), Lenn (1987), Urick (1947) and Young et al. (1982). Wedlock et al. (1990) describe a method based on monitoring the passage of an ultrasonic beam of known frequency through a test suspension and measuring the time it takes for the beam to travel between a pair of sensors. The velocity of the ultrasonic beam which is then calculated is related to the solids volume concentration. Whilst this technique enjoys the advantage of being completely non-intrusive and non-invasive, it has been reported that calibration problems are encountered at high solids volume fractions, ($\phi_s > 0.4$). Thus, suspensions become increasingly acoustically opaque thus making it difficult to directly relate the ultrasonic beam velocity to the solids concentration due to internal scattering effects which greatly reduce instrument sensitivity (Howe and Robins, 1990). Although it is possible to improve the resolution of ultrasonic sensors so that they are capable of monitoring suspensions for which $\phi_s > 0.4$, the increase in complexity and extra costs incurred are rarely justifiable.

5.4 Penetrative Radiation Techniques

The use of penetrative radiation techniques such as neutron deflection, x-rays and γ-rays for the characterisation of the behaviour of settling suspensions can be inherently expensive. Some of this expense is usually associated with the implementation of measures targeted at mitigating the harmful effects of radiation. Another factor that makes radiation techniques unattractive for field applications is that they are difficult to implement in practice often requiring skilled operation. Another disadvantage of some existing radiation methods is that they sometimes provide partial information. Thus, they may measure the solids volume concentration but not the particle settling velocity and therefore, it becomes difficult to determine the solids flux (Williams et al., 1990). Some of the these limitations apply to techniques such as nuclear magnetic resonance (NMR) and the use of radiation tracers (Genthe, 1974; Hansen et al., 1985).

5.5 Transducers

Transducers are devices that convert one physical variable into another. These devices are not restricted to electrical signal conversion although, in the main, this is the most common application. In the wider context, any measurement device capable of converting one variable into another can be defined as a transducer. In general, transducers exploit convenient signals as a means to monitor processes and may be capable of recording real time measurements. They are also usually capable of amplifying the small changes detected in the test environment prior to using them and amplification factors as high as 10^6 have been reported (see for example Peter, 1985).

Transducers based on the principle of sensing changes in electrical properties are popular primarily because electrical signals are relatively easy to convey whilst avoiding the need for complicated mechanical linkage. However, in practice there are several limitations that undermine the ability of these devices to provide accurate and reproducible results. Some of the factors that can be used to assess the performance of transducers in relation to process monitoring include reliability, mechanical integrity and the effects of environmental factors such as temperature, pressure, sensing volume,

humidity, solubility and susceptibility to corrosion. In recent years, a variety of transducers have been applied to the monitoring of settling suspensions for the purpose of obtaining sedimentation kinetic data (Shi et al., 1993).

5.5.1 Electrical Transducers

Electrical sensing techniques involve measurement of signals derived from an electrical excitation source. Typically, input signals are modulated as sensors are exposed to the suspension and output signals are received by suitable detectors. Direct signal processing as well as system automation is possible and several configurations of this nature are reported in the open literature. The exact configuration of the electrical circuits used is application dependent. Some electrical sensing methods have characteristically fast response times and are therefore suitable for the analysis of transient behaviour in test environments (Huang et al., 1988; Myers and Saville, 1989). The fast response time feature is of great importance since this means that data can be obtained in real time.

Unfortunately, most electrical transducers have the disadvantage of being inherently susceptible to effects such as electric field distortion caused by external electromagnetic interference as well as changes in the condition of the fluid medium. Another limitation is that in most applications of electrical devices, electric currents tend to follow the path of least resistance (Shi et al., 1993). In the context of monitoring sedimenting suspensions this can translate to underestimation of the solids concentration and settling velocity. This is in contrast to penetrative radiation techniques where the working principle relies on the transmission of neutrons which follow well-defined linear paths through suspensions.

In order to obtain measurements, electrodes of a suitable geometry are used and there must be a sufficient contrast in the measured electrical property between the solid and the fluid phase. There are three principal electrical properties which can be exploited to interrogate sedimenting suspensions. These are resistance, capacitance and inductance

which are related through a collective electrical property known as the complex impedance. This is given by the expression:

$$Z_x = R_x + j\left(\omega L_x + \frac{1}{\omega C_x}\right) \qquad (5.2)$$

where, Z_x, L_x , C_x and R_x are the impedance, inductance, capacitance and resistance respectively. ω, is the angular frequency of the electrical excitation signal. The impedance of a given electrical system is a complex function which represents the division of the energy supplied into two components. These are dissipative heat and magnetic/electric field energy.

The resistance, capacitance and inductance components can be resolved and determined as separate quantities and the choice of the appropriate electrical sensing property depends on the characteristics of the system under investigation. Judicious choice of the appropriate sensing technique must also take practical considerations such as vessel geometry and operating conditions into account. This is because the electrical property chosen usually dictates the size, geometry and location of electrodes.

When handling suspensions of fine particles, especially those in the colloidal sub-range, it is especially desirable for electrodes to be non-intrusive and non-invasive to the test environment. It has been shown to be possible to design electrical transducers that observe this constraint (Xie et al., 1990). For instance in some applications electrodes are mounted on the outer walls of sedimentation vessels. Unfortunately, while this approach is non-invasive it is commonly accompanied with a reduction in instrument sensitivity. This is because the sensing electrodes are not in intimate contact with the test environment which renders the detection of small changes difficult. Intuitively, a balance needs to be established between the intrusive/invasive nature and the sensitivity of a sensor.

5.5.1.1 Capacitance Transducers

Transducers based on the measurement of electrical capacitance are commonly used for a wide range of sensing applications. Some of these devices tend to be invasive in the sense that they are in direct contact with the test environment. They can, however, be considered non-intrusive since they occupy a small fraction of the sensing volume (Simons, 1991). In essence the capacitance sensing technique relies on the existence of a finite difference in dielectric constant (effective permittivity) between dispersed and continuous phases. In the case of a settling suspension this contrast depends on the fluid-particle pairing as well as the solids concentration. The technique is, therefore, not suitable for analysing electrically neutral suspensions in which there is no dielectric contrast between solid and fluid phases.

As sedimentation occurs the concentration of suspended particles changes. This in turn causes a change in system dielectric constant and it is this change that capacitance transducers measure and use to characterise the settling behaviour of the suspension. These devices tend to be highly sensitive and their capability to provide reliable measurements is often affected by the smallest of changes in electrode size, location and configuration. With regard to electrode configuration, flat plates, rings or helical structures can all be used with varying degrees of success. Furthermore, electrodes can either be flush mounted onto the inner wall of the settling vessel or they can be allowed to protrude into the vessel in direct contact with the suspension.

Due to the high sensitivity of capacitor electric fields, capacitance transducers can be susceptible to external electromagnetic interference. This problem can, however, be overcome by using earthed electromagnetic shields which surround the entire sedimentation column in the manner described by Simons (1991). It is also important to note that fluctuations in temperature and power supply are capable of destabilising the system response. Another source of instability comes in the guise of finite changes in the base-line capacitance over extended periods of usage. This phenomenon is commonly referred to as transducer base-line drift. The base-line capacitance can be defined as the background reading for a well mixed suspension of known composition.

The drift effect is caused by changes in charging voltage and it is usually necessary to perform regular re-calibrations which can be inconvenient in continuous applications.

There are a variety of working principles upon which capacitance transducers can be based. These include charge/discharge, voltage excitation/current detection, current excitation/voltage detection, resonance, capacitance balance and frequency response mechanisms (Huang et al., 1988; Noltingk, 1987; Simons et al., 1989).

The most commonly used of these is the charge/discharge method in which an excitation voltage is applied to a source electrode. A second electrode (the detector) then receives the charged pulse which is transmitted from the source electrode through the suspension medium. The detecting electrode therefore measures and monitors the charge recovered which is a function of solids concentration. It is essential for the applied excitation voltage to be of high frequency. This is because the use of low excitation frequencies often results in high effective permittivity values induced by polarisation of the electric double layers that surround particles (Williams, 1992). Myers and Saville (1989) report the existence of high effective permittivities for excitation frequencies below 20 kHz. In addition, it may also be necessary to minimise the duration between electrode charging and discharging cycles. This precautionary measure effectively reduces the influence of resistive components on the true value of capacitance since the these two electrical properties are related by the expression:

$$C_x = C_m - 0.5\,\tau_c\,G_x \qquad (5.3)$$

where, C_x and C_m are the true and measured capacitance values respectively, τ_c is the charge pulse duration and G_x is the conductance (the reciprocal of resistance). It is important to note that $C_x \rightarrow C_m$ as $\tau_c \rightarrow 0$ as well as $G_x \rightarrow 0$. Thus, even with a short pulse duration, it is quite possible for an appreciable difference to exist between C_x and C_m if the fluid phase (electrolyte) has a high conductivity. Another problem associated with the use of capacitance transducers based on the charge transfer principle is the charging of ancillary electronic circuitry, switches for example, by the applied

excitation voltage. It is essential that such 'stray' charges do not report to the detector electrode. Huang et al. (1988) developed a high frequency stray-immune capacitance transducer based on the charge transfer principle in which stray charges are discharged to earth. In this configuration only the sensor capacitance C_X is detected. The transformer-ratio-arm capacitance transducer is another commonly used stray-immune configuration (Shi et al., 1993). It is, however, restricted to excitation frequencies below 100 kHz.

The degree to which suspensions are homogeneous can also affect instrument sensitivity. Very often, suspensions are concentrated and polydisperse and effects such as channelling also known as cross-sectional stratification occur (see section 3.4, chapter 3). Under these settling conditions capacitance transducers are unlikely to provide an accurate measure of solids concentration due to significant lateral variations.

Another disadvantage of capacitance sensing is that several calibrations are often required. Simons (1991) describes experiments in which eight capacitance transducers mounted at various positions along a sedimentation vessel are calibrated at several values of initial solids concentration. This calibration must be done each time a different suspension is considered for analysis which is inconvenient. In addition, when using a multiplicity of sensors to obtain profiles of sedimentation kinetic data such as settling velocities and concentrations, there is a need to 'focus' the electric field of each device in order to minimise 'cross-talk' (interference). Simons (1991) describes a method of simultaneous excitation of several transducers which keeps electric field lines between adjacent sensors parallel thus minimising interference.

5.5.1.2 Resistance Transducers

Electrical resistance or its reciprocal conductance, is also often used to characterise the behaviour of settling suspensions. In contrast to capacitance sensing where the dielectric contrast between phases is exploited this technique relies on detecting changes in the ionic strength of suspensions during sedimentation. The conductance of

a given suspension can be attributed to either the presence of polar molecules or an ionised fluid phase. These sensors therefore rely on measuring the resistance to the flow of a current through the suspension when an electric field is applied. The current transmitted through the suspension can either be direct (DC) or alternating (AC) although the latter is usually preferred since the problem of polarisation of particles on the surfaces of electrodes is alleviated (Shi et al., 1993).

As in the case of capacitance sensing, two electrodes are used; one for excitation and the other for detection. The main difference between resistance as compared to capacitance sensing is that the attenuation of the input current signal is measured instead of the corresponding change in capacitance. The frequency at which the excitation current is supplied has to be above a certain threshold value in order to reduce polarisation effects (Myers and Saville, 1989). When two-electrode configurations are used polarisation may occur at the electrode-electrolyte interface resulting in a voltage drop additional to that established between the two electrodes. This effect can render the interpretation of results difficult and is an inherent source of error especially when handling dilute suspensions in which the signal-to-noise ratio is low (Myers and Saville, 1989).

Myers and Saville (1989) developed an alternative four-electrode device based on the work of Hayakawa et al. (1975) and Nakamura et al. (1981). This four-electrode configuration is reported to be free of polarisation effects due to separation of electrode functions. In this device no electrode is simultaneously required to pass current and measure voltage. Myers and Saville (1989) also describe a further improvement of the basic four-electrode configuration. The frequency difference dielectric spectrometer utilises a resistance-capacitance parallel circuit which "mimics" the behaviour of the fluid phase (pure electrolyte) to provide a constant reference level. Although this feature pre-supposes that the behaviour of the pure electrolyte is known, it represents an auto-calibrated system.

The applied current is converted to a proportional voltage using a current-to-voltage converter. This is a convenient feature since it is relatively easier to measure voltage

than it is to measure current directly. For this reason, dielectric spectrometers are more sensitive and accurate than traditional Wheatstone bridge based devices as well as conventional four-electrode systems. The experimental data of Myers and Saville (1989) validates the superior performance of the dielectric spectrometer.

Unfortunately, four-electrode configurations are more invasive to the test environment than conventional two-electrode arrangements. Therefore, there are two opposing effects for such systems; small electrodes that result in reduced invasivity but high polarisation and large electrodes are more invasive but less susceptible to polarisation. Overall, resistance transducers are both invasive and intrusive since they have to be in direct contact with the suspension (Shi et al., 1993). Compared to capacitance transducers, however, resistance sensors are more reliable since their performance is not significantly affected by external electromagnetic fields. In all, there are fewer factors that affect the performance of these devices compared to their capacitive counterparts. For this reason, resistance measurement techniques are currently more popular. Particularly, the influence of 'stray' resistances is not significant. However, calibration specific to the type of suspension handled is still required. The bulk resistivity of a given suspension can also change with time if the solubility of the solid phase in the fluid changes. For instance, fluctuations in temperature may induce changes in the solubility of the solid phase. For this reason, temperature control may be required to ensure stability.

Like capacitance, the measured resistance is a function of solids concentration (Meredith and Tobias, 1962). Similarly there are several working principles on which resistance transducers can be based. These include voltage excitation/current measurement, current excitation/voltage measurement and resistance balance techniques. It is also possible to have a sensitive analogue of the transformer-ratio-arm capacitance transducer. In this circuit capacitors are simply replaced by suitable resistors. Wakeman and Holditch (1989) used several resistance transducers mounted along a sedimentation vessel to infer information pertaining to solids concentration profiles.

5.5.1.3 Inductance Transducers

Inductance transducers are very uncommon. These devices work on the basis of monitoring the inductance of metallic coils mounted around a sedimentation vessel (Williams, 1990). The inductance of the coils changes accordingly with time as the concentration of solids in the bulk suspension decreases. Several coils can be mounted at different locations along the settling zone to obtain measurements that can be used to infer solids concentrations and particle settling velocity profiles.

The coils used in inductance sensing applications are usually mounted on the external surface of the sedimentation vessel. The technique can therefore be non-intrusive and non-invasive. However, sensitivity to slight changes in inductance brought about by correspondingly small changes in solids concentration is limited by the remoteness of the transducers from the suspension.

5.5.1.4 Impedance Transducers

Hybrid systems that combine capacitance, C_x resistance, R_x and inductance, L_x sensing components are also possible. This is because suspensions experience changes in resistance and capacitance simultaneously as the concentration of solids varies. Devices that measure both resistive and capacitive components of the complex impedance are known as impedance transducers. These systems exploit the fact that a 90° phase lag exists between the three electrical properties, C_x, R_x and L_x. Techniques such as phase sensitive detection (PSD) developed by Xie et al. (1988) exploit the phase difference between capacitance and conductance to give measurements in the form of resolved components of these two electrical properties. Transformer-ratio-arm transducers that simultaneously determine resistance and capacitance components have also been developed. Shi et al. (1993) describe such hybrid systems that can be used to interrogate settling suspensions.

5.6 Pressure Sensors

During sedimentation, the hydrostatic pressure in the settling zone varies with time since the solid phase is removed continuously. Therefore, at any given level within the settling zone the total hydrostatic pressure is the sum of the fluid pressure head and the weight of the remaining suspended particles. The hydrostatic pressure exerted by the suspended particles is, in essence, an excess pressure. Thus, it is an additional pressure to the hydrostatic pressure of the fluid on a solids free basis.

Pressure transducers work on the principle of measuring small changes in total hydrostatic pressure resulting from changes in excess pressure. The first notable application of pressure sensors was by Duncombe and Withrow (1932) who used a sensitive manometric method to monitor the variation of hydrostatic pressure with time for dilute suspensions. Unfortunately, as particles settle, the excess hydrostatic pressure progressively decreases and manometers discharge fluid back into the bulk suspension. This disrupts the fluid hydrodynamics of the suspension and therefore, interferes with the sedimentation process. Another notable limitation of conventional manometric methods is that short-term fluctuations in excess pressure are not easy to detect and transducer response time can be very poor.

Raffle (1976) also describes the application of pressure transducers which exploit changes in fluid hydrostatic pressure to obtain data from which particle settling velocities can be inferred. This technique differs from that of Duncombe and Withrow in the sense that the effect of decreasing excess pressure can be minimised by careful design. In this improved technique filters are used at the connection points between each manometer and the suspension in order to prevent fluid back-flow.

More recently, very sensitive solid-state pressure transducers have been invented. These devices are pressure sensitive membranes (diaphragms) which are flush-mounted to the walls of sedimentation vessels in direct contact with the suspension. The excess pressure caused by the presence of particles in the fluid is exerted on the membranes resulting in a proportional deflection. These devices have characteristically short

response times which allows for fast and continuous measurement of excess pressure from which particle settling velocities and concentrations can be inferred. For instance measurements can be taken at different locations along the settling zone in order to provide effective pressure-time profiles from which the solids flux can be inferred (Simons, 1991). In this method the settling velocities of particles are deduced from the initial slopes of effective pressure-time profiles.

Unfortunately, most existing solid-state pressure transducers are delicate since they are fabricated from silicon. These devices are, therefore, not suitable for use in aggressive environments. Whilst it is possible to fabricate more robust devices from materials such as steel difficulties arise from a reduction in sensitivity (Blasquez et al., 1989; Xie et al., 1990).

It is also noteworthy that since pressure transducers are usually flush mounted they are unlikely to provide representative bulk settling measurements even in the absence of wall effects.

5.7 Conclusion

Table 1 represents a summary of the relative merits/disadvantages of the most commonly used methods for sedimentation analysis as described in the preceding sections. All of these systems involve monitoring the variation of some property over a defined sensing volume. The derived information is then used in conjunction with an initial calibration in order to determine the settling behaviour of a given suspension.

Unfortunately, the majority of these techniques are unreliable since the type of calibration they require is suspension-specific. Consequently, few devices are capable of continuous on-line operation and, therefore, operators still have to rely on direct sampling methods in which samples are extracted for analysis in order to approximate the dynamic behaviour of the settling process. This approach is itself prone to errors

Table 1. Advantages and disadvantages of common methods of obtaining sedimentation kinetic data

Method	Working Principle	Limitations	Cost	On line?
Light extinction	Light absorbed is proportional to solids concentration	changes in refractive index, not applicable to optically opaque systems	Low	No
Ultrasonic sensing	Ultrasound beam velocity is function of solids concentration	occurrence of internal scattering effects, not applicable to acoustically opaque systems	High	No
Radiation imaging	Radiation absorbed/deflected is function of concentration	may provide partial information, usually concentration only	High	No
Pressure sensing	Hydrostatic pressure related to suspended solids content	prone to fouling, fragile, poor response time and sensitivity	Low	Yes
Electrical sensing	Electrical resistance/capacitance is function of concentration	susceptible to external electromagnetic interference	High	No

and evidently non-representative since suspension composition may change rapidly with time.

Although flush mounted pressure transducers can be used to provide on-line sedimentation kinetic data by exploiting changes in the fluid hydrostatic head, complications associated with the influence of wall effects on the settling behaviour of particles arise. This limitation has recently been addressed by the development of devices which extend well into the core of the suspension. However, these sensors are still prone to fouling and their sensitivity decreases with usage. The current practice is to periodically replace sensors which is neither cost effective nor reliable.

On the basis of the above considerations, it is evident that there is still a strong incentive to develop alternative techniques that are capable of providing direct sedimentation data on an on-line basis. It is particularly desirable to obtain such information in a model-independent manner for both monodisperse and polydisperse suspensions.

CHAPTER 6

EXPERIMENTAL

DESIGN AND DEVELOPMENT OF THE VIBRATING REED SEDIMENTATION ANALYSER

6.0 Introduction

This chapter describes the design and development of a multiple vibrating reed analyser for the routine on-line measurement of particle settling velocities and the solids flux (mass settling per unit area per unit time) during sedimentation. The associated electronic drive and detection systems are also given.

The development of a bench-top unit utilising a single reed is described first. This coupled with theoretical modelling (Mahgerefteh and Al-Khoory, 1991(a)) are used for determining the optimal design and operational characteristics required for the multiple reed system.

The principle of operation of the device is simple and relies on the fact that the resonance of a stiff reed performing simple harmonic motion in a fluid medium is directly related to the fluid hydrodynamic head. In the case of a settling suspension, the fluid bulk density and hence the hydrodynamic head decreases with time as solids settle out of suspension. Particle settling velocities and solids flux profiles may in turn be easily obtained by continuous monitoring of the resonance frequencies of a number of reeds positioned at set levels along a settling tank.

An ancillary electronic data acquisition system has been developed for use in conjunction with the multiple reeds. This system comprises a multiplexed array of electronic counters with a capability to provide frequency measurements at a rate of ca. 10^{-3} s per channel. The output from this system is linked to a computerised data processing and collection interface.

It is noteworthy that in recent years, there have also been several other applications of the remote drive vibrating reed system. These for example include fluid density measurement under aggressive process conditions and thermogravimetric analysis (Mahgerefteh et al., 1994, 1990, 1988; Mahgerefteh and Al-Khoory, 1991a, 1991b; Briscoe et al., 1987; Briscoe and Mahgerefteh, 1985, 1984). More recently, a vibrating reed device has been used to study added mass effects in two-phase liquid/solid media (Mahgerefteh and Khoderverdian, 1996; Khoderverdian, 1994).

6.1 The Remote Drive Arrangement

Figure 6.1 shows a schematic representation of the basic layout of the remote drive system. A detailed design is given later.

The unit comprises a stainless steel rod (1) clamped at an intermediate point along its length. One end (the 'remote side') is exposed to the settling suspension whilst the other (the 'drive side') is driven into transverse vibration at resonance by an alternating current electromagnet (5). The first harmonic resonance frequency is the preferred mode of operation due to its characteristically linear variation (Roy and Ganesan, 1994). Second and higher order harmonics tend to be distinctly non-linear, not pronounced and, therefore, more difficult to interpret. Vibrations are transmitted through the clamp and optically detected using a suitable detector (6) placed on the drive side. With length ratios of the drive to the remote spans of the reed of less than 0.4, the resonance frequency of the reed becomes predominantly sensitive to changes occurring on the remote side only (Mahgerefteh et al., 1990). A particularly novel feature of the device is the fact that the drive and detection mechanisms are effectively isolated from the test fluid.

6.1.1 The Electronic Drive and Detection System

Figure 6.2 shows the vibrating reed electronic drive and detection circuit. The system automatically tunes to the first harmonic resonance frequency of the reed on the basis

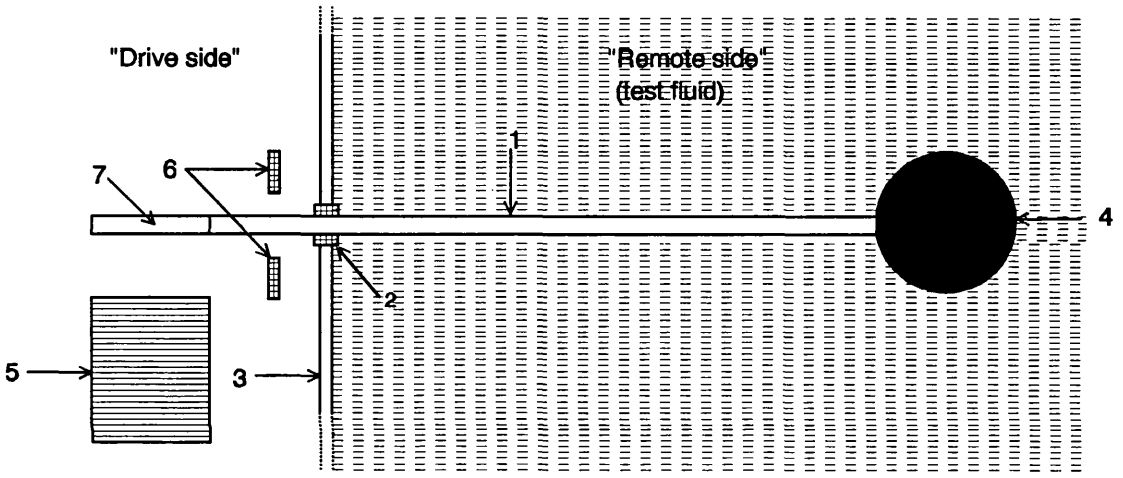

Figure 6.1 A schematic representation of the remote drive vibrating reed analyser showing the reed (1), clamp (2), container wall (3), attached mass (4), electromagnet (5), optical detector assembly (6) and flux linkage plate (7)

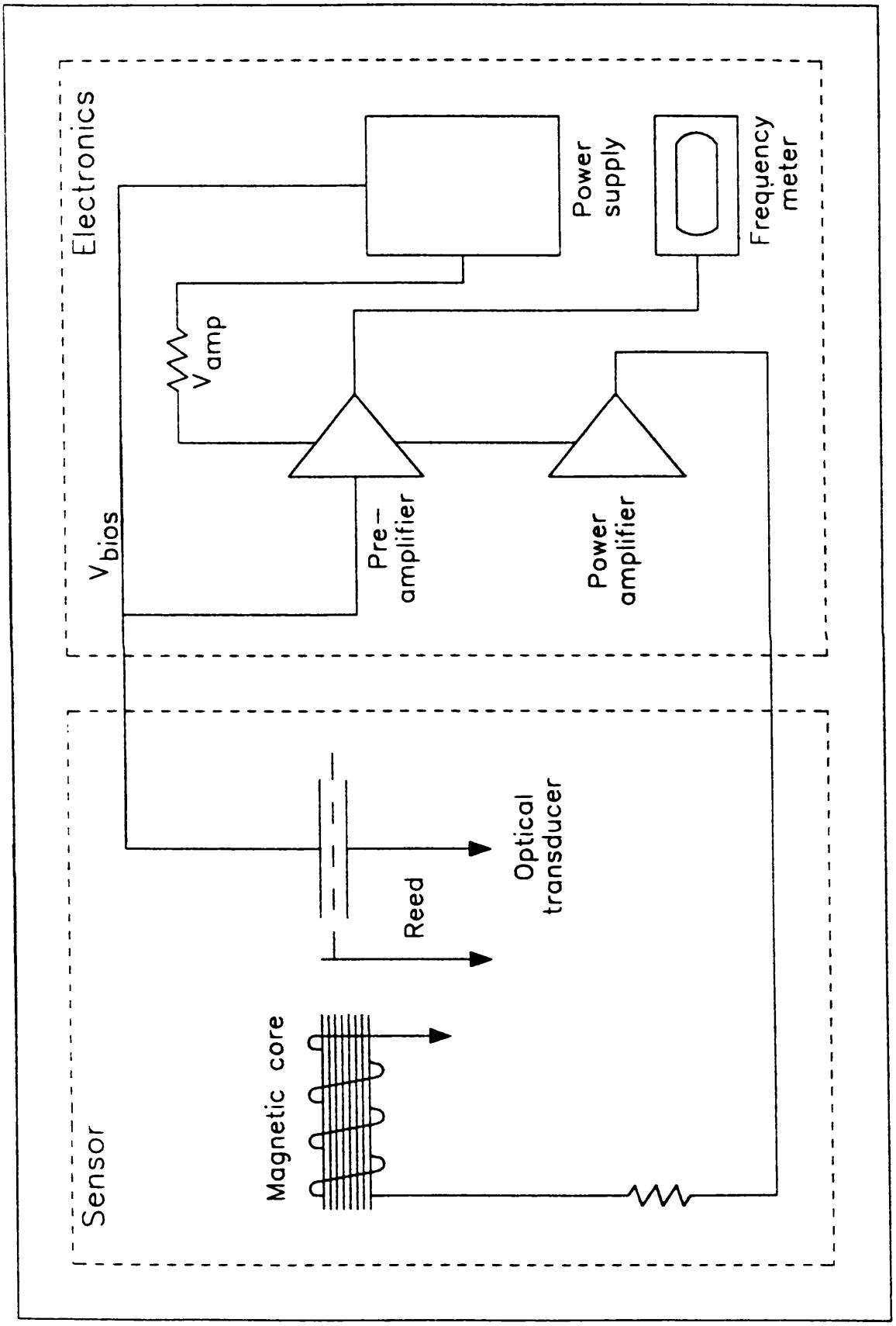

Figure 6.2 Vibrating reed electronic circuit diagram (Khodaverdian, 1994)

of a regenerative feed back loop (Seely, 1958). In this case, the vibration induced voltage signal picked up by optical sensors is returned to drive the electromagnet via a 30 watt pulsating alternating current power amplifier thus forming a closed loop. The electromagnet comprises a laminated rectangular soft iron core wound with 1200 turns of 0.1 mm diameter copper wire. Also shown in figure 6.2, is the system power supply (range 0 - 30 volts) which consists of a 50 watt transformer (RS type 223-8257). This unit is used to drive the electromagnet and excite the optical detector (6).

The latter comprises a 5 mm infra-red emitter (Farnell, type TSUS 5400) and a pair of photo-diode detectors (Farnell, type BPW 41N). In essence, these operate by illuminating the reed with an infra-red light source of known wavelength in order to cast a shadow across the photo-diodes which in turn produce photo-currents proportional to the light intensity (Cimmino and Davis, 1985). As the reed vibrates, the shadow oscillates across the surfaces of the photo-diodes thereby modulating the photo-currents. The difference between the photo-currents of the two detectors provides a measure of the reed displacement. The system response in relation to the reed displacement is linear provided the shadow overlaps the two photo-diodes. With this arrangement it is possible to detect amplitudes of vibration as low as 1×10^{-3} mm.

The output from the power amplifier is modulated to produce a pulsed drive signal which attracts the reed towards the electromagnet for only part of the full cycle. This feature has been observed to improve the stability of the detected signal by minimising the degree of interaction between the drive and the reed (Bak, 1986). A variable bandpass filter (range 0 - 230 Hz) eliminates second and higher order harmonics (see later). The amplifier circuit (see later) also incorporates special provisions for controlling the drive pulse width as well as its phase lag (normally set at 90° relative to the detected signal to ensure resonance (French, 1970)). The detected amplitude and resonance frequency are, respectively, displayed at ca. 2 s intervals using a universal frequency meter (Racal-Dana type 1990, range 0 - 100 MHz), and a digital multi-meter (Keithley type 175, range 0 - 250 volts). A suitable oscilloscope (Telequipment type DM64) is used to monitor the phase lag and pulse width.

6.1.2 Modelling of the Vibration Mechanics and Optimal Design Criteria

The mathematical representation of the vibration characteristics of a horizontal beam oscillating in the transverse direction is described by Bickley and Talbot (1961) who applied the elementary Euler - Bernoulli equation:

$$\frac{\partial^4 y}{\partial x^4} + \left(\frac{\rho a}{EI} . \frac{\partial^2 y}{\partial t^2} \right) = 0 \qquad (6.1)$$

where, 'ρ' is the density of the beam, 'a' is the cross sectional area of the beam, 'E' is Young's modulus of elasticity and 'I' is the area moment of inertia of the beam cross section about the neutral axis. 'y' represents the transverse deflection at any point 'x' along the beam and can be expressed as a function of time, 't'.

Thus:

$$y(x,t) = Y(x).F(t) \qquad (6.2)$$

where, Y(x) defines the normal mode of vibration and F(t) is a function describing the motion of the vibrating beam experiencing simple harmonic motion at an angular frequency, 'ω'. The function F(t) is in turn given by the equation:

$$F(t) = \alpha \sin(\omega t) + \beta \cos(\omega t) \qquad (6.3)$$

where 'α' and 'β' are arbitrary constants. By combining equations 6.1 to 6.3 it can be shown that:

$$\frac{d^4 Y}{dx^4} - \lambda^4 Y = 0 \qquad (6.4)$$

where:

$$\lambda^4 = \frac{\rho a \omega^2}{EI} \qquad (6.5)$$

Equation 6.5 is known as the beam equation and the term 'EI' is commonly referred to as the flexural rigidity (Beards, 1995). In this analysis, it is assumed that beam rotation is negligible compared to transverse deflection. In addition, shear deformation is considered to be negligible compared to bending deformation.

The general solution to equation 6.5 is given by:

$$Y = A\cos(\lambda x) + B\sin(\lambda x) + C\cosh(\lambda x) + D\sinh(\lambda x) \qquad (6.6)$$

where A, B, C and D are constants whose values depend on the boundary conditions of the system which in turn depend on the manner in which the beam is supported. The solution of equation 6.6 yields an infinite number of possible resonance frequencies and amplitudes of vibration. In the case of a beam clamped well away from its mid point, the effect of the surrounding fluid becomes much more pronounced on the longer span provided the system is vibrated at its short end at the first harmonic resonance frequency (Mahgerefteh and Al-Khoory, 1991a).

Al-Khoory (1992) applied the appropriate boundary conditions to produce three sets of solutions for the constants A, B, C and D for three spans (the drive, the remote and the clamped section) of the reed. The resulting system of equations was then used in conjunction with a computational model based on the finite element method of analysis to predict the effect of various design parameters on the reed resonance frequency.

In summary, for a cylindrical shaped reed, the optimal design and operating criteria resulting in a stable response as well as giving rise to a maximum change in the resonance frequency in response to a change in mass at the remote end require:

(i) Maximising the ratio of Young's modulus of elasticity to the density of the reed material of construction.

(ii) Minimising the length ratio of the drive span to the overall length of the reed.

(iii) Minimising the ratio of the remote side attached mass to the overall mass of the reed.

(iv) Minimising the distance over which the reed is clamped.

(v) Minimising the overall length of the reed.

(vi) Maximising the diameter of the reed.

(vii) Operating at the first harmonic resonance frequency of vibration.

6.2 Design of the Bench-Top Analyser

A bench top analyser has been especially developed so as to allow changes in the reed's characteristic dimensions (length and diameter) along those based on the optimal design criteria discussed in section 6.1.2. This is carried out whilst at the same time bearing in mind the practical implications on the overall system design. For example, criterion (i) above dictates a reed material of construction with a high ratio of Young's modulus to density thus making a ceramic such as quartz an obvious choice. Unfortunately this was not practical due to difficulties associated with its fabrication as well as clamping. In this study, we have chosen stainless steel as the next best choice particularly in view of its corrosion resistance properties. Criterion (ii) on the other hand dictates a minimum clamping ratio (ratio of drive span length to the overall reed length). In this study we choose a clamping ratio of 0.35. Smaller ratios although more desirable, are impractical due to excessive power requirement by the electromagnet which in turn results in its considerable Ohmic heating and eventual burn-out.

Figure 6.3 and plate 6.1 show, respectively, a scaled drawing and a photograph of the bench-top analyser. Figure 6.4 on the other hand, shows a scale drawing of the reed in isolation. The reed is assembled from three interchangeable parts comprising a remote section, joining piece and drive section. The joining piece is suitably threaded in order to take on different length and diameter reeds. Returning to figure 6.3, the reed (1) is horizontally held via a 36 mm diameter, 0.06 mm thick pinning disk (2) (see later). The latter is in turn connected to a 102 mm long × 70 mm wide × 20 mm thick stainless steel supporting block (3) via six 12 mm long M4 × 10 screws (4). The supporting block (3) is securely mounted on a 274 mm long × 140 mm wide × 20 mm thick lead slab (5) which in turn stands on four rubber legs (6). The latter minimise the transfer of vibrations to the surroundings.

The drive side of the reed is suitably threaded to take on a 13 × 13 mm, 3 mm thick mild steel plate (7) in order to provide magnetic flux linkage with the electromagnet (8). The separation between the electromagnet (8) and the plate (7) may be adjusted at will using two 20 mm long M4 × 10 screws (9). The remote side of the reed on the other hand is mounted with a 20 mm diameter fine meshed (ca 40 μm) wire gauze supported on a 2 mm thick brass ring (10). This member enhances the effect of the fluid environment on the reed's vibration characteristics. At the same time, close visual observation of settling water/glass ballotini suspensions has revealed that the wire gauze has the advantage of reducing the vibration induced perturbations in the immediate vicinity of the reed. Also, the selection of a wire gauze as opposed to a flat plate results in a reduction in the attached mass compared to the mass of the reed thus complying with the optimal design criterion (iii) (see section 6.1.2).

The optical detector (11) is strategically positioned at ca. 12 mm from the supporting block (3). It is found that although larger separations result in an increase in sensitivity, this is however at a cost of reduction in stability of the detected signal.

Previous designs (see for example Mahgerefteh and Khodaverdian (1996)) of the remote drive system involved the use of plastic compression fittings as a means of clamping the reed to the supporting structure.

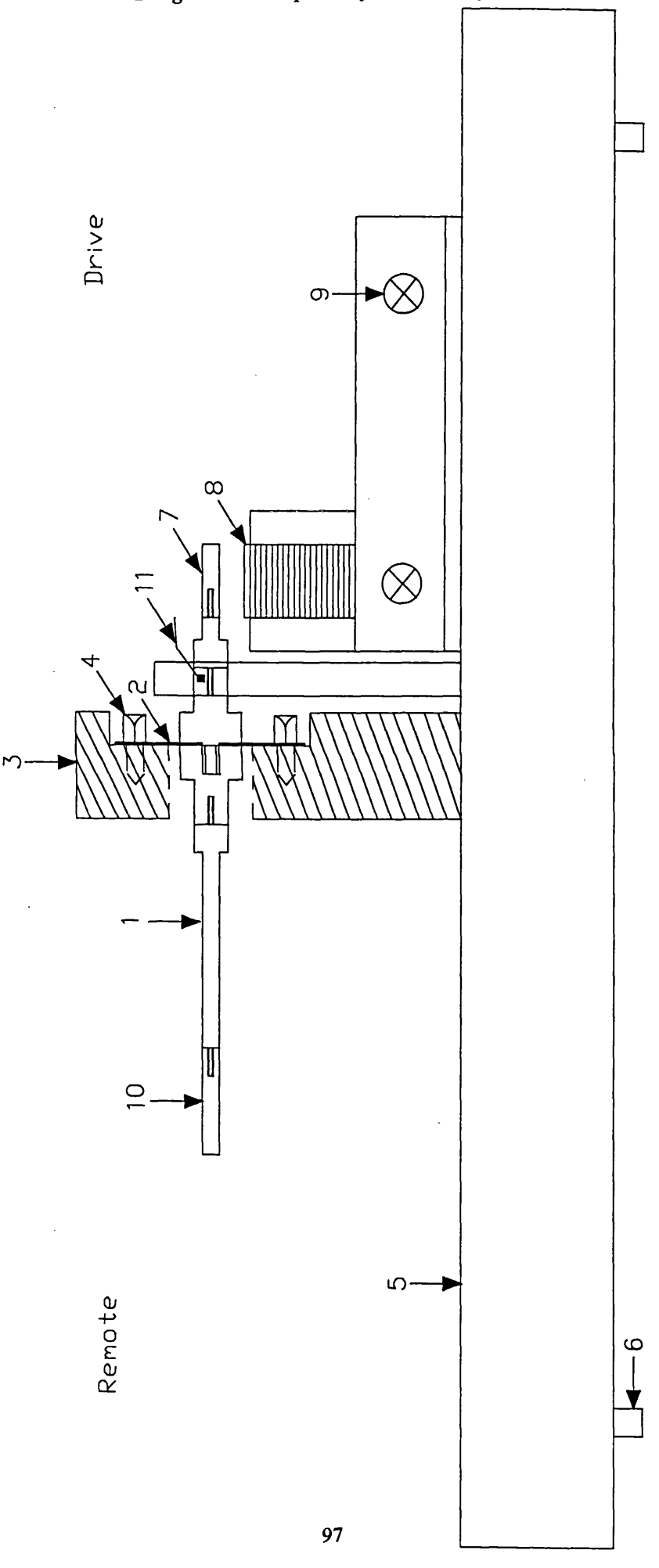

Figure 6.3 A scaled drawing of the bench-top vibrating reed analyser.

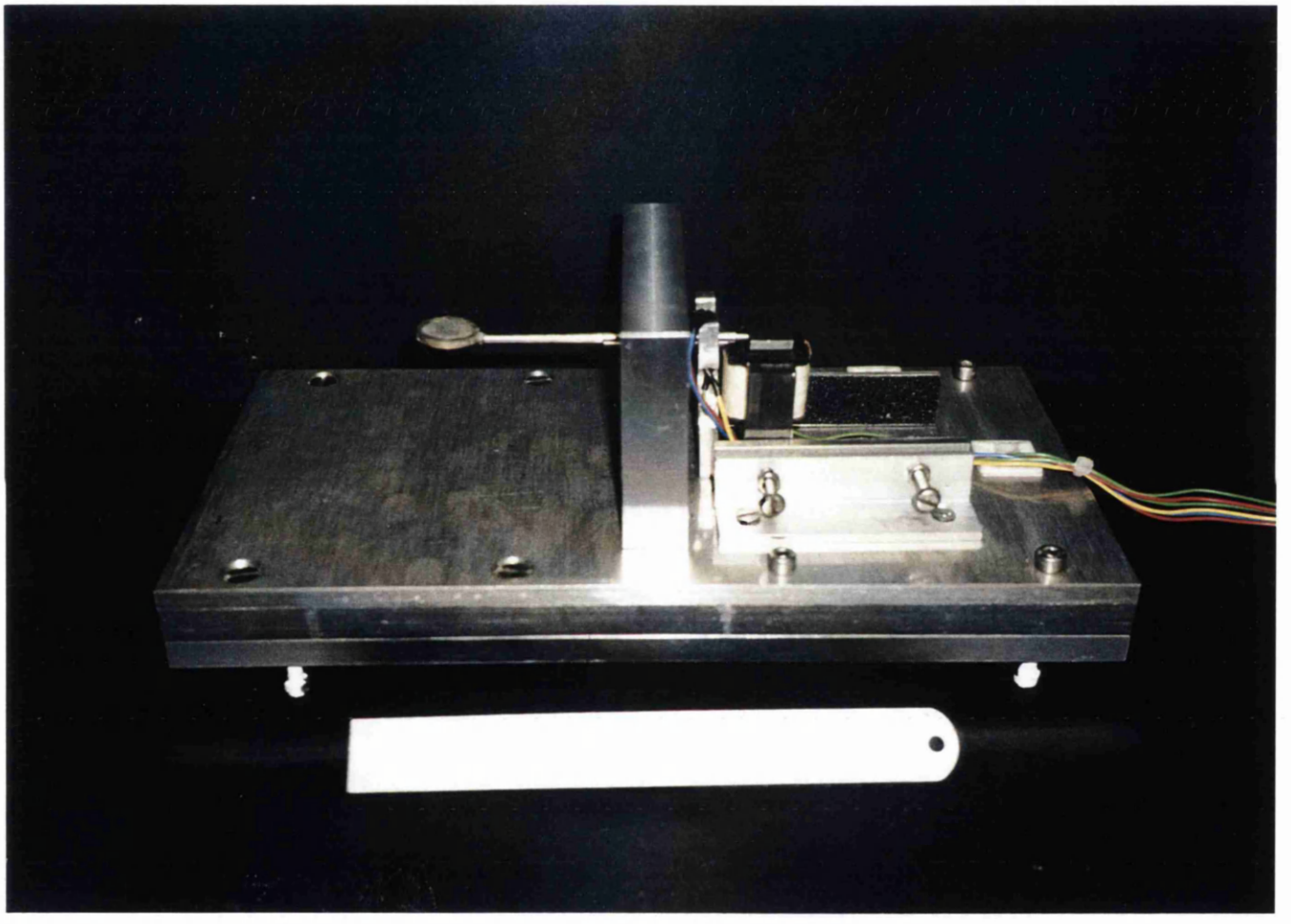

Plate 6.1 Photograph of the bench-top vibrating reed analyser.

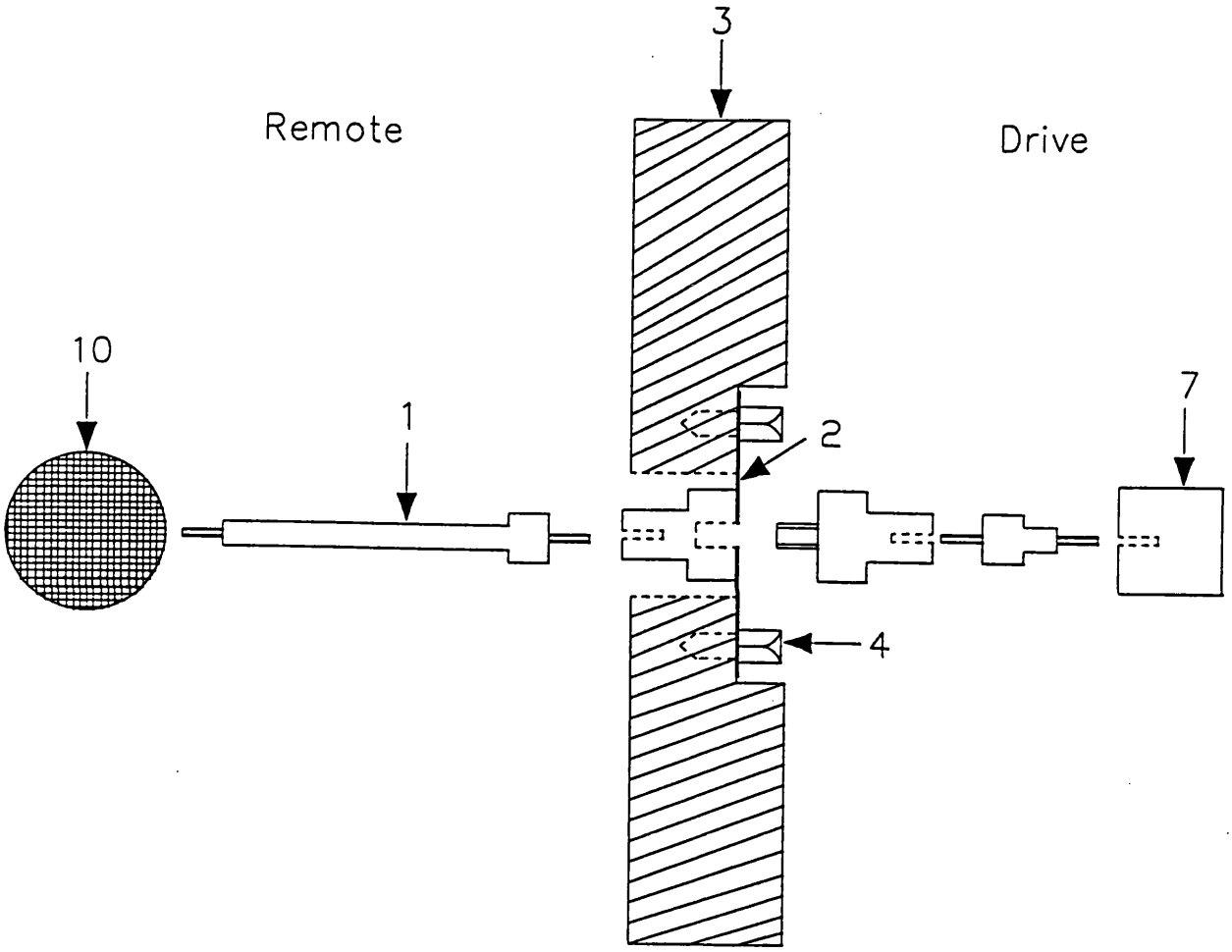

Figure 6.4 A scaled drawing showing the various components of the bench-top unit in isolation.

Our experience has shown that although this arrangement acts as an effective seal for isolating the fluid environment from the drive side, it has the disadvantage of damping vibrations thus reducing the system's quality factor. Also, the resonance frequency is marginally, but significantly affected by the clamping pressure produced as a result of the degree of tightness of the locking nut which is in turn difficult to control. This can be a significant problem in the design of the multiple reed system (see later) as it may give rise to inconsistent behaviour of the reeds.

In our new design we overcome this problem by replacing the compression fitting clamp with a 'pinned support'. Here the reed is effectively pinned at a point along its length via a 36 mm diameter, 0.06 mm thick stainless steel disk which is welded around its circumference. The disk is in turn securely attached around its circumference to the supporting slab in the manner described above.

The very small clamping distance produced as a result of pinning the reed significantly improves the efficiency of transfer of vibrations from the drive to the remote span, thereby minimising the interference of the supporting structure with the reed's vibration characteristics. The result is a much more stable and sensitive response (see later), consistent with the optimal design criteria (see section 6.1.2).

6.2.1 Design Optimisation Studies

In the proceeding section, the performance of the system is mainly quantified in terms of the magnitude of the change of resonance frequency in response to a change in attached mass (Hz/g) as well as the stability of the frequency response.

6.2.1.1 Optimisation of Reed Length

Different length remote and drive spans of the reed were machined ensuring a constant pinning ratio (ratio of drive span length to the overall reed length) of ca. 0.35.

Figure 6.5 shows the variation of resonance frequency with remote side attached mass in air for 3 mm diameter stainless steel reeds of various overall lengths in the range 110 - 196 mm. Figure 6.6 on the other hand shows the corresponding variation in system sensitivity, (Hz/g) obtained from the slope of the linear regression lines fitted to the data in figure 6.5 plotted as a function of reed length. A typical amplitude of vibration as measured at the remote end is 0.5 mm.

Returning to figure 6.6, it is evident that system sensitivity improves as the overall length of the reed decreases. This result is consistent with the predictive design criteria described previously (see section 6.1.2). It is interesting to observe that there is little further improvement in the system's sensitivity for reed lengths below 130 mm.

It is important to note that the optimal reed length is that which provides the best combination of mass sensitivity (as measured from the slope of frequency versus attached mass data) and stability in response. We determine the latter by monitoring the system's resonance frequency for a constant attached mass (in this case 1.6513 g) over a period of ca. 20 minutes. As frequency readings are taken at 2 s intervals, this corresponds to 600 measurements.

For each reed length, the maximum deviation from the mean resonance frequency over the test interval is then determined and added to the maximum frequency deviation from the resonance frequency versus attached mass calibration lines (see figure 6.6).

The resulting cumulative error (Hz) is then divided by the corresponding sensitivity (Hz/g) to determine the system mass resolution (per g). The latter corresponds to the minimum detectable mass and, therefore, can be considered as a reliable parameter with respect to the evaluation of the system's performance.

Figure 6.7 shows the variation of system mass resolution with overall reed length for 3 mm diameter uniform reeds with a constant pinning ratio of 0.35. Clearly, the sensitivity of the system with respect to mass measurement decreases markedly for

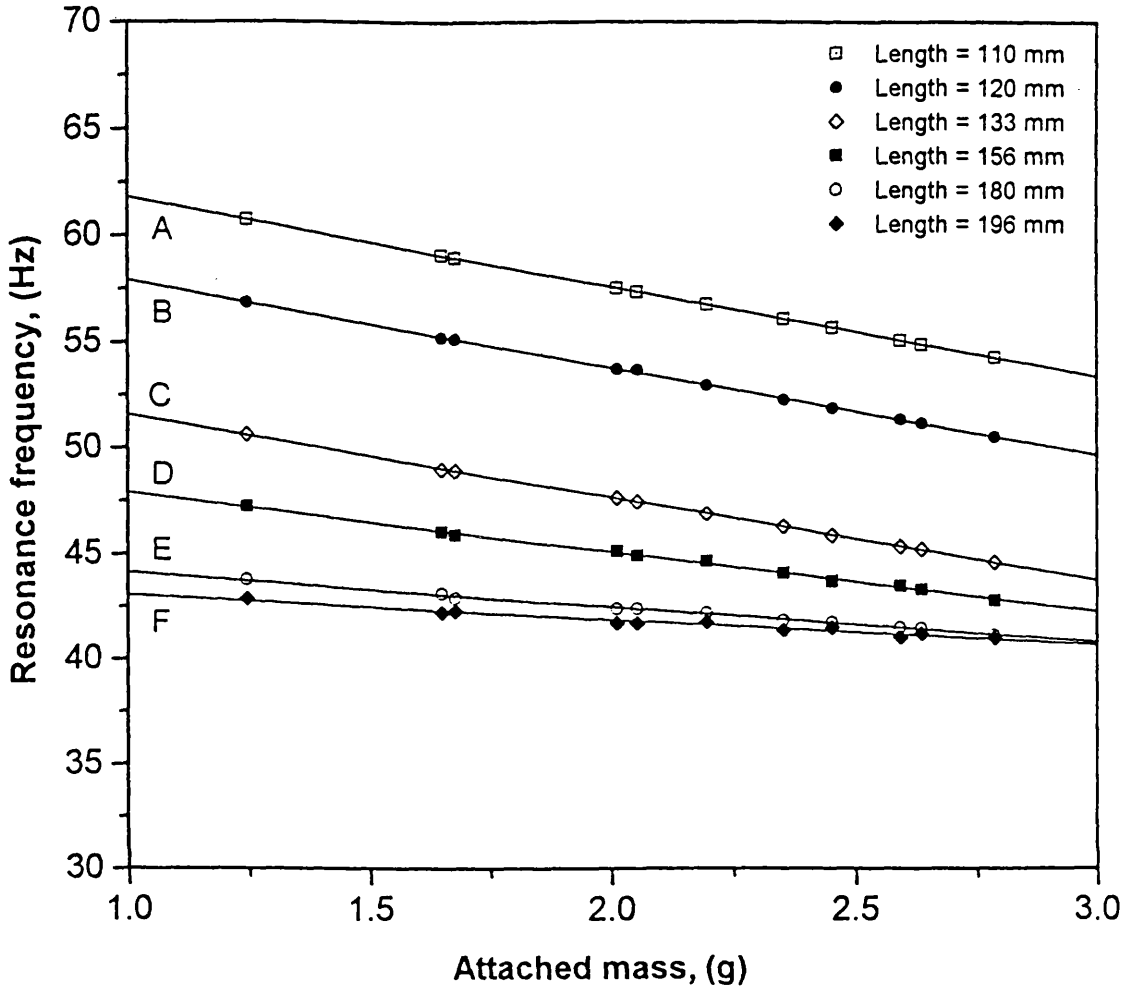

Figure 6.5

The variation of resonance frequency with remote side attached mass for 3 mm diameter uniform reeds of various overall lengths: curve A, 110 mm; curve B, 120 mm; curve C, 133 mm; curve D, 156 mm; curve E, 180 mm and curve F, 196 mm. The data is for a constant pinning ratio of 0.35

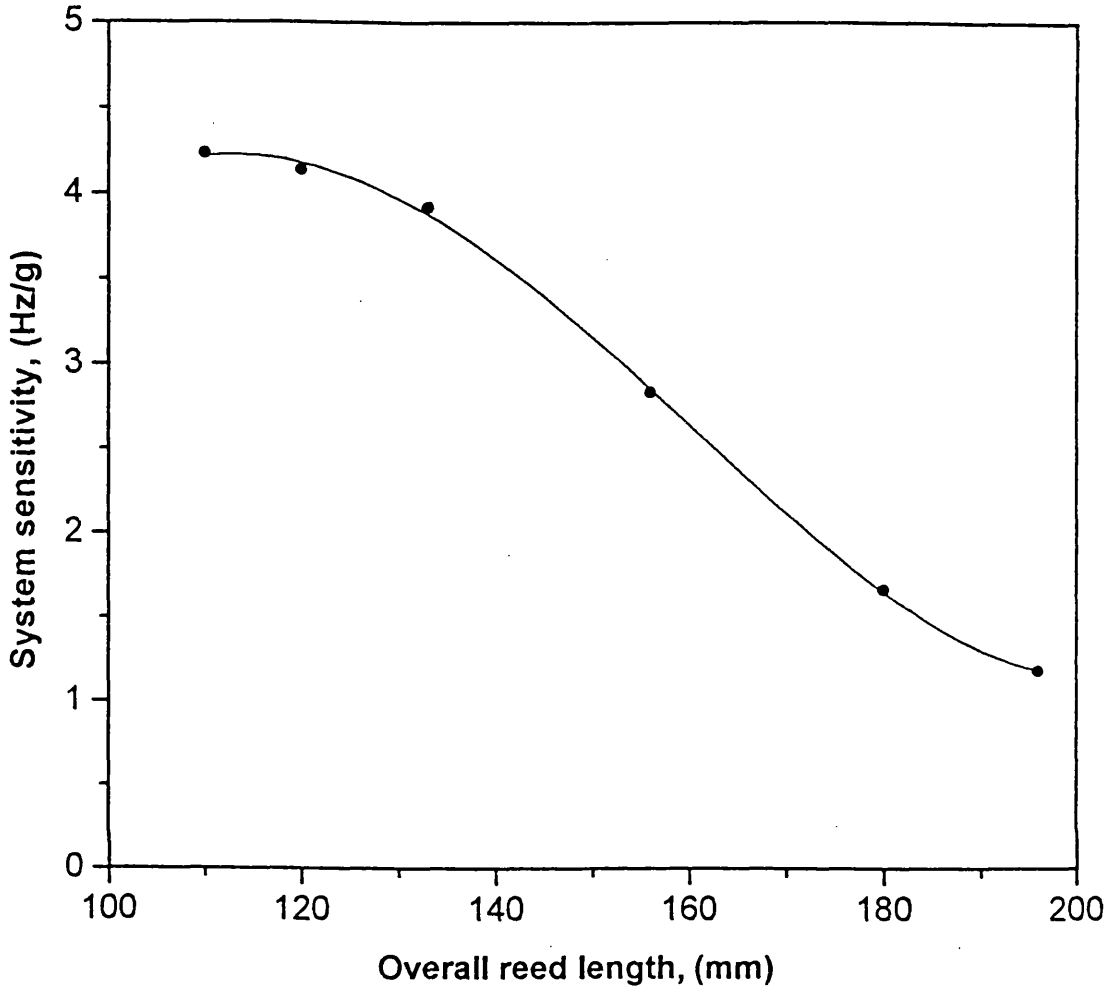

Figure 6.6
The variation of system sensitivity with overall reed length for 3 mm diameter uniform reeds with a constant pinning ratio of 0.35

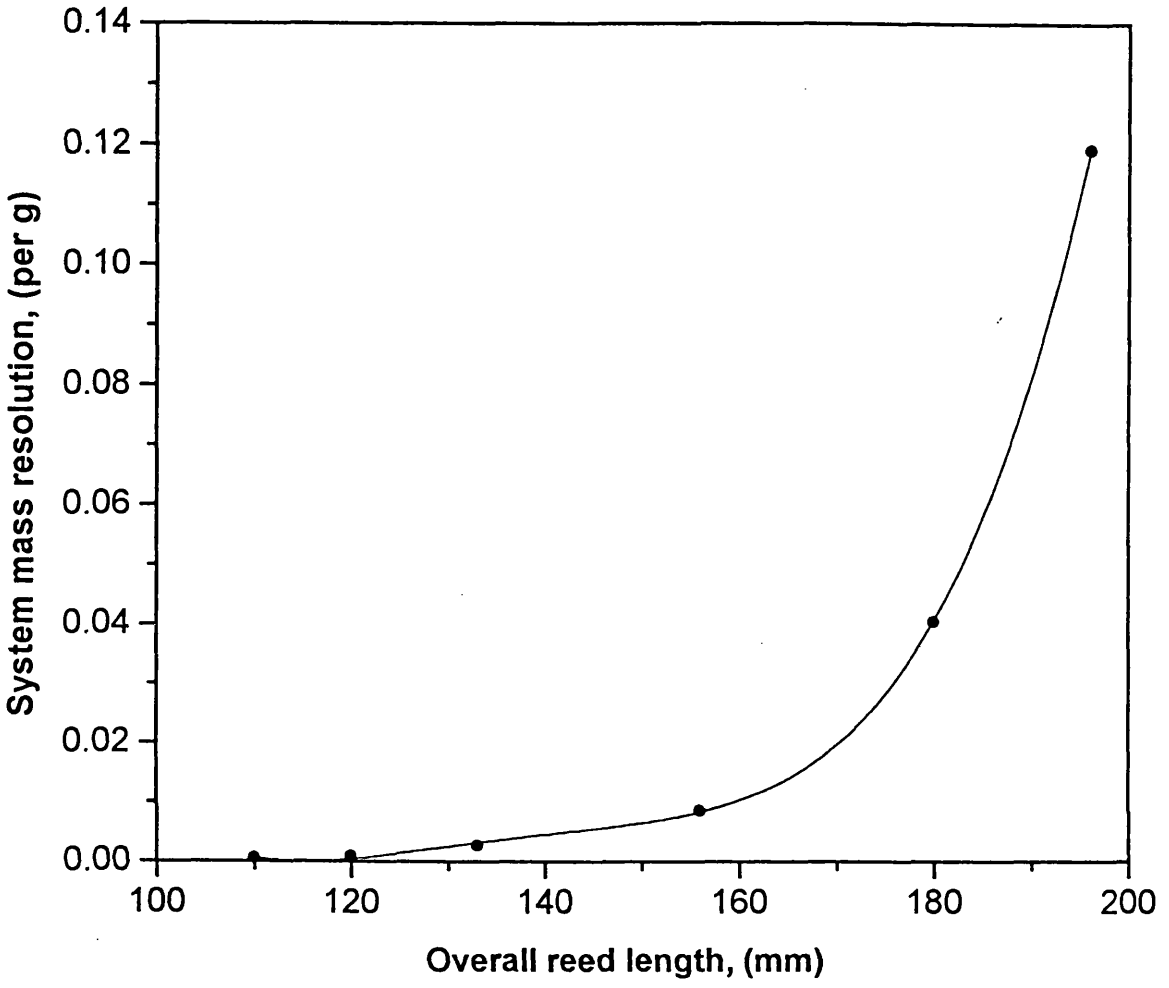

Figure 6.7
The variation of system mass resolution with overall reed length for 3 mm diameter uniform reeds with a constant pinning ratio of 0.35

reed lengths above 150 mm. Table 6.1 shows a summary of the main results obtained from the reed length optimisation study.

The data shows that the optimal reed length is ca. 110 mm. This corresponds to ± 4.85 x 10^{-4} g^{-1} mass resolution. The frequency/attached mass linear correlation coefficient is 0.9999. It is interesting to note that the above represents an order of magnitude improvement in mass sensitivity as compared to previously designed remote drive systems (Mahgerefteh and Khodaverdian (1996)) utilising a plastic compression fitting as a clamp.

Further reductions in the overall reed length were not practical as these were found to require unacceptably high magnetic flux linkages in order to induce vibration. In addition, the optimal location of the optical sensor places a constraint on the minimum practicable length of the drive span and, hence, the overall reed length.

6.2.1.2 Optimisation of Reed Diameter

Figure 6.8 shows a comparison of the variation of system sensitivity (Hz/g) with reed length for 3 mm (curve A) and 4 mm (curve B) diameter reeds. The pinning ratio is 0.35. As in the previous study, the sensitivity of the reeds is obtained from a slope of the linear regression of resonance frequency versus remote side attached mass plots. The data are in good accord with predictive criterion (vi) (see section 6.1.2), in that they clearly show the system sensitivity improves as the reed diameter increases. However, the effect becomes much less pronounced as the reed length decreases. This is probably because as the reed length decreases, there is a corresponding reduction in its mass and hence, an increase in its sensitivity consistent with criterion (vi) above. An increase in diameter on the other hand results in an increase in reed mass. The two factors effectively counteract one another when the reed length falls below ca. 130 mm. In such ranges there is no net effect on the system's sensitivity.

Figure 6.9 shows the corresponding changes in the system's stability. Curves A and B respectively show, the data for the 3 mm and 4 mm diameter reeds. It is clear from

Overall Reed Length (mm)	Sensitivity (=A) (Hz/g)	Maximum deviation from linear fit to data (=B) (Hz)	Maximum fluctuation in frequency recorded over 20 minutes (=C) (Hz)	System Mass Resolution (=(B+C)/A) (g)
110	4.23	1.93×10^{-3}	1.21×10^{-4}	4.85×10^{-4}
120	4.14	3.25×10^{-3}	3.91×10^{-4}	8.79×10^{-4}
133	3.92	9.51×10^{-3}	8.31×10^{-4}	2.64×10^{-3}
156	2.83	2.33×10^{-2}	1.03×10^{-3}	8.60×10^{-3}
180	1.66	5.11×10^{-2}	1.59×10^{-2}	4.04×10^{-2}
196	1.18	1.21×10^{-1}	1.94×10^{-2}	1.19×10^{-1}

Table 6.1

A summary of the main results obtained from the reed length optimisation study. The data relates to 3 mm diameter reeds with a constant pinning ratio of 0.35

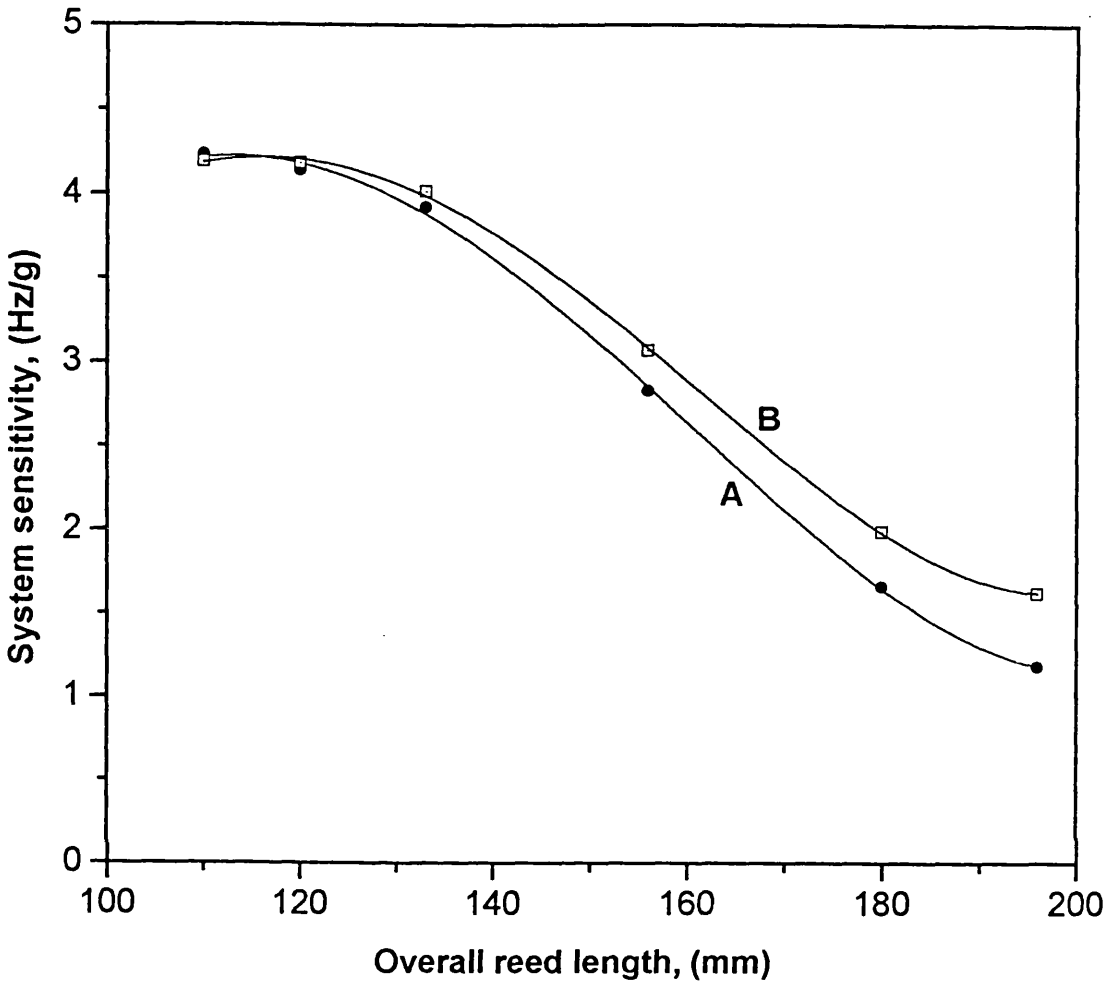

Figure 6.8
A comparison of the variation of system sensitivity with overall reed length for 3 mm (curve A) and 4 mm (curve B) diameter uniform reeds with a constant pinning ratio of 0.35. The data shows the effect of increasing reed diameter on the system response.

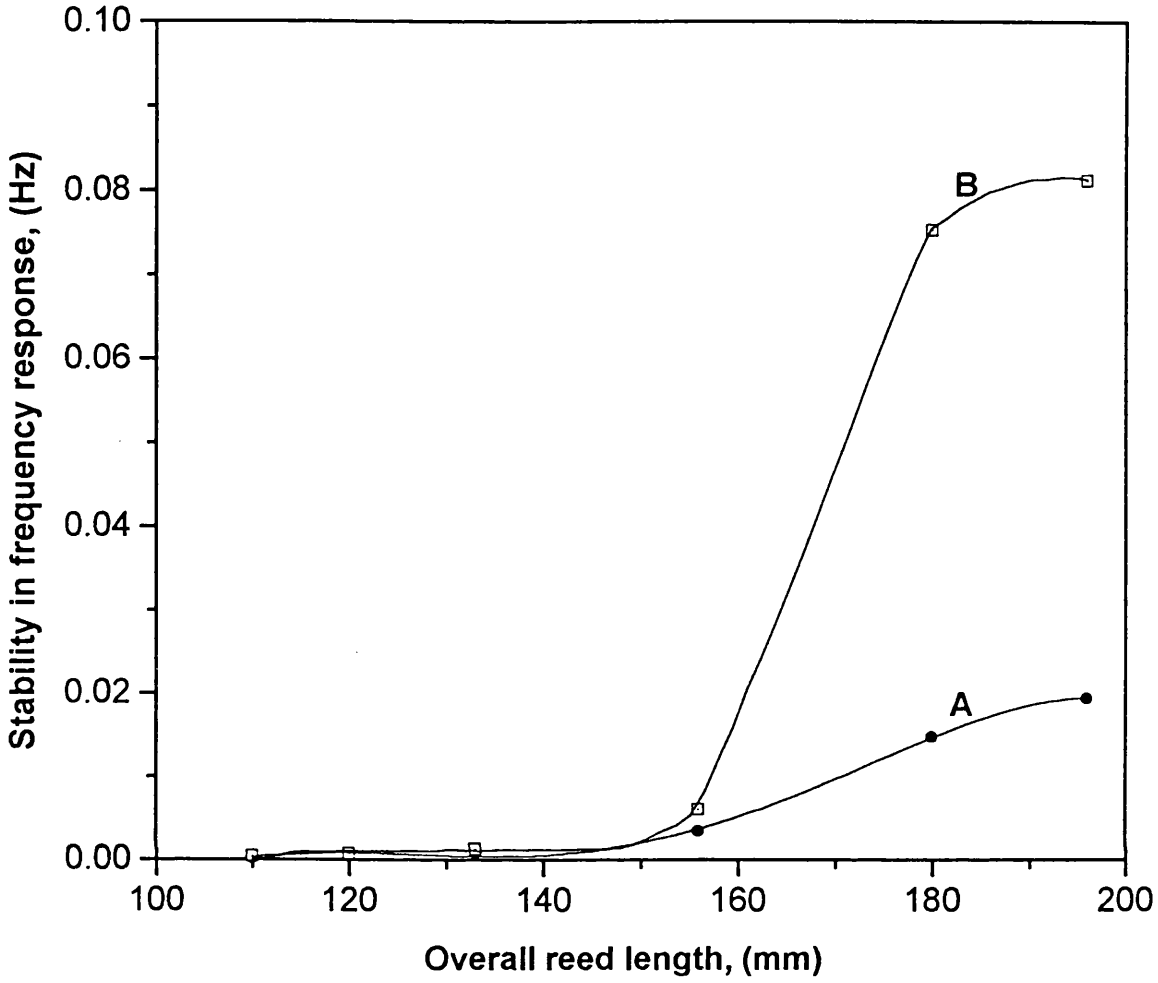

Figure 6.9
A comparison of the variation of system stability in response with overall reed length for 3 mm (curve A) and 4 mm (curve B) diameter uniform reeds with a constant pinning ratio of 0.35. The data shows the effect on increasing reed diameter on the system's stability.

the data that the system's stability decreases as the reed diameter increases. We believe this is because larger diameter reeds require higher driving powers for maintaining the same amplitude of vibration which in turn results in less efficient operation of the electromagnet due to Ohmic heating. The latter was indeed observed in practice.

Figure 6.10 shows the corresponding combined effects of system stability and sensitivity plotted in terms of mass resolution versus reed length for the two reed diameters. Curve A shows the data for the 3 mm reeds whereas curve B refers to the 4 mm diameter reeds. It is clear from the data that the smaller diameter reed offers a better degree of performance and hence, is selected in the proceeding studies.

In summary, on the basis of our analysis, the optimally designed reed is 110 mm long, 3 mm in diameter made from stainless steel. The corresponding pinning ratio is 0.35. The variation in the resonance frequency in response to changes in mass occurring at the remote side is, to a good degree of approximation linear (correlation coefficient 0.9999, maximum frequency deviation from a straight line is $\pm$ 1.93 $\times$ 10^{-3} Hz). The system sensitivity with respect to changes in mass at the remote side is ca. 4.23 Hz/g. The stability of the frequency response is better than $\pm$ 1.21 $\times$ 10^{-4} Hz. The corresponding mass resolution of the system is therefore ca. $\pm$ 4.85 $\times$ 10^{-4} g.

6.3 Design of the Optimised Unit for Sedimentation Analysis

Figure 6.11 shows, in perspective, a schematic representation of the optimised unit ready for mounting onto the settling tank as viewed from the drive side. Figure 6.12 on the other hand shows, in perspective, a schematic representation of the same unit as viewed from the remote side. Figure 6.13 shows a perspective scaled drawing of the various components of the sedimentation analyser in isolation. Figure 6.14(a) is a scaled drawing of the sedimentation analyser, viewed in section, to show how it is connected at its remote side to the settling tank. Figure 6.14(b) is a scaled drawing of the sedimentation analyser, viewed from above. Finally, plates 6.2(a) and 6.2(b) are photographs showing side and top views of the sedimentation analyser respectively.

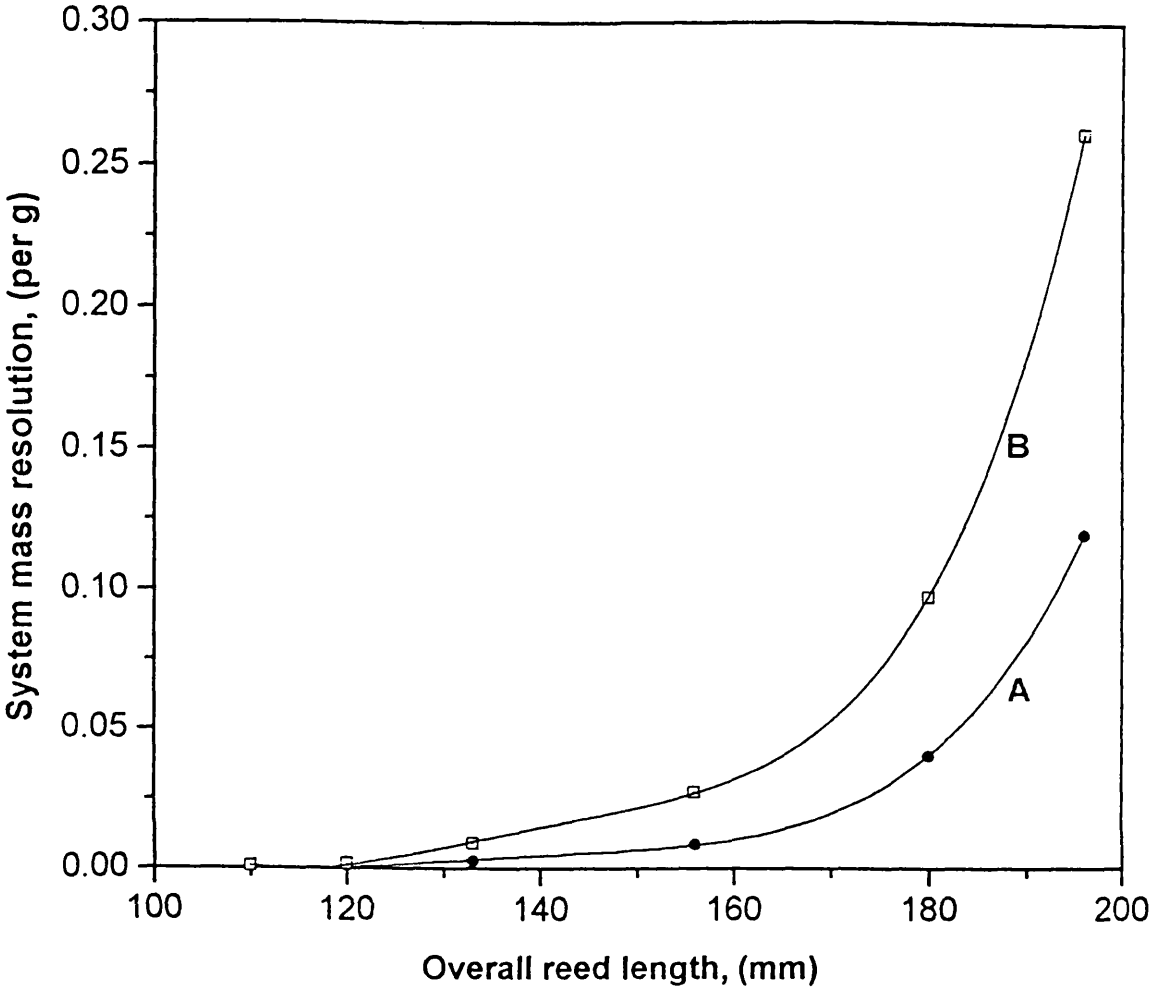

Figure 6.10
A comparison of the variation of system mass resolution with overall reed length for 3 mm (curve A) and 4 mm (curve B) diameter uniform reeds with a constant pinning ratio of 0.35. The data shows the effect on increasing reed diameter on the system response.

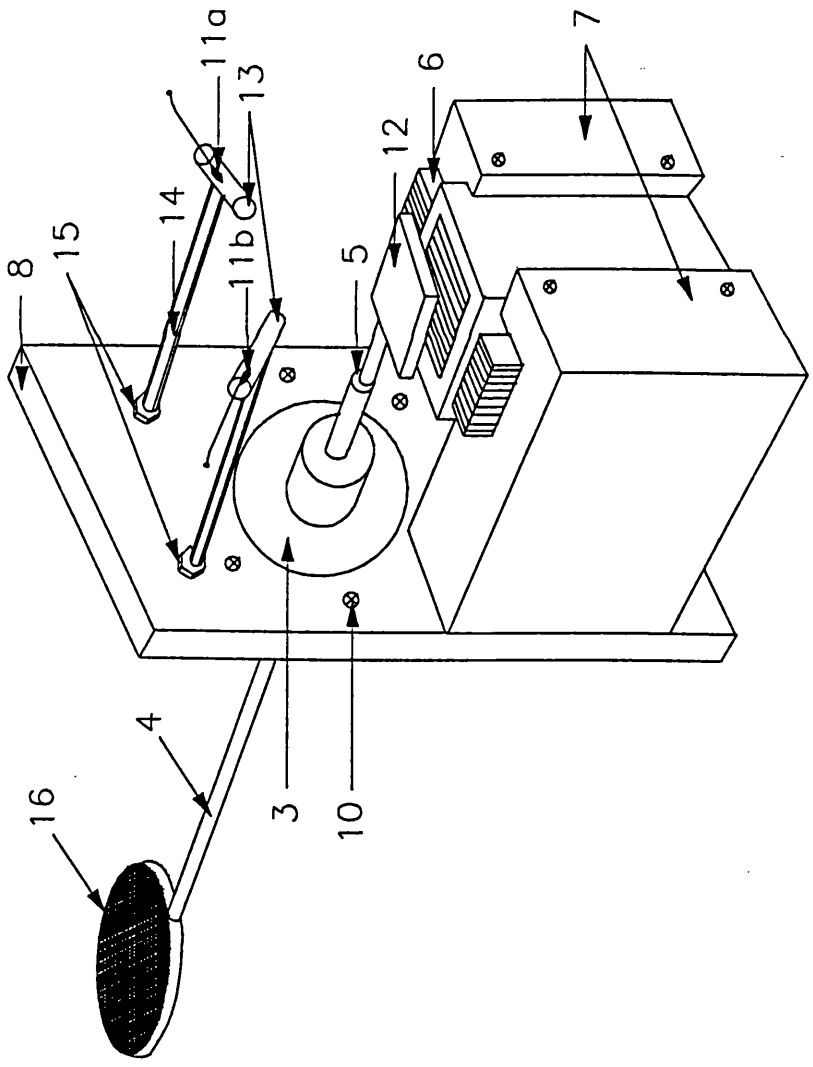

Figure 6.11 A perspective drawing of the optimised vibrating reed sedimentation analyser as viewed from the drive side.

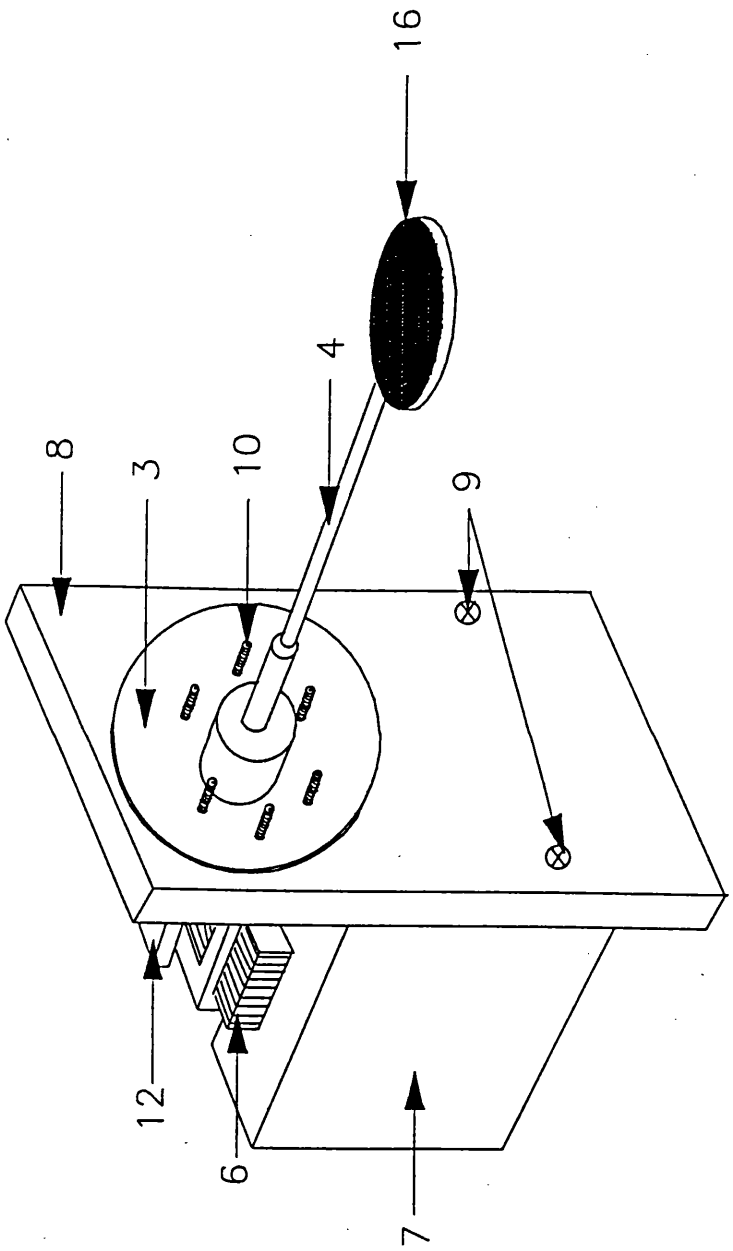

Figure 6.12 A perspective drawing of the optimised vibrating reed sedimentation analyser as viewed from the remote side.

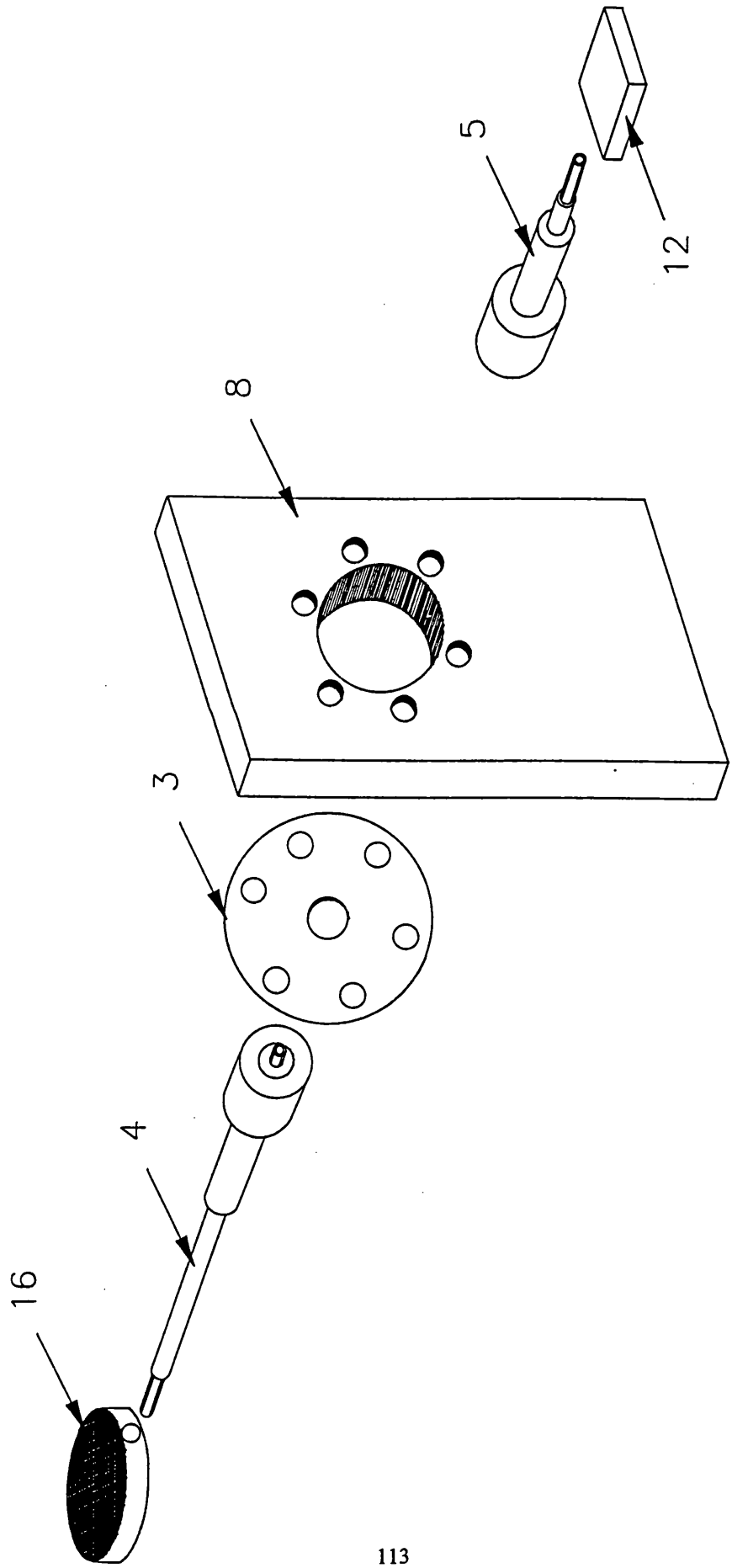

Figure 6.13 A perspective scaled drawing showing the various components of the optimised vibrating reed sedimentation analyser in isolation.

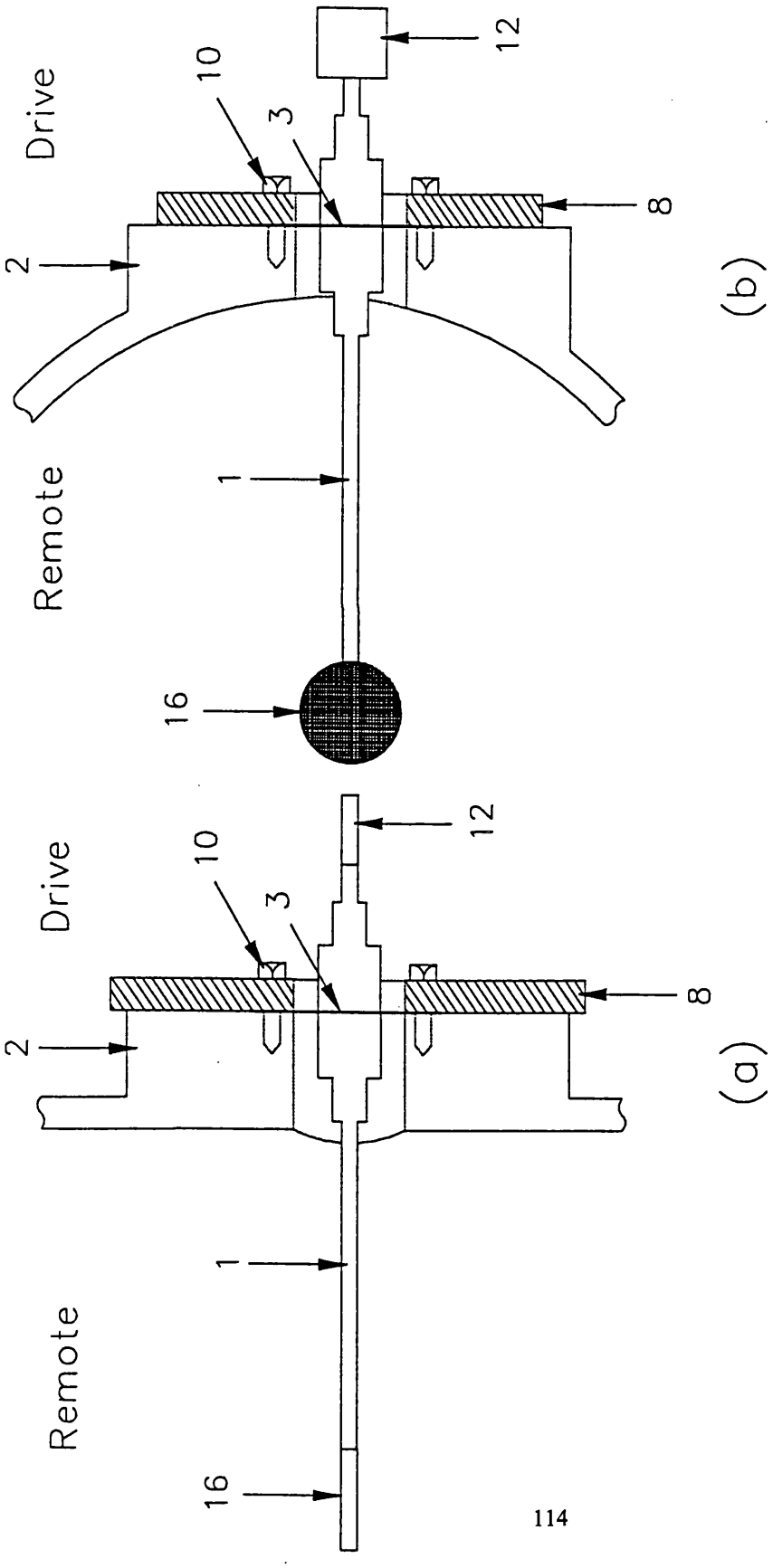

Figure 6.14 Scaled drawings showing how the vibrating reed sedimentation analyser is connected to the settling tank; a) section view and b) viewed from above.

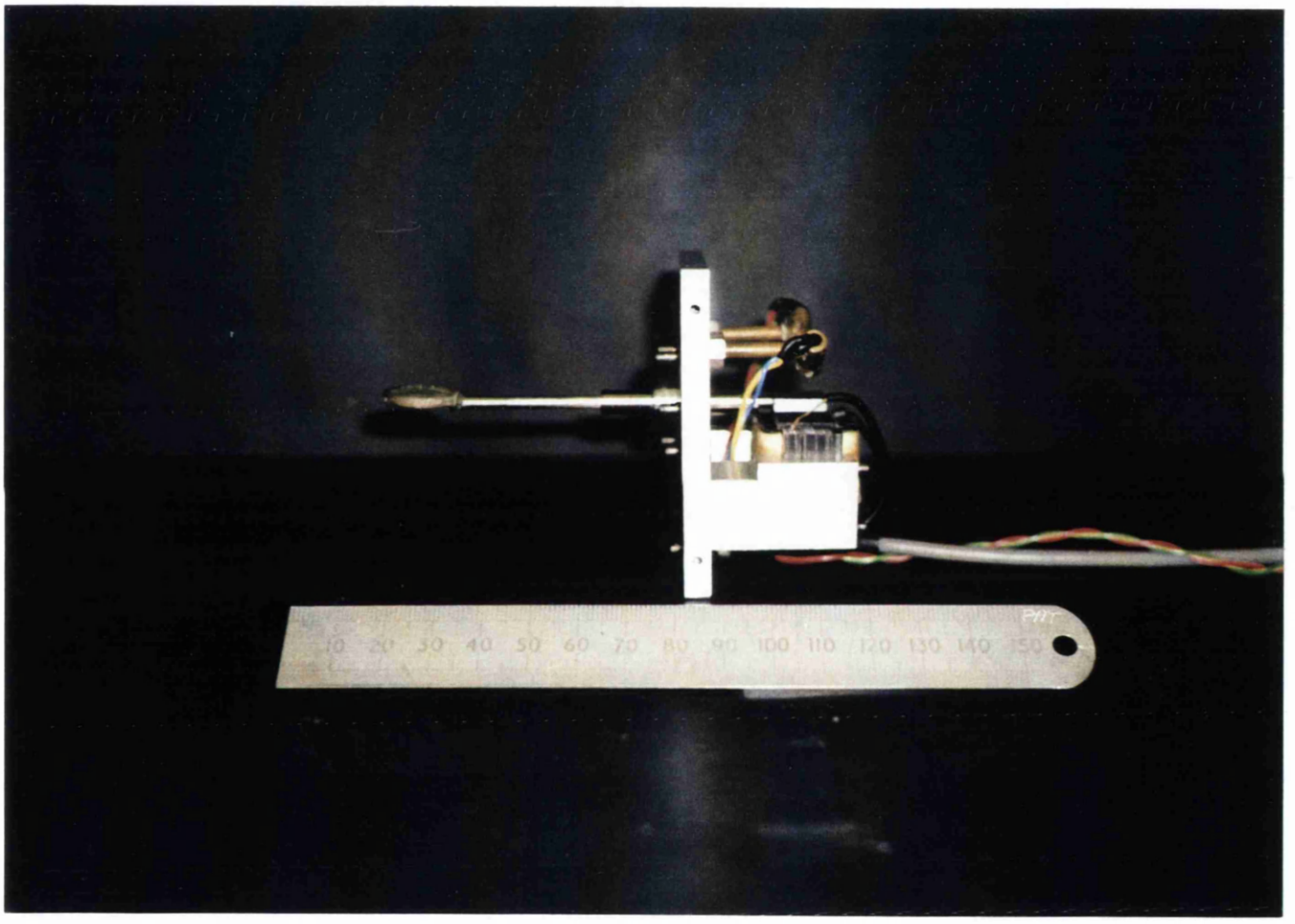

Plate 6.2(a) Photograph showing a side view of the vibrating reed sedimentation analyser.

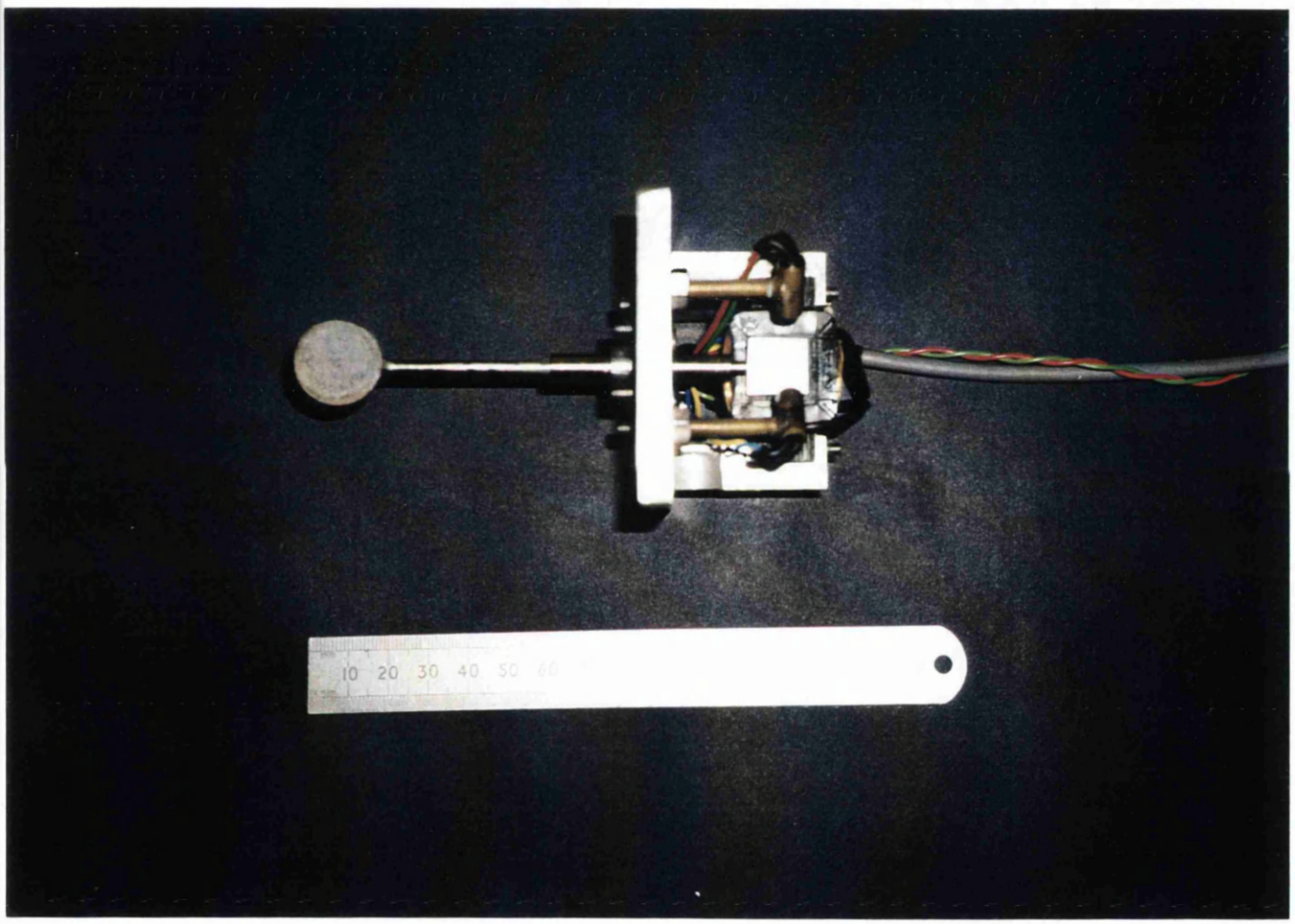

Plate 6.2(b) Photograph showing a top view of the vibrating reed sedimentation analyser.

In this system, the photo-diode detector (see section 6.1.1) is replaced with a photo-transistor detector (RS type SF309FA). The resulting higher sensitivity enables the use of relatively small currents (ca. 0.3 Amps) for driving the electromagnet thus resulting in almost an order of magnitude improvement in the system stability (cf $\pm$ 8.75 $\times$ 10^{-5} Hz with $\pm$ 1.21 $\times$ 10^{-4} Hz). This affords us the possibility of positioning the reed further away from the clamping point (ca. 30 mm as compared to the photo-diode system) where vibrations are more pronounced.

Referring to figures 6.11 - 6.14, the electromagnet (6) is securely held in position by two suitably shaped aluminium brackets (7). The latter are connected to a rectangular stainless steel supporting block (8) by two 10 mm long, M4 $\times$ 10 screws (9). The supporting block (8) is also suitably machined in order to allow the mounting of the reed (1) to the settling tank (2) via the pinning disk (3) using six equi-spaced 10 mm long, M4 $\times$ 10 screws (10). This unit is then connected to the settling tank (2) using the same six screws (10). The pinning disk (3) forms a liquid tight seal with the settling tank (2).

Vibrations are transmitted through the pinning disk (3) and detected on the drive side by an infrared emitter (11a) and photo-transistor (11b). These are mounted at ca. 10 mm above the mild steel plate (12) at a separation of ca. 25 mm from one another. The emitter (11a) and the photo-transistor (11b) are each housed in a hollow brass cylinder (13) which is in turn connected to a 22 mm long, M5 $\times$ 10 brass thread (14) whose free end screws into the supporting block (8). The emitter (11a) and photo-transistor (11b) are suitably angled (ca. 90° relative to the mild steel plate (12)) in order to ensure that the emitted signal reaches the photo-transistor (11b). When aligned, the emitter (11a) and photo-transistor (11b) are then each clamped by tightening a restraining bolt (15) situated at the free end of the supporting brass thread (14).

The free end of the remote span (4) of the reed is mounted with a 20 mm diameter fine meshed (ca. 40 μm) wire gauze supported on a 2 mm thick brass ring (16) which magnifies the effect of the test suspension on the resonance frequency (see section 6.2). Finally, the distance between the mild steel plate (12) and the electromagnet (6) is

set at ca. 5 mm and the entire drive section of the reed is covered with a 85 mm long × 50 mm wide × 68 mm deep aluminium casing in order to block out light interference from surroundings.

6.4 On-Line Multiple Reed System and the Associated Sedimentation Rig

Figure 6.15 and plate 6.3 show, respectively, a schematic representation (not to scale) and a photograph of the multiple reed system and the associated sedimentation rig.

The system comprises a 218 cm high by 15 cm diameter cylindrical perspex column (1) with four vibrating reed sedimentation analysers (2) strategically positioned along its length (see later). A 114 litre base hold-up tank (3) contains the suspending liquid which is in turn circulated through the perspex column (1) using a 3 kW (Stuart Turner: type 50CR125) centrifugal pump (4). The settling particles are confined within the perspex column by two woven wire (ca. 35 μm mesh) stainless steel supporting grids (5) placed at the base and at the top of the settling zone. The top grid rests on a suitably machined ledge and is held in position by a brass O-ring whilst the grid at the bottom is an integral part of an 8 cm deep copper catch-pot in which test samples are placed. Plate 6.4 shows a photograph of the sample catch-pot.

The base of the perspex column (1) consists of a 36 cm long section which contains a 28 cm high 14 × 14 cm square multi-channel copper flow distributor (6). This unit provides a uniform flow field of the suspending liquid to the bed of particles in the catch-pot. Plate 6.5 shows a photograph of this member.

The disposition of the four reeds (2) along the length of the settling zone is such that each device sees a fresh flow field thus minimising the possibility of cross-interference.

This is achieved by using the helical mounting arrangement shown in figure 6.15. The separation distance between neighbouring reeds is ca. 20 cm. Figure 6.16 shows the position of each reed relative to the top of the settling zone.

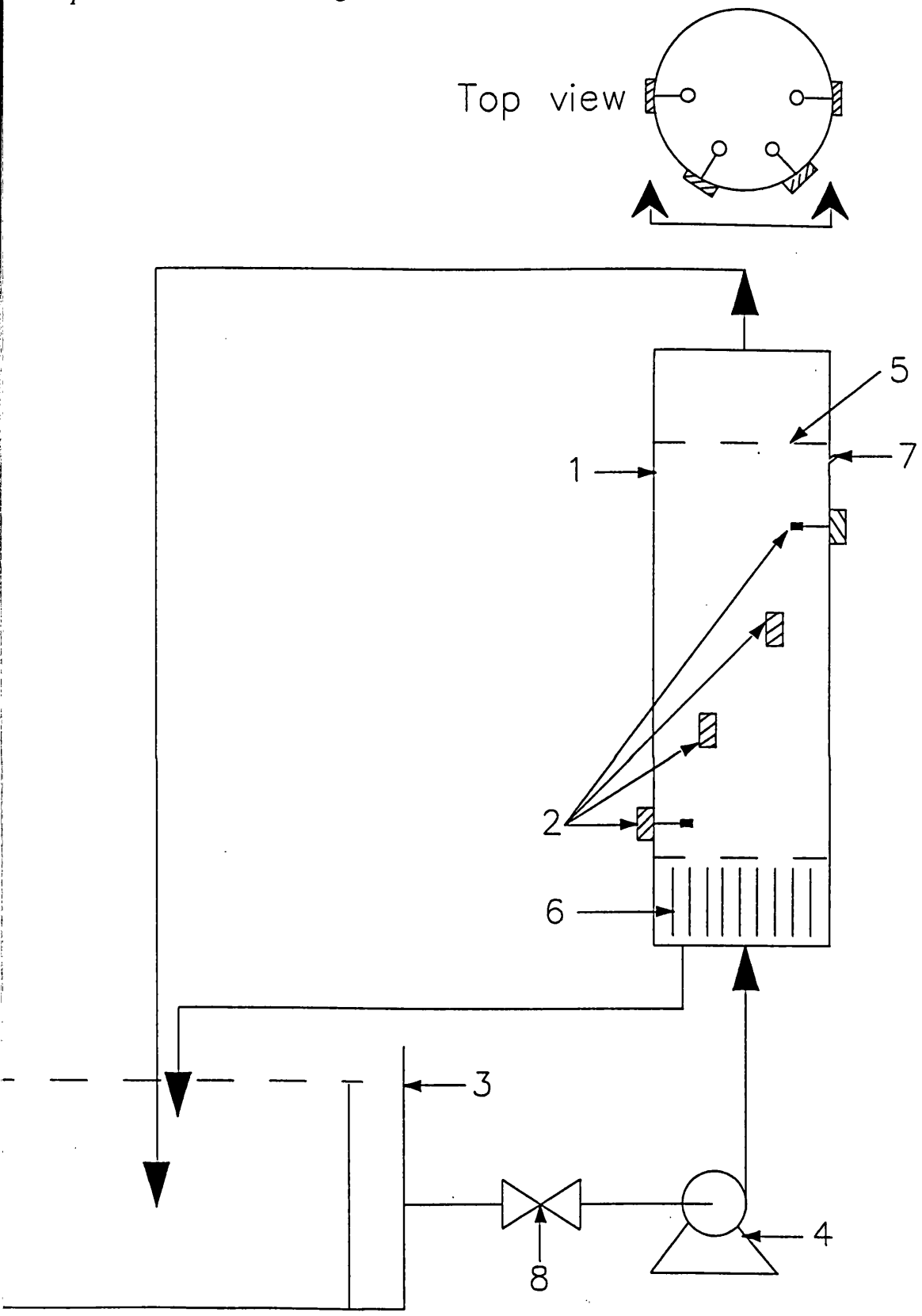

Figure 6.15 A schematic representation (not to scale) of the multiple vibrating reed system and the associated sedimentation rig.

Plate 6.3 Photograph of the multiple vibrating reed system and the associated sedimentation rig.

Plate 6.4 Photograph of the sample catch-pot.

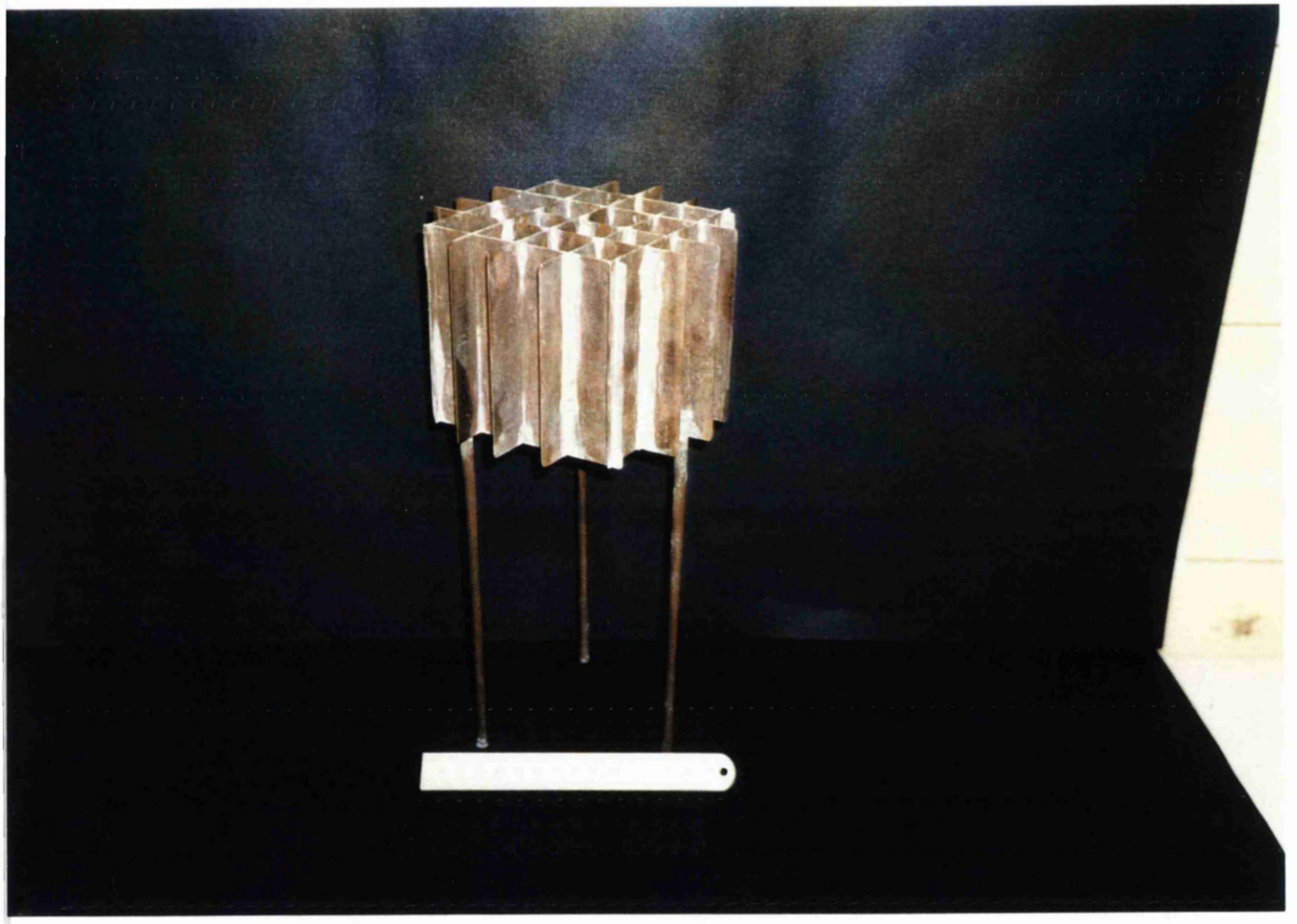

Plate 6.5 Photograph of the multi-channel copper flow distributor.

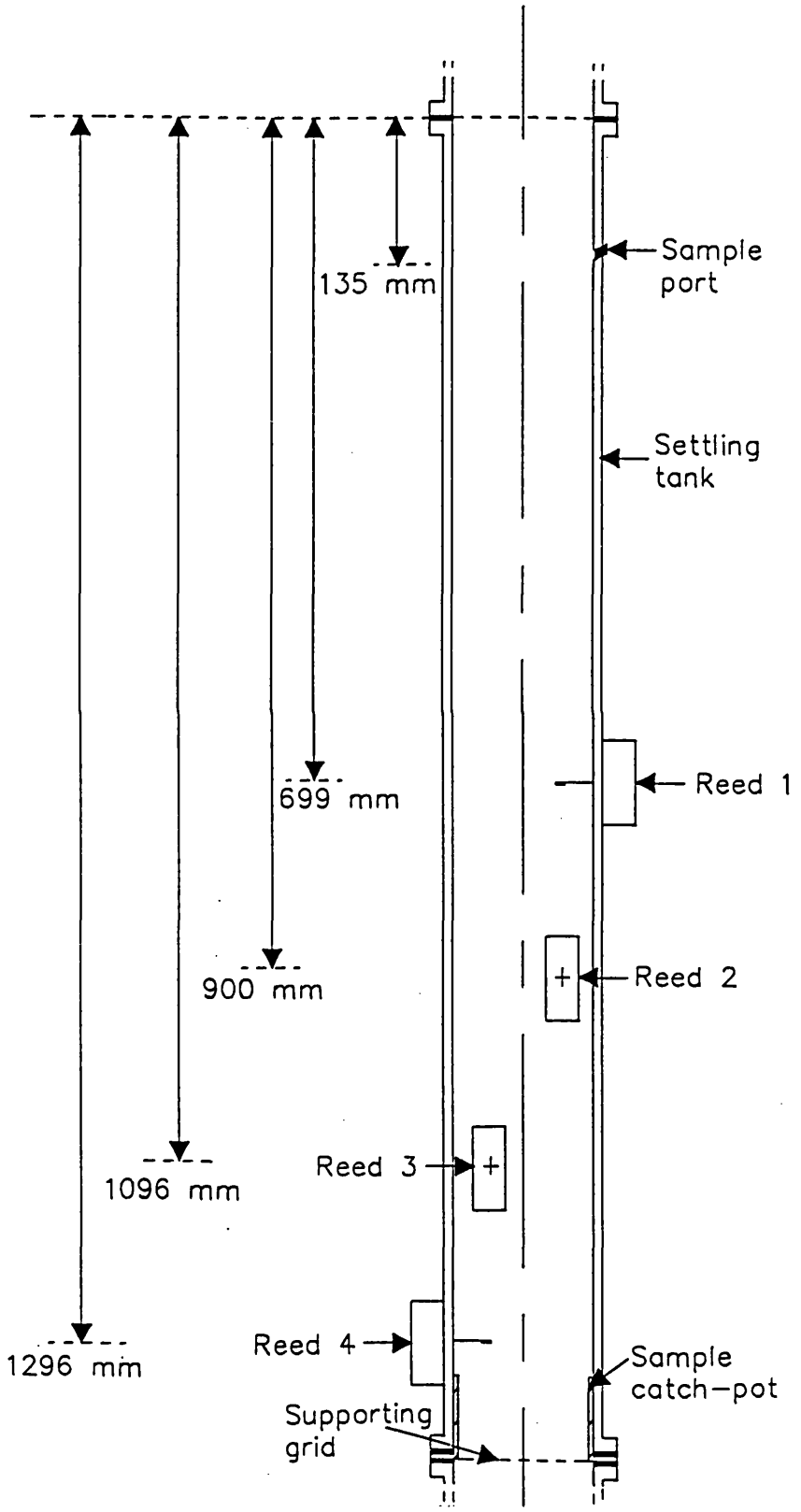

Figure 6.16 A scaled drawing showing the disposition of each reed relative to the top of the settling zone.

The bulk flow of the liquid is sufficient to uniformly fluidise the particles within the settling zone. On switching off the pump, the particles fall under gravity following which resonance frequency measurements are automatically recorded using a specially developed electronic data acquisition system. The latter consists of a multiplexed array of electronic counters with a capability of providing resonance frequency measurements at a rate of ca. 10^{-3} s per channel. A detailed explanation is given in section 6.4.1. The output from this system is linked to a computerised data processing and collection interface.

6.4.1 Ancillary Electronics and a Computerised Data Acquisition System

6.4.1.1 System Power Regulators

A power regulator is used to control and stabilise the voltage supplied to the electromagnets. Figure I in appendix A shows the electronic circuit diagram. This unit is based around a voltage regulator (RS: type LM 338, output range 0-30 volts) and is duplicated for the four electronic channels corresponding to each of the four reeds. All other system components (see below) are powered using a single 50 watt a.c power supply (RS: type 805-142, output range 0-15 volts).

6.4.1.2 The Photo-Transistor Detectors

The optical detectors used to monitor the responses of the reeds each have a light emitting diode source which is interrupted by the reed prior to reaching a photo-transistor. The output voltage signal from the photo-transistor is then sent to the buffer amplifier (RS: type TL071, output range 0-15 volts). Figure II in appendix A shows the appropriate circuit diagram. This unit buffers the output signal by lowering its impedance. The modulated signal is then relayed to the front panel of a multi-channel power amplifier unit.

6.4.1.3 The Variable Bandpass Filter

Figure III in appendix A shows the electronic circuit diagram for the variable bandpass filter. The system is based on a Master Frequency Clock (RS: type MF10C, output range 0-5 volts) integrated circuit which comprises a switched capacitor filter (RS: type 4047, output range 0-5 volts) with a variable clock input controlled from the front panel of the multi-channel power amplifier. The clock input frequency of this device allows for the selection of the resonance frequency of each reed. This effectively limits the range of operational frequencies for each reed so as to avoid self-tuning to modes other than the primary harmonics.

6.4.1.4 Pulsed Power Amplifier

Figure IV in appendix A shows the electronic circuit diagram for the pulsed power amplifier used to drive the electromagnets. This unit is based on a triggered input integrated circuit (RS: type 4049, output range 0-15 volts). The input to this device is converted from analogue into a 'switched signal' before being relayed to an output socket on the front panel of the multi-channel system. This output is then used to drive all subsequent circuitry including the electromagnets and optical detectors. In addition, part of this output is relayed to a pair of test sockets on the front panel from which the drive pulse width and phase lag of the system can be monitored. The amplitude of vibration of all four reeds is maintained constant throughout measurements using a comparitor circuit (RS: type LM 311, output range 0-15 volts).

Figure V in appendix A shows the appropriate circuit developed to maintain each reed at its primary resonance frequency during measurements. In this arrangement, the triggered signal from the comparitor is fed to a first delay circuit (RS: types 74HCT74, output range 0-5 volts). This signal, also known as the 'phase' is controlled from the front panel of the multi-channel system. The output from the first delay circuit is in turn used to trigger a second delay circuit (RS: types 74HCT4017, output range 0-5 volts). This is also controlled from the front panel and is known as the 'pulse'. The

output signal from the second delay circuit is then used to drive the electromagnets via a power transistor (RS: type BDX 53C) thus forming a self tuning closed circuit.

6.4.1.5 The Computer Data Logging Interface

Resonance frequencies are continuously logged by a 486 computer via a digital input/output card with external circuitry. This card (Blue Chip: type ADC - 44d) has 3 × 8 bit digital input/output ports which are used as 20 bit input ports and 4 bit control ports. The former are used to measure and record resonance frequencies whilst the latter control the rate at which data is collected using a Visual Basic programme (see appendix A).

Figures V and VI, in appendix A, show detailed circuits of the current data logging system. The detected vibration signal from each reed is amplified by the power pulse amplifier. The output from this unit is then used as the input signal to a Master Clock generator (RS: type MCLK, 1 MHz or 1 μs resolution) which measures the period of the input square signal by counting the time between two successive peaks. Figure VII in appendix A shows a schematic illustration of the manner in which the counts are taken. The circuitry is then commanded channel by channel to send the number of pulses counted to the computer via the Visual Basic programme (see appendix A). The programme then converts the measured period to a frequency value.

Returning to Figure VII in appendix A, the 1 MHz Master Clock is generated along with a 4 MHz timing clock (RS: type CCLK) which is used internally by a crystal oscillator module (RS: type IC7) to take counts. The Master Clock count is then fed to a chain of three counter integrated circuits (RS: types 74HCT393(IC1), 74HCT374(IC2) and 74HCT393(IC3)) each capable of counting up to 2^{24} bits of which only 20 bits are used. The 4 MHz timing clock is used in conjunction with a decoder (RS: type 74HCT138) (see figure VI in appendix A) whose additional timing circuitry generates 'latch-end' clear pulses. These clear pulses are used at the start of the each count to initialise the counter circuits. This procedure is then followed by the first count from the Master Clock which continues until the start of the second count

period and so on. Between counts, a pulse is generated to 'latch' onto the value accumulated in the three counter stages. This pulse is stored in an output 'latch' where it remains valid for reading by the computer via the Visual Basic programme until the next signal cycle. The cycle is then repeated in sequence and all four channels are counted independently. This is also achieved via the visual basic programme which uses a decoder (RS: type 74HCT138) to select the active channel. This circuit outputs a 4 bit value which is used to select the frequency channel to be read back. Various integrated circuits (RS: types 74HCT374(IC4), 74HCT393(IC5) and 74HCT374(IC6)) then convert the 4 bit value into individual channel select signals which enable a set of latches onto the common 20 bit input ports. Figure VIII in appendix A shows a layout of the computerised data logging system. Figure IX in appendix A on the other hand shows a detailed layout of the multiple reed electronic drive and detection system.

Logged resonance frequencies are read to an Excel (version 5.0) output file in real time basis via the Visual Basic programme. This file is also commanded via the programme to record the data for each reed to a separate address. Consequently, the data for the four reeds is displayed as four distinct columns which can be analysed separately. Since the output file is overwritten each time the programme is run, it is necessary transfer all data to a second Excel file in which a series of macros are used to filter out stray signals and reduce the volume of data by averaging measurements over ca. 5 s intervals.

CHAPTER 7

EXPERIMENTAL PROCEDURES

7.0 Introduction

This chapter describes the results of a series of experiments elucidating the performance characteristics of the vibrating reed system. These in the main, demonstrate the effects of the reed amplitude of vibration, the suspension bulk viscosity as well as its temperature on the system's response. Performance data relating to system sensitivity were given in chapter 6.

This is then followed by a number of further studies the results of which form the basis for establishing the feasibility and reliability of the vibrating reed system in providing sedimentation kinetic data. The latter include the determination of settling velocities as well as the solids flux. The reliability of the system is primarily verified by comparison with data obtained from direct visual observation of the rate of descent of the suspension-clear liquid interface for nominal monodisperse suspensions comprising various concentrations of 200 - 212 μm glass ballotini in water.

The methods and equipment used to prepare and characterise test samples as well as the manner in which test suspensions are prepared and monitored are described first.

7.1 Particulate Specification and Preparation

The material chosen for use in model sedimentation experiments is soda glass ballotini beads, supplied by Jencons Scientific Ltd. (Bedfordshire, UK). Appendix B gives a typical chemical composition as well as important physical properties.

These samples, varying in the range 55 - 212 μm were separated to various size fractions using sieving performed in accordance to British Standards recommendations (BS 1796: part 1: 1989).

The calibration of the multiple vibrating reed sedimentation analyser requires the use of a monodisperse sample. Ideally, such a sample should consist of identical (with respect to both size and density) non-aggregating particles which settle through the fluid medium at the same rate. This allows for the direct verification of the experimental technique on the basis of visual observation of the rate of fall of the sharp suspension-clear liquid interface and comparison with the resonance frequency response data as well as validation of the appropriate theoretical models for monodisperse particles.

Unfortunately, single sized particles are difficult to prepare in practice and are prohibitively expensive particularly when considering the quantities required in this study (>1 kg). Here, we use glass ballotini in the range 200 - 212 μm as representing a nominal mono-size sample. This is the narrowest sieve cut available. In addition, particles in this size range are sufficiently coarse so that their settling behaviour in aqueous media is much more likely to be dominated by particle-particle hydrodynamic interactions rather than surface charge related electrostatic effects. The latter tend to be more prevalent in conjunction with smaller particles (< 50 μm).

Once a good understanding of the response of the multiple reeds in relation to the settling behaviour of a monodisperse suspension has been attained, the settling behaviour of more complex polydisperse suspensions can be studied. In this study, the samples used for this purpose comprise glass ballotini in the ranges; 55 - 100 μm, 80 - 115 μm, 90 - 135 μm and 100 - 200 μm.

The size distribution of each sieve cut was determined using a laser diffraction particle size analyser (Malvern: type Mastersizer S). Each sample was prepared prior to analysis in accordance with Allen's (1990) recommendations. This involved washing with 2.5 mol dm^{-3} hydrochloric acid in order to remove any traces of iron which may

be present as a result of the manufacturer's handling process followed by rinsing with distilled water and finally drying.

The particle size distribution analysis for each sample is repeated at least 10 times in order to ensure that the results are reproducible. The water used in the above procedure and all subsequent tests is free of all impurities which may otherwise affect experimental results. This involves passing through a primary disinfection cartridge where ionic and organic impurities are removed by ultraviolet radiation and finally filtration in a reverse osmosis ultra-microfilter. After this stage the processed water has a virtually neutral pH.

Figures 7.1 - 7.5 show the particle size distribution data for the various glass ballotini samples used in this study. The data is presented in the form of the percentage number frequency in the analysed population versus particle size. In the case of the 'monodisperse' 200 - 212 μm sample, the particle size distribution plot is symmetrical and can be fitted by a normal distribution function with the general form (Rumpf, 1990):

$$f(x,\mu,\sigma) = \frac{1}{\sqrt{2\pi}\,\sigma} \exp -\left[\frac{(x-\mu)^2}{2\sigma^2}\right] \qquad (7.1)$$

where x is the particle size, μ is the arithmetic mean of the particle size distribution and σ is the standard deviation of the distribution. The data shows that the sieving operation is reasonably effective since the cumulative count for sizes in the range 200 - 212 μm is 95.2 %.

The particle size distribution data for the majority of the polydisperse samples is slightly skewed towards the small particle size end of the distribution curve which indicates the presence of a disproportionately high number of smaller particles. This is probably due to errors incurred during sub-sampling. However, the particle size distribution data for the various polydisperse samples are still best fitted by normal distribution functions. Table 7.1 shows a summary of the main parameters of the

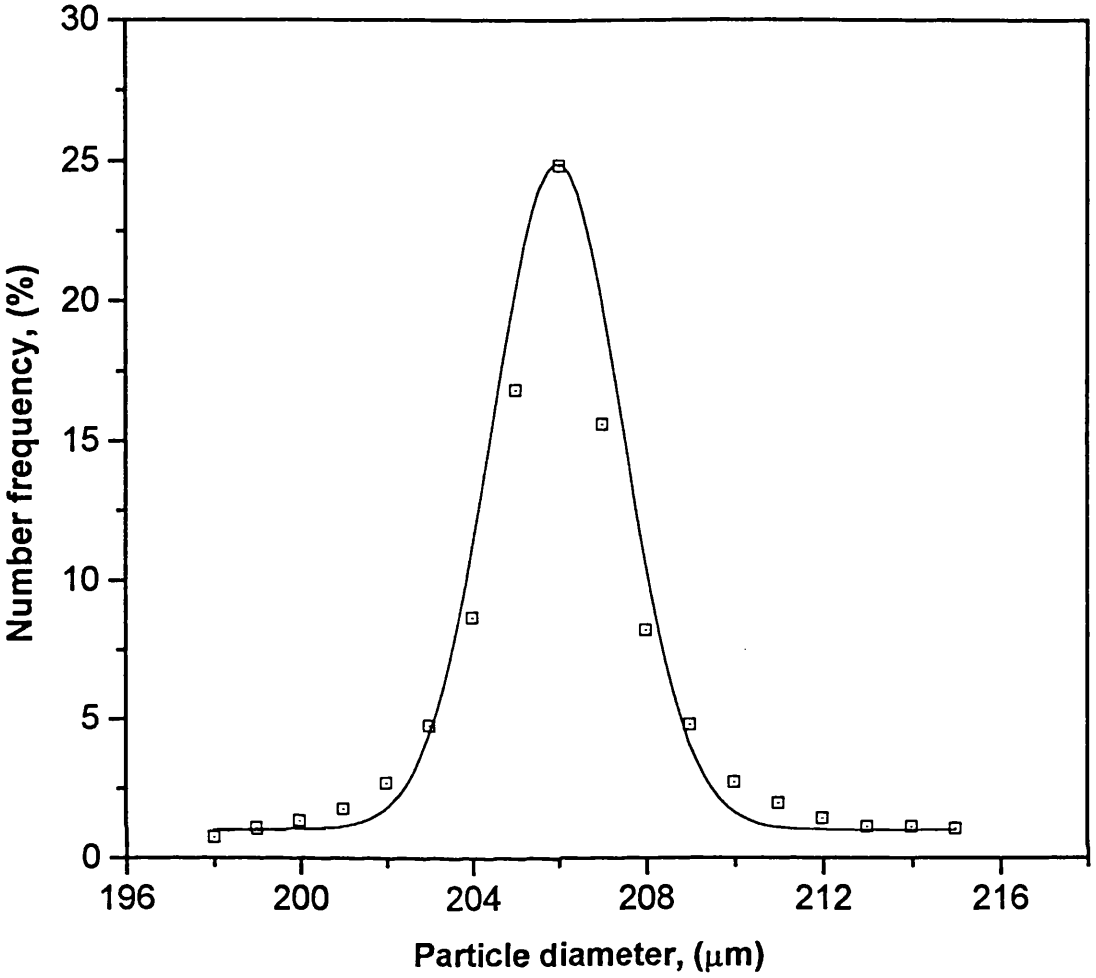

Figure 7.1
Particle size distribution data for the monodisperse 200 - 212 μm glass ballotini sample (density 2550 kgm^{-3})

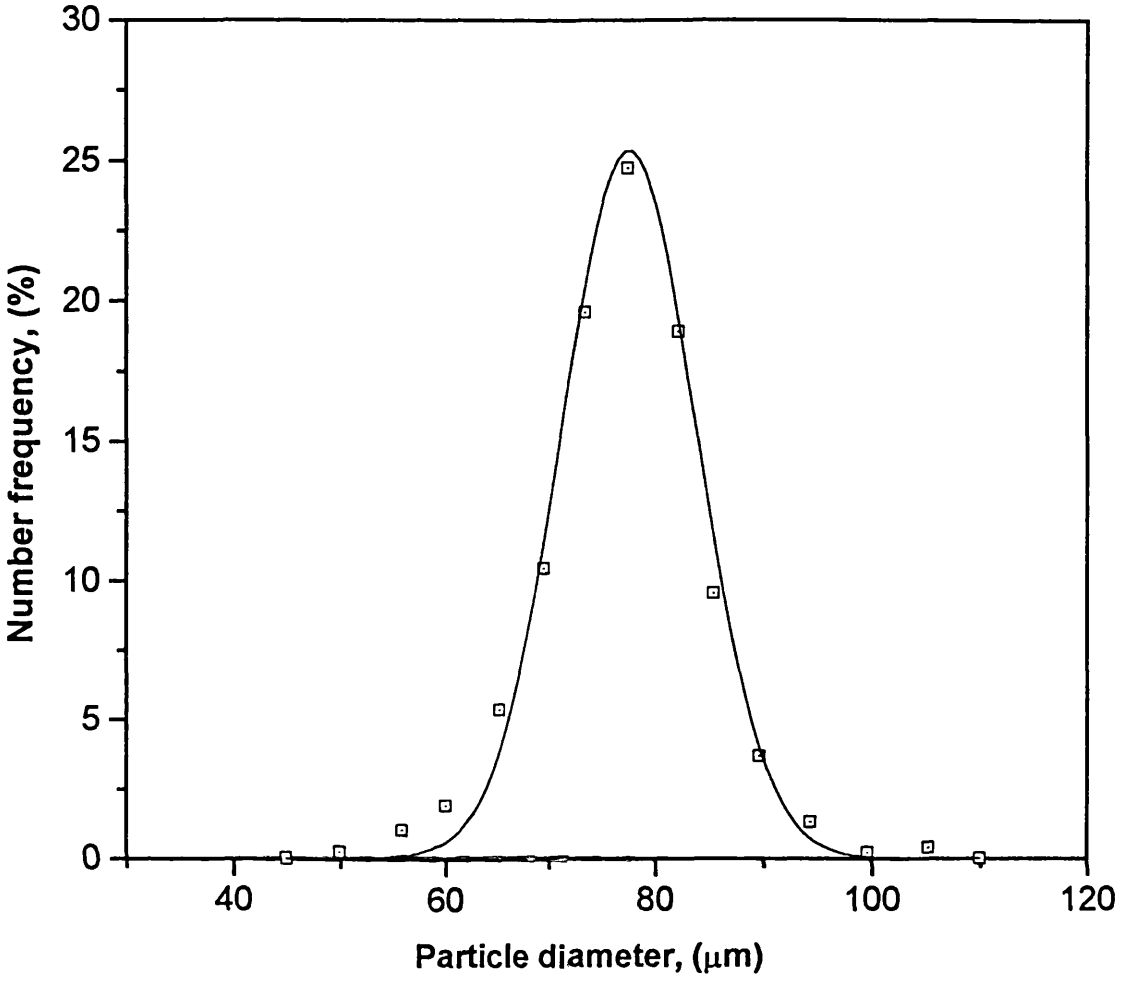

Figure 7.2
Particle size distribution data for the polydisperse 55 - 100 μm glass ballotini sample (density 2550 kgm^{-3})

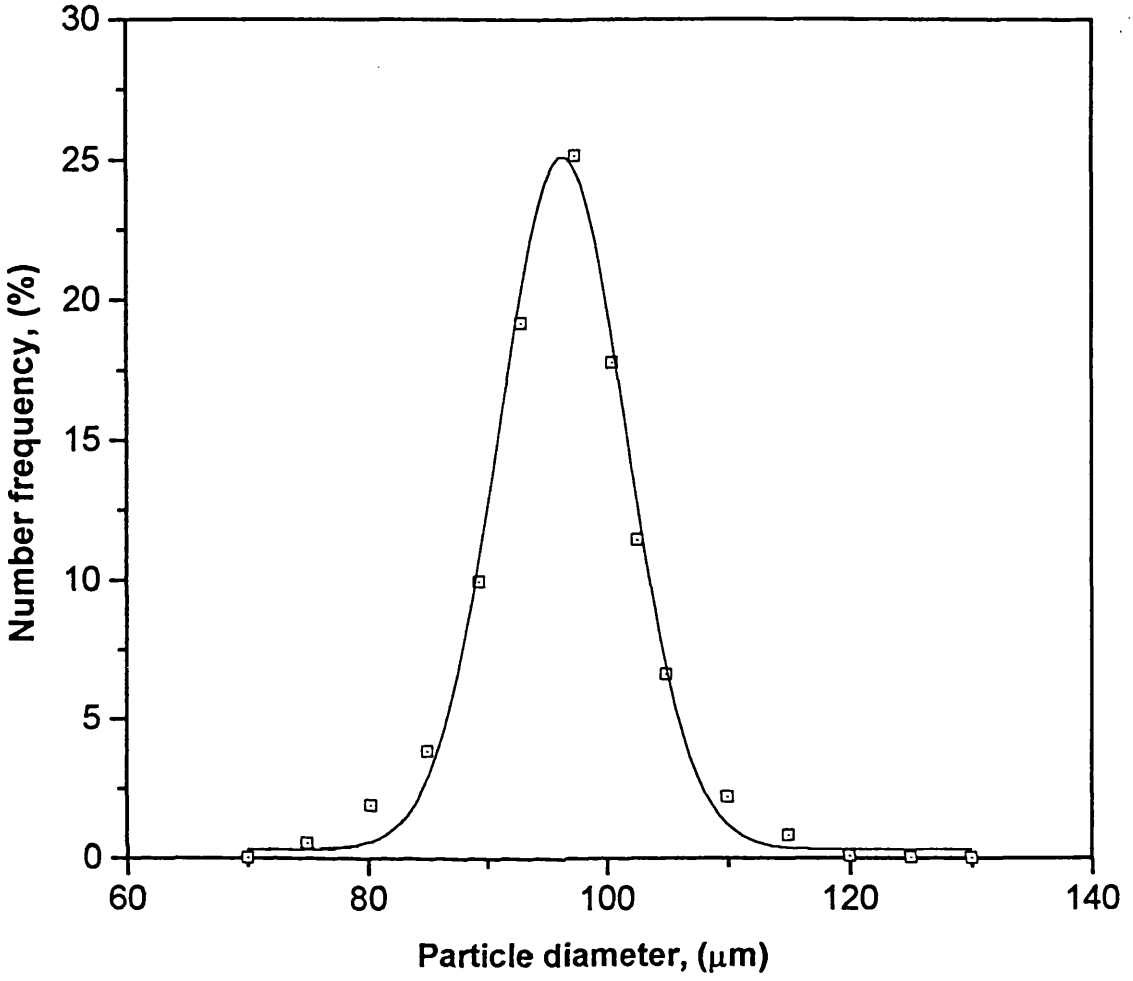

Figure 7.3
Particle size distribution data for the polydisperse 80 - 115 μm glass ballotini sample (density 2550 kgm^{-3})

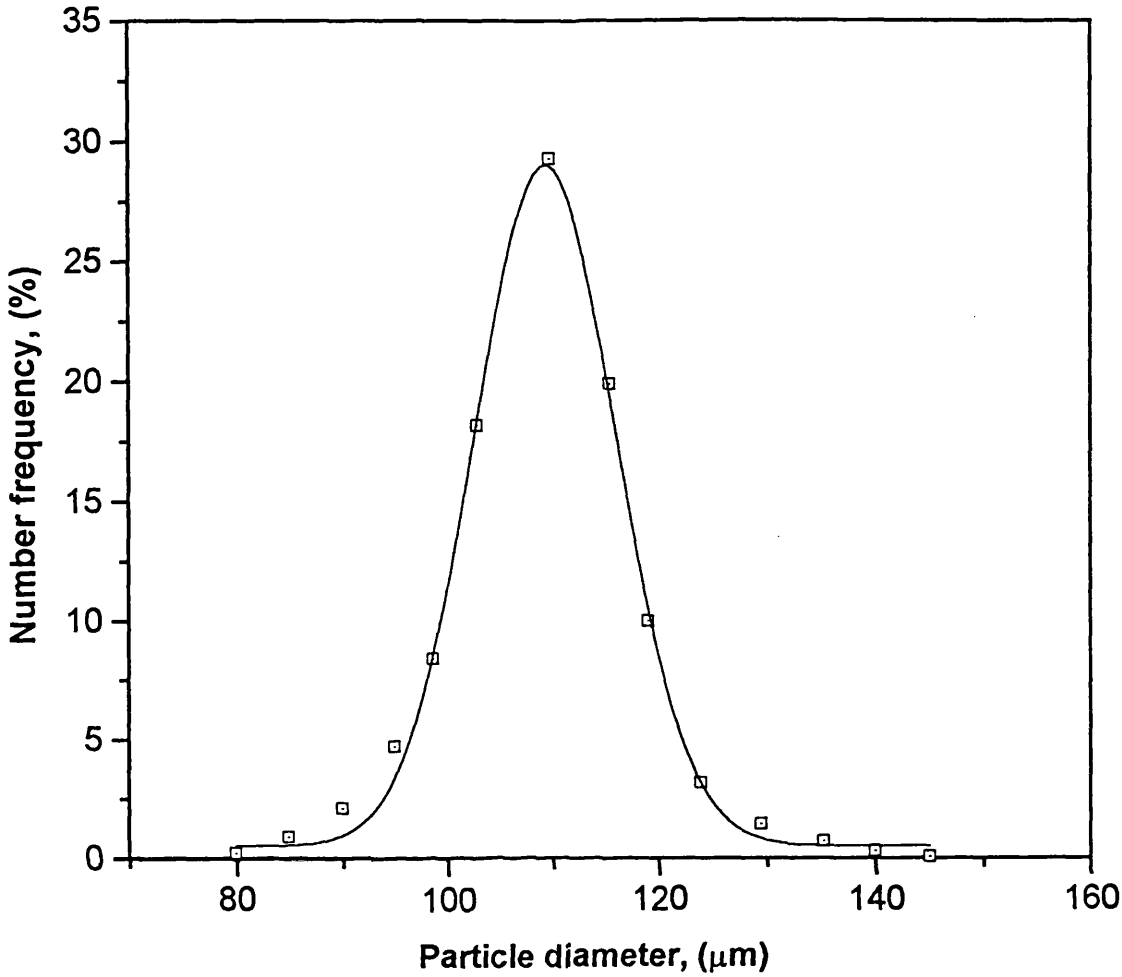

Figure 7.4
Particle size distribution data for the polydisperse 90 - 135 μm glass ballotini sample (density 2550 kgm^{-3})

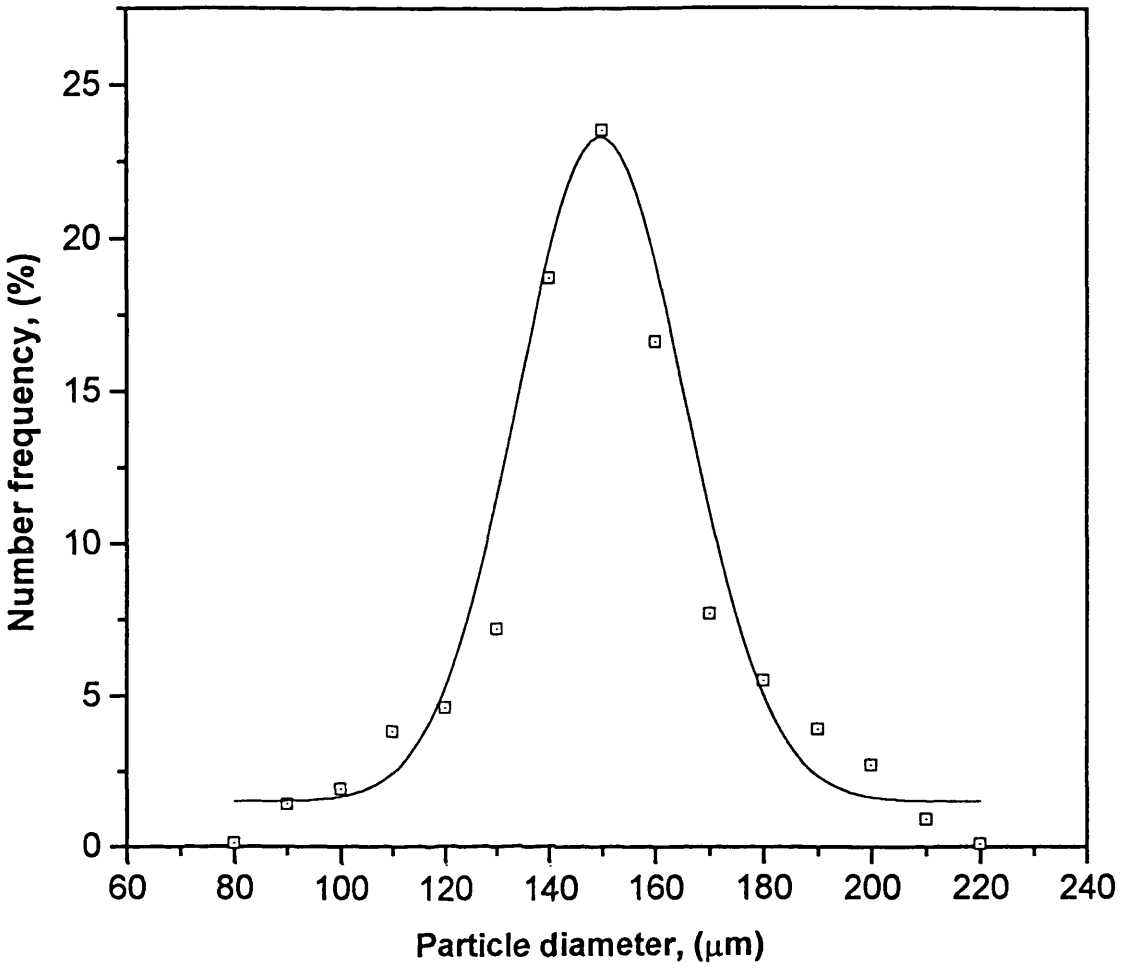

Figure 7.5
Particle size distribution data for the polydisperse 100 - 200 μm glass ballotini sample (density 2550 kgm^{-3})

Particle Size Range (μm)	Description	Mean Particle Size (μm)	Standard Deviation of fit (σ)	Percentage within Size Range (%)
200 - 212	Monodisperse	206.0	0.21	95.22
55 - 100	Polydisperse	77.5	0.69	96.48
80 - 115	Polydisperse	96.4	0.35	98.71
90 - 135	Polydisperse	109.3	0.42	97.82
100 - 200	Polydisperse	149.7	2.53	96.11

Table 7.1. A summary of the main parameters of the normal distribution curves which best fit the particle size analysis data for all samples at a 95 % confidence level.

normal distribution curves which best fit the particle size analysis data for all samples at a 95 % confidence level.

7.2 Preparation of Two-Phase Solid/Liquid Suspensions

The manner in which the two-phase solid/liquid suspensions are prepared for use in the proceeding sedimentation studies is described with reference to figure 6.15, chapter 6.

The first stage involves filling the hold-up tank (3) with the suspending liquid (water) followed by switching on of the centrifugal pump (4). The flow of water is then adjusted via a flow control valve (8) so that the settling tank (1) is gently filled up to a level a few centimetres below the particle inlet port situated ca. 135 mm from the top of the settling zone (7). Once the desired water level has been reached, the pump is switched off and a pre-determined volume of the test particles is slowly poured into the setting tank via the inlet port using a funnel. The sample port is then closed following which the pump is switched on again, this time in a re-circulating mode in which the water leaving the top of the settling tank returns to the base hold-up tank and re-pumped back into the base of the settling tank. The flow of water is gradually increased in order to expand and uniformly mix the bed of particles in the catch-pot over the entire settling zone. Once a uniform suspension has been observed the pump is switched off. This marks the start of the sedimentation process which is monitored by measuring the resonance frequencies of the reeds in the manner described in section 6.4.1, chapter 6.

The samples are weighed prior to being introduced to the settling zone so that the solid mass concentration can be determined for subsequent mass balance calculations. The operating temperature is measured using a digital thermometer placed in the base hold-up tank.

7.3 Study of the Performance Characteristics of the Vibrating Reed System.

7.3.1 Effect of Amplitude of Vibration

Figure 7.6 shows the effect of an increase in the amplitude of vibration on the resonance frequency of reed 1 vibrating in water at 17 °C. In this test, the amplitude of vibration is increased by gradually increasing the power supplied to the electromagnet. As it is clear, at certain ranges, the resonance frequency dramatically decreases with increase in the amplitude of vibration. This is a commonly observed phenomenon, and is mainly due to 'softening spring behaviour'. Timoshenko(1937), attributes this effect to the strain induced in the beam following its deflection which in turn reduces the Young's modulus. As a result, the reed's resonance frequency is reduced. Figures 7.7 - 7.9 on the other hand show the corresponding data obtained at the same time as those shown in figure 7.6 using reeds 2 - 4 repectively. The data show similar trends.

In the context of the present study, the above may give rise to complications during sedimentation analysis as changes in the resonance frequency of vibration may not be wholly attributed to variations in the fluid properties.

Here, we overcome this potential problem by operating each reed at a constant amplitude of vibration of 0.65 V. As it is clear from the data in figures 7.6 - 7.9, even slight fluctuations in this amplitude will have negligible effect on the resonance frequency. For example, the maximum changes in the resonance frequencies in the amplitude range 0.5 - 0.8 V for reeds 1, 2, 3, and 4 are $\pm 2.44 \times 10^{-4}$, $\pm 2.75 \times 10^{-4}$, $\pm 2.36 \times 10^{-4}$ and $\pm 2.67 \times 10^{-4}$ Hz respectively. The corresponding estimated errors in mass resolution are sufficiently small so that they may be considered as negligible (i.e $\pm 5.02 \times 10^{-5}$, $\pm 5.66 \times 10^{-5}$, $\pm 4.86 \times 10^{-5}$ and $\pm 5.49 \times 10^{-5}$ g respectively).

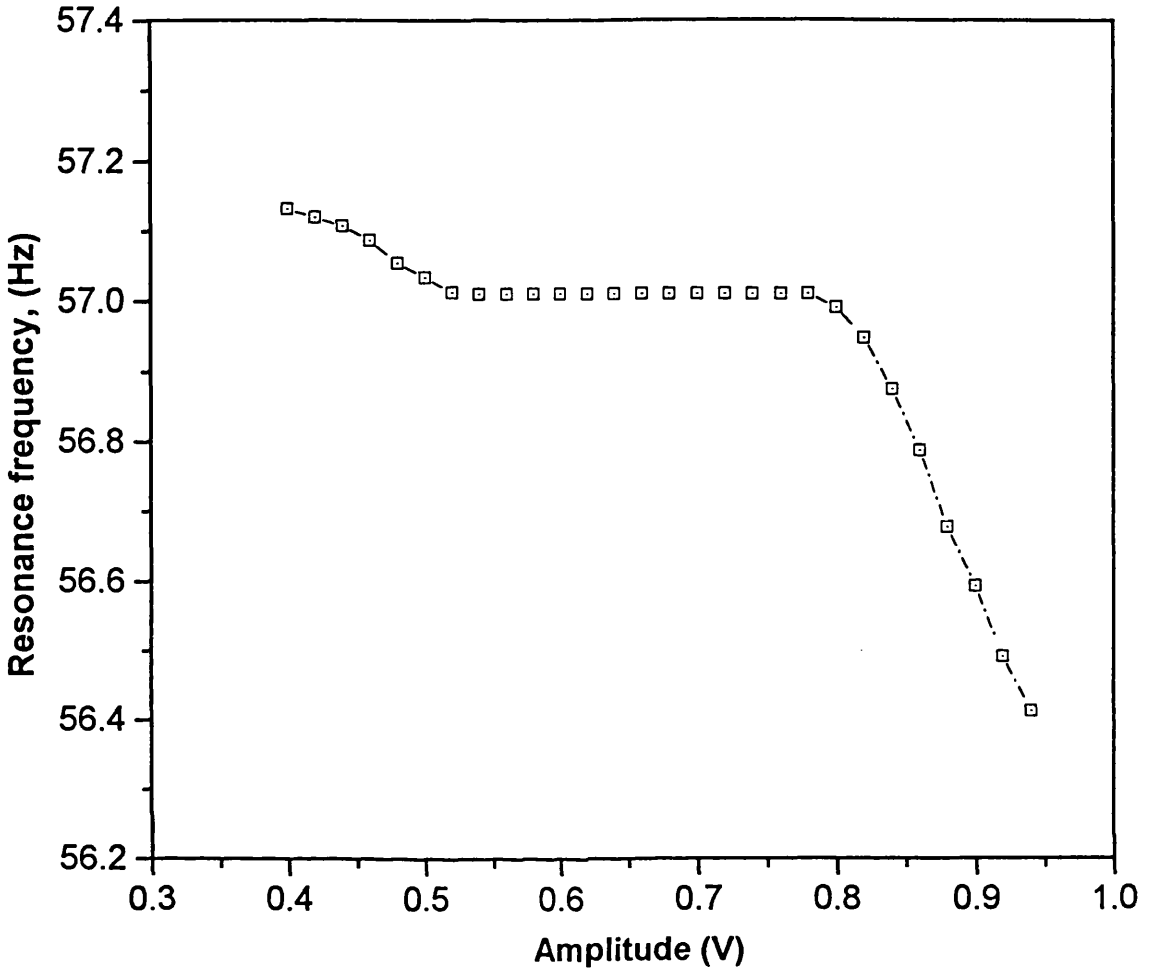

Figure 7.6
The effect of amplitude of vibration on resonance frequency for reed 1 vibrating in water @ 17 °C. The head of water above the reed is 699 mm.

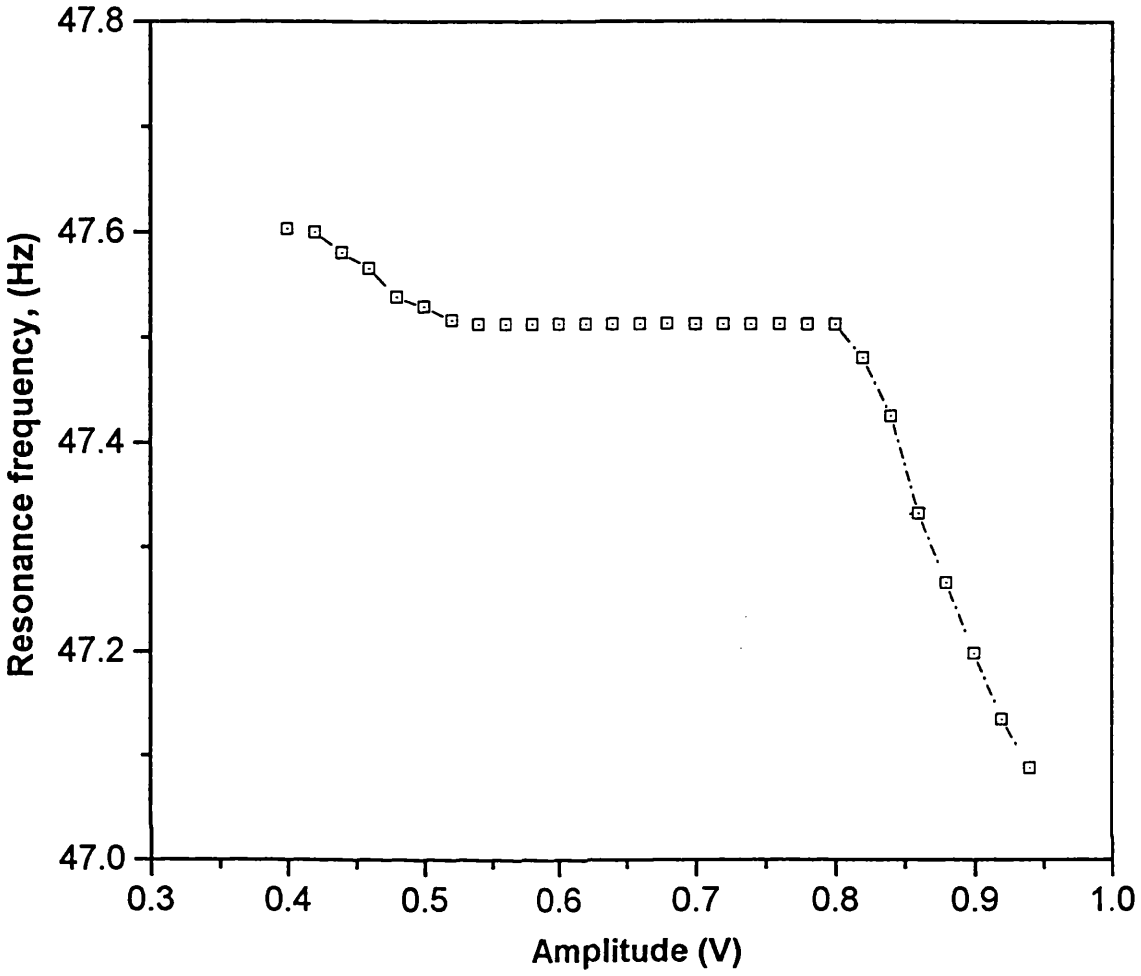

Figure 7.7
The effect of amplitude of vibration on resonance frequency for reed 2 vibrating in water @ 17 °C. The head of water above the reed is 900 mm.

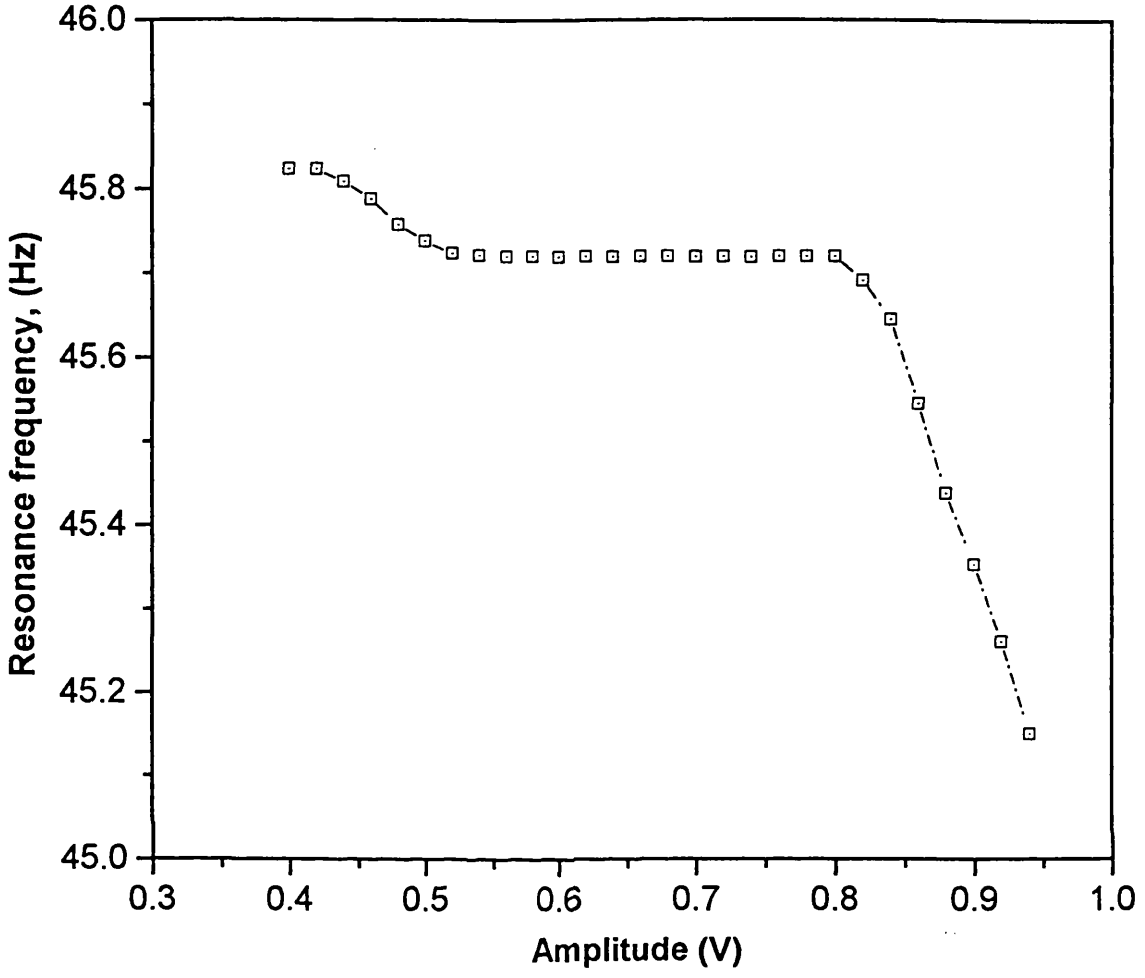

Figure 7.8
The effect of amplitude of vibration on resonance frequency for reed 3 vibrating in water @ 17 °C. The head of water above the reed is 1096 mm.

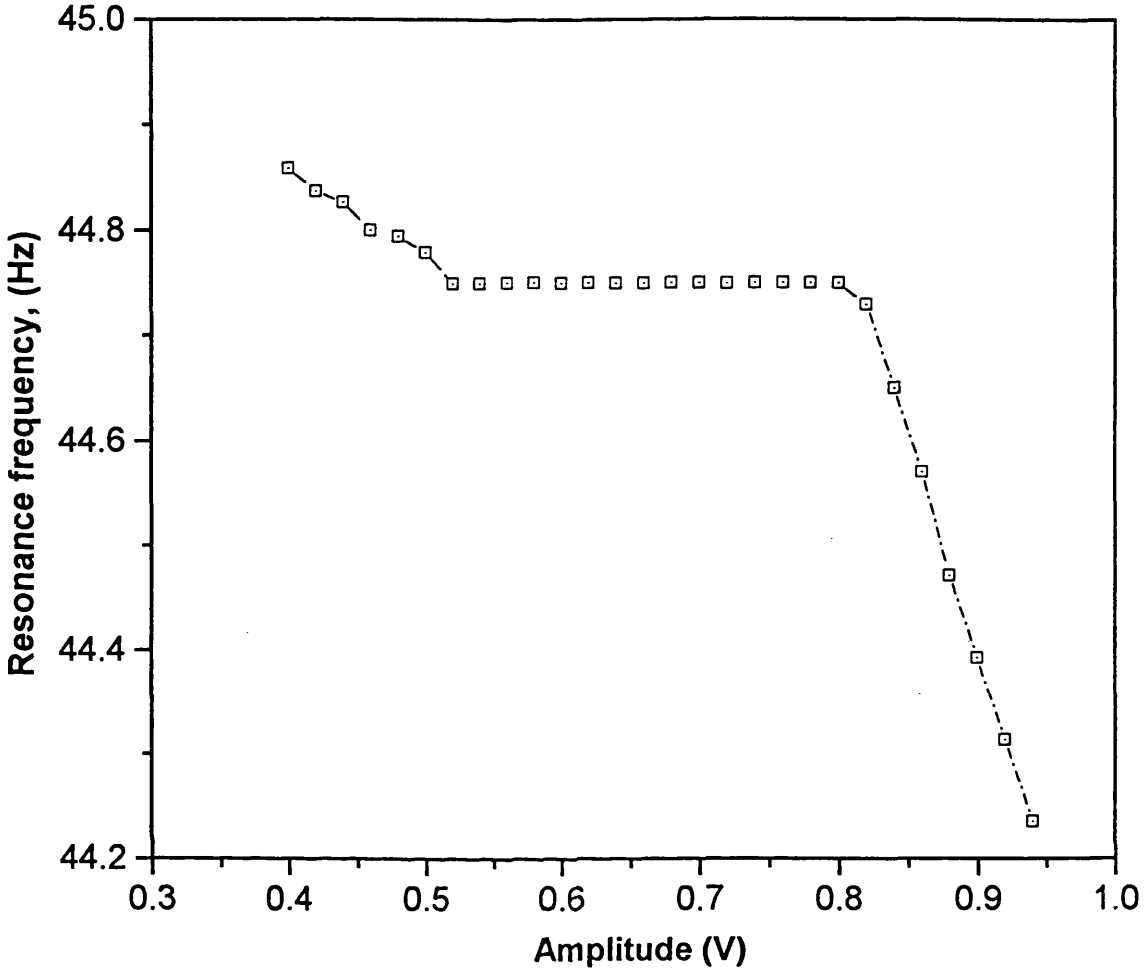

Figure 7.9
The effect of amplitude of vibration on resonance frequency for reed 4 vibrating in water @ 17 °C. The head of water above the reed is 1296 mm.

7.3.2 Effect of Fluid Viscosity and Temperature

The vibration characteristics of a reed are dictated by both the density and viscosity of the fluid medium in which it vibrates (Retsina et al. 1986, 1987). Accordingly, since the vibrating reed sedimentation analysers rely on detecting changes in the bulk density and therefore, the hydrodynamic head of settling suspensions, it is essential to determine the effect of viscosity on the system response.

The fluid bulk viscosity is a function of both temperature and solids concentration.

Dealing with the effect of the temperature first, figure 7.10 shows the variation of the suspending fluid viscosity, in this case pure water with increase in temperature in the range 10 and 60 °C (Perry's Chemical Engineers' Handbook, 1973).

Figure 7.11 on the other hand, shows the corresponding variation of frequency with amplitude around resonance for reed 2 chosen as an example. As it may be observed, the amplitude of vibration increases markedly with increase in the fluid temperature. This is probably due to a reduction in the damping effect of the fluid medium since an increase in temperature results in the reduction in the fluid viscosity (see figure 7.10). However, since the maximum amplitude attained at resonance is still within the range 0.5 - 0.8 V (see figures 7.6 - 7.9), the resonance frequency (the frequency corresponding to the maximum amplitude of vibration) remains unchanged.

Dealing with the effect of solids concentration next, in the case of a settling suspension changes in the fluid viscosity are implicit within the solids volume concentration. For dilute (solids volume concentrations < 5 % v/v) systems, suspension bulk viscosity can be estimated from Einstein's empirical viscosity correlation (Einstein, 1906) presented in section 4.2, chapter 4. Figure 7.12 shows the corresponding predicted variation of suspension viscosity with solids volume fraction at various temperatures in the range 10 - 25 °C. The data covers the typical range of solids volume concentrations (1.75 - 2.81 % v/v) used in the proceeding sedimentation experiments with glass ballotini

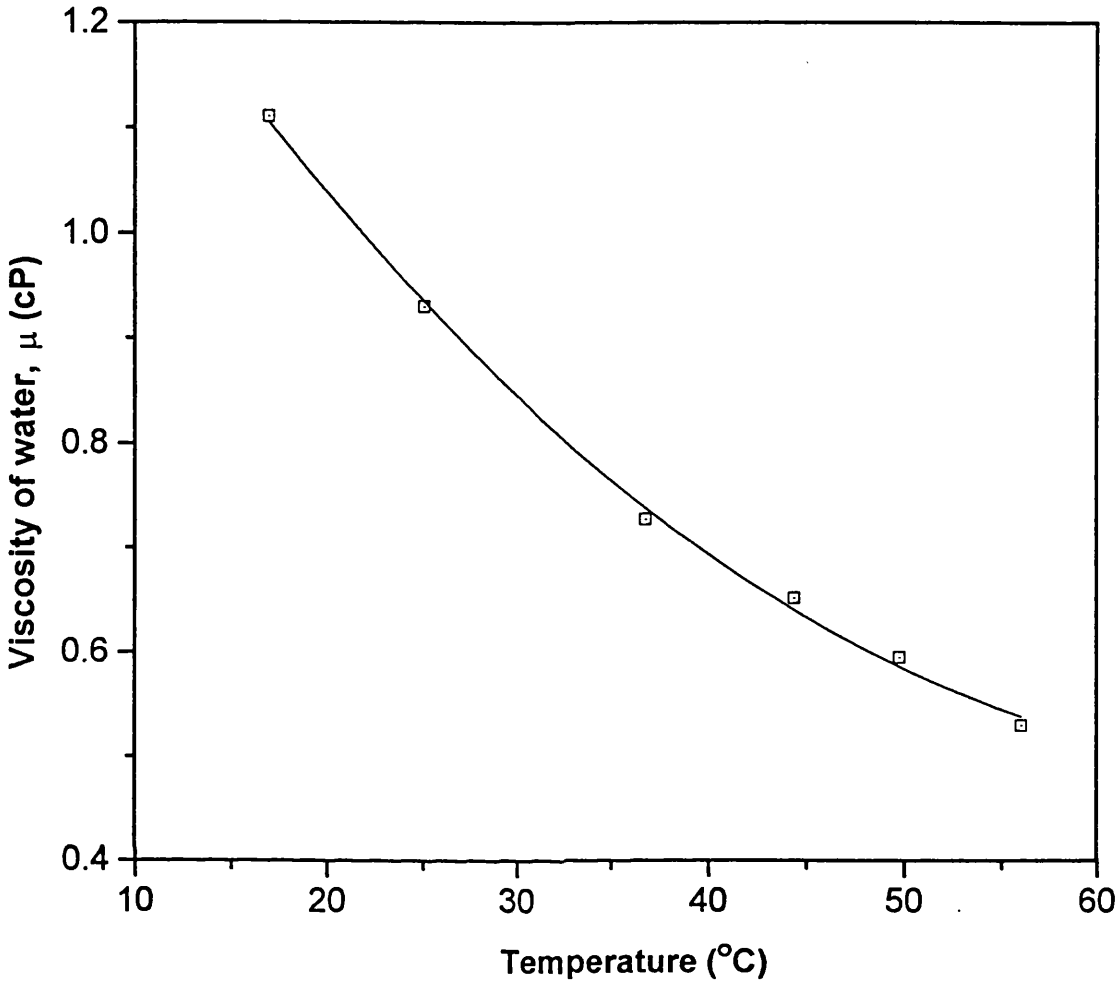

Figure 7.10
The variation of viscosity with temperature for water (Perry's Chemical Engineer's Handbook, 1973).

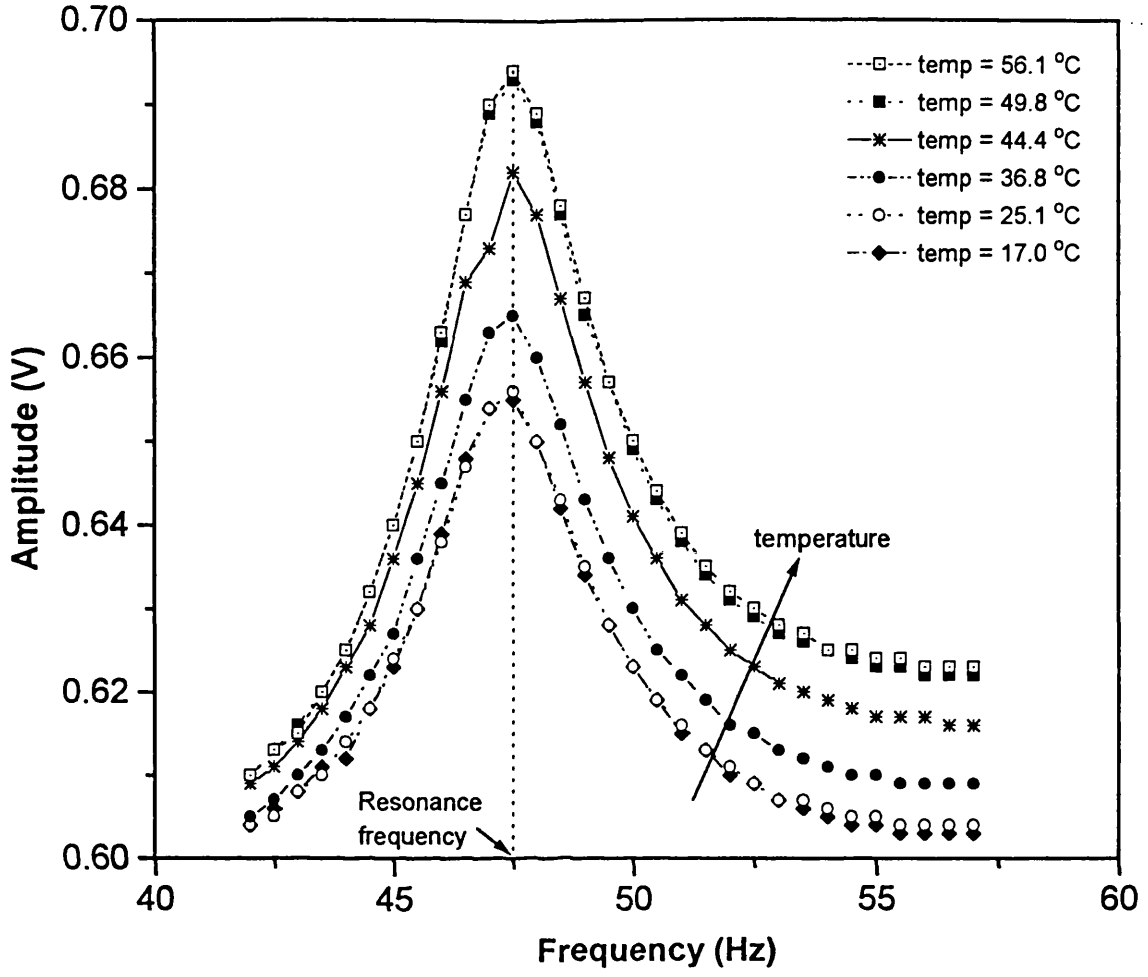

Figure 7.11
The effect of fluid (water) temperature on the amplitude-frequency response of reed 2 for a constant driving power of 3.5 W

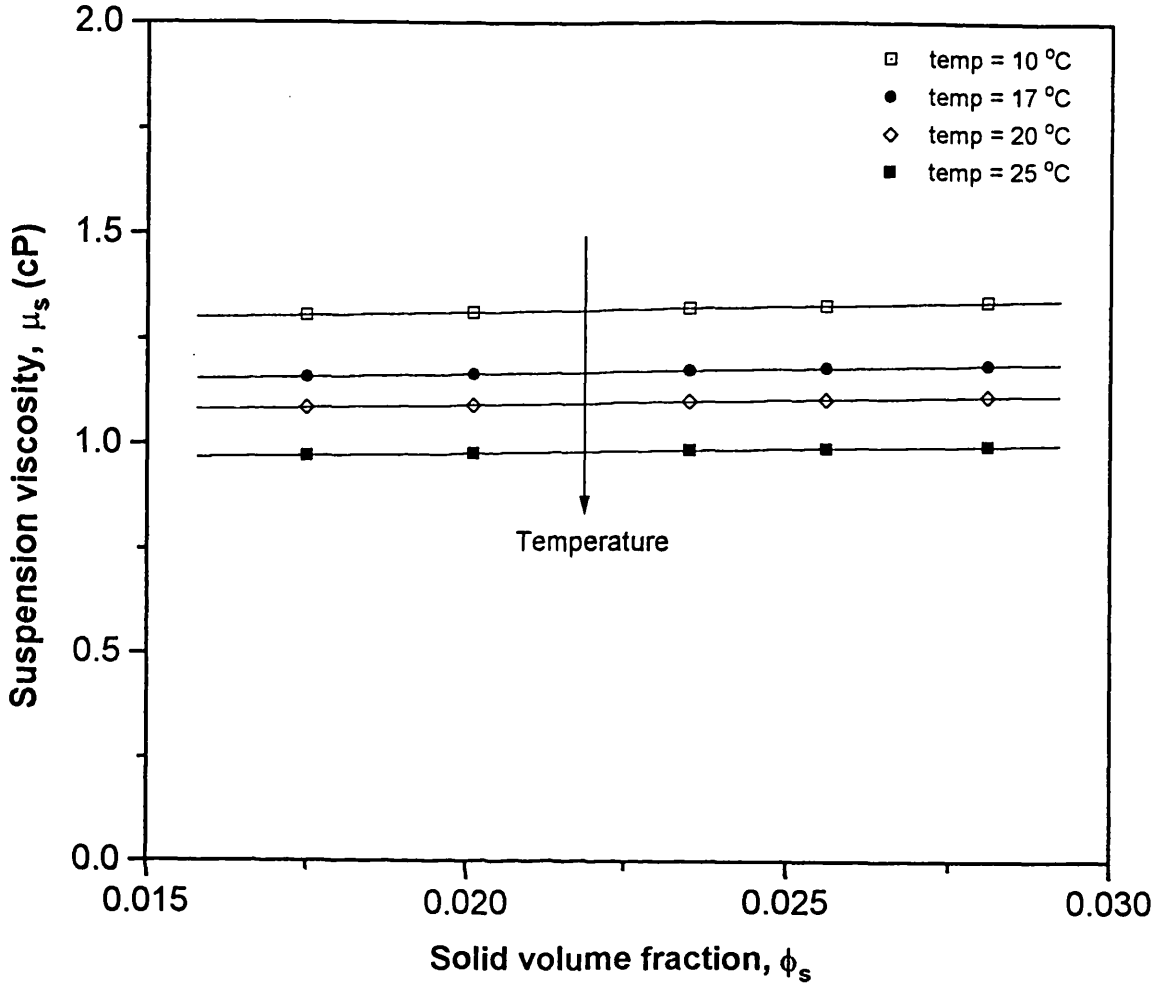

Figure 7.12
Theoretical variation of suspension viscosity with solids volume fraction based on Einstein's viscosity correlation for settling hard spheres (Einstein, 1906) for various temperatures

(density 2550 kgm^{-3}) particles. Clearly, within the ranges tested, provided temperature remains constant, there is no net change in the suspension bulk viscosity as a result of an increase in the solid concentration.

On the basis of the above observations, it may therefore be concluded that changes in the reed's resonance frequency may be predominantly attributable to variations in suspension bulk density and hence the fluid hydrodynamic head.

Therefore, the principle of operation of the system with respect to monitoring the behaviour of a settling suspension relies on detecting changes in the hydrodynamic head above each reed which decreases with time as the solid phase settles to leave a clear fluid.

7.3.3 Effect of Fluid Hydrodynamic Head

It is noteworthy that each reed detects global rather than local changes in the bulk concentration of the suspension since the effective sensing volume of each device is the entire volume above its reference position. This is confirmed by monitoring the system response following changes in the fluid hydrodynamic head.

Figure 7.13 shows the variation of normalised resonance frequency with fluid (water @ 17 °C) hydrodynamic head for the multiple reeds. The data is obtained by adjusting the fluid level in the settling tank and recording the resonance frequency. Measurements are then normalised by dividing by the corresponding resonance frequency of each reed in air at 17 °C. The response of each reed is advantageously linear and as expected, resonance frequency decreases as the hydrodynamic head increases. It is important to note that during this experiment the local inertial forces acting on each reed remain constant since the fluid density and viscosity do not change. Therefore, the data shown in figure 7.13 simulates the system's response to changes in the hydrodynamic head exerted by a suspension during sedimentation.

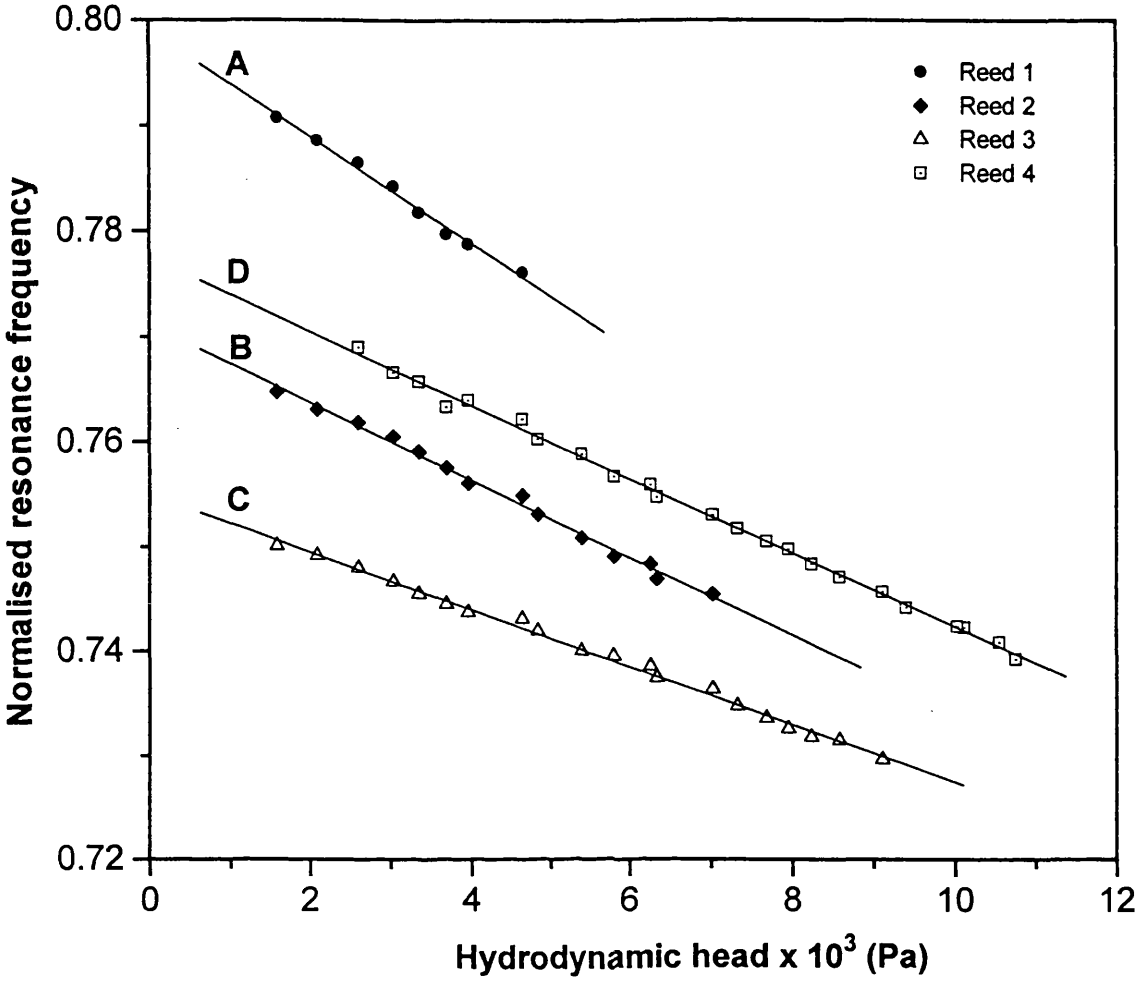

Figure 7.13
The variation of normalised resonance frequency with hydrodynamic head (water @ 17 °C) for various reed positions as measured from the top of the settling zone: reed 1, 699 mm; reed 2, 900 mm; reed 3, 1096 mm and reed 4, 1296 mm.

Close inspection of the data indicates differences in sensitivity of each reed (the fitted lines have different gradients). This is probably due to the finite differences in the material and characteristic dimensions of each reed during its fabrication. Accordingly, it is necessary to calibrate the response of each reed independently.

7.4 Calibration of System Response

In order to calibrate the vibrating reed sedimentation analysers, dilute suspensions of known initial solids volume concentrations (1.75, 2.01, 2.35, 2.56 and 2.81 % v/v) are prepared in the manner described in section 7.3 using the nominally monodisperse 200 - 212 μm glass ballotini sample. The resonance frequency response of each reed is then monitored as a function of time from which sedimentation kinetic data such as the particle settling velocity and the solids flux may be inferred.

Figure 7.14 shows the variation of system resonance frequency with time for various initial suspended solids volume concentrations of 200 - 212 μm glass ballotini spheres (density 2550 kgm^{-3}) settling in water at 17 °C. The data (recorded and displayed in real time using the specially developed electronic data acquisition system described in section 6.4.1, chapter 6) is obtained from reed 1 which is located at a distance of 699 mm from the top of the setting zone. Figures 7.15 - 7.17 on the other hand show the corresponding data obtained at the same time as those shown in figure 7.14 using reeds 2 - 4 respectively. Reeds 2, 3 and 4 are situated 900, 1096 and 1296 mm respectively, from the top of the settling zone (see figure 6.16, chapter 6).

The data indicate an initial flat region corresponding to steady state operation in which all the particles are in a fluidised state (see later; section 8.1, chapter 8). As particles settle past the reed, the resonance frequency continuously increases since the hydrodynamic head above it decreases. A constant value is reached when all particles have past the reed to leave a clear liquid (the supernatant). The corresponding time lapsed measured relative to the onset of settling at which this occurs is here referred to as the 'breakthrough time', Δt_b (see for example figure 7.14). As expected, the

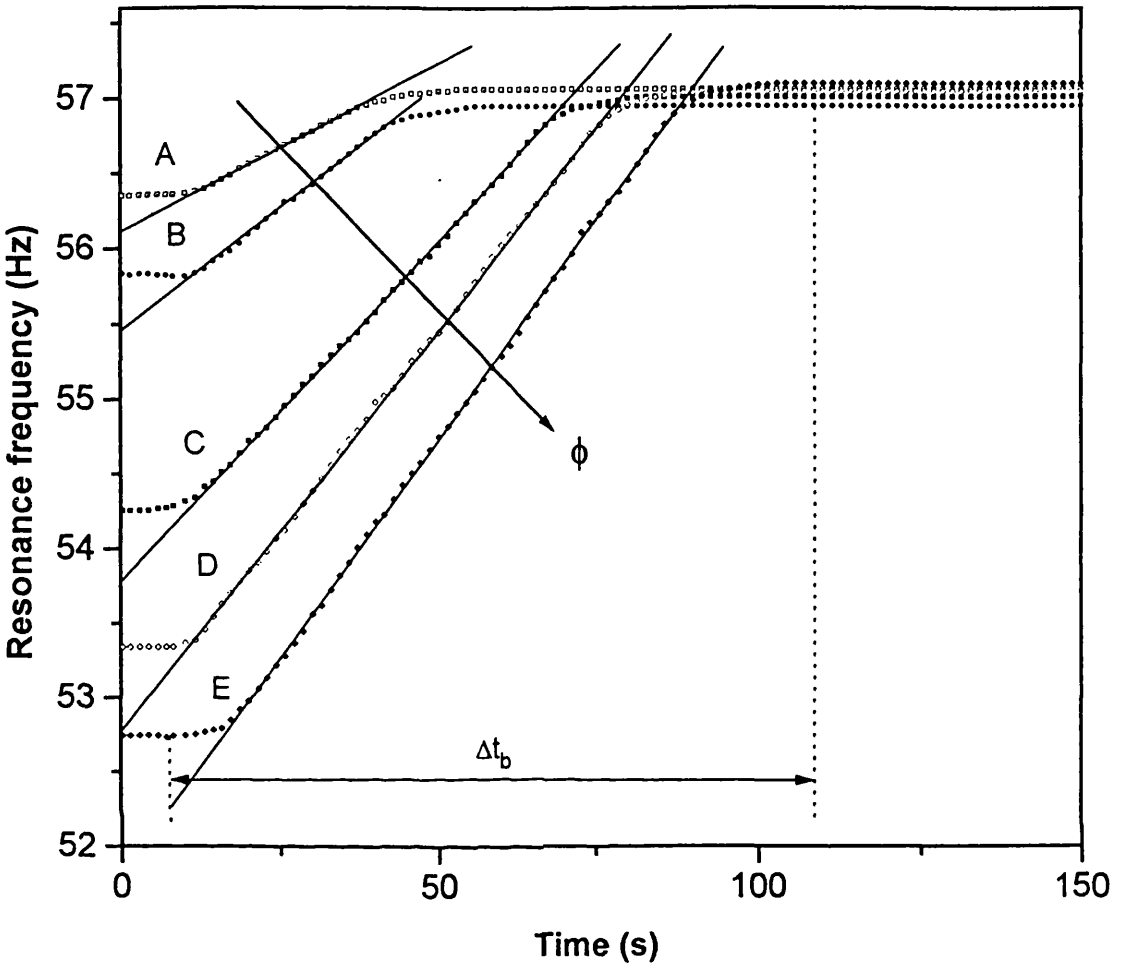

Figure 7.14
The variation of resonance frequency with time at reed position 1 (699 mm from top of settling zone) for monodisperse 200 - 212 μm glass ballotini spheres (density 2550 kgm^{-3}) settling in water @ 17 °C at various initial suspended solids volume concentrations, ϕ: curve A, ϕ = 1.75 %; curve B, ϕ = 2.01 %; curve C, ϕ = 2.35 %; curve D, ϕ = 2.56 % and curve E, ϕ = 2.81 %

	Fitting equation	Correlation coefficient
Curve A	y = 0.02217x + 56.11	0.9991
Curve B	y = 0.03375x + 55.45	0.9986
Curve C	y = 0.04849x + 53.78	0.9973
Curve D	y = 0.05749x + 52.77	0.9984
Curve E	y = 0.06884x + 51.80	0.9973

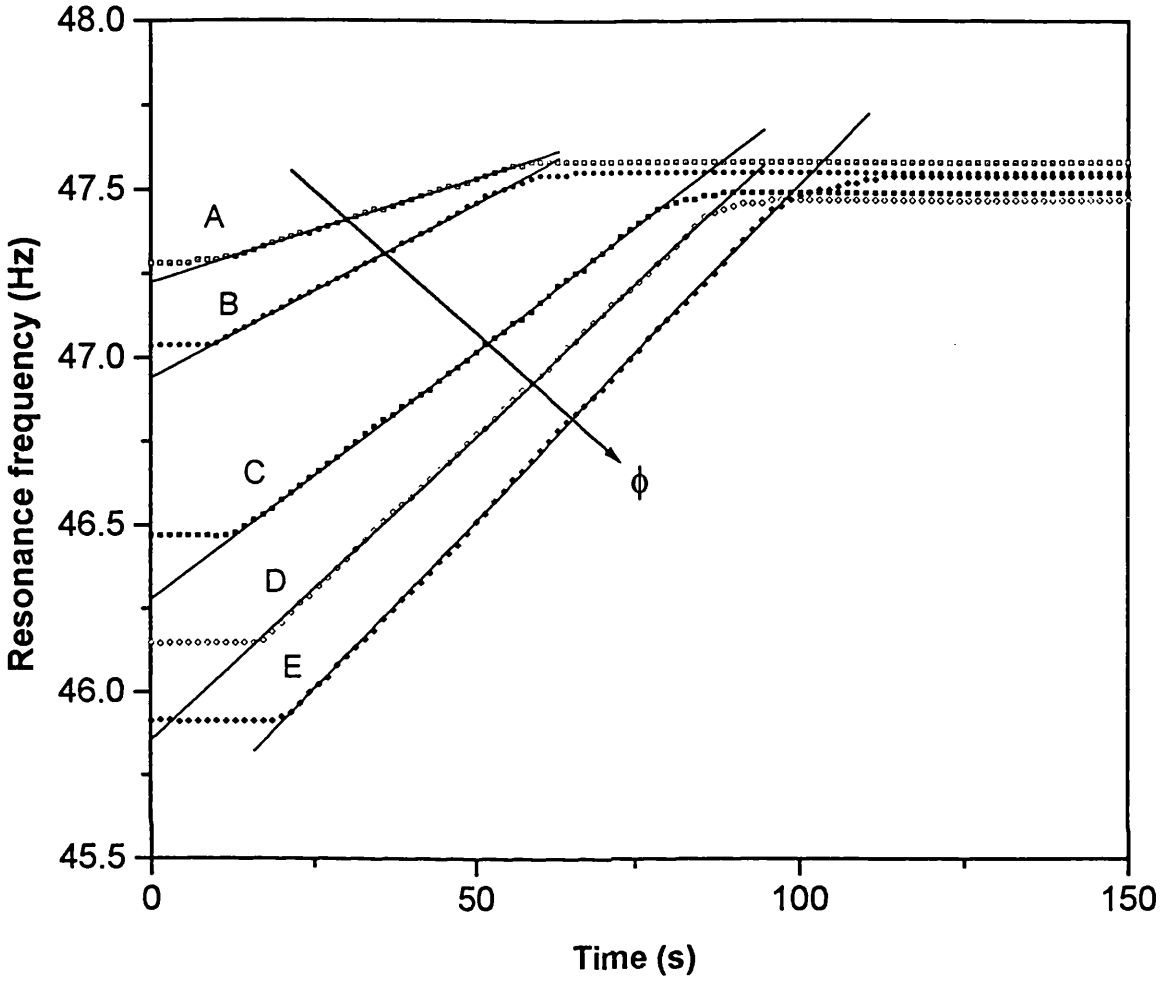

Figure 7.15
The variation of resonance frequency with time at reed position 2 (900 mm from top of settling zone) for monodisperse 200 - 212 μm glass ballotini spheres (density 2550 kgm^{-3}) settling in water @ 17 °C at various initial suspended solids volume concentrations, ϕ: curve A, ϕ = 1.75 %; curve B, ϕ = 2.01 %; curve C, ϕ = 2.35 %; curve D, ϕ = 2.56 % and curve E, ϕ = 2.81 %

	Fitting equation	Correlation coefficient
Curve A	y = 0.00601x + 47.22	0.9962
Curve B	y = 0.01073x + 46.94	0.9958
Curve C	y = 0.01624x + 46.28	0.9977
Curve D	y = 0.01950x + 45.85	0.9974
Curve E	y = 0.02451x + 45.50	0.9954

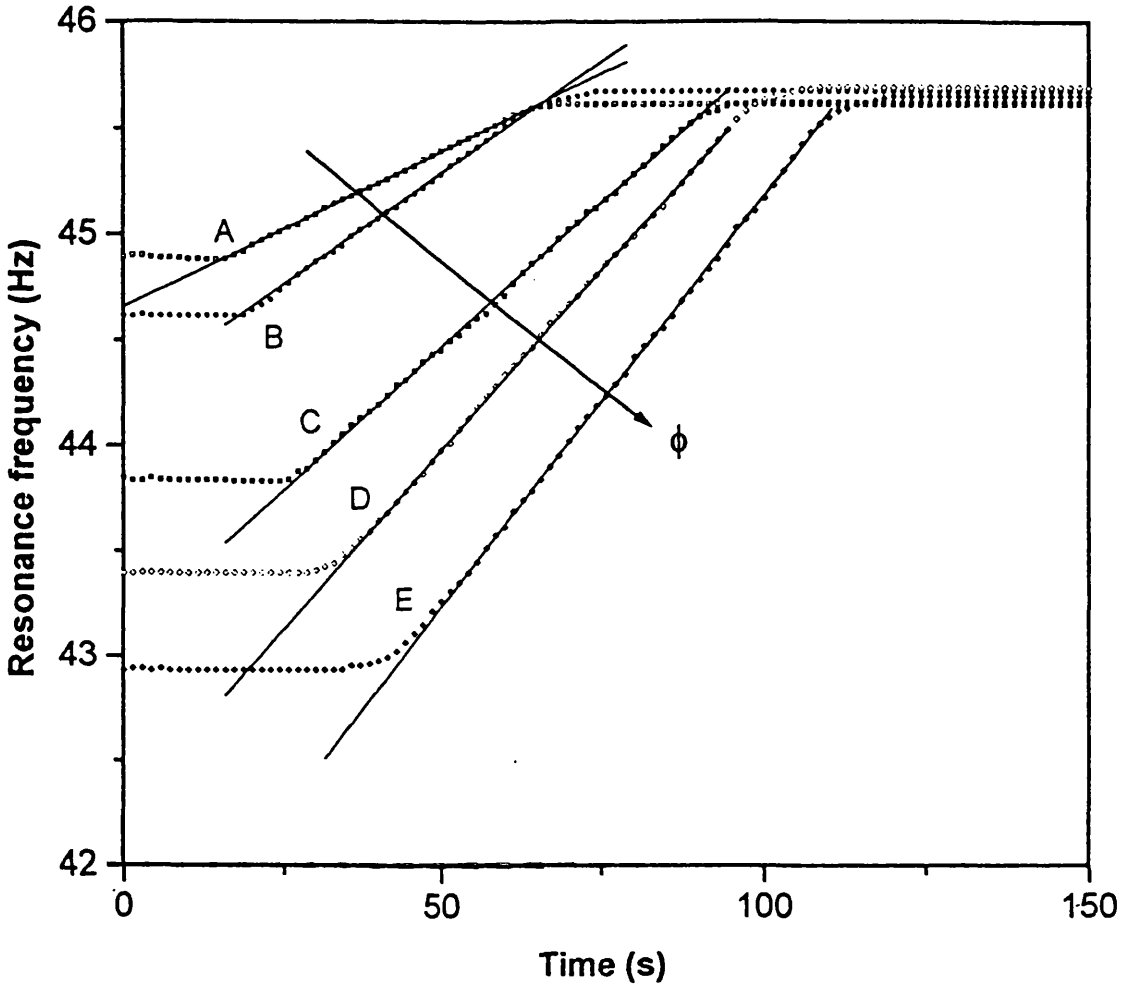

Figure 7.16
The variation of resonance frequency with time at reed position 3 (1096 mm from top of settling zone) for monodisperse 200 - 212 μm glass ballotini spheres (density 2550 kgm^{-3}) settling in water @ 17 °C at various initial suspended solids volume concentrations, ϕ: curve A, ϕ = 1.75 %; curve B, ϕ = 2.01 %; curve C, ϕ = 2.35 %; curve D, ϕ = 2.56 % and curve E, ϕ = 2.81 %

	Fitting equation	Correlation coefficient
Curve A	y = 0.01466x + 44.66	0.9987
Curve B	y = 0.02137x + 44.24	0.9981
Curve C	y = 0.03124x + 43.11	0.9977
Curve D	y = 0.03632x + 42.27	0.9989
Curve E	y = 0.04277x + 41.27	0.9972

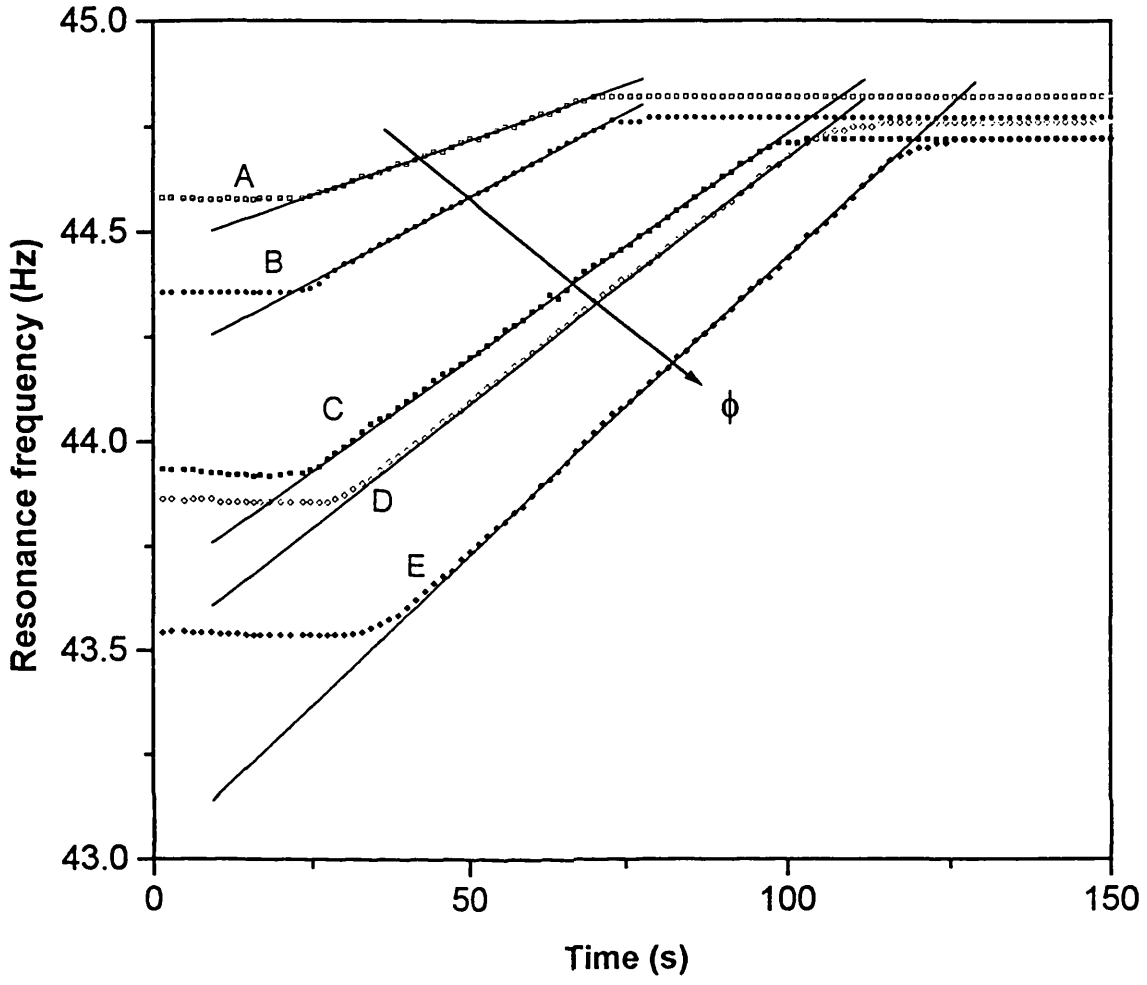

Figure 7.17

The variation of resonance frequency with time at reed position 4 (1296 mm from top of settling zone) for monodisperse 200 - 212 μm glass ballotini spheres (density 2550 kgm^{-3}) settling in water @ 17 °C at various initial suspended solids volume concentrations, ϕ: curve A, ϕ = 1.75 %; curve B, ϕ = 2.01 %; curve C, ϕ = 2.35 %; curve D, ϕ = 2.56 % and curve E, ϕ = 2.81 %

	Fitting equation	Correlation coefficient
Curve A	y = 0.00528x + 44.46	0.9961
Curve B	y = 0.00789x + 44.18	0.9986
Curve C	y = 0.01097x + 43.66	0.9983
Curve D	y = 0.01298x + 43.50	0.9944
Curve E	y = 0.01550x + 43.01	0.9973

breakthrough time increases with increase in particle concentration as well as the distance of each reed relative to the top of the settling zone.

According to the data in figures 7.14 - 7.17, the variation of the resonance frequency with time during the transition period may be assumed to be linear. This indicates that for this special case of a nominally monodisperse suspension, all particles settle at approximately the same rate and hence, the rate of descent of the suspension-clear liquid interface accurately represents the average settling rate of the particles.

The tables in the figures show the corresponding linear fitting equations in the transition region as well as the correlation coefficients. The slopes of the fitted lines provide information on the solids flux (see later) via appropriate calibration.

Figure 7.18 shows the variation of suspension-supernatant interface height with time relative to the bottom of the settling zone for the above range of initial solids volume concentrations. This data was obtained by direct visual observation of the sharp suspension-clear liquid interface and is primarily intended for evaluating the performance of the vibrating reed system in obtaining sedimentation kinetic data.

It is evident that the suspensions settle at a constant rate and the gradients of the fitting lines correspond to the interface velocity. Figure 7.19 shows the variation of solids breakthrough time, Δt_b, with reed position relative to the top of the settling zone as extracted from the data in figures 7.14 - 7.17. The experimental interface velocity may be determined from this data by taking the reciprocal of the gradients of the fitted lines A to E.

Figure 7.20 shows a comparison of experimental (figure 7.19) and visually obtained (figure 7.18) interface velocities. The data points correspond to different solids volume concentrations and lie on a 45° line thus validating the capability of the vibrating reeds in providing relatively accurate settling velocity data.

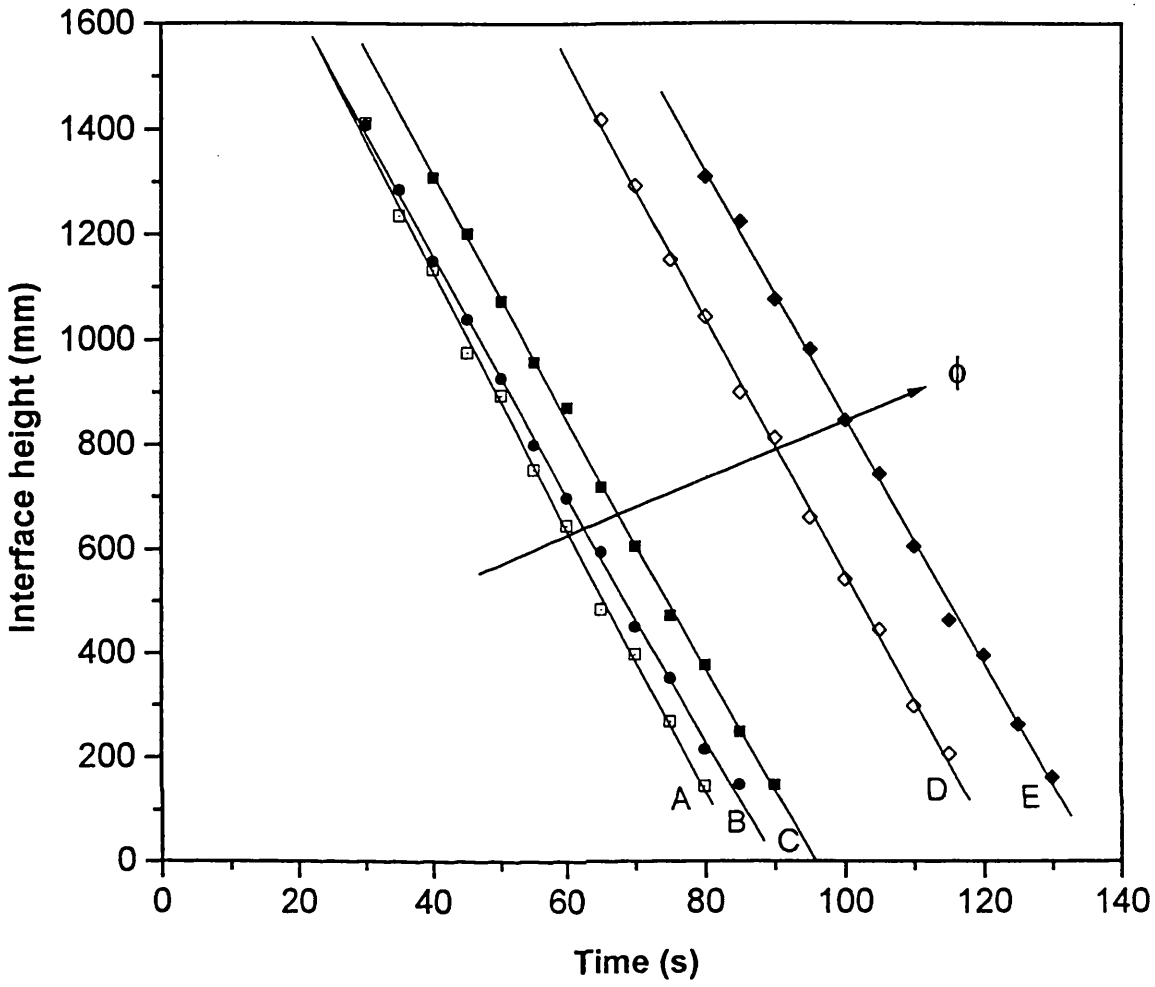

Figure 7.18

The variation of suspension-clear liquid interface height with time as determined by direct visual observation relative to the bottom of the settling zone for monodisperse 200 - 212 μm glass ballotini spheres (density 2550 kgm^{-3}) settling in water @ 17 °C at various initial suspended solids volume concentrations, ϕ: curve A, ϕ = 1.75 %; curve B, ϕ = 2.01 %; curve C, ϕ = 2.35 %; curve D, ϕ = 2.56 % and curve E, ϕ = 2.81 %

	Fitting equation	Interface velocity (mms^{-1})
Curve A	y = -24.83x +2123	24.83
Curve B	y = -24.36x + 2087	24.36
Curve C	y = -23.56x + 2255	23.56
Curve D	y = -23.48x + 2988	23.48
Curve E	y = -23.18x + 3198	23.18

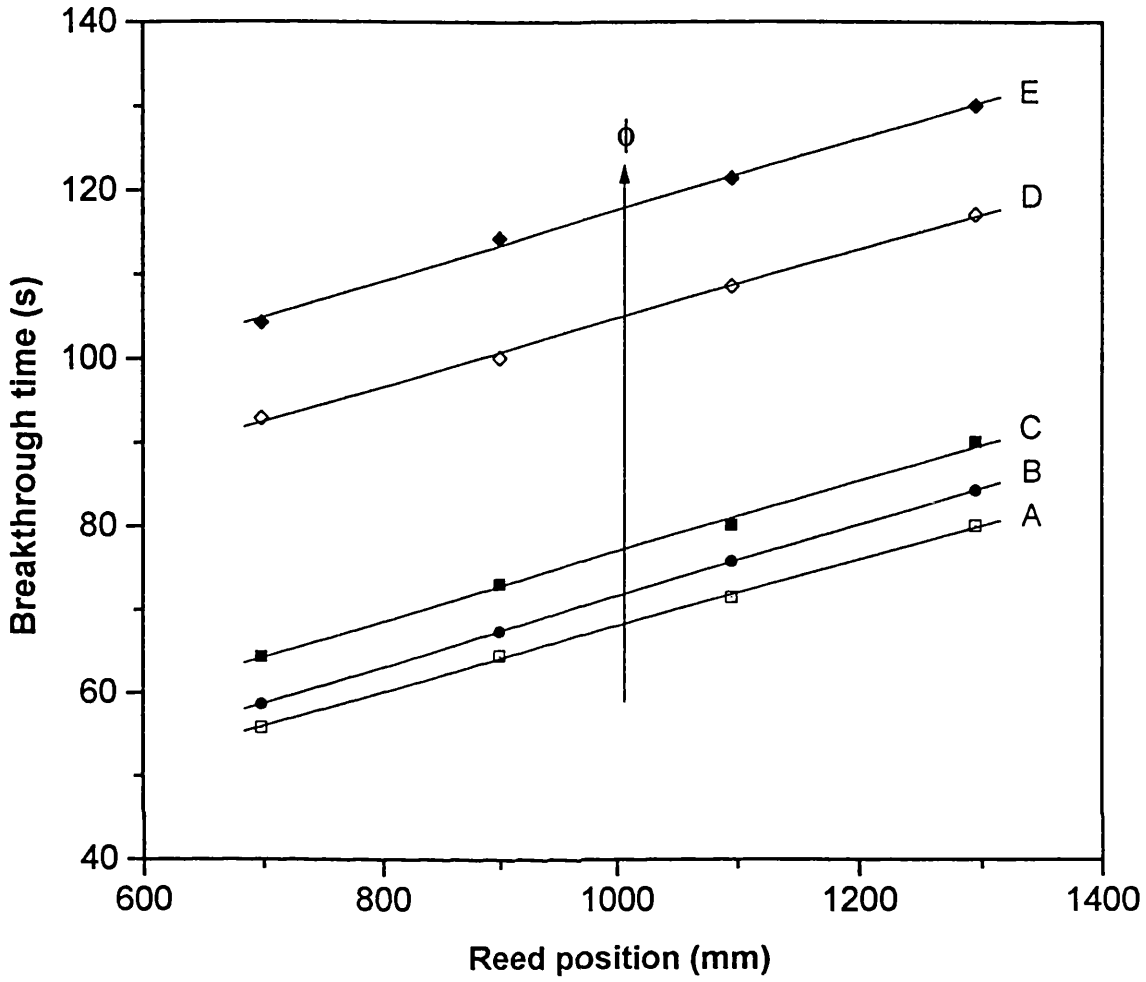

Figure 7.19
The variation of solids breakthrough time with reed position relative to the top of the settling zone for monodisperse 200 - 212 μm glass ballotini spheres (density 2550 kgm^{-3}) settling in water @ 17 °C at various initial suspended solids volume concentrations, ϕ: curve A, ϕ = 1.75 %; curve B, ϕ = 2.01 %; curve C, ϕ = 2.35 %; curve D, ϕ = 2.56 % and curve E, ϕ = 2.81 %

	Fitting equation	Interface velocity (mms^{-1})
Curve A	y = 0.0403x + 27.73	24.81
Curve B	y = 0.0410x + 28.45	24.39
Curve C	y = 0.0424x + 34.51	23.58
Curve D	y = 0.0424x + 63.82	23.58
Curve E	y = 0.0431x + 75.23	23.20

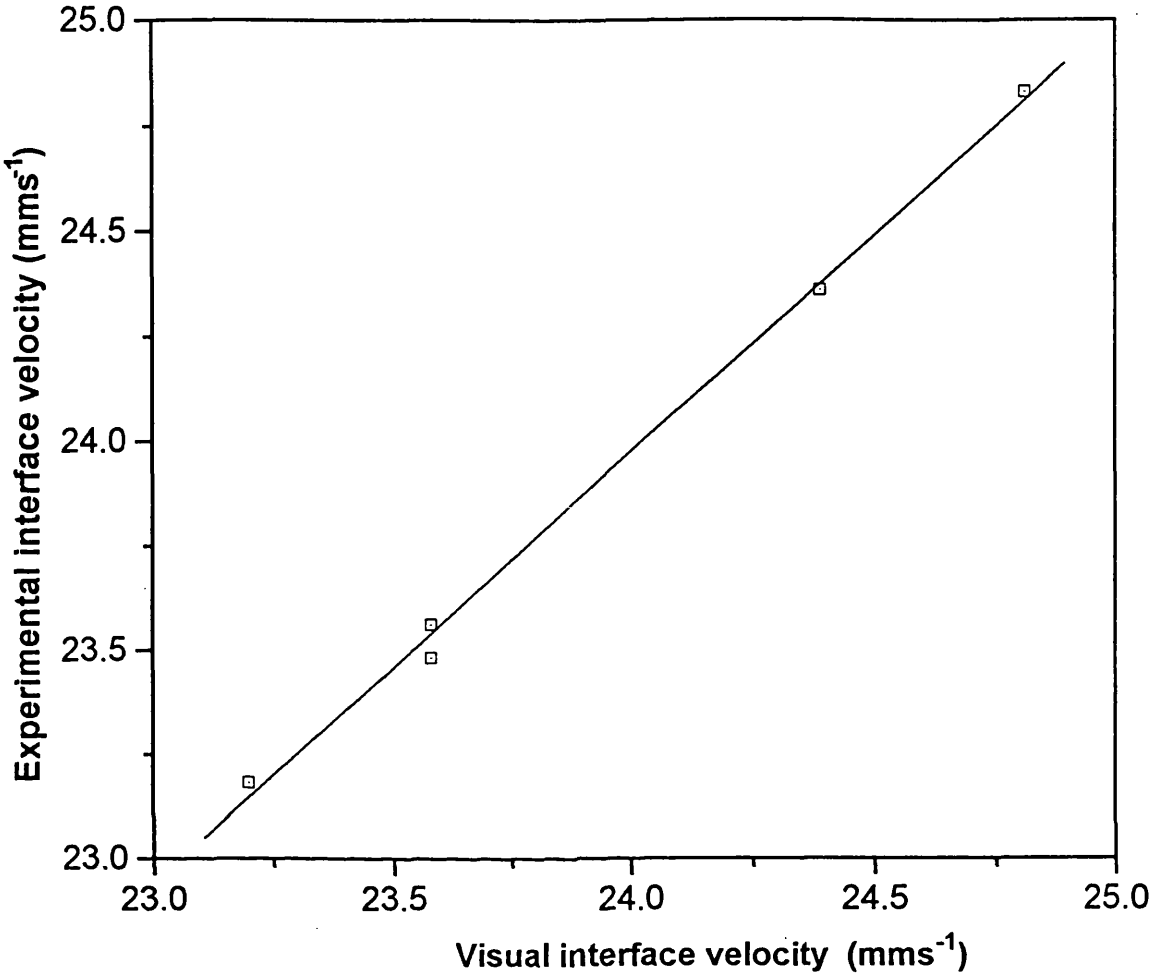

Figure 7.20
A comparison of experimental and visual interface velocities for monodisperse 200 - 212 μm glass ballotini spheres (density 2550 kgm^{-3}) settling in water @ 17 °C. Each data point corresponds to a different initial solids volume concentration, ϕ

Returning to figures 7.14 - 7.17, it is evident that for the nominally monodisperse suspensions chosen in this study, the rate of change of resonance frequency with time is constant and can be determined by linear regression of the fitted lines A to E. Also, since corresponding values of the initial solids volume concentration and the settling velocity (based on reed breakthrough times) are known for each suspension, the solids flux (product of settling velocity and solids volume concentration) can be determined.

Figures 7.21 - 7.24 show the variation of solids flux versus rate of change of resonance frequency for reeds 1 - 4 respectively. The solids volume concentrations vary in the range 1.75 - 2.81 %. These data were obtained in the manner described above in conjunction with the mono-sized particles and may be accurately represented by 4^{th} degree polynomials. These equations can in turn be used to determine the solids flux profiles in other test suspensions from a direct measurement of the rate of change of resonance frequency with time data. It is important to note that the above data represent absolute values of the solids flux which is negative since particles leave the settling zone (i.e. the solids volume concentration decreases with time).

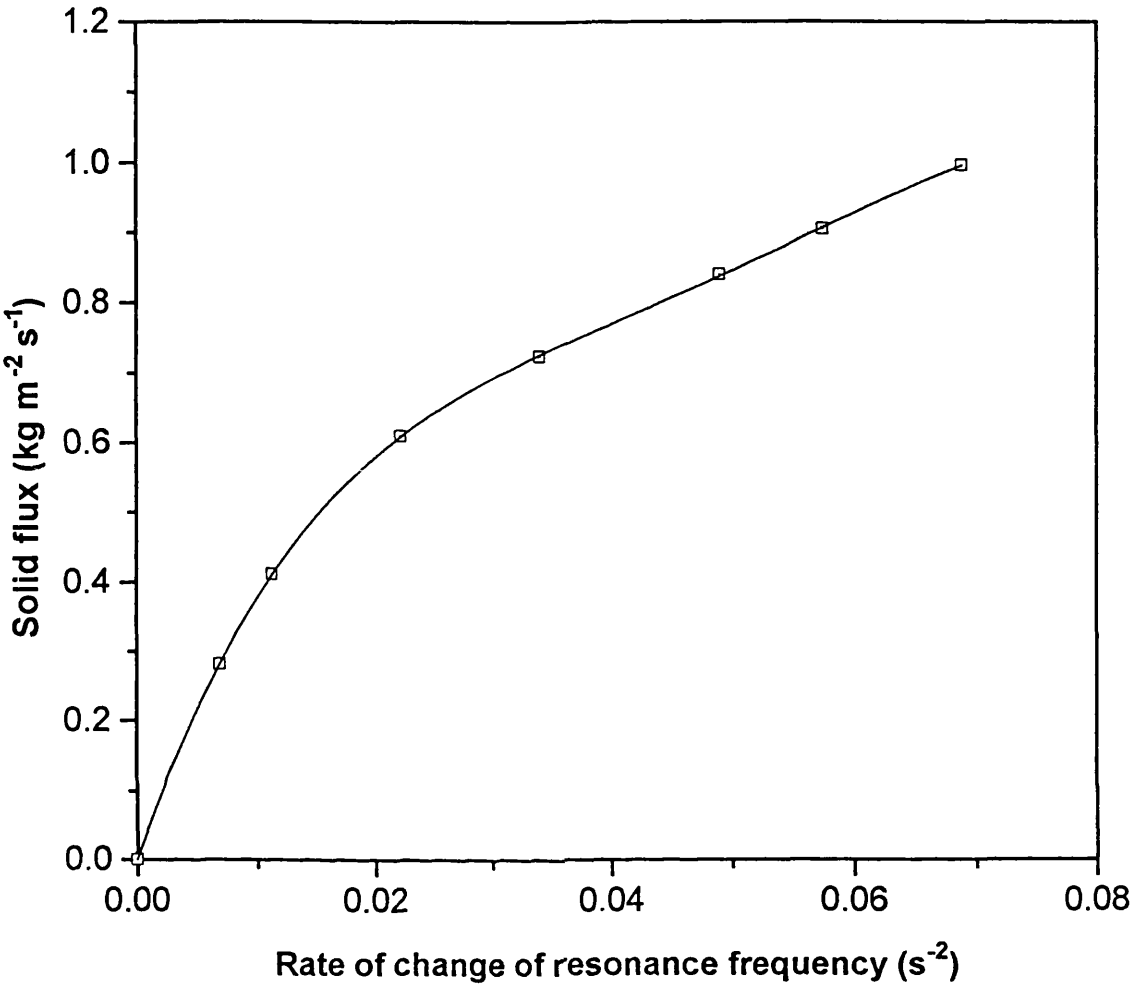

Figure 7.21
Calibration curve showing solids flux versus rate of change of resonance frequency at reed position 1 (699 mm from top of settling zone) for monodisperse 200 - 212 μm glass ballotini spheres (density 2550 kgm^{-3}) settling in water @ 17 °C

Fitting equation
$y = -101878.78x^4 + 19703.025x^3 - 1383.3522x^2 + 49.550264x + 5.8059886E-5$

Correlation coefficient
$R^2 = 0.9999$

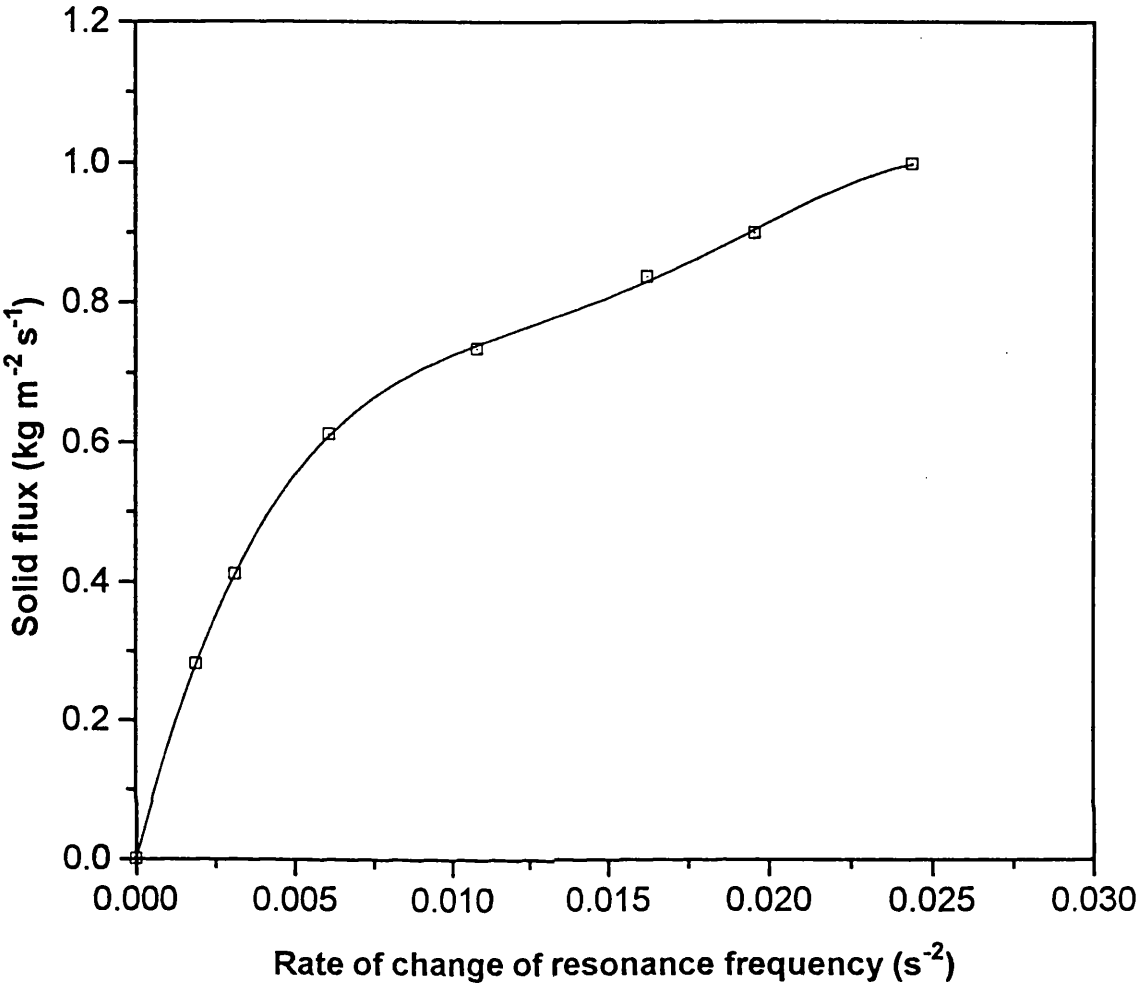

Figure 7.22

Calibration curve showing solids flux versus rate of change of resonance frequency at reed position 2 (900 mm from top of settling zone) for monodisperse 200 - 212 μm glass ballotini spheres (density 2550 kgm^{-3}) settling in water @ 17 °C

Fitting equation

$y = -11216174x^4 + 719277.68x^3 - 16404.394x^2 + 175.8275x + 3.4421938E\text{-}5$

Correlation coefficient

$R^2 = 0.9999$

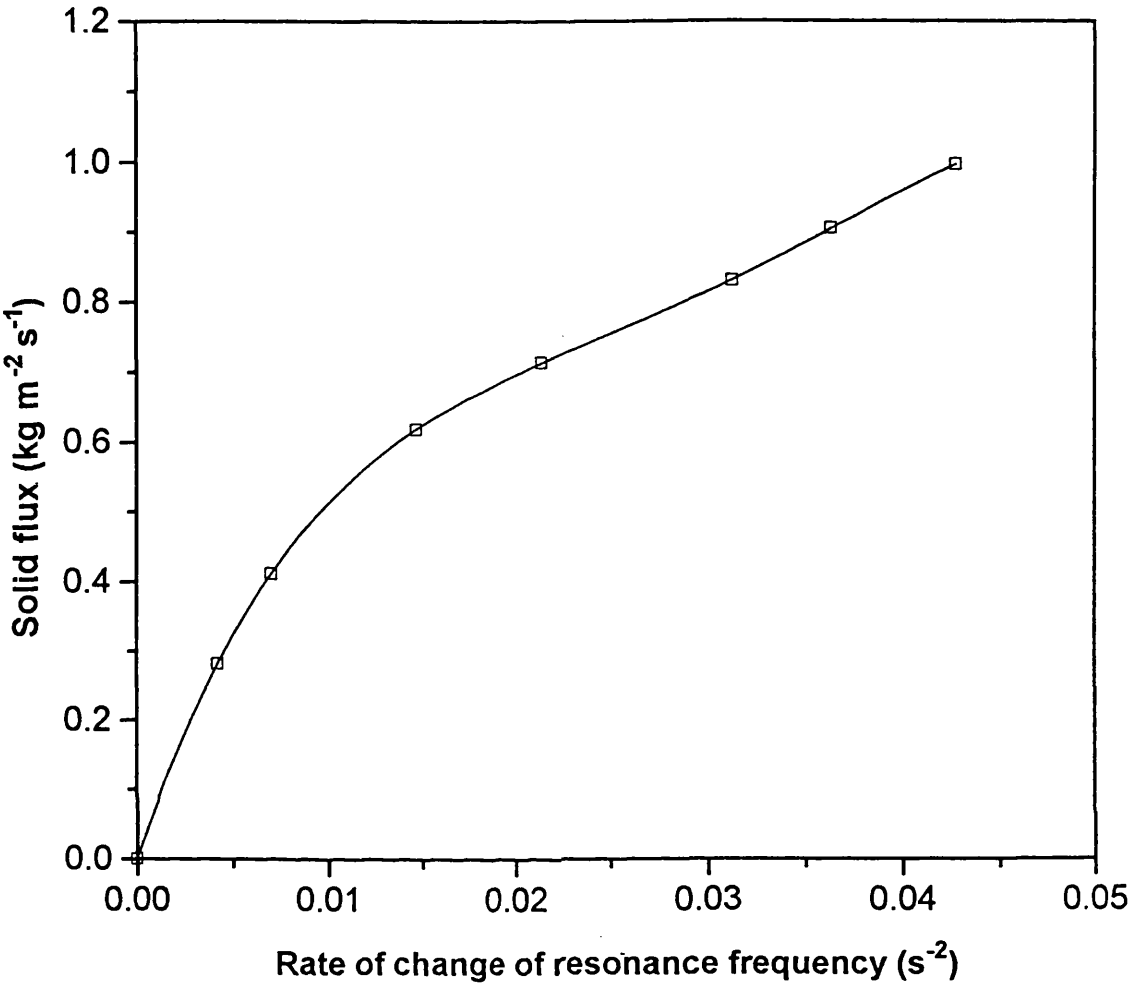

Figure 7.23
Calibration curve showing solids flux versus rate of change of resonance frequency at reed position 3 (1096 mm from top of settling zone) for monodisperse 200 - 212 μm glass ballotini spheres (density 2550 kgm^{-3}) settling in water @ 17 °C

Fitting equation

$y = -735659.57x^4 + 88302.456x^3 - 3777.9957x^2 + 80.893072x - 1.966342E-5$

Correlation coefficient

$R^2 = 0.9998$

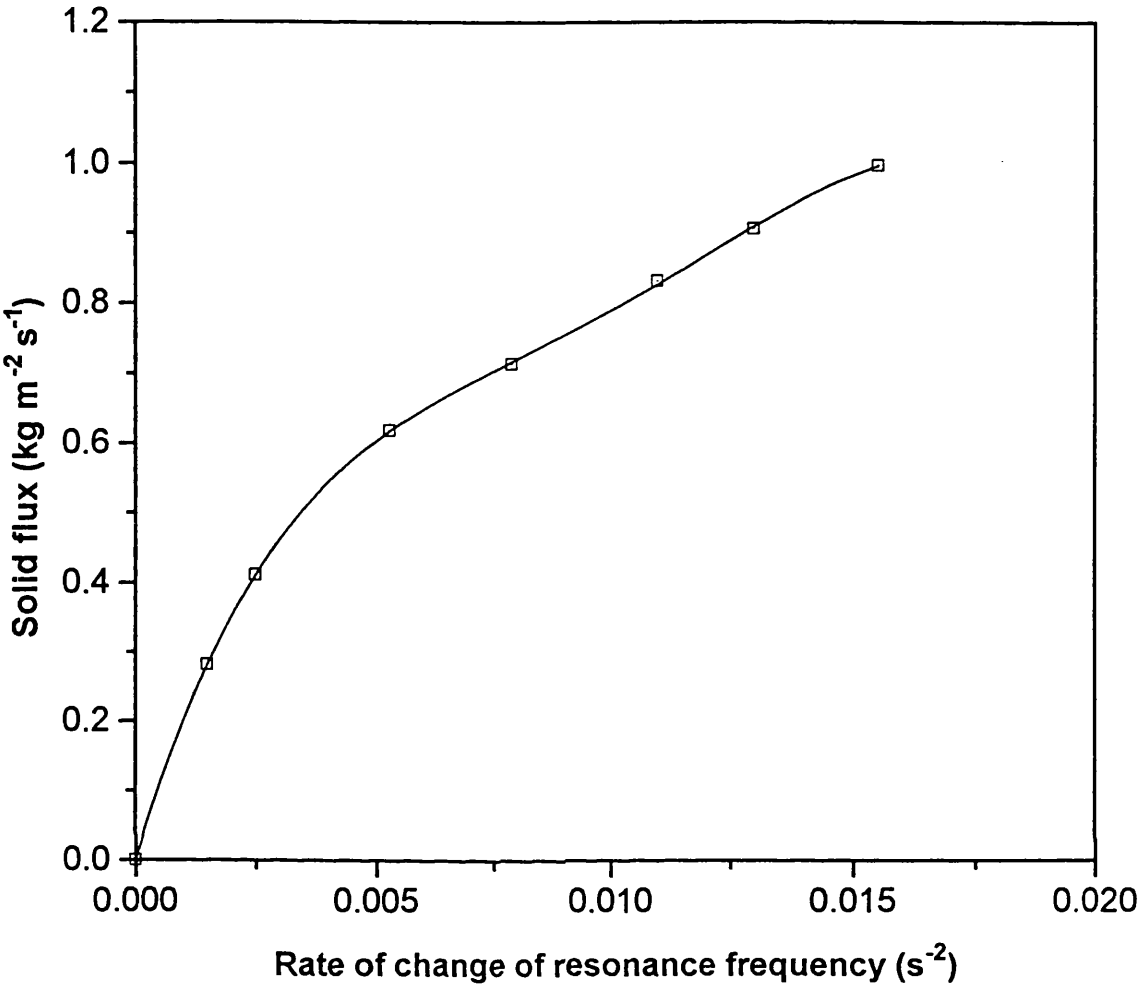

Figure 7.24
Calibration curve showing solids flux versus rate of change of resonance frequency at reed position 4 (1296 mm from top of settling zone) for monodisperse 200 - 212 μm glass ballotini spheres (density 2550 kgm^{-3}) settling in water @ 17 °C

Fitting equation

$y = -52664362x^4 + 2145854.9x^3 - 31303.342x^2 + 229.96065x + 8.8930806E-5$

Correlation coefficient

$R^2 = 0.9998$

CHAPTER 8

RESULTS AND DISCUSSION

8.0 Introduction

In chapter 7, the capability of the multiple vibrating reed system in providing sedimentation kinetic data such as particle settling velocities and the solids flux was demonstrated in conjunction with experimental data for nominally monodisperse 200 - 212 μm glass ballotini/water suspensions. In particular, the rate of change of resonance frequency with time for each reed was calibrated against the solids flux. Interface velocities on the other hand were obtained directly from the breakthrough times of frequency versus time profiles.

This chapter deals with the utilisation of the solids flux calibration plots to characterise the settling behaviour of polydisperse glass ballotini/water suspensions comprising the normally distributed particle size ranges: 55 - 100 μm, 80 - 115 μm, 90 - 135 μm and 100 - 200 μm presented in chapter 7. This is achieved by taking the first derivative of resonance frequency versus time profiles obtained during the sedimentation of each suspension. These data are in turn used in conjunction with the system calibration plots to produce solids flux ($kgm^{-2}s^{-1}$) versus time profiles the accuracy of which is validated by direct mass balance. The latter involves determining the area under each solids flux curve (kgm^{-2}) and multiplying by the cross-sectional area of the settling tank to obtain the experimental solids mass throughputs (kg). The results are then compared with the corresponding volume-based estimates of the solids mass throughputs calculated from the known initial solids concentration (kgm^{-3}) and the suspension volume above each reed.

The performance of the relevant empirical models described in chapter 4 is evaluated by comparing predicted setting velocities with those obtained from experiment. The above analysis is however limited to monodisperse 200 - 212 μm glass ballotini/water

suspensions for which the appropriate theoretical correlations exist. The settling behaviour of dilute (< 5 % v/v) polydisperse suspensions is inherently more complex. This is demonstrated by the occurrence of highly diffuse interfaces which arise from the differential settling of particles during sedimentation. As such reliable models for the prediction of particle settling behaviour for such systems are not available. Unfortunately due to practical difficulties associated with achieving good mixing within the settling tank the present study mainly deals with dilute polydisperse suspensions (1.75 - 2.81 % v/v) in which particles experience differential rather than hindered settling.

The results of preliminary investigations on the effects of solids concentration and mean particle size on the speed at which the two-phase system responds to the change from 'steady state' to 'unsteady state' operation following the onset of the sedimentation process are also presented. The chapter concludes with a presentation of sedimentation kinetic data obtained in conjunction with an industrially relevant system comprising flocculated kaolin/water slurries. In addition, the feasibility of application of the measurement technique in monitoring the stability of two-phase liquid/liquid emulsions is demonstrated by presenting data on different concentration oil/water emulsions.

8.1 Resonance Frequency/Time Profiles

Figure 8.1 shows the variation of resonance frequency with time for polydisperse 55 - 100 μm glass ballotini spheres (density 2550 kgm^{-3}) settling in water at 17 °C for various initial solids concentrations in the range 1.75 - 2.81 % v/v. The data is obtained from reed 1 (positioned nearest to the top of the settling tank; see figure 6.16). Figures 8.2 - 8.4 on the other hand show the corresponding data obtained at the same time as those shown in figure 8.1 using reeds 2 - 4 respectively. Some of the important trends in the results may be summarised as follows:

i) As expected, the breakthrough time, Δt_b increases with increase in the initial solids concentration.

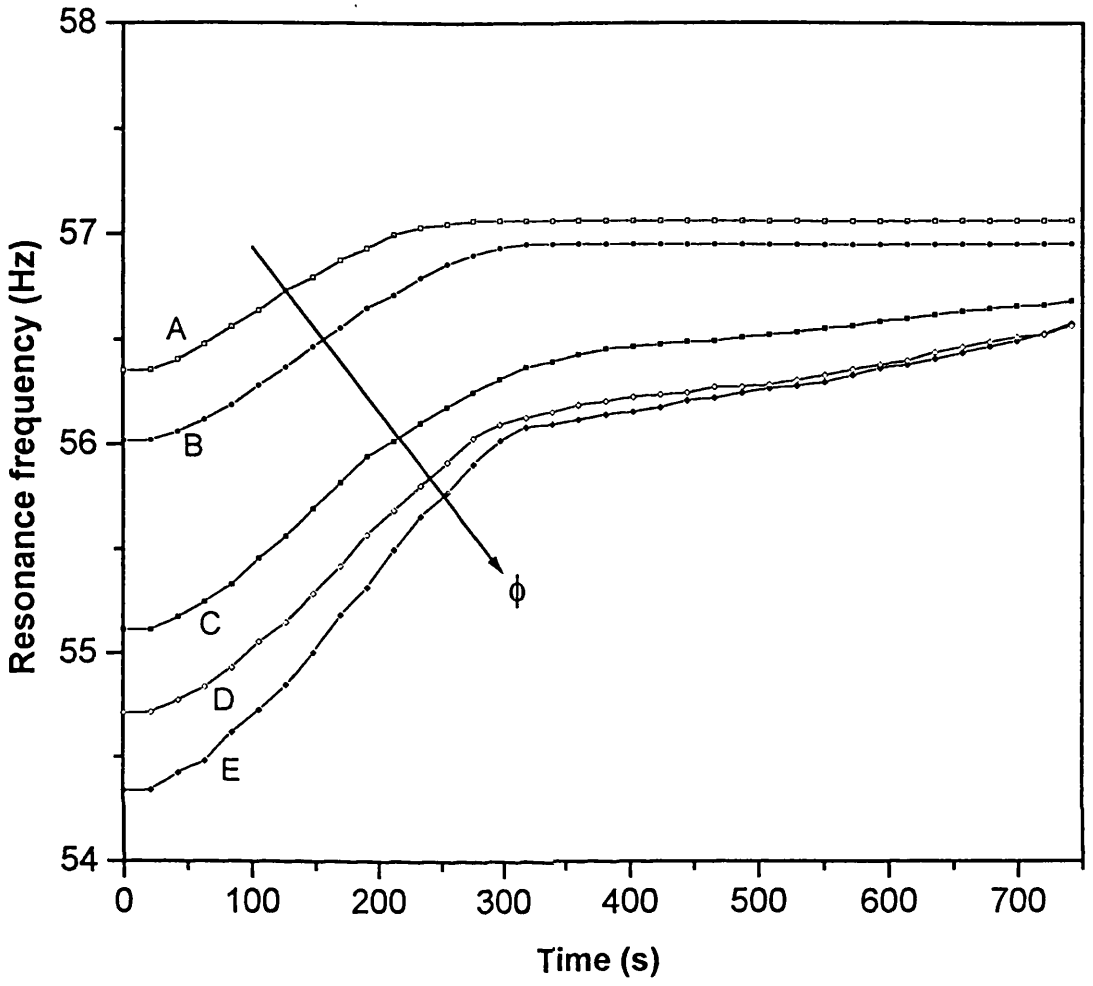

Figure 8.1
The variation of resonance frequency with time at reed position 1 (699 mm from top of settling zone) for polydisperse 55 - 100 μm glass ballotini spheres (density 2550 kgm^{-3}) settling in water @ 17 °C at various initial suspended solids volume concentrations, ϕ: curve A, ϕ = 1.75 %; curve B, ϕ = 2.01 %; curve C, ϕ = 2.35 %; curve D, ϕ = 2.56 % and curve E, ϕ = 2.81 %

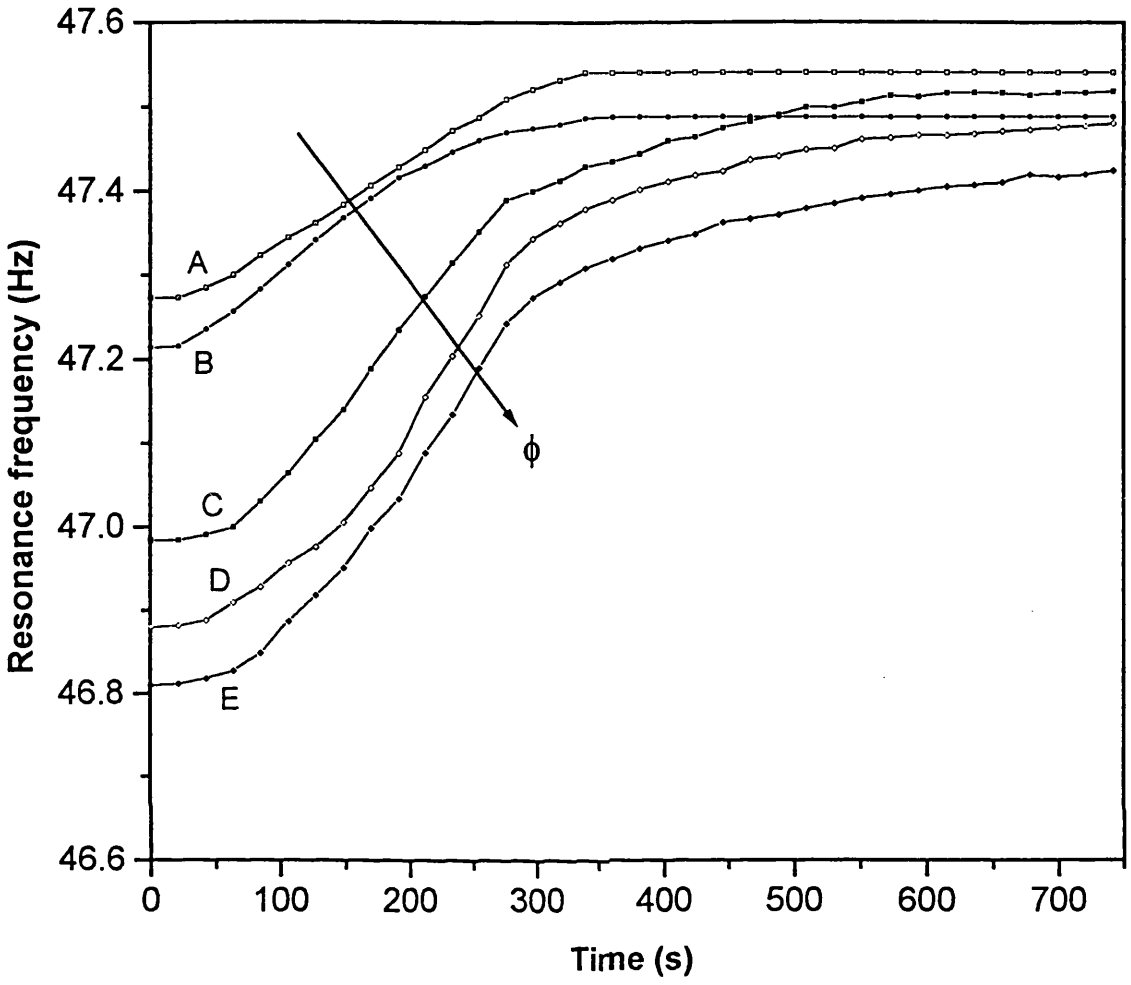

Figure 8.2
The variation of resonance frequency with time at reed position 2 (900 mm from top of settling zone) for polydisperse 55 - 100 μm glass ballotini spheres (density 2550 kgm^{-3}) settling in water @ 17 °C at various initial suspended solids volume concentrations, ϕ: curve A, ϕ = 1.75 %; curve B, ϕ = 2.01 %; curve C, ϕ = 2.35 %; curve D, ϕ = 2.56 % and curve E, ϕ = 2.81 %

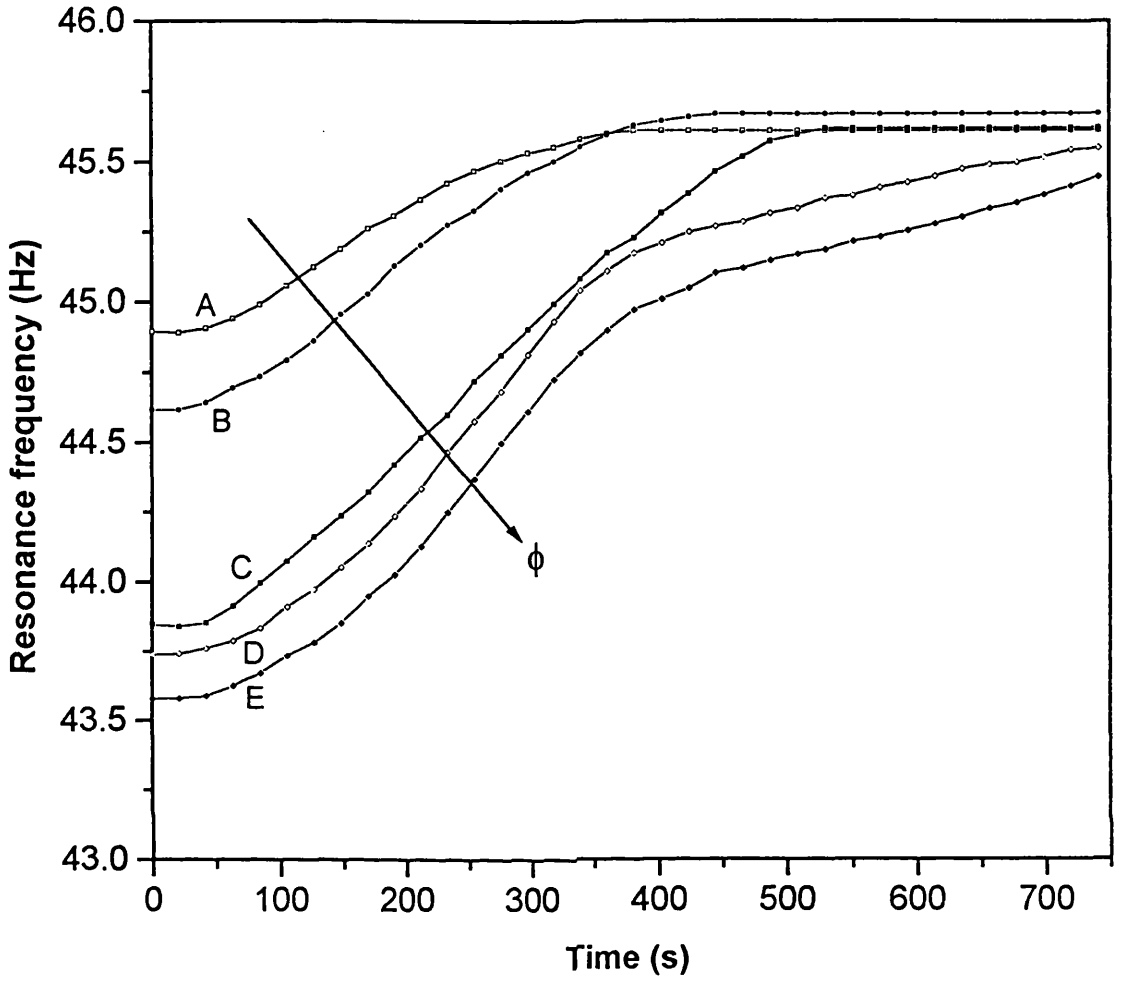

Figure 8.3
The variation of resonance frequency with time at reed position 3 (1096 mm from top of settling zone) for polydisperse 55 - 100 μm glass ballotini spheres (density 2550 kgm^{-3}) settling in water @ 17 °C at various initial suspended solids volume concentrations, ϕ: curve A, ϕ = 1.75 %; curve B, ϕ = 2.01 %; curve C, ϕ = 2.35 %; curve D, ϕ = 2.56 % and curve E, ϕ = 2.81 %

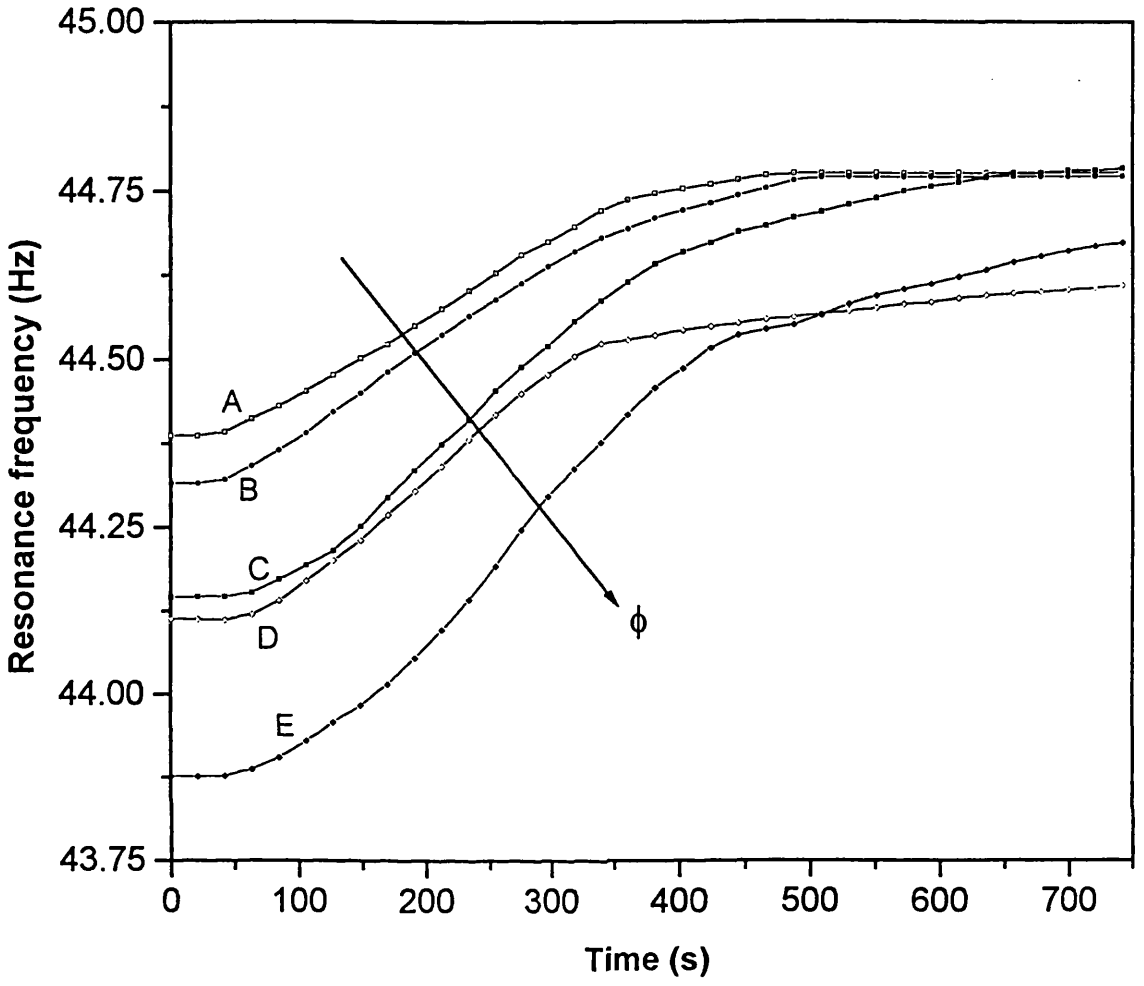

Figure 8.4

The variation of resonance frequency with time at reed position 4 (1296 mm from top of settling zone) for polydisperse 55 - 100 μm glass ballotini spheres (density 2550 kgm^{-3}) settling in water @ 17 °C at various initial suspended solids volume concentrations, ϕ: curve A, ϕ = 1.75 %; curve B, ϕ = 2.01 %; curve C, ϕ = 2.35 %; curve D, ϕ = 2.56 % and curve E, ϕ = 2.81 %

ii) The switching off of the circulation pump (time zero) does not immediately lead to a change in the resonance frequency but that rather there is a small time delay before this occurs. This is probably due to the finite amount of time required for the disturbance wave produced as a result of a change from steady state to unsteady state operation to propagate from the top of the settling zone to the position of each reed. This phenomenon is analysed further in section 8.6.1.

iii) At any given time and initial solids volume concentration, the resonance frequency decreases with distance between the reed position and the top of the settling zone. This is consistent with the fact that resonance frequency decreases with increase in the hydrodynamic head.

iv) In contrast to the data obtained in conjunction with the monodisperse 200 - 212 μm suspensions (see figures 7.14 - 7.17, chapter 7), the variation of resonance frequency with time in the transition region is non-linear. This is due to the size segregation and hence differential settling rate of the polydisperse sample. Accordingly, the rate of change of resonance frequency with time goes through a maximum following which it starts to decrease once the faster settling particles have left the reed sensing volume. As the remaining fine particles continue to settle past the reed the system response gradually tends to the clear liquid resonance frequency (for example 57 Hz in the case of reed 1; figure 8.1). In contrast to the monodisperse 200 - 212 μm suspensions (see figure 7.14, chapter 7), these size-dependent differential settling effects result in diffuse interfaces thus making a direct estimation of the breakthrough time, Δt_b by visual observation more difficult. Accordingly, such data for all polydisperse systems employed in this study will be more accurately extracted from subsequently derived solids flux profiles (see later).

Figures 8.5 - 8.8, show resonance frequency/time profiles for 80 - 115 μm size fraction glass ballotini/water suspensions obtained in conjunction with reeds 1 - 4 respectively. The trends in the data are similar to those for the slightly more

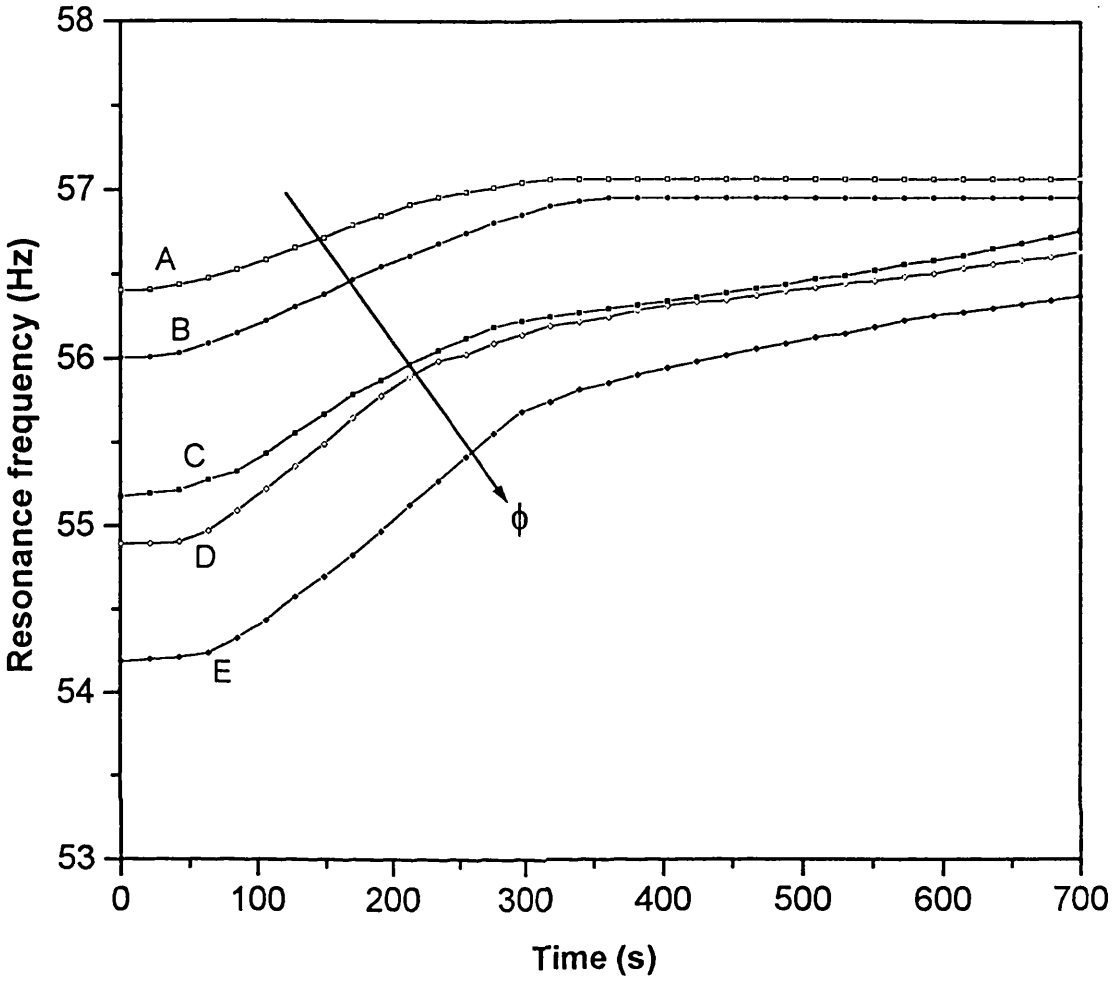

Figure 8.5
The variation of resonance frequency with time at reed position 1 (699 mm from top of settling zone) for polydisperse 80 - 115 μm glass ballotini spheres (density 2550 kgm^{-3}) settling in water @ 17 °C at various initial suspended solids volume concentrations, ϕ: curve A, ϕ = 1.75 %; curve B, ϕ = 2.01 %; curve C, ϕ = 2.35 %; curve D, ϕ = 2.56 % and curve E, ϕ = 2.81 %

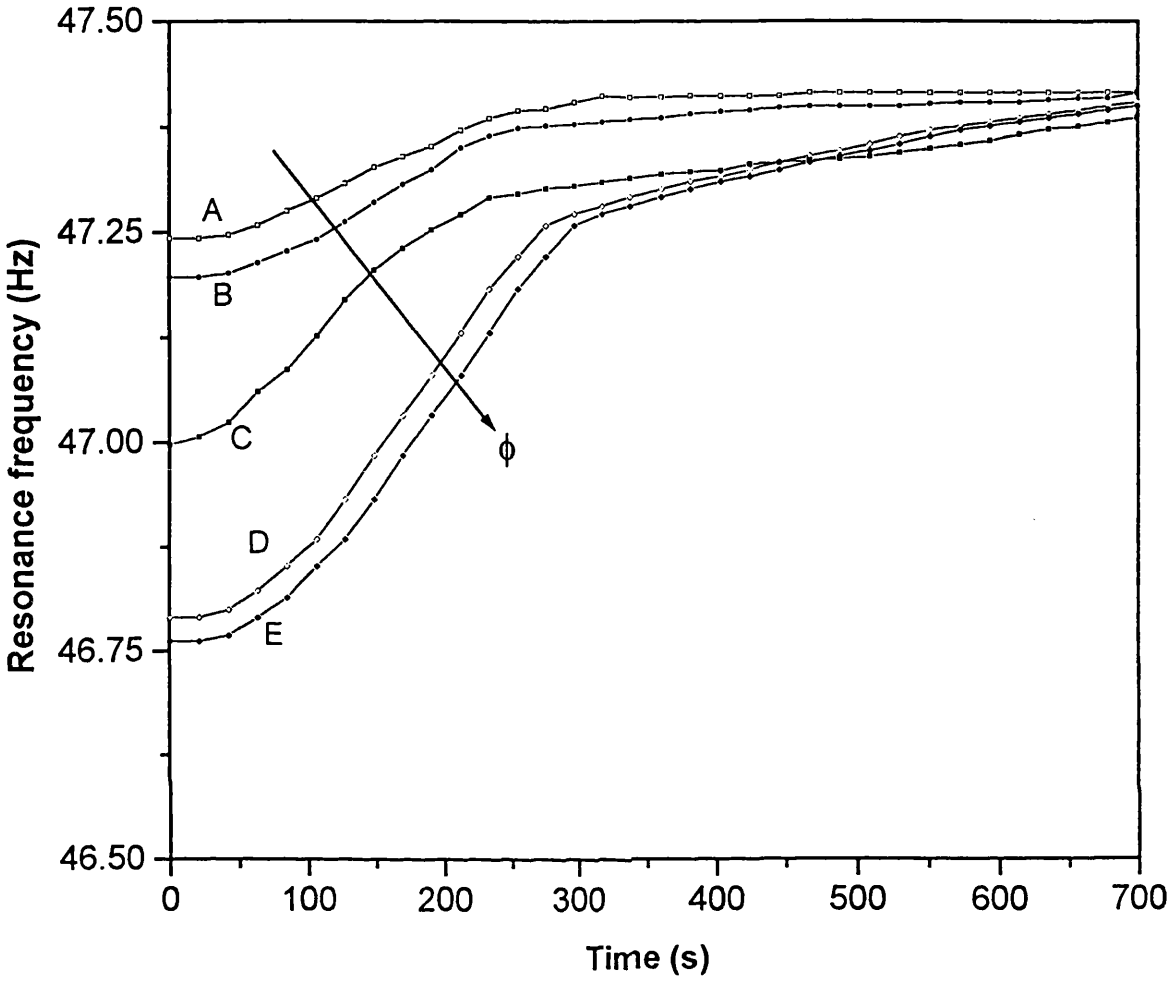

Figure 8.6

The variation of resonance frequency with time at reed position 2 (900 mm from top of settling zone) for polydisperse 80 - 115 μm glass ballotini spheres (density 2550 kgm^{-3}) settling in water @ 17 °C at various initial suspended solids volume concentrations, ϕ: curve A, ϕ = 1.75 %; curve B, ϕ = 2.01 %; curve C, ϕ = 2.35 %; curve D, ϕ = 2.56 % and curve E, ϕ = 2.81 %

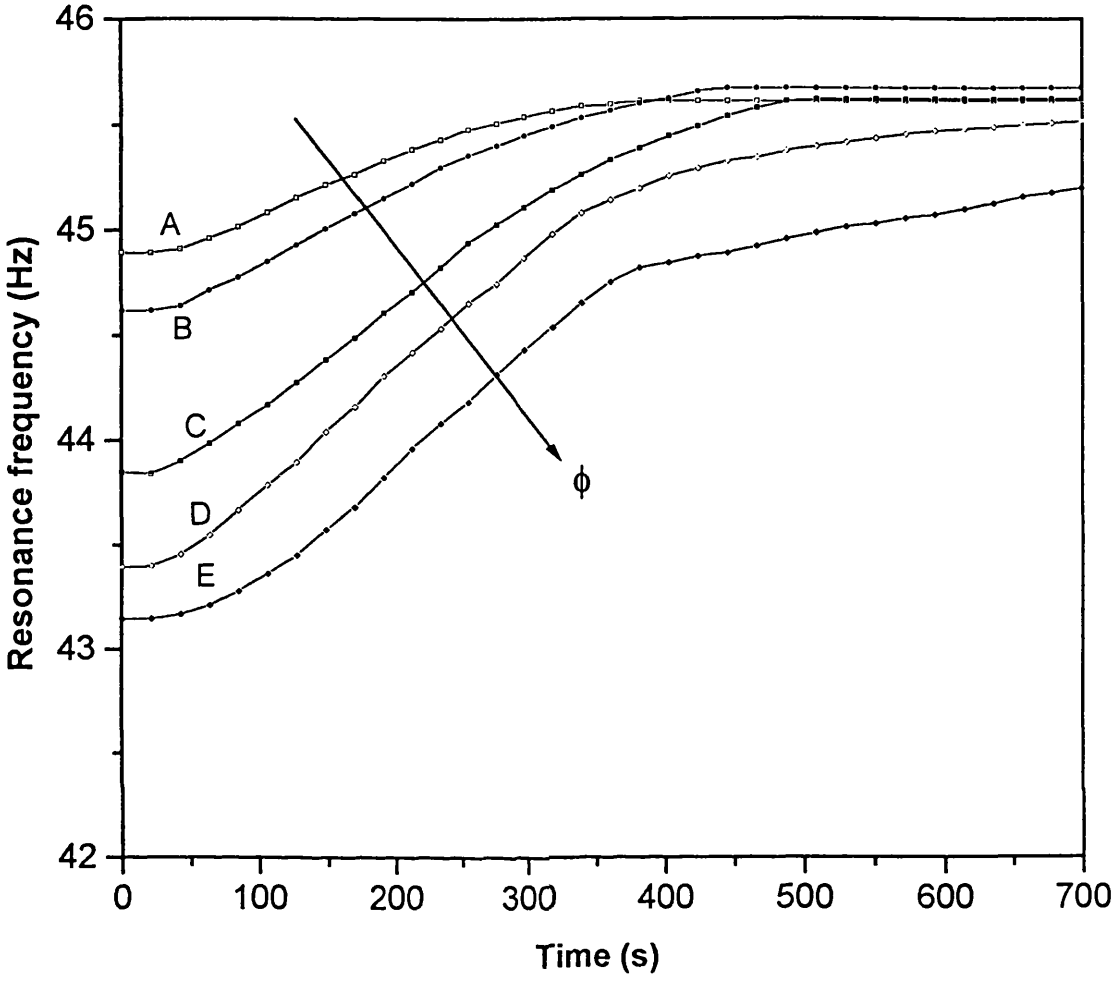

Figure 8.7
The variation of resonance frequency with time at reed position 3 (1096 mm from top of settling zone) for polydisperse 80 - 115 μm glass ballotini spheres (density 2550 kgm^{-3}) settling in water @ 17 °C at various initial suspended solids volume concentrations, ϕ: curve A, ϕ = 1.75 %; curve B, ϕ = 2.01 %; curve C, ϕ = 2.35 %; curve D, ϕ = 2.56 % and curve E, ϕ = 2.81 %

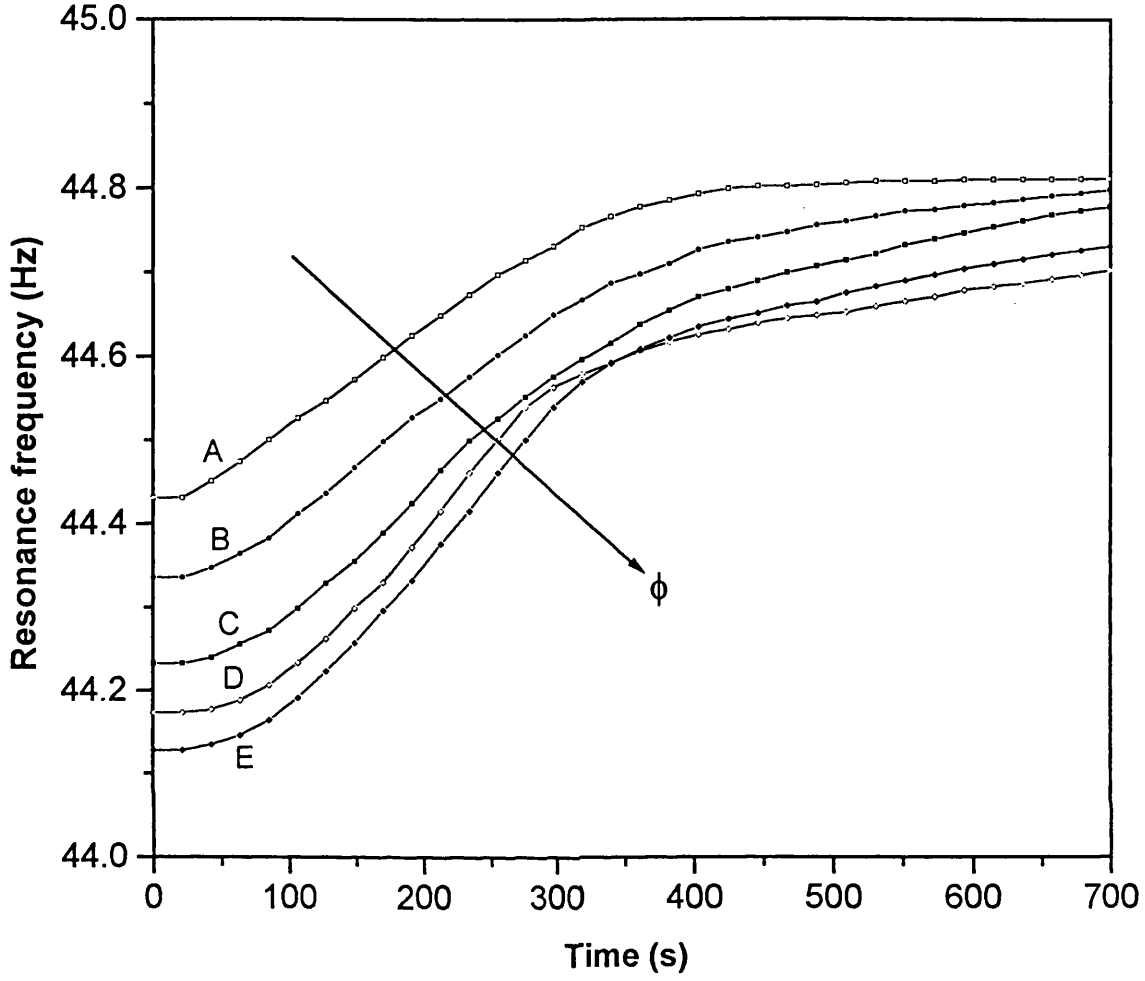

Figure 8.8
The variation of resonance frequency with time at reed position 4 (1296 mm from top of settling zone) for polydisperse 80 - 115 μm glass ballotini spheres (density 2550 kgm^{-3}) settling in water @ 17 °C at various initial suspended solids volume concentrations, ϕ: curve A, ϕ = 1.75 %; curve B, ϕ = 2.01 %; curve C, ϕ = 2.35 %; curve D, ϕ = 2.56 % and curve E, ϕ = 2.81 %

polydisperse (wider size distribution) 55 - 100 μm size fraction. However, for the same reed and solids volume concentration, there is a slight decrease in the breakthrough time (see later) and hence a faster settling rate in the case of the 80 - 115 μm sample due to its larger mean diameter (96.4 μm as compared with 77.5 μm).

Figures 8.9 - 8.12 show resonance frequency/time profiles obtained from reeds 1 - 4 respectively, for 90 - 135 μm size fraction glass ballotini suspensions. These systems have the same degree of polydispersity (range 45 μm) as the 55 - 100 μm size fraction (figures 8.1 - 8.4). However, compared to the behaviour of the 80 - 115 μm size fraction (figures 8.5 - 8.8), settling rates for these suspensions are clearly higher as reed breakthrough times decrease by ca. 100 s for the same initial solids volume concentrations. This is probably due to the larger mean particle diameter ($\overline{d}_p$ = 109.3 μm) of the 90 - 135 μm size fraction.

Figures 8.13 - 8.16 show respective resonance frequency/time profiles obtained from reeds 1 - 4 in conjunction with 100 - 200 μm size fraction glass ballotini suspensions. Compared to all the preceding systems, these suspensions are highly polydisperse (range 100 μm, $\overline{d}_p$ = 149.7 μm). However, despite the wider particle size distribution, the resulting system response is characterised by well defined solids breakthrough times. This is somewhat unexpected and is probably due to the limited time available for size segregation to occur during sedimentation since overall settling rates are high.

8.2 The Effect of Particle Size

Figures 8.17 - 8.20 show the variation of the initial (time zero) resonance frequency with initial solids concentration for reeds 1 - 4 respectively in various size range polydisperse glass ballotini/water suspensions. The data are extracted from the resonance frequency profiles shown in figures 8.1 - 8.16 and relate to the well mixed suspensions just before the onset of the settling process. As it is clear the system response is independent of particle size and decreases in a linear manner with increase in solids volume concentration and hence the system bulk density.

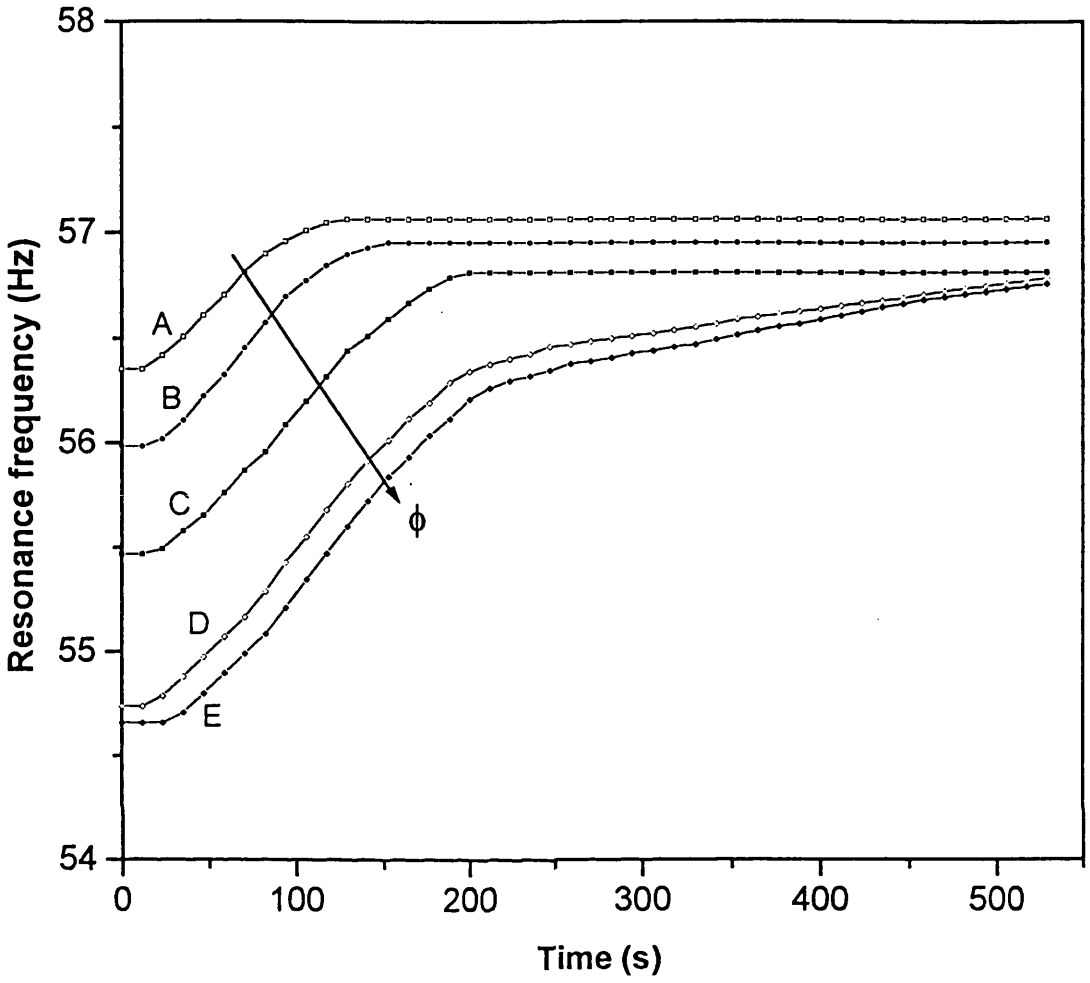

Figure 8.9
The variation of resonance frequency with time at reed position 1 (699 mm from top of settling zone) for polydisperse 90 - 135 μm glass ballotini spheres (density 2550 kgm^{-3}) settling in water @ 17 °C at various initial suspended solids volume concentrations, ϕ: curve A, ϕ = 1.75 %; curve B, ϕ = 2.01 %; curve C, ϕ = 2.35 %; curve D, ϕ = 2.56 % and curve E, ϕ = 2.81 %

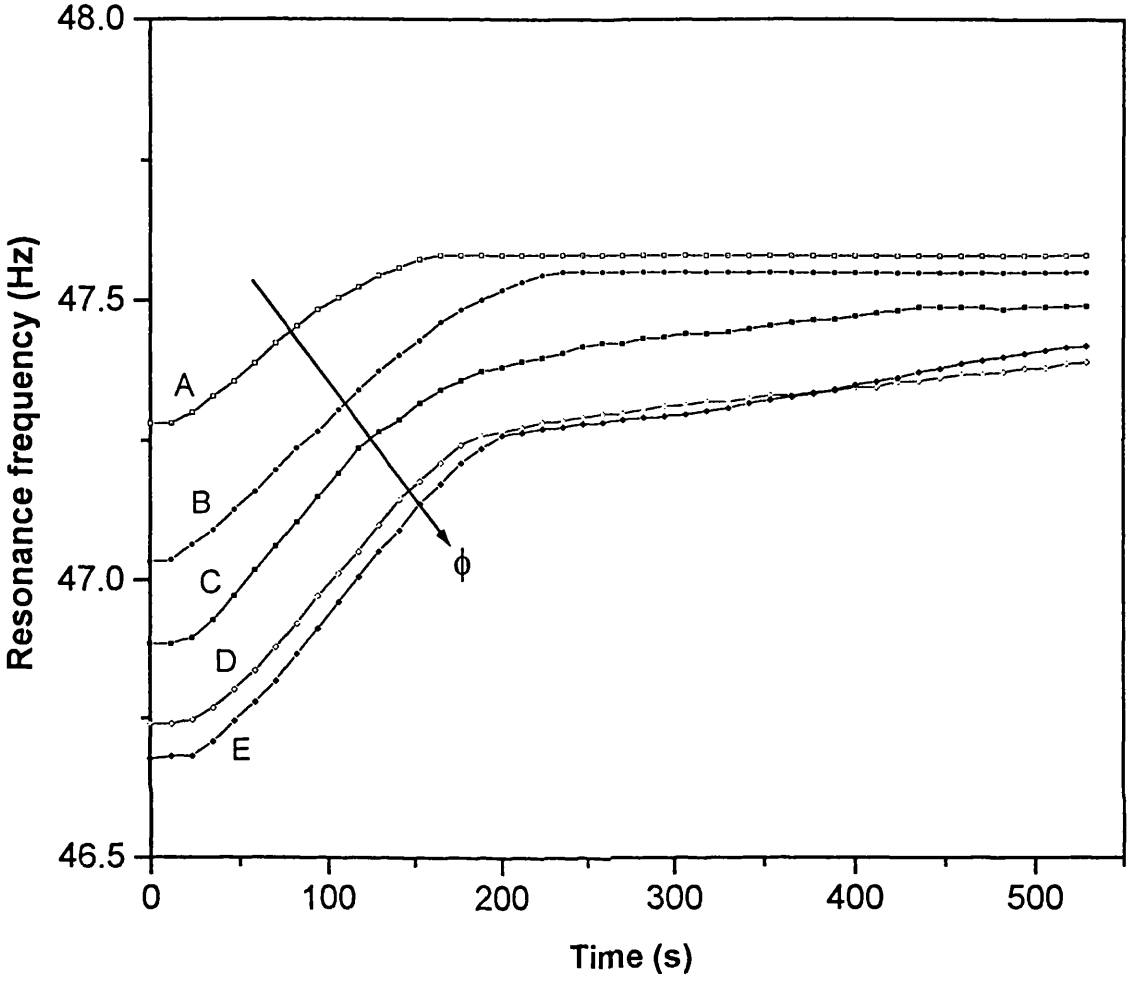

Figure 8.10

The variation of resonance frequency with time at reed position 2 (900 mm from top of settling zone) for polydisperse 90 - 135 μm glass ballotini spheres (density 2550 kgm^{-3}) settling in water @ 17 °C at various initial suspended solids volume concentrations, ϕ: curve A, ϕ = 1.75 %; curve B, ϕ = 2.01 %; curve C, ϕ = 2.35 %; curve D, ϕ = 2.56 % and curve E, ϕ = 2.81 %

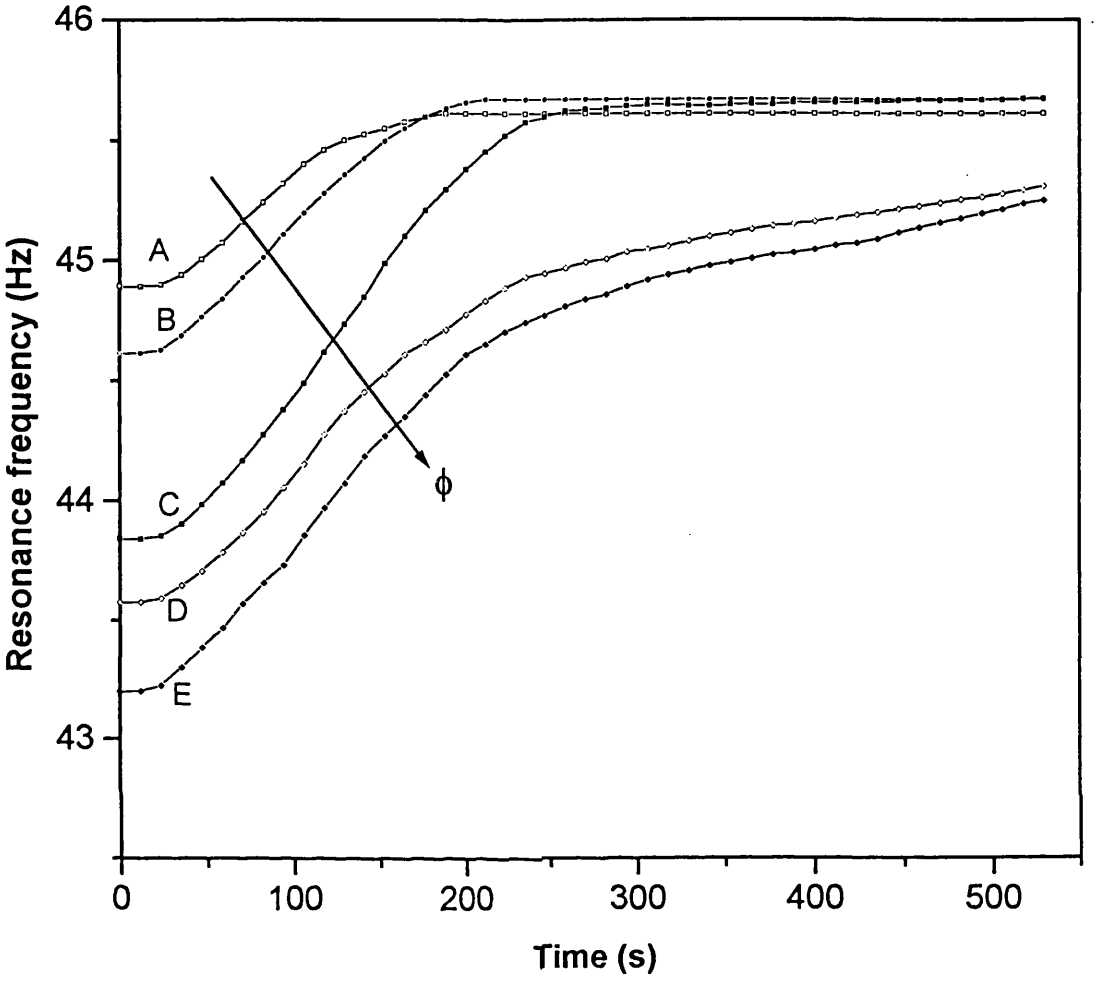

Figure 8.11

The variation of resonance frequency with time at reed position 3 (1096 mm from top of settling zone) for polydisperse 90 - 135 μm glass ballotini spheres (density 2550 kgm^{-3}) settling in water @ 17 °C at various initial suspended solids volume concentrations, ϕ: curve A, ϕ = 1.75 %; curve B, ϕ = 2.01 %; curve C, ϕ = 2.35 %; curve D, ϕ = 2.56 % and curve E, ϕ = 2.81 %

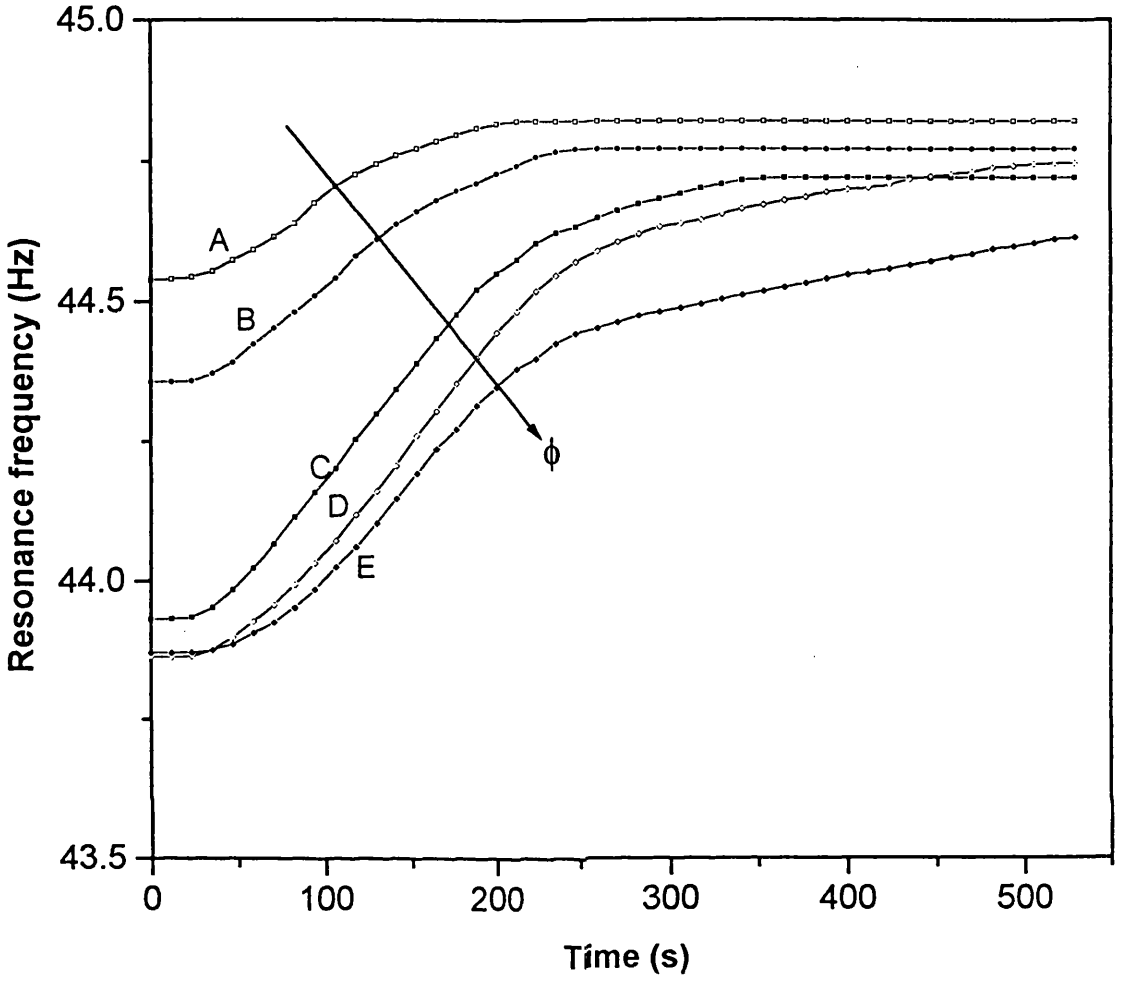

Figure 8.12
The variation of resonance frequency with time at reed position 4 (1296 mm from top of settling zone) for polydisperse 90 - 135 μm glass ballotini spheres (density 2550 kgm^{-3}) settling in water @ 17 °C at various initial suspended solids volume concentrations, ϕ: curve A, ϕ = 1.75 %; curve B, ϕ = 2.01 %; curve C, ϕ = 2.35 %; curve D, ϕ = 2.56 % and curve E, ϕ = 2.81 %

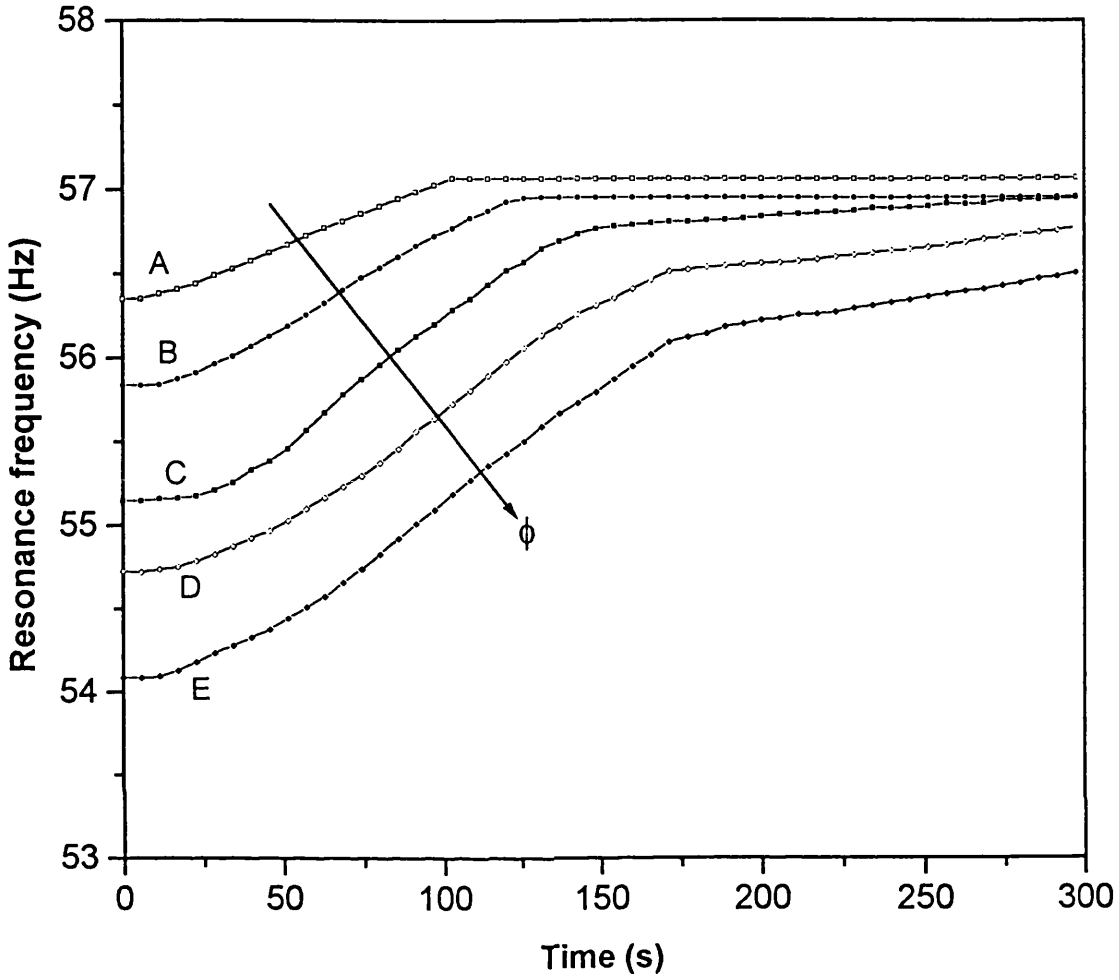

Figure 8.13
The variation of resonance frequency with time at reed position 1 (699 mm from top of settling zone) for polydisperse 100 - 200 μm glass ballotini spheres (density 2550 kgm^{-3}) settling in water @ 17 °C at various initial suspended solids volume concentrations, ϕ: curve A, ϕ = 1.75 %; curve B, ϕ = 2.01 %; curve C, ϕ = 2.35 %; curve D, ϕ = 2.56 % and curve E, ϕ = 2.81 %

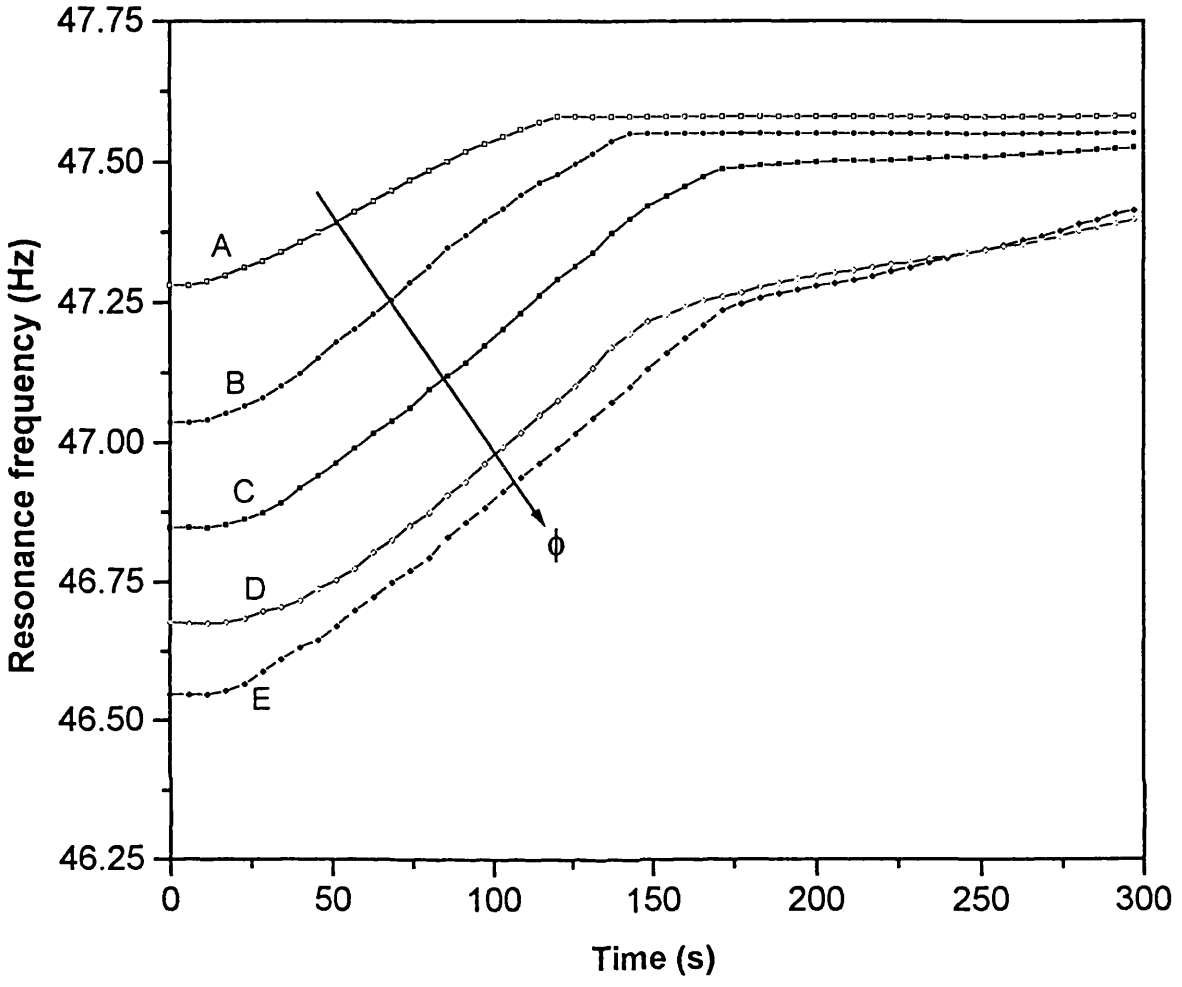

Figure 8.14

The variation of resonance frequency with time at reed position 2 (900 mm from top of settling zone) for polydisperse 100 - 200 μm glass ballotini spheres (density 2550 kgm^{-3}) settling in water @ 17 °C at various initial suspended solids volume concentrations, ϕ: curve A, ϕ = 1.75 %; curve B, ϕ = 2.01 %; curve C, ϕ = 2.35 %; curve D, ϕ = 2.56 % and curve E, ϕ = 2.81 %

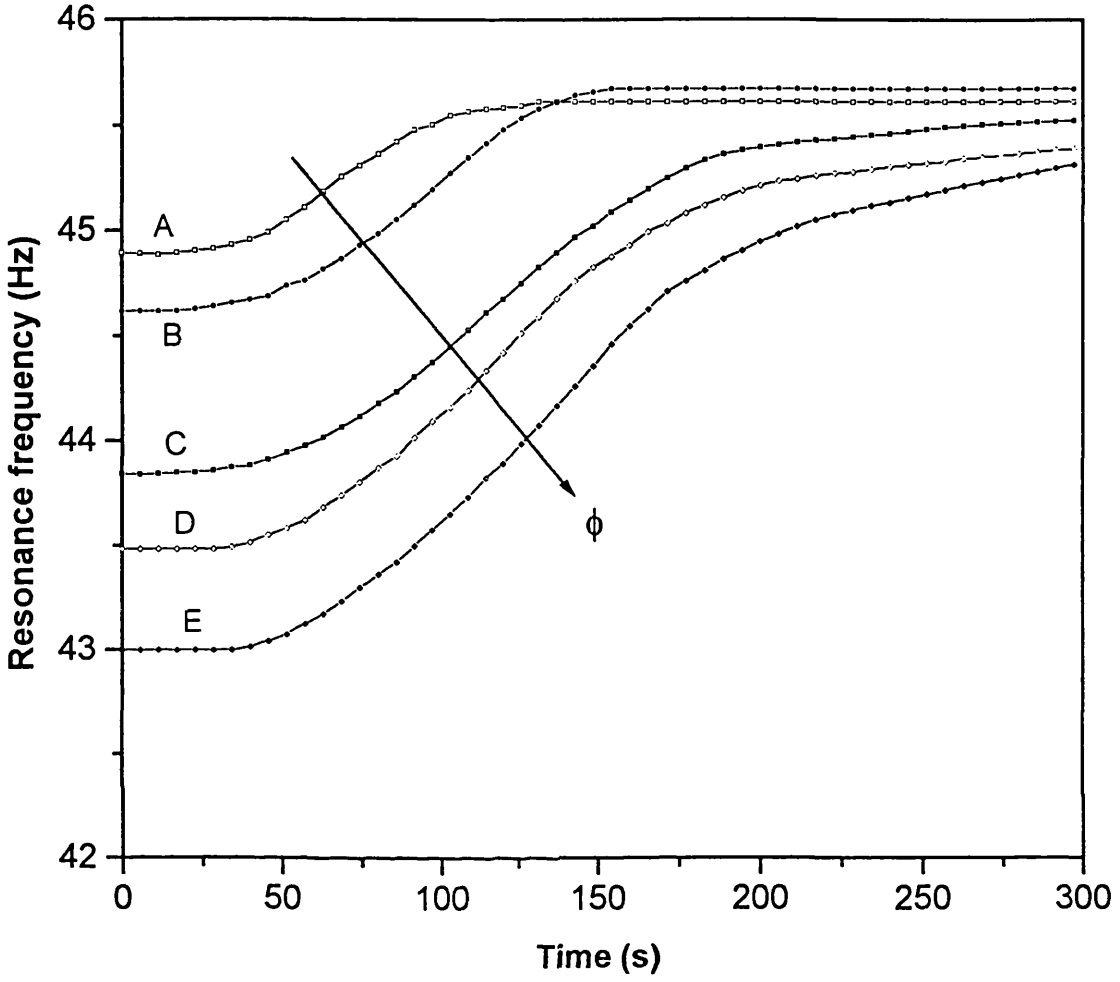

Figure 8.15
The variation of resonance frequency with time at reed position 3 (1096 mm from top of settling zone) for polydisperse 100 - 200 μm glass ballotini spheres (density 2550 kgm^{-3}) settling in water @ 17 °C at various initial suspended solids volume concentrations, ϕ: curve A, ϕ = 1.75 %; curve B, ϕ = 2.01 %; curve C, ϕ = 2.35 %; curve D, ϕ = 2.56 % and curve E, ϕ = 2.81 %

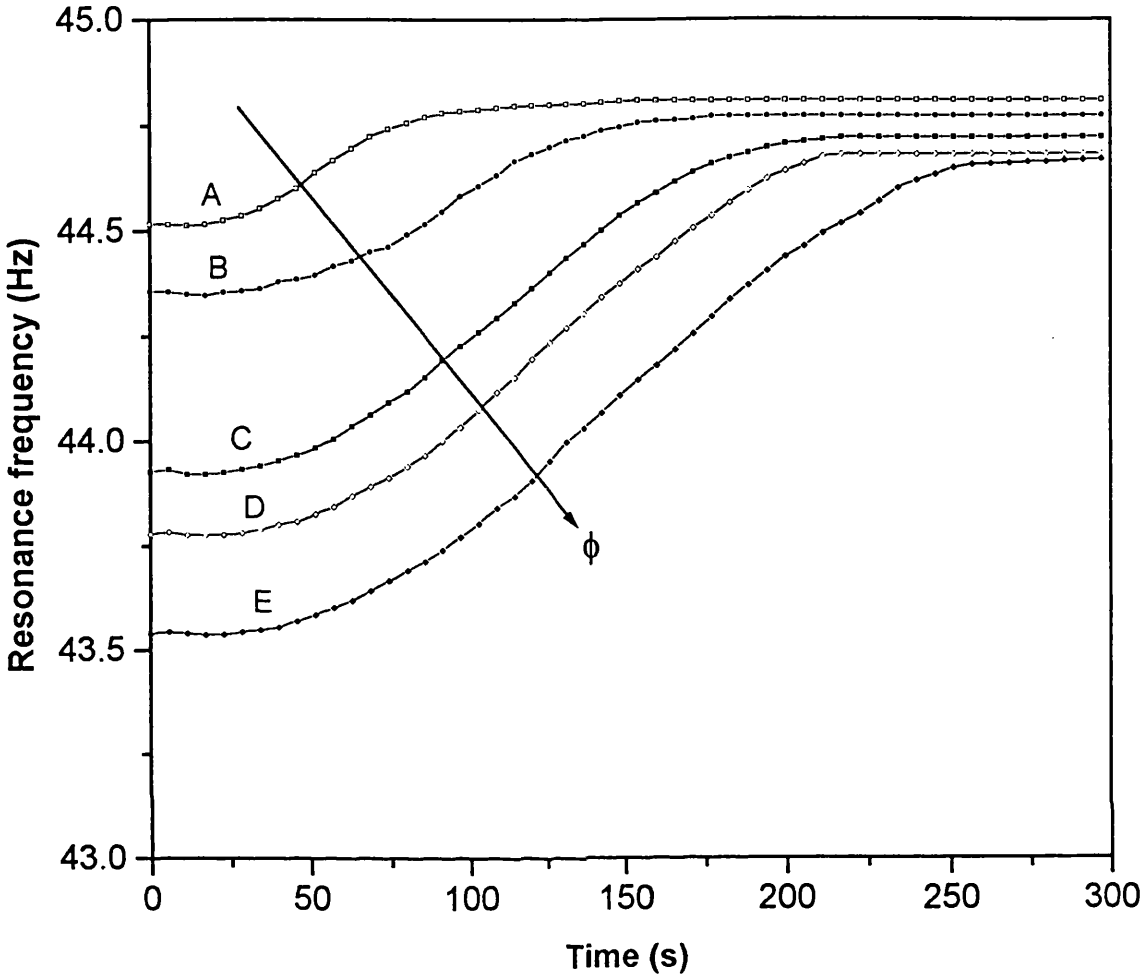

Figure 8.16

The variation of resonance frequency with time at reed position 4 (1296 mm from top of settling zone) for polydisperse 100 - 200 μm glass ballotini spheres (density 2550 kgm^{-3}) settling in water @ 17 °C at various initial suspended solids volume concentrations, ϕ: curve A, ϕ = 1.75 %; curve B, ϕ = 2.01 %; curve C, ϕ = 2.35 %; curve D, ϕ = 2.56 % and curve E, ϕ = 2.81 %

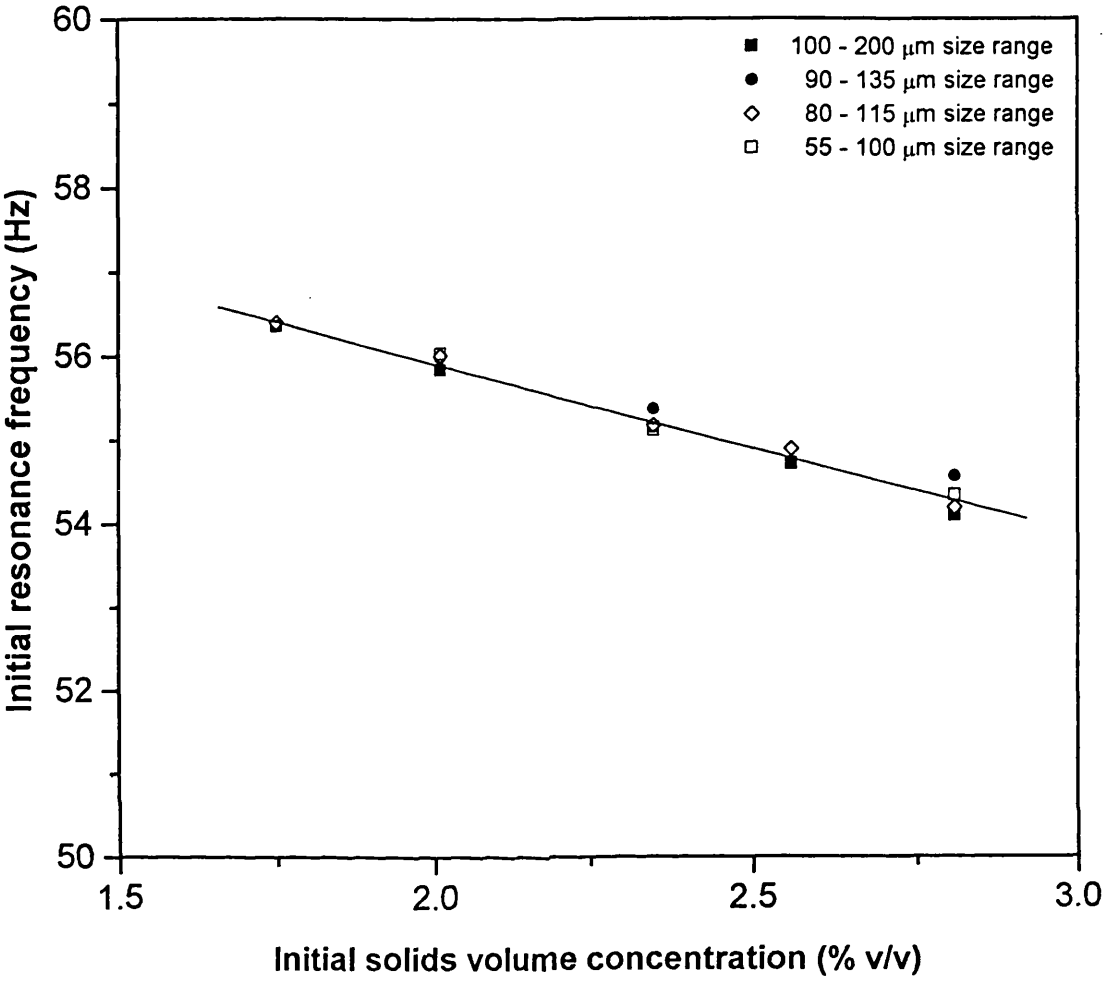

Figure 8.17
The variation of initial (time t = 0) resonance frequency with solids volume concentration at reed position 1 (699 mm from top of setting zone) for various polydisperse glass ballotini/water suspensions @ 17 °C. The data relates to uniformly mixed suspensions at the start of sedimentation.

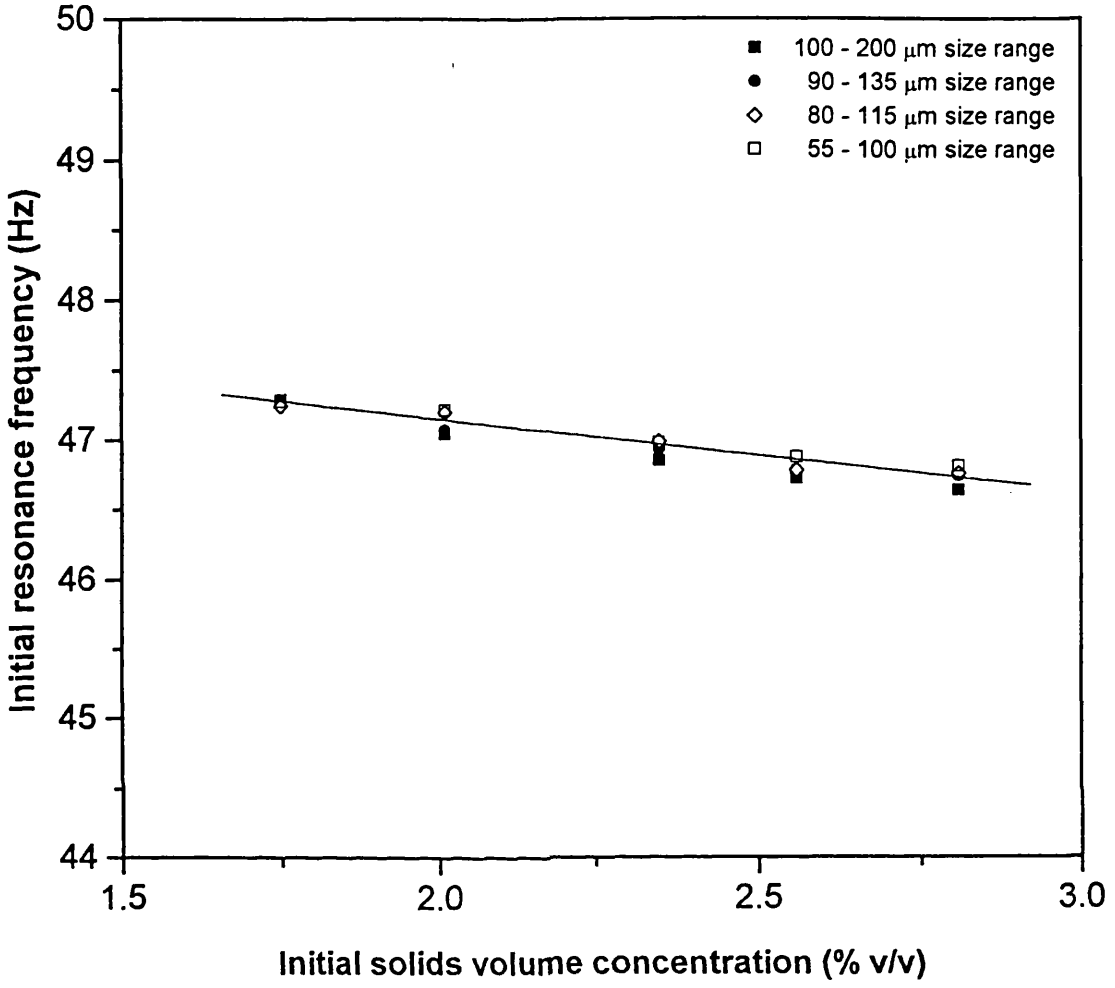

Figure 8.18
The variation of initial (time t = 0) resonance frequency with solids volume concentration at reed position 2 (900 mm from top of setting zone) for various polydisperse glass ballotini/water suspensions @ 17 °C. The data relates to uniformly mixed suspensions at the start of sedimentation.

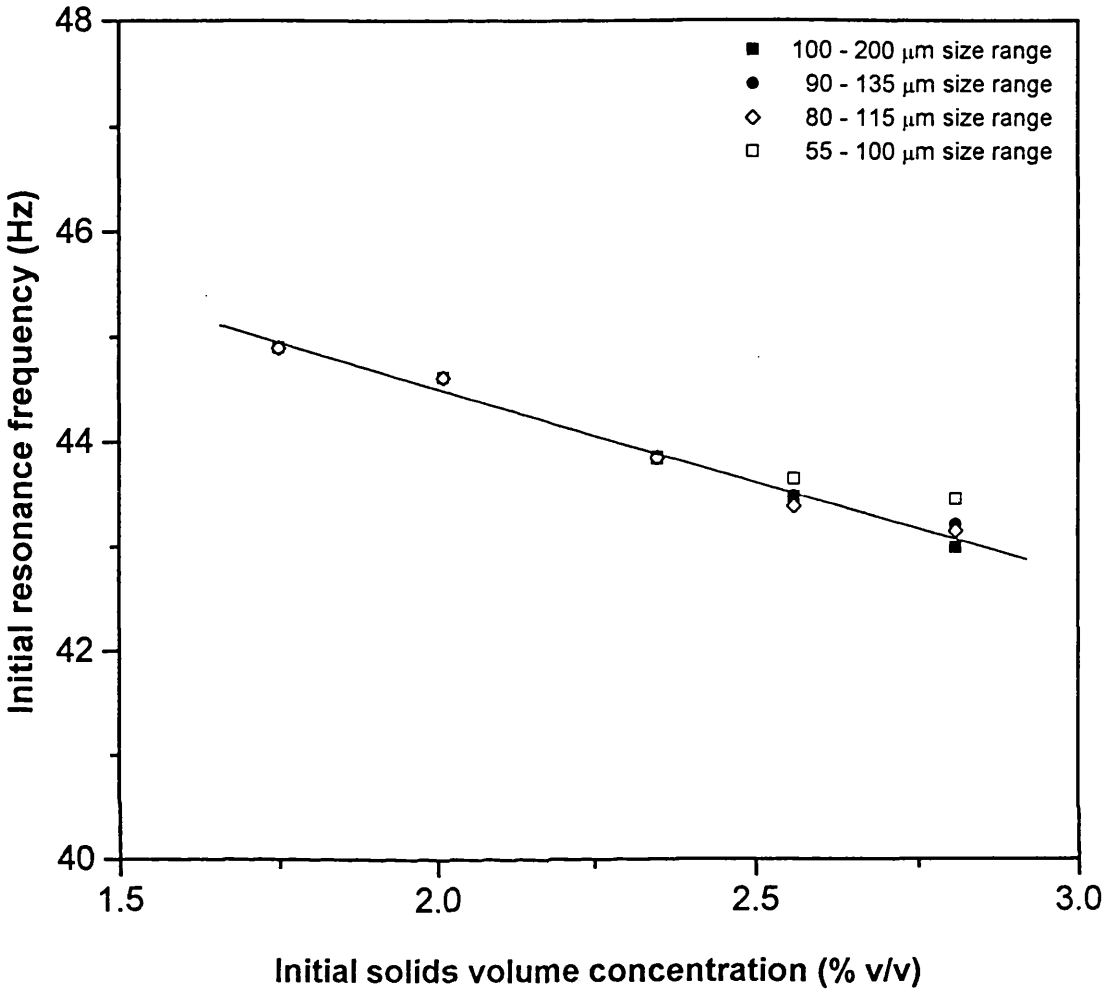

Figure 8.19
The variation of initial (time t = 0) resonance frequency with solids volume concentration at reed position 3 (1096 mm from top of setting zone) for various polydisperse glass ballotini/water suspensions @ 17 °C. The data relates to uniformly mixed suspensions at the start of sedimentation.

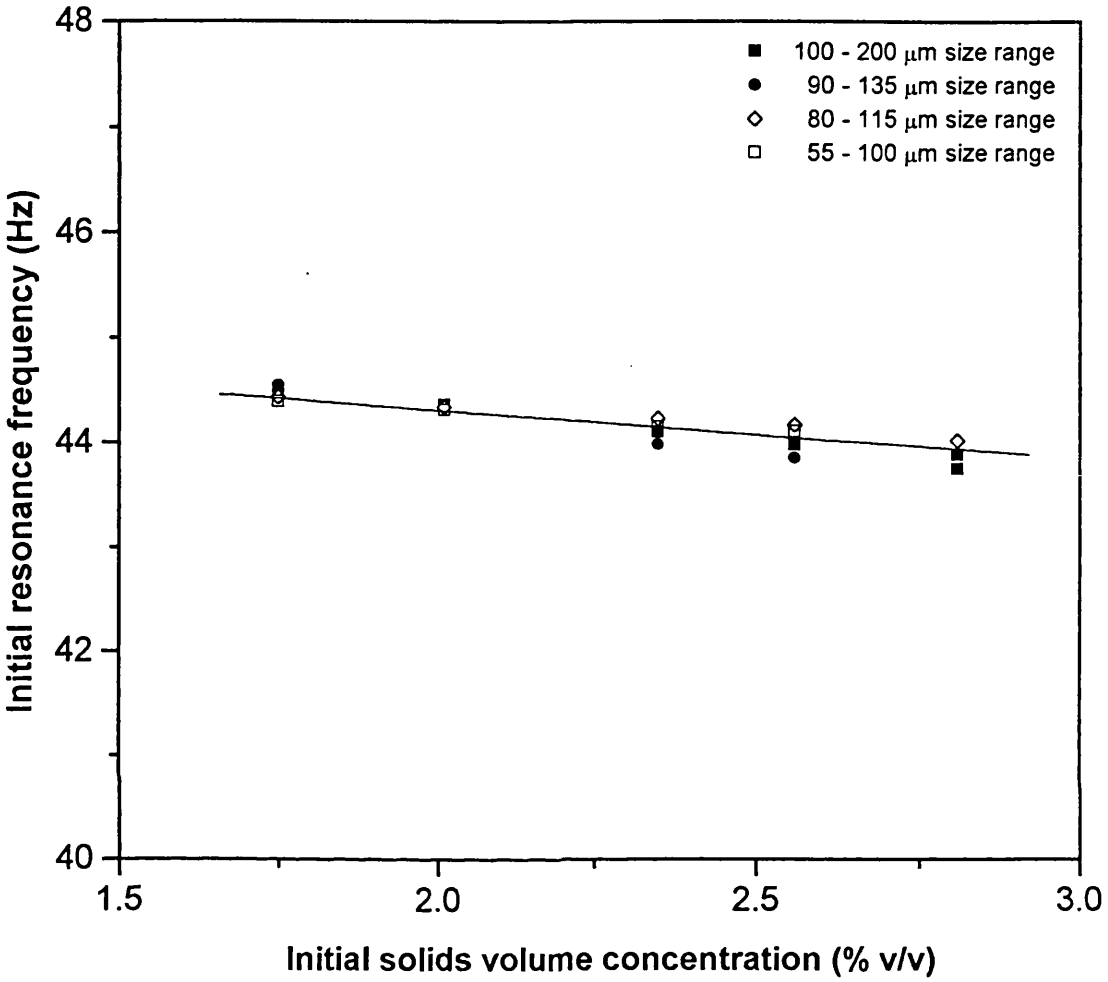

Figure 8.20
The variation of initial (time t = 0) resonance frequency with solids volume concentration at reed position 4 (1296 mm from top of setting zone) for various polydisperse glass ballotini/water suspensions @ 17 °C. The data relates to uniformly mixed suspensions at the start of sedimentation.

The data in figures 8.17 - 8.20 may therefore serve as calibration lines for the subsequent determination of solids concentration from a knowledge of the resonance frequency. This is of course provided that the bulk viscosity of the system does not affect the resonance frequency (see figures 7.10 - 7.12, chapter 7).

8.3 Sedimentation Kinetic Data

Figure 8.21 shows the variation of the rate of change of resonance frequency with time for polydisperse 55 - 100 μm glass ballotini spheres settling in water at 17 °C at various initial suspended solids volume concentrations. The data relate to the system response for reed 1 and is obtained by fitting ninth degree polynomials to the resonance frequency versus time profiles shown in figure 8.1, taking their first derivatives and plotting the result versus time. Figures 8.22 - 8.24 respectively show the corresponding data obtained using reeds 2 - 4. Table 8.1 shows the fitting equations as well as the corresponding correlation coefficients.

Referring to figures 8.21 - 8.24, it is clear that for a given initial solids volume concentration, the settling rate starts from a low, effectively zero value, goes through a peak and then reverts back to zero. This type of behaviour is highly indicative of size segregation of the settling particles in the test suspension. Also, it is clear that the maximum settling rate increases with increase in solids concentration.

Considering curve A in figure 8.21 as an example, it is clear that the sensing volume above reed 1 contains no particles after ca. 340 s (breakthrough time) since the rate of change of resonance frequency is zero. The reed is exposed to the clear liquid for which there is no further change in the resonance frequency. As before, the breakthrough time increases with the initial solids concentration (see curves B - E). This is accompanied by a more diffuse suspension-clear liquid interface as confirmed by direct visual observation of the settling zone during experiments.

It is interesting to note that as the sensing zone moves away from the top of the settling zone (see the response for reeds 1 - 4, figures 8.21 - 8.24), the peaks of the

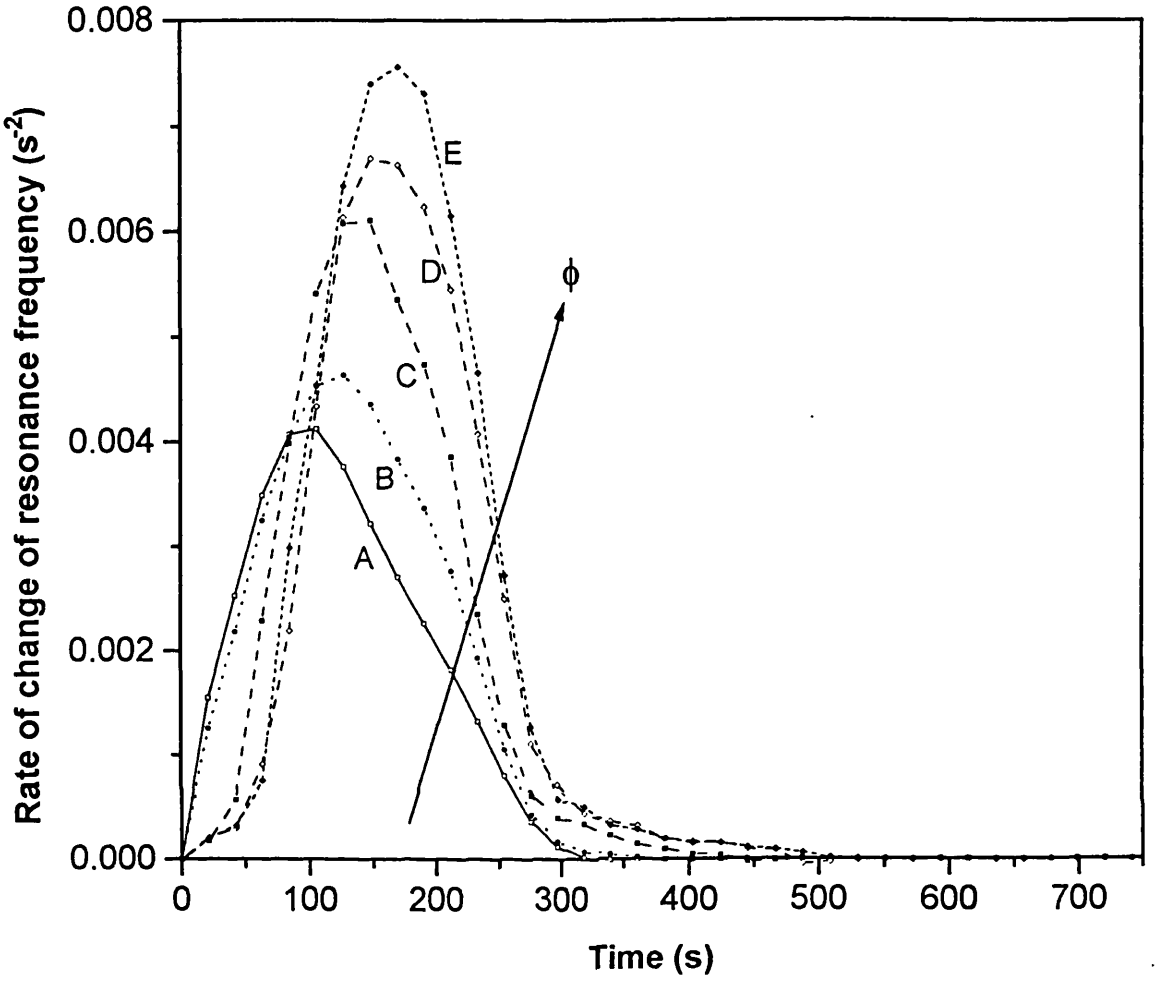

Figure 8.21

The variation of rate of change of resonance frequency with time at reed position 1 (699 mm from top of settling zone) for polydisperse 55 - 100 μm glass ballotini spheres (density 2550 kgm^{-3}) settling in water @ 17 °C at various initial suspended solids volume concentrations, ϕ: curve A, ϕ = 1.75 %; curve B, ϕ = 2.01 %; curve C, ϕ = 2.35 %; curve D, ϕ = 2.56 % and curve E, ϕ = 2.81 %

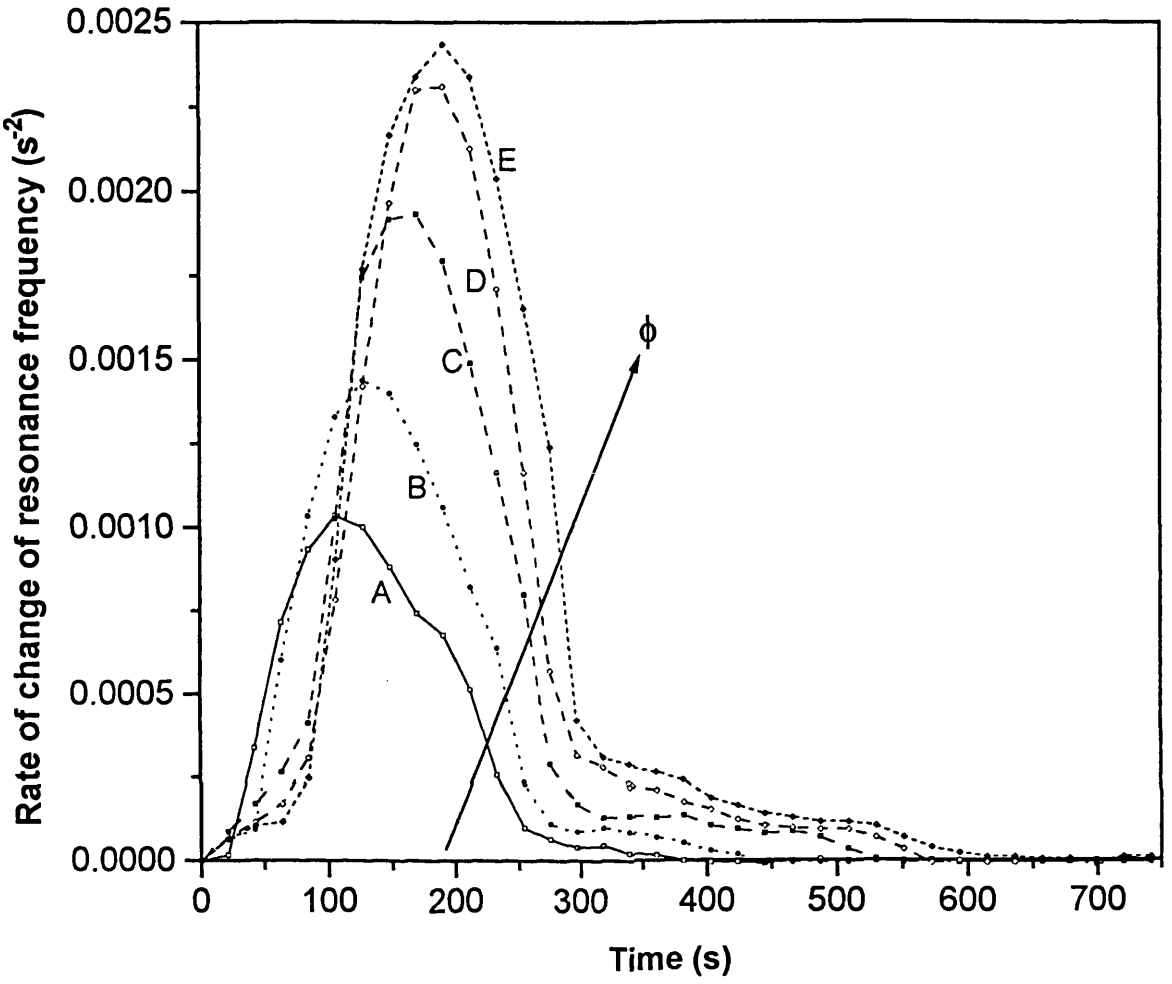

Figure 8.22
The variation of rate of change of resonance frequency with time at reed position 2 (900 mm from top of settling zone) for polydisperse 55 - 100 μm glass ballotini spheres (density 2550 kgm^{-3}) settling in water @ 17 °C at various initial suspended solids volume concentrations, ϕ: curve A, ϕ = 1.75 %; curve B, ϕ = 2.01 %; curve C, ϕ = 2.35 %; curve D, ϕ = 2.56 % and curve E, ϕ = 2.81 %

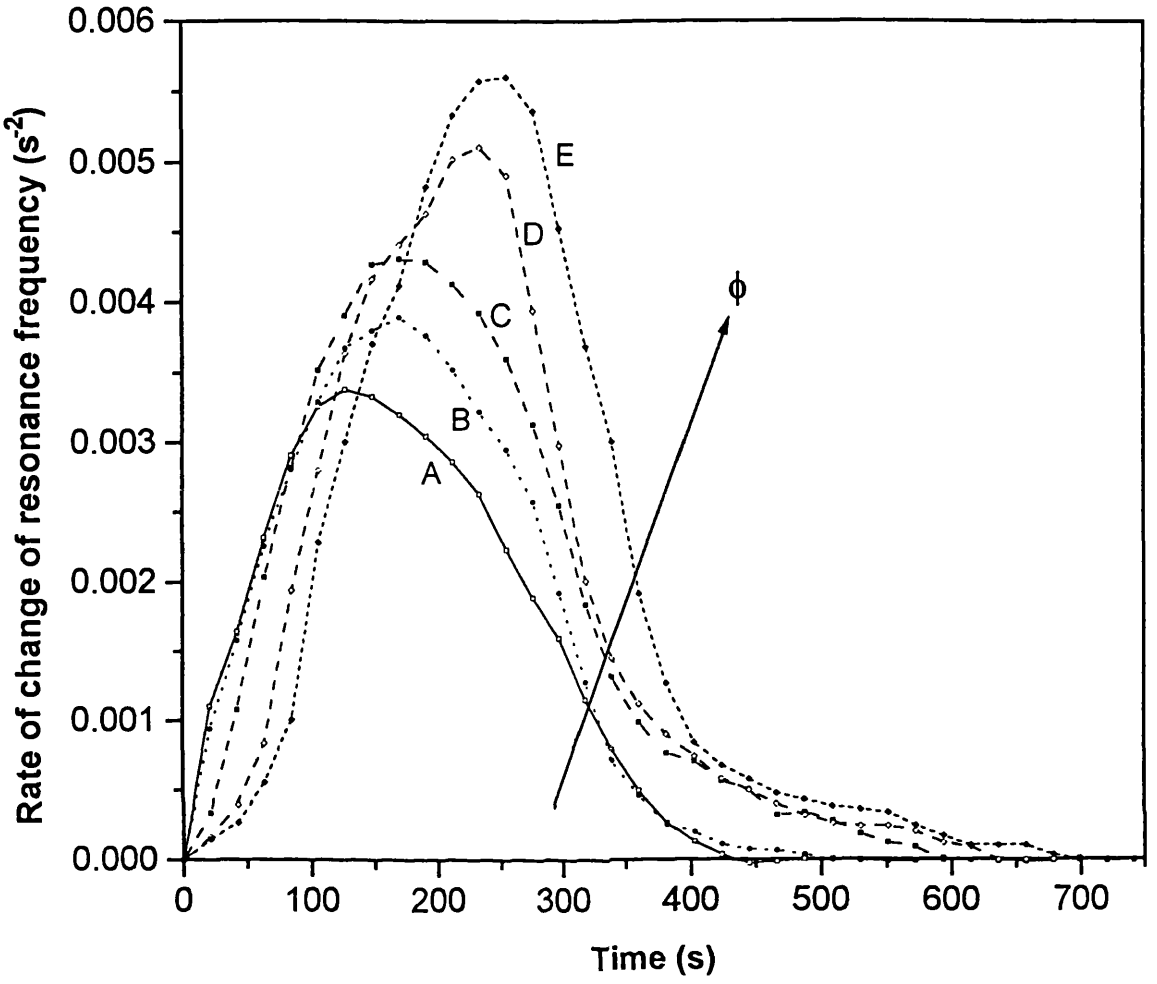

Figure 8.23

The variation of rate of change of resonance frequency with time at reed position 3 (1096 mm from top of settling zone) for polydisperse 55 - 100 μm glass ballotini spheres (density 2550 kgm^{-3}) settling in water @ 17 °C at various initial suspended solids volume concentrations, ϕ: curve A, ϕ = 1.75 %; curve B, ϕ = 2.01 %; curve C, ϕ = 2.35 %; curve D, ϕ = 2.56 % and curve E, ϕ = 2.81 %

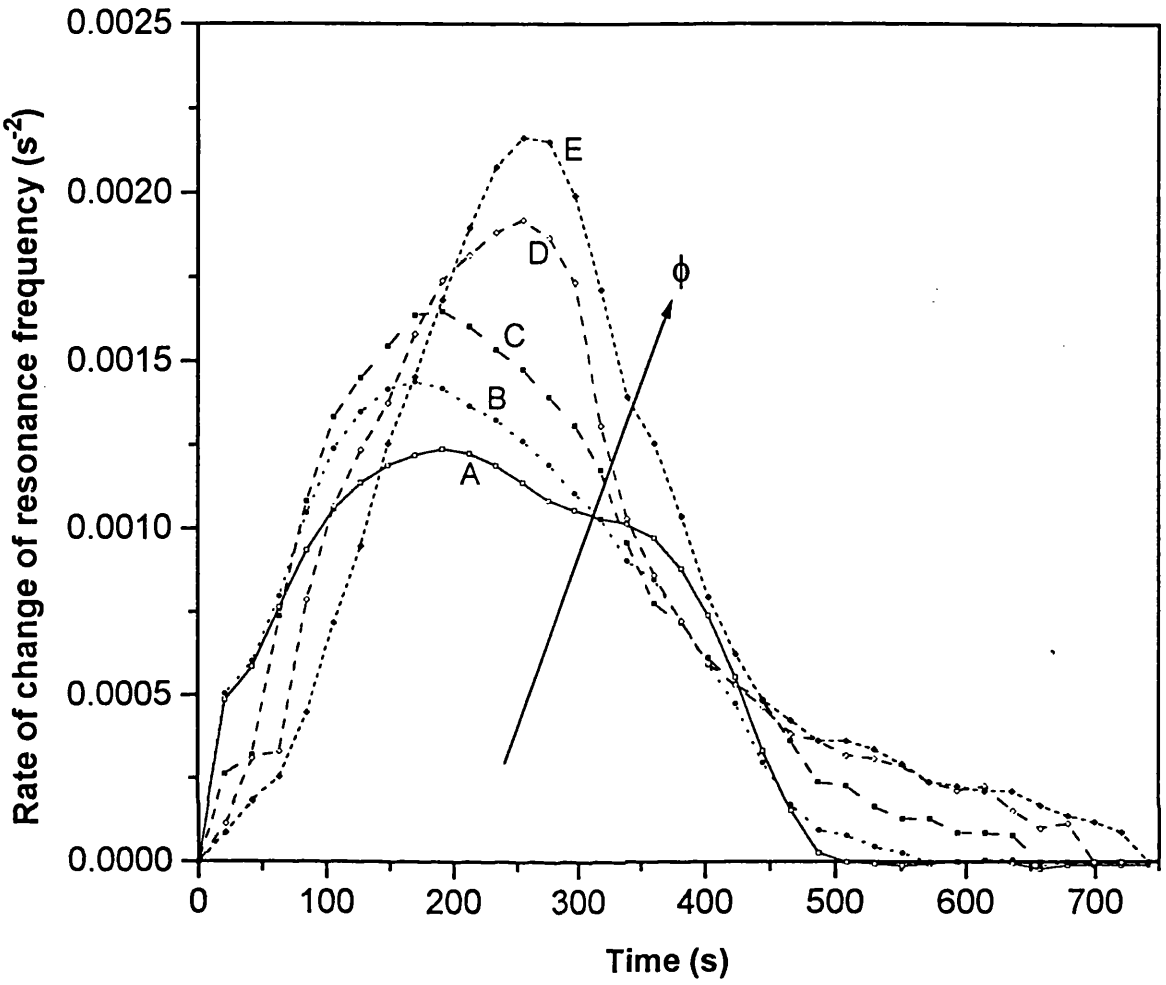

Figure 8.24

The variation of rate of change of resonance frequency with time at reed position 4 (1296 mm from top of settling zone) for polydisperse 55 - 100 μm glass ballotini spheres (density 2550 kgm^{-3}) settling in water @ 17 °C at various initial suspended solids volume concentrations, ϕ: curve A, ϕ = 1.75 %; curve B, ϕ = 2.01 %; curve C, ϕ = 2.35 %; curve D, ϕ = 2.56 % and curve E, ϕ = 2.81 %

Reed 1	Fitting equation	Correlation coefficient
Curve A	$y = 56.35 + 1.13E\text{-}05x + 3.42E\text{-}05x^2 + 7.06E\text{-}09x^3 - 1.35E\text{-}09x^4 + 6.49E\text{-}12x^5 - 1.43E\text{-}14x^6 + 1.69E\text{-}17x^7 - 1.04E\text{-}20x^8 + 2.59E\text{-}24x^9$	0.9998
Curve B	$y = 56.01 - 5.42E\text{-}04x + 4.57E\text{-}05x^2 - 2.57E\text{-}07x^3 + 1.41E\text{-}09x^4 - 6.73E\text{-}12x^5 + 1.91E\text{-}14x^6 - 2.98E\text{-}17x^7 + 2.38E\text{-}20x^8 - 7.64E\text{-}24x^9$	0.9999
Curve C	$y = 55.11 - 4.12E\text{-}04x + 4.16E\text{-}05x^2 + 2.47E\text{-}08x^3 - 1.46E\text{-}09x^4 + 6.93E\text{-}12x^5 - 1.65E\text{-}14x^6 + 2.21E\text{-}17x^7 - 1.61E\text{-}20x^8 + 4.91E\text{-}24x^9$	0.9998
Curve D	$y = 54.71 + 1.02E\text{-}05x + 3.94E\text{-}05x^2 - 1.87E\text{-}07x^3 + 1.51E\text{-}09x^4 - 8.76E\text{-}12x^5 + 2.57E\text{-}14x^6 - 3.94E\text{-}17x^7 + 3.06E\text{-}20x^8 - 9.55E\text{-}24x^9$	0.9999
Curve E	$y = 54.33 - 1.90E\text{-}04x + 7.10E\text{-}05x^2 - 7.11E\text{-}07x^3 + 5.84E\text{-}09x^4 - 2.77E\text{-}11x^5 + 7.23E\text{-}14x^6 - 1.04E\text{-}16x^7 - 5.20E\text{-}17x^8 - 2.41E\text{-}23x^9$	0.9998

Reed 2	Fitting equation	Correlation coefficient
Curve A	$y = 47.27 - 5.88E\text{-}04x + 3.13E\text{-}05x^2 - 3.49E\text{-}07x^3 + 2.26E\text{-}09x^4 - 8.64E\text{-}12x^5 + 1.95E\text{-}14x^6 - 2.54E\text{-}17x^7 + 1.78E\text{-}20x^8 - 5.20E\text{-}24x^9$	0.9999
Curve B	$y = 47.21 - 2.20E\text{-}04x + 2.10E\text{-}05x^2 - 1.34E\text{-}07x^3 + 4.64E\text{-}10x^4 - 1.11E\text{-}12x^5 + 1.89E\text{-}15x^6 - 2.17E\text{-}18x^7 + 1.44E\text{-}21x^8 - 4.11E\text{-}25x^9$	0.9999
Curve C	$y = 46.98 + 2.60E\text{-}05x - 2.83E\text{-}06x^2 + 1.70E\text{-}07x^3 - 9.80E\text{-}10x^4 + 2.19E\text{-}12x^5 - 1.52E\text{-}15x^6 - 1.72E\text{-}18x^7 + 3.31E\text{-}21x^8 - 1.47E\text{-}24x^9$	0.9999
Curve D	$y = 46.88 - 4.77E\text{-}04x + 3.56E\text{-}05x^2 - 5.52E\text{-}07x^3 + 4.67E\text{-}09x^4 - 2.08E\text{-}11x^5 + 5.13E\text{-}14x^6 - 7.12E\text{-}17x^7 + 5.23E\text{-}20x^8 - 1.58E\text{-}23x^9$	0.9997
Curve E	$y = 46.81 - 5.82E\text{-}04x + 2.70E\text{-}05x^2 - 3.29E\text{-}07x^3 + 2.74E\text{-}09x^4 - 1.24E\text{-}11x^5 + 3.10E\text{-}14x^6 - 4.34E\text{-}17x^7 + 3.19E\text{-}20x^8 - 9.65E\text{-}24x^9$	0.9997

Reed 3	Fitting equation	Correlation coefficient
Curve A	$y = 44.90 - 1.31E\text{-}03x + 4.34E\text{-}05x^2 - 2.00E\text{-}07x^3 + 4.69E\text{-}10x^4 - 6.41E\text{-}13x^5 + 3.29E\text{-}16x^6 + 4.92E\text{-}19x^7 - 9.03E\text{-}22x^8 + 4.21E\text{-}25x^9$	0.9999
Curve B	$y = 44.61 + 3.34E\text{-}04x + 8.68E\text{-}07x^2 + 2.86E\text{-}07x^3 - 2.35E\text{-}09x^4 + 9.15E\text{-}12x^5 - 2.07E\text{-}14x^6 + 2.74E\text{-}17x^7 - 1.98E\text{-}20x^8 + 5.97E\text{-}24x^9$	0.9999
Curve C	$y = 43.85 - 2.28E\text{-}03x + 8.43E\text{-}05x^2 - 6.78E\text{-}07x^3 + 3.55E\text{-}09x^4 - 1.20E\text{-}11x^5 + 2.57E\text{-}14x^6 - 3.39E\text{-}17x^7 + 2.50E\text{-}20x^8 - 7.79E\text{-}24x^9$	0.9999
Curve D	$y = 43.75 - 2.58E\text{-}03x + 1.01E\text{-}04x^2 - 1.13E\text{-}06x^3 + 7.36E\text{-}09x^4 - 2.64E\text{-}11x^5 + 5.39E\text{-}14x^6 - 6.26E\text{-}17x^7 + 3.85E\text{-}20x^8 - 9.76E\text{-}24x^9$	0.9999
Curve E	$y = 43.59 - 2.35E\text{-}03x + 9.60E\text{-}05x^2 - 1.13E\text{-}06x^3 + 7.64E\text{-}09x^4 - 2.83E\text{-}11x^5 + 5.98E\text{-}14x^6 - 7.24E\text{-}17x^7 + 4.69E\text{-}20x^8 - 1.26E\text{-}23x^9$	0.9999

Reed 4	Fitting equation	Correlation coefficient
Curve A	$y = 44.39 - 6.79E\text{-}04x + 2.84E\text{-}05x^2 - 2.66E\text{-}07x^3 + 1.50E\text{-}09x^4 - 5.08E\text{-}12x^5 + 1.02E\text{-}14x^6 - 1.20E\text{-}17x^7 + 7.62E\text{-}21x^8 - 2.03E\text{-}24x^9$	0.9999
Curve B	$y = 44.32 - 5.16E\text{-}04x + 1.98E\text{-}05x^2 - 1.11E\text{-}07x^3 + 4.17E\text{-}10x^4 - 1.18E\text{-}12x^5 + 2.39E\text{-}15x^6 - 3.17E\text{-}18x^7 + 2.40E\text{-}21x^8 - 7.74E\text{-}25x^9$	0.9999
Curve C	$y = 44.15 + 1.21E\text{-}04x - 9.32E\text{-}06x^2 + 2.23E\text{-}07x^3 - 1.45E\text{-}09x^4 + 5.09E\text{-}12x^5 - 1.09E\text{-}14x^6 + 1.42E\text{-}17x^7 - 1.02E\text{-}20x^8 + 3.09E\text{-}24x^9$	0.9999
Curve D	$y = 44.11 - 7.19E\text{-}04x + 2.02E\text{-}05x^2 - 1.64E\text{-}07x^3 + 1.19E\text{-}09x^4 - 5.23E\text{-}12x^5 + 1.29E\text{-}14x^6 - 1.76E\text{-}17x^7 + 1.26E\text{-}20x^8 - 3.71E\text{-}24x^9$	0.9999
Curve E	$y = 43.88 - 6.32E\text{-}04x + 2.02E\text{-}05x^2 - 1.66E\text{-}07x^3 + 9.42E\text{-}10x^4 - 2.85E\text{-}12x^5 + 4.37E\text{-}15x^6 - 3.02E\text{-}18x^7 + 3.68E\text{-}22x^8 + 3.51E\text{-}25x^9$	0.9999

Table 8.1. Polynomial fitting functions for resonance frequency versus time profiles for reeds 1 - 4 for 55 - 100 μm glass ballotini particles settling in water at 17°C at initial solids concentrations in the range 1.75 - 2.81 % v/v.

rate of change of resonance frequency with time profiles become progressively broader exhibiting a smaller degree of size segregation.

Figures 8.25 - 8.36 show the corresponding sedimentation kinetic data as those shown in figures 8.21 - 8.24 but this time obtained in conjunction with ballotini particles in the size ranges 80 - 115 μm (figures 8.25 - 8.28), 90 - 135 μm (figures 8.29 - 8.32) and 100 -200 μm (figures 8.33 - 8.36). Once again, the data go through a maximum indicating size segregation. It is however, notable that the peaks become progressively flatter as the mean particle size increases indicating a smaller extent of size segregation.

8.4 Solids Flux Profiles

Figure 8.37 shows the variation of solids flux ($kgm^{-2}s^{-1}$) at each reed position with time for polydisperse 55 - 100 μm glass ballotini spheres (density 2550 kgm^{-3}) settling in water at 17 °C. The data refers to an initial solids volume concentration, ϕ of 1.75 % v/v. The significance of the data in the accompanying table as well as those given in the tables in figures 8.38 - 8.41 will be discussed later.

Solids flux has been calculated from the corresponding rate of change of resonance frequency profiles (see section 8.3) at each reed position in conjunction with the system solids flux calibration plots (see figures 7.21 to 7.24) in the manner described in section 7.4, chapter 7.

Curves A to D in figure 8.37 represent the variation of the solids flux along the length of the settling zone. As expected, the solids flux (product of settling velocity and solids concentration) at time, t = 0 s is zero since the settling velocity of the suspension is zero. This is followed by a sharp increase in the suspension velocity and therefore, the solids flux as particles accelerate to reach their terminal velocities. At the same time, the suspension concentration starts to decrease as particles continuously leave the settling zone. Accordingly, the solids flux goes through a maximum following which it starts to decrease tending to zero as the suspension-clear liquid interface approaches each reed. At breakthrough (for example t = 340 s for reed 1), the solids concentration

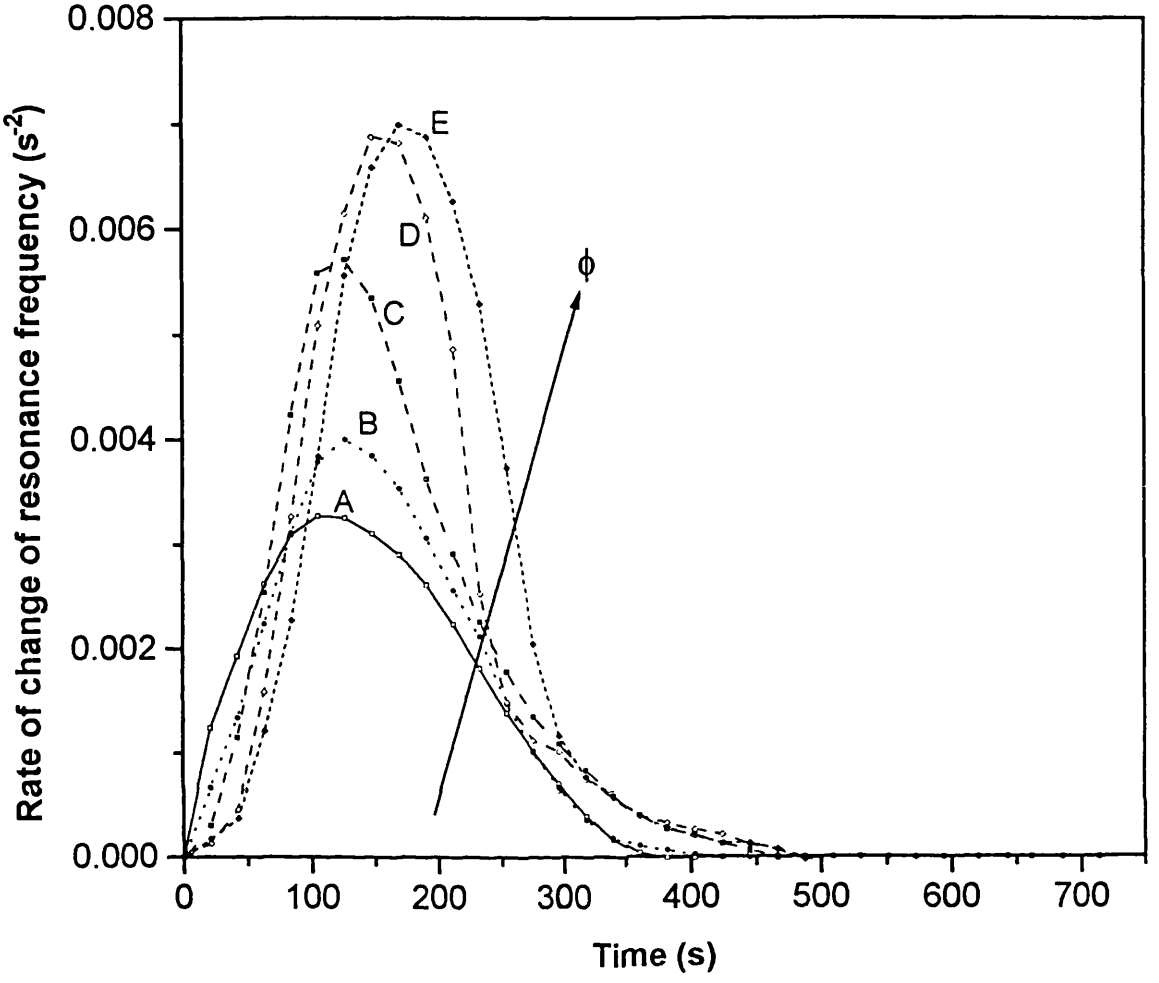

Figure 8.25
The variation of rate of change of resonance frequency with time at reed position 1 (699 mm from top of settling zone) for polydisperse 80 - 115 μm glass ballotini spheres (density 2550 kgm^{-3}) settling in water @ 17 °C at various initial suspended solids volume concentrations, ϕ: curve A, ϕ = 1.75 %; curve B, ϕ = 2.01 %; curve C, ϕ = 2.35 %; curve D, ϕ = 2.56 % and curve E, ϕ = 2.81 %

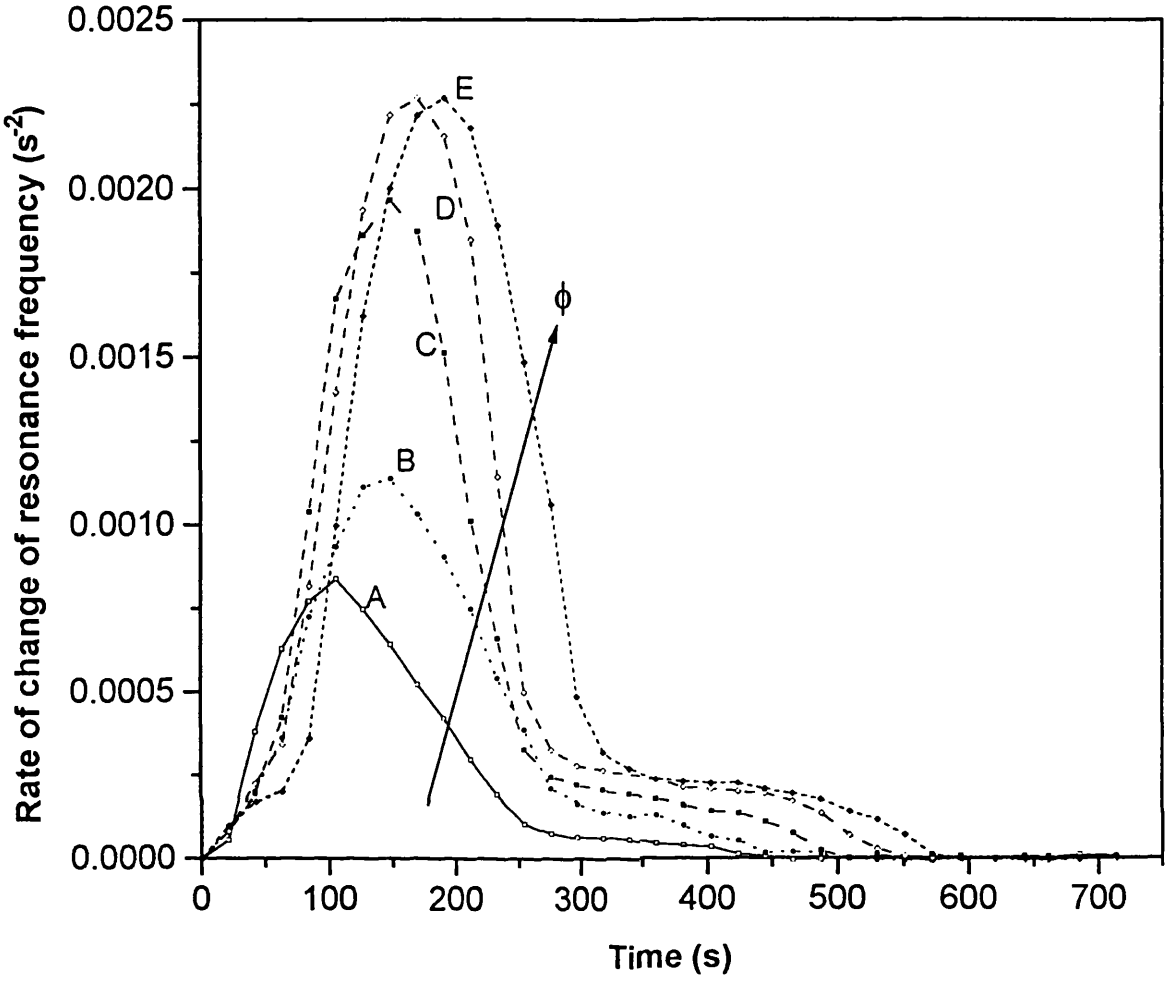

Figure 8.26

The variation of rate of change of resonance frequency with time at reed position 2 (900 mm from top of settling zone) for polydisperse 80 - 115 μm glass ballotini spheres (density 2550 kgm^{-3}) settling in water @ 17 °C at various initial suspended solids volume concentrations, ϕ: curve A, ϕ = 1.75 %; curve B, ϕ = 2.01 %; curve C, ϕ = 2.35 %; curve D, ϕ = 2.56 % and curve E, ϕ = 2.81 %

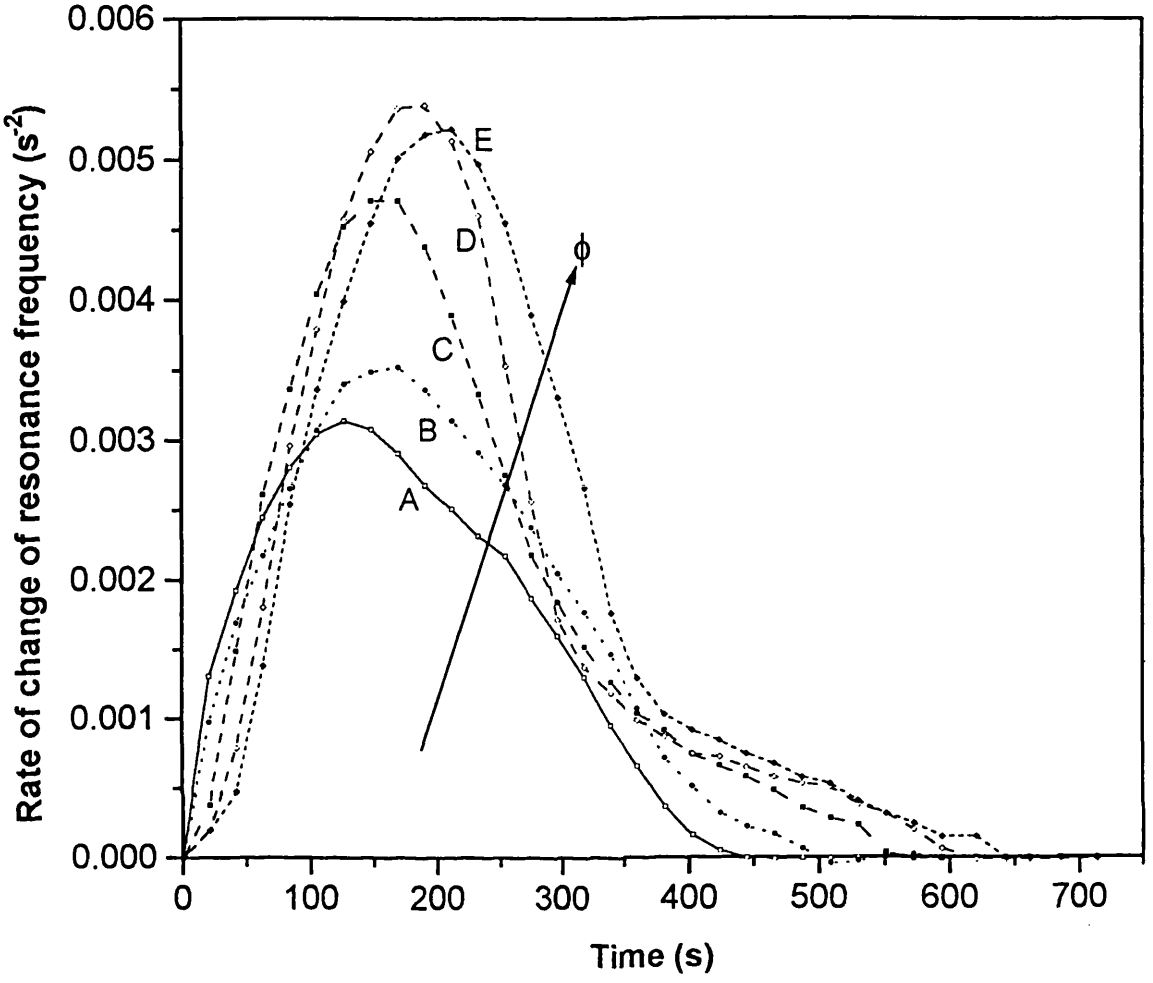

Figure 8.27
The variation of rate of change of resonance frequency with time at reed position 3 (1096 mm from top of settling zone) for polydisperse 80 - 115 μm glass ballotini spheres (density 2550 kgm^{-3}) settling in water @ 17 °C at various initial suspended solids volume concentrations, ϕ: curve A, ϕ = 1.75 %; curve B, ϕ = 2.01 %; curve C, ϕ = 2.35 %; curve D, ϕ = 2.56 % and curve E, ϕ = 2.81 %

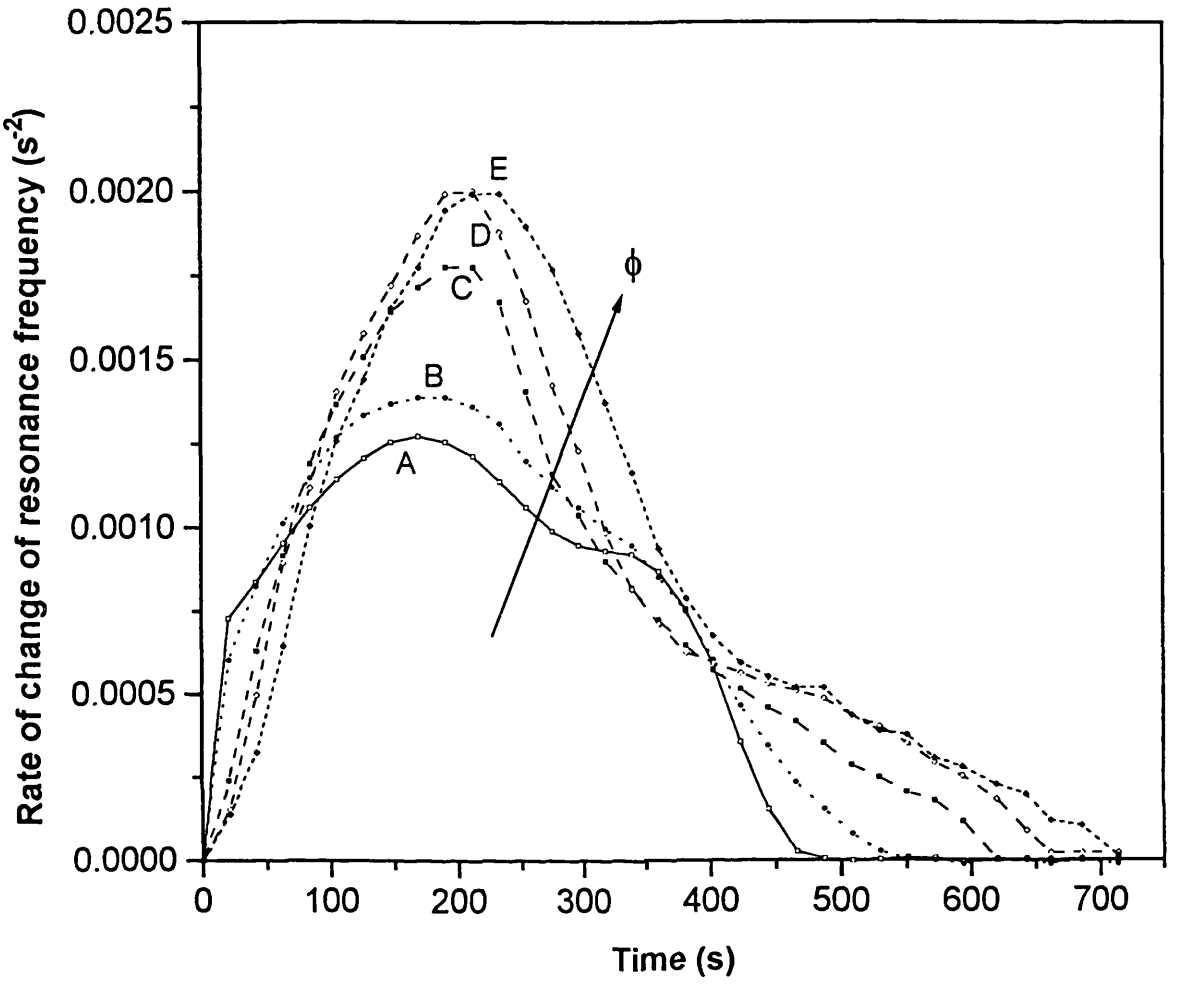

Figure 8.28

The variation of rate of change of resonance frequency with time at reed position 4 (1296 mm from top of settling zone) for polydisperse 80 - 115 μm glass ballotini spheres (density 2550 kgm^{-3}) settling in water @ 17 °C at various initial suspended solids volume concentrations, ϕ: curve A, ϕ = 1.75 %; curve B, ϕ = 2.01 %; curve C, ϕ = 2.35 %; curve D, ϕ = 2.56 % and curve E, ϕ = 2.81 %

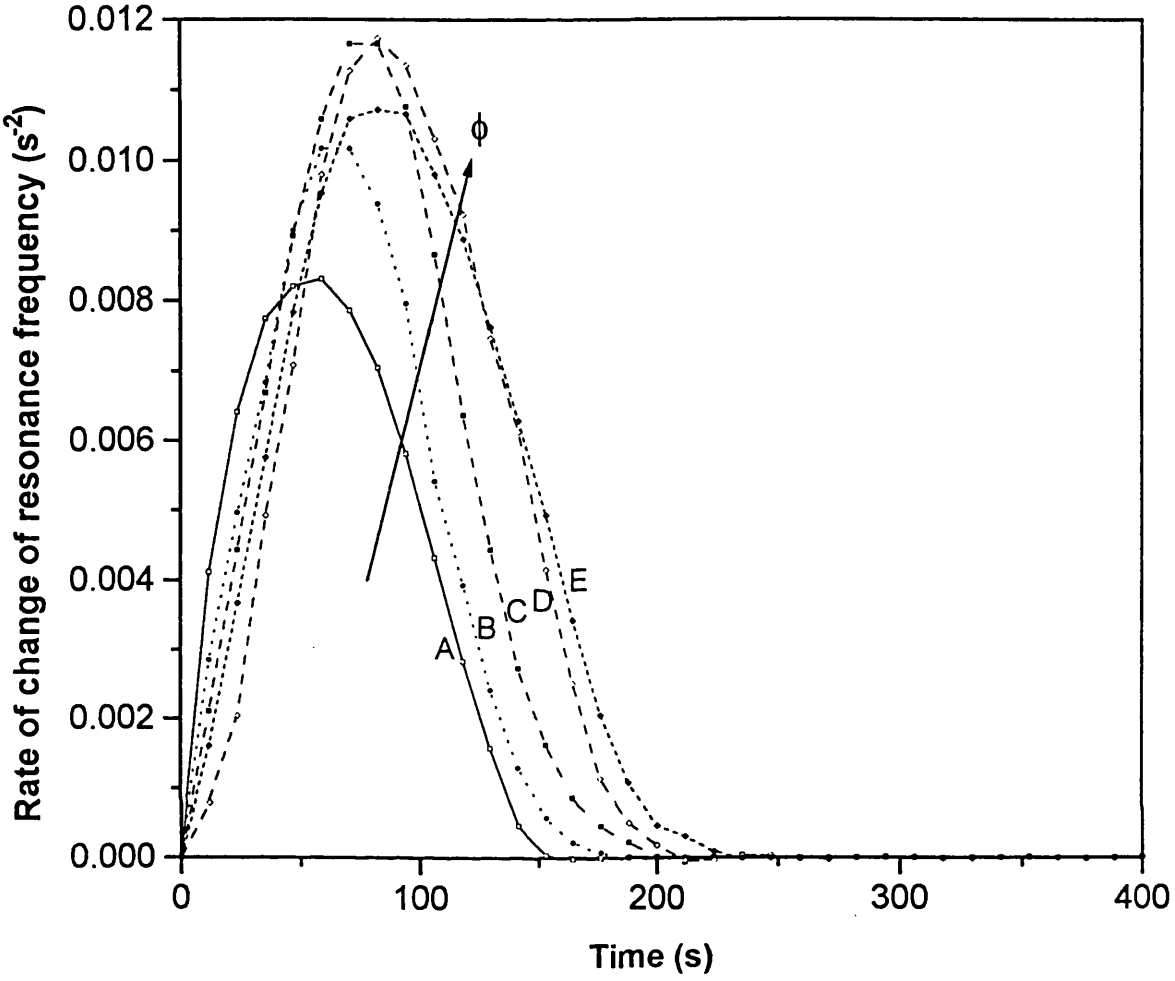

Figure 8.29

The variation of rate of change of resonance frequency with time at reed position 1 (699 mm from top of settling zone) for polydisperse 90 - 135 μm glass ballotini spheres (density 2550 kgm^{-3}) settling in water @ 17 °C at various initial suspended solids volume concentrations, ϕ: curve A, ϕ = 1.75 %; curve B, ϕ = 2.01 %; curve C, ϕ = 2.35 %; curve D, ϕ = 2.56 % and curve E, ϕ = 2.81 %

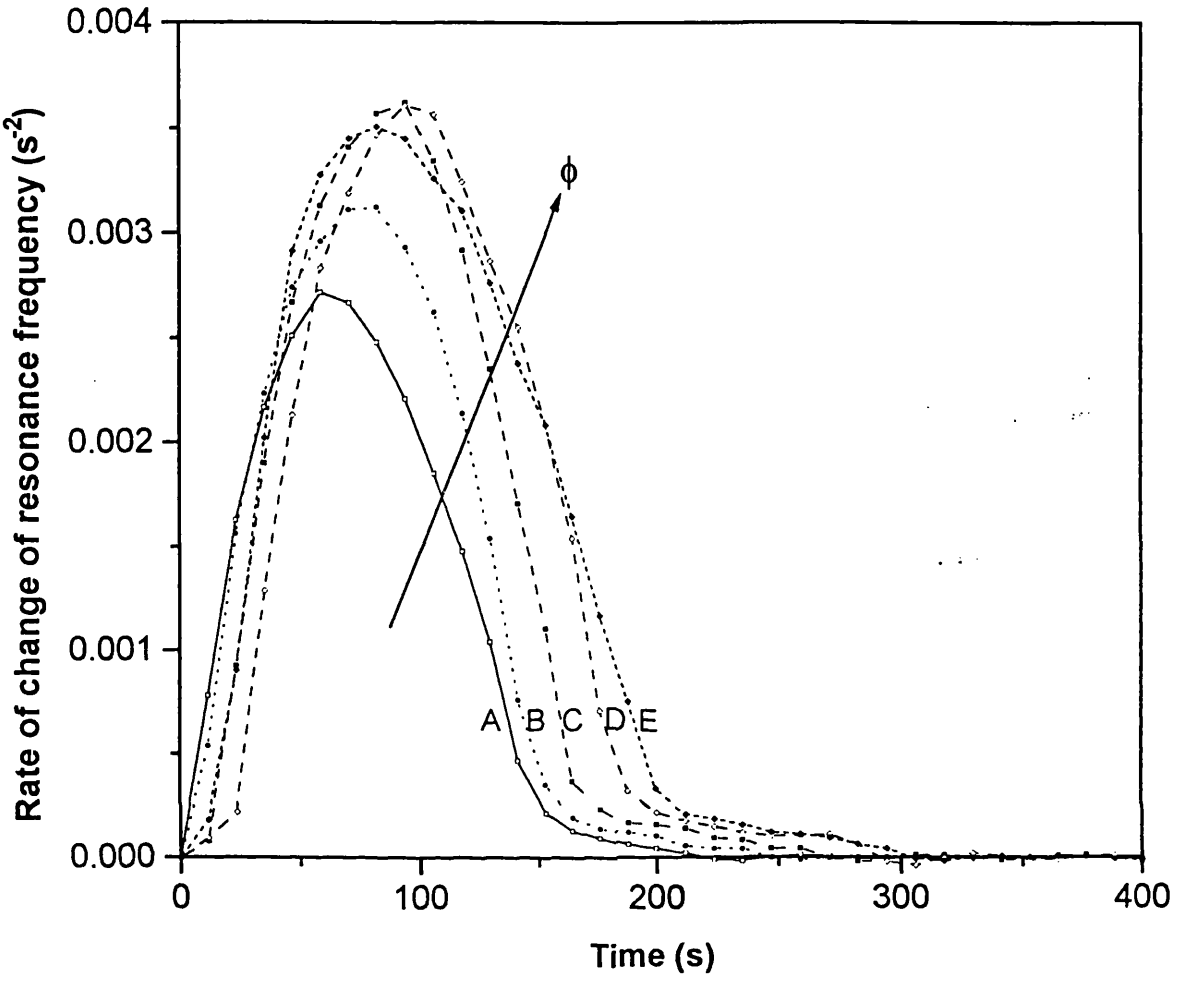

Figure 8.30

The variation of rate of change of resonance frequency with time at reed position 2 (900 mm from top of settling zone) for polydisperse 90 - 135 μm glass ballotini spheres (density 2550 kgm^{-3}) settling in water @ 17 °C at various initial suspended solids volume concentrations, ϕ: curve A, ϕ = 1.75 %; curve B, ϕ = 2.01 %; curve C, ϕ = 2.35 %; curve D, ϕ = 2.56 % and curve E, ϕ = 2.81 %

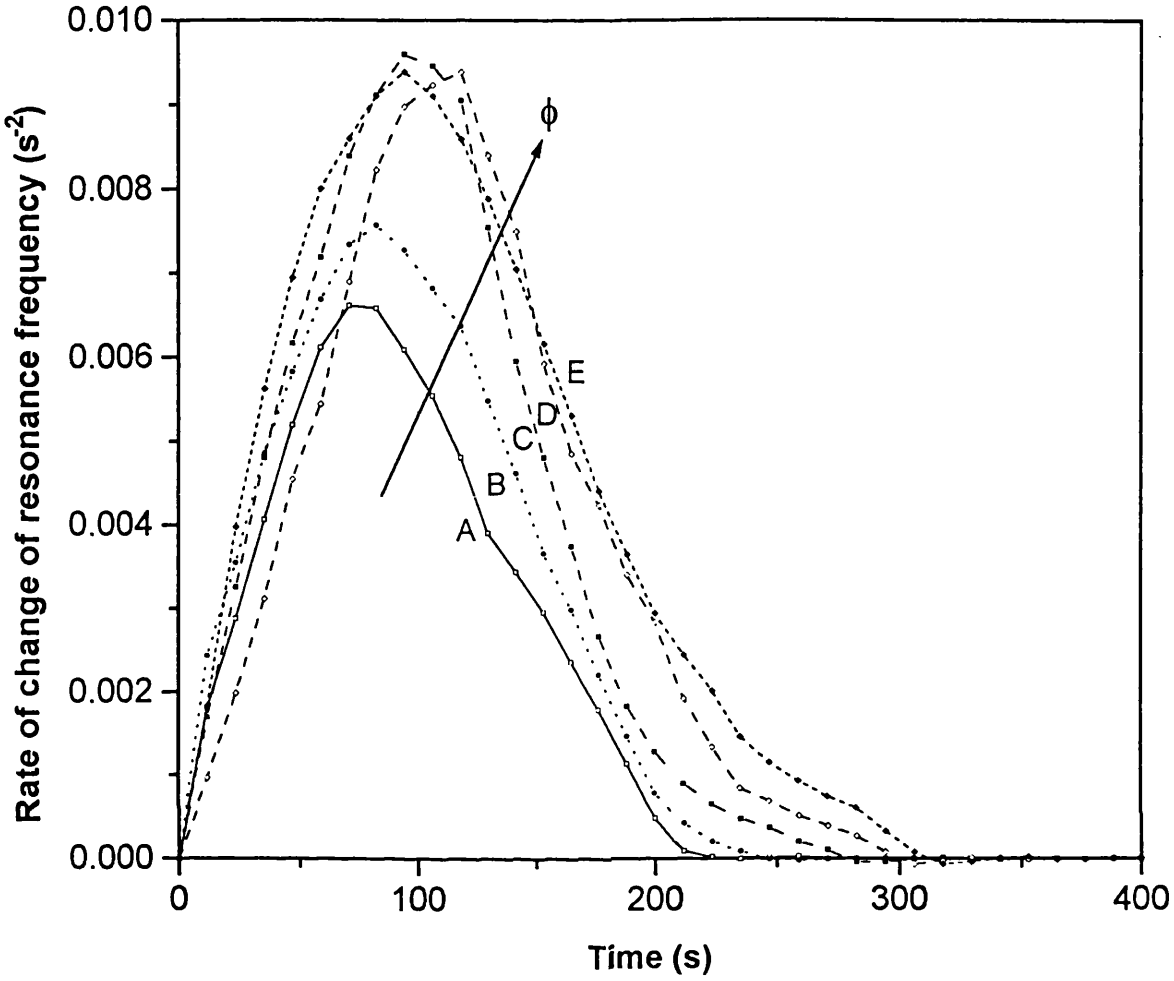

Figure 8.31

The variation of rate of change of resonance frequency with time at reed position 3 (1096 mm from top of settling zone) for polydisperse 90 - 135 μm glass ballotini spheres (density 2550 kgm^{-3}) settling in water @ 17 °C at various initial suspended solids volume concentrations, ϕ: curve A, ϕ = 1.75 %; curve B, ϕ = 2.01 %; curve C, ϕ = 2.35 %; curve D, ϕ = 2.56 % and curve E, ϕ = 2.81 %

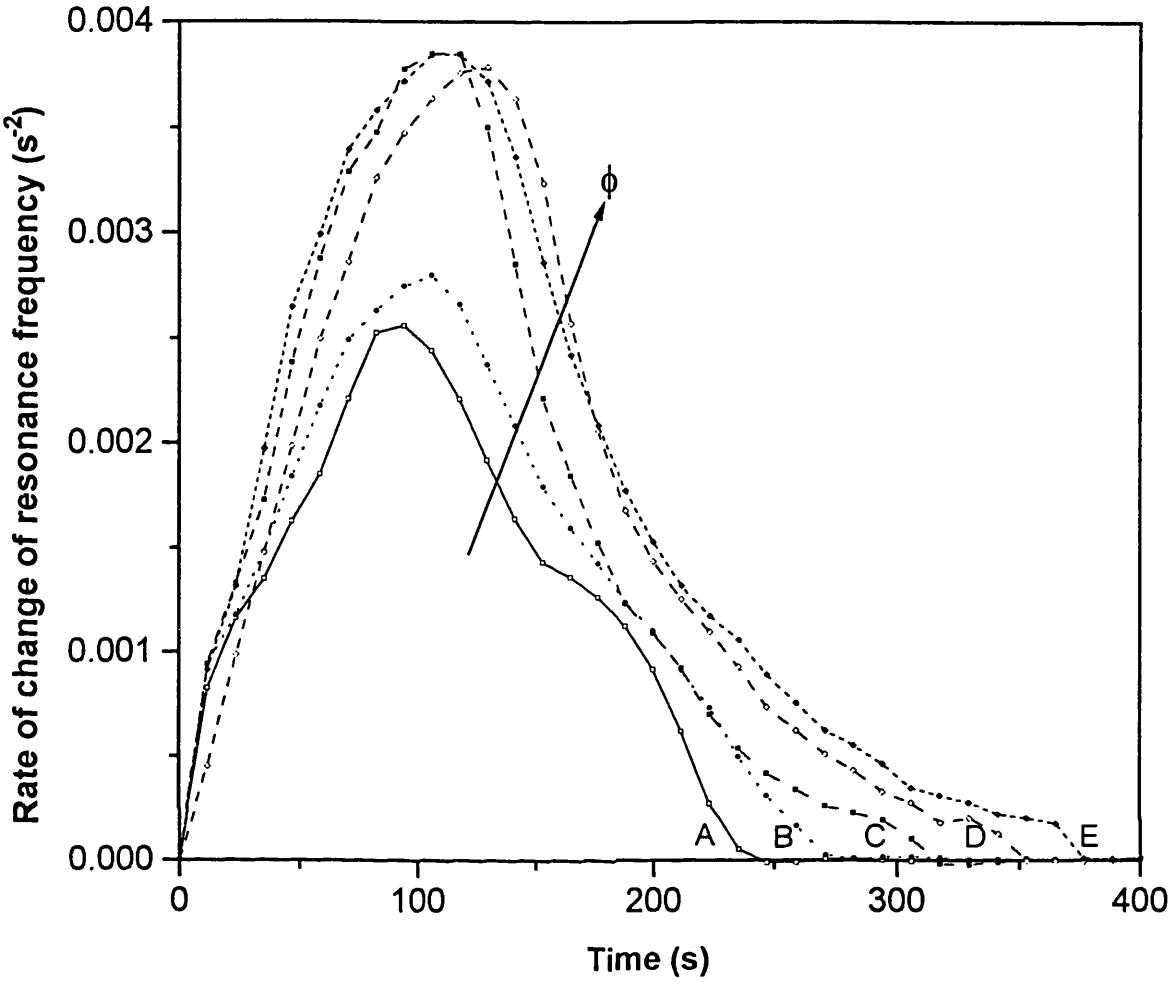

Figure 8.32
The variation of rate of change of resonance frequency with time at reed position 4 (1296 mm from top of settling zone) for polydisperse 90 - 135 μm glass ballotini spheres (density 2550 kgm^{-3}) settling in water @ 17 °C at various initial suspended solids volume concentrations, ϕ: curve A, ϕ = 1.75 %; curve B, ϕ = 2.01 %; curve C, ϕ = 2.35 %; curve D, ϕ = 2.56 % and curve E, ϕ = 2.81 %

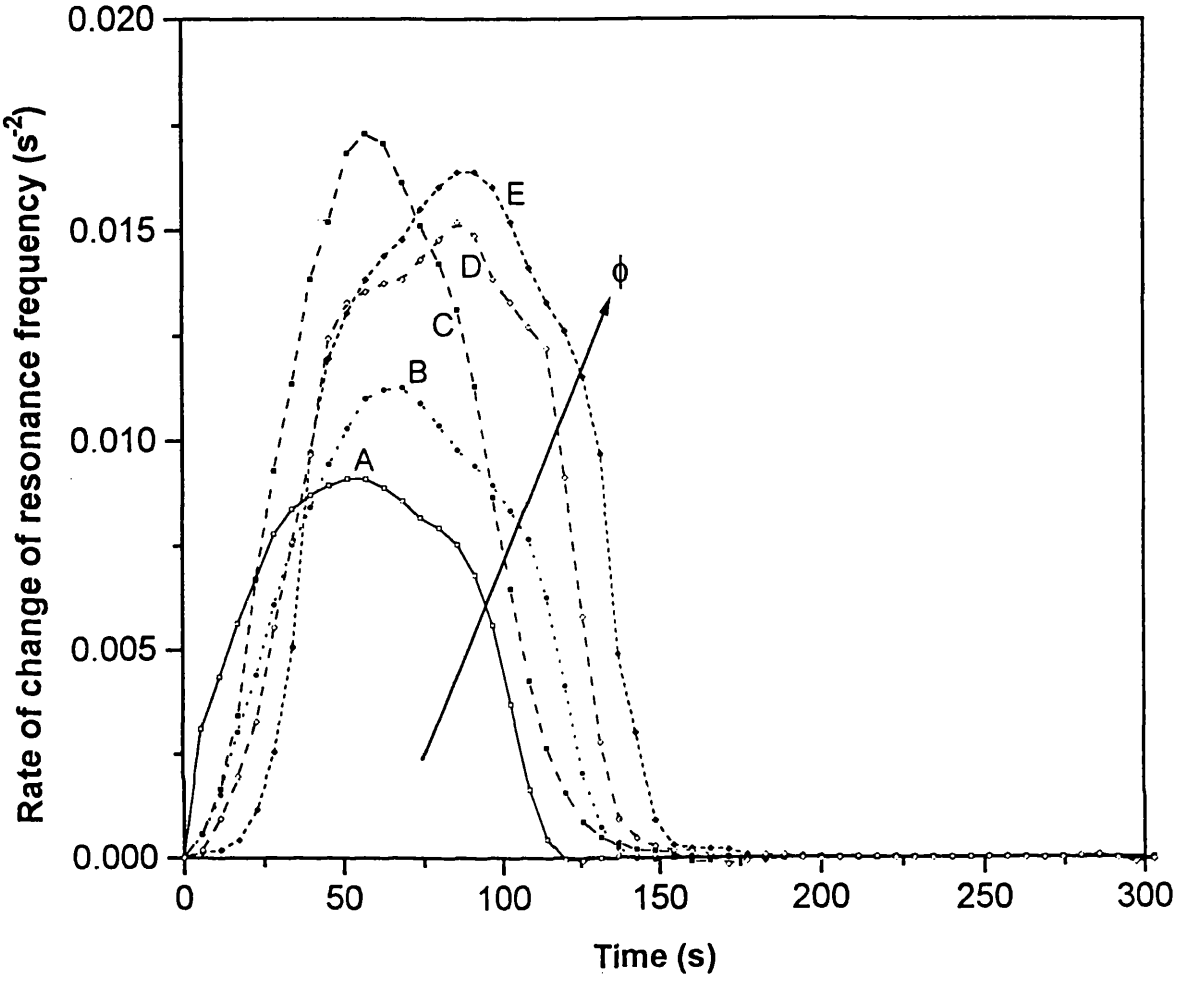

Figure 8.33

The variation of rate of change of resonance frequency with time at reed position 1 (699 mm from top of settling zone) for polydisperse 100 - 200 μm glass ballotini spheres (density 2550 kgm^{-3}) settling in water @ 17 °C at various initial suspended solids volume concentrations, ϕ: curve A, ϕ = 1.75 %; curve B, ϕ = 2.01 %; curve C, ϕ = 2.35 %; curve D, ϕ = 2.56 % and curve E, ϕ = 2.81 %

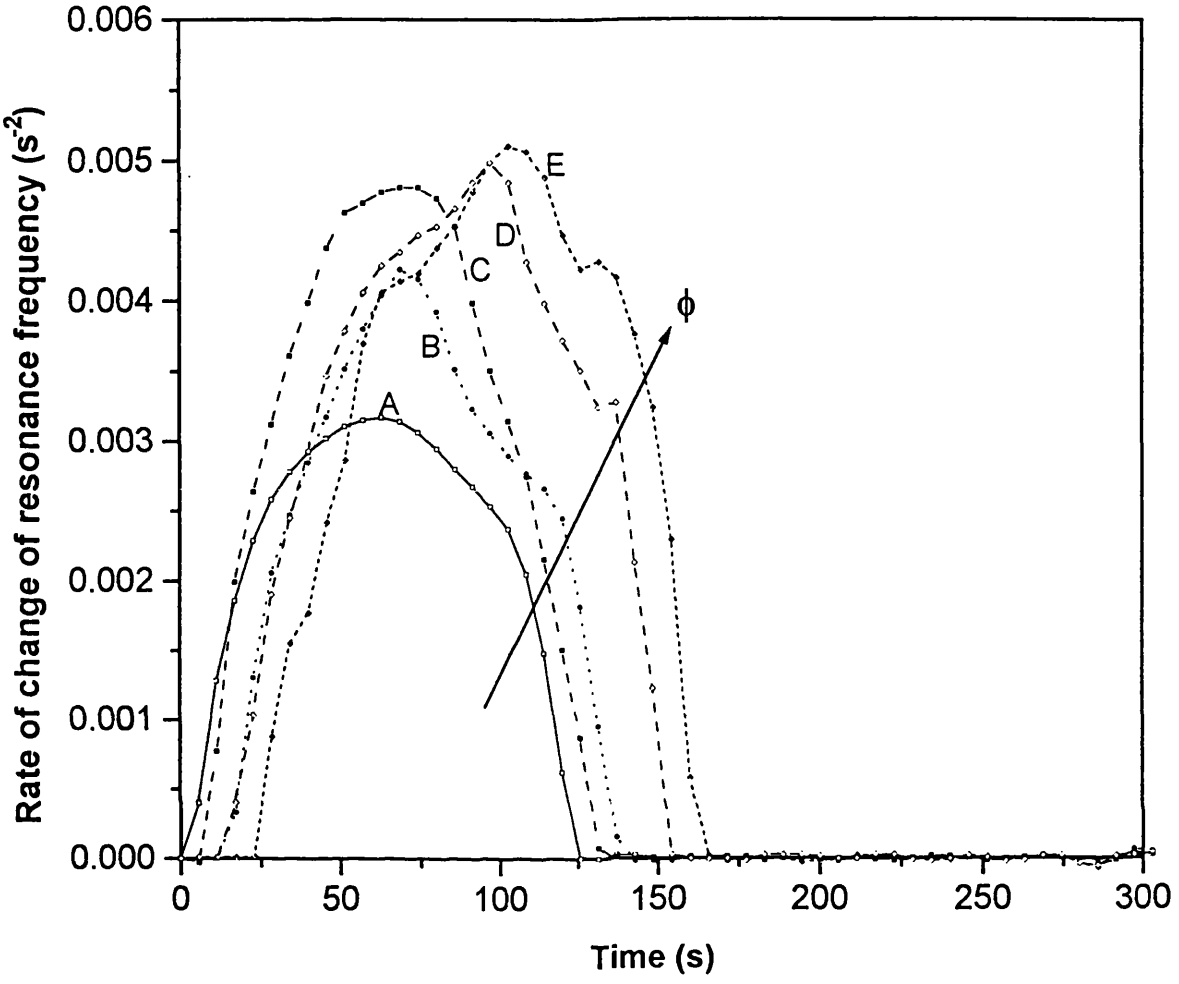

Figure 8.34

The variation of rate of change of resonance frequency with time at reed position 2 (900 mm from top of settling zone) for polydisperse 100 - 200 μm glass ballotini spheres (density 2550 kgm^{-3}) settling in water @ 17 °C at various initial suspended solids volume concentrations, ϕ: curve A, ϕ = 1.75 %; curve B, ϕ = 2.01 %; curve C, ϕ = 2.35 %; curve D, ϕ = 2.56 % and curve E, ϕ = 2.81 %

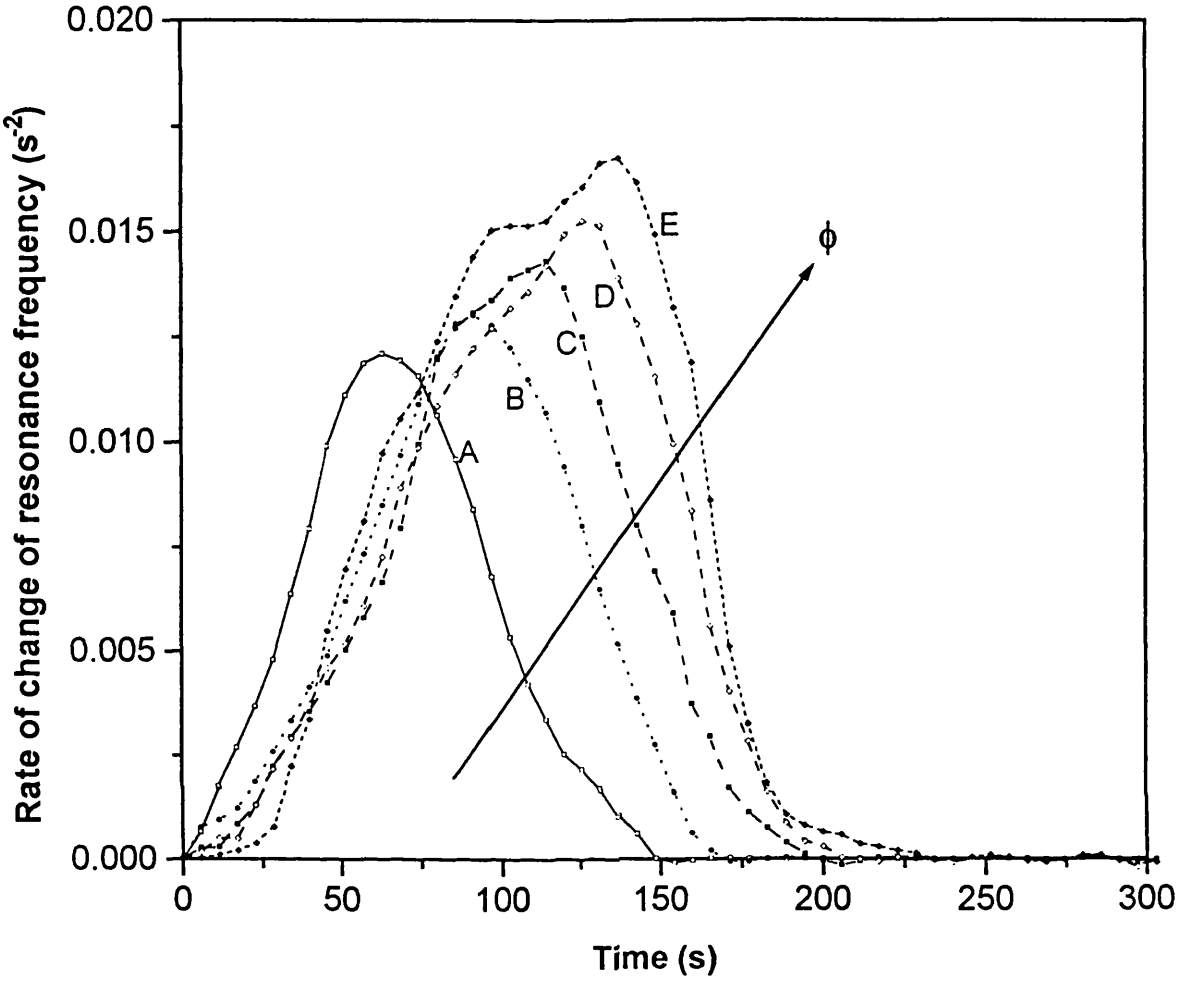

Figure 8.35

The variation of rate of change of resonance frequency with time at reed position 3 (1096 mm from top of settling zone) for polydisperse 100 - 200 μm glass ballotini spheres (density 2550 kgm^{-3}) settling in water @ 17 °C at various initial suspended solids volume concentrations, ϕ: curve A, ϕ = 1.75 %; curve B, ϕ = 2.01 %; curve C, ϕ = 2.35 %; curve D, ϕ = 2.56 % and curve E, ϕ = 2.81 %

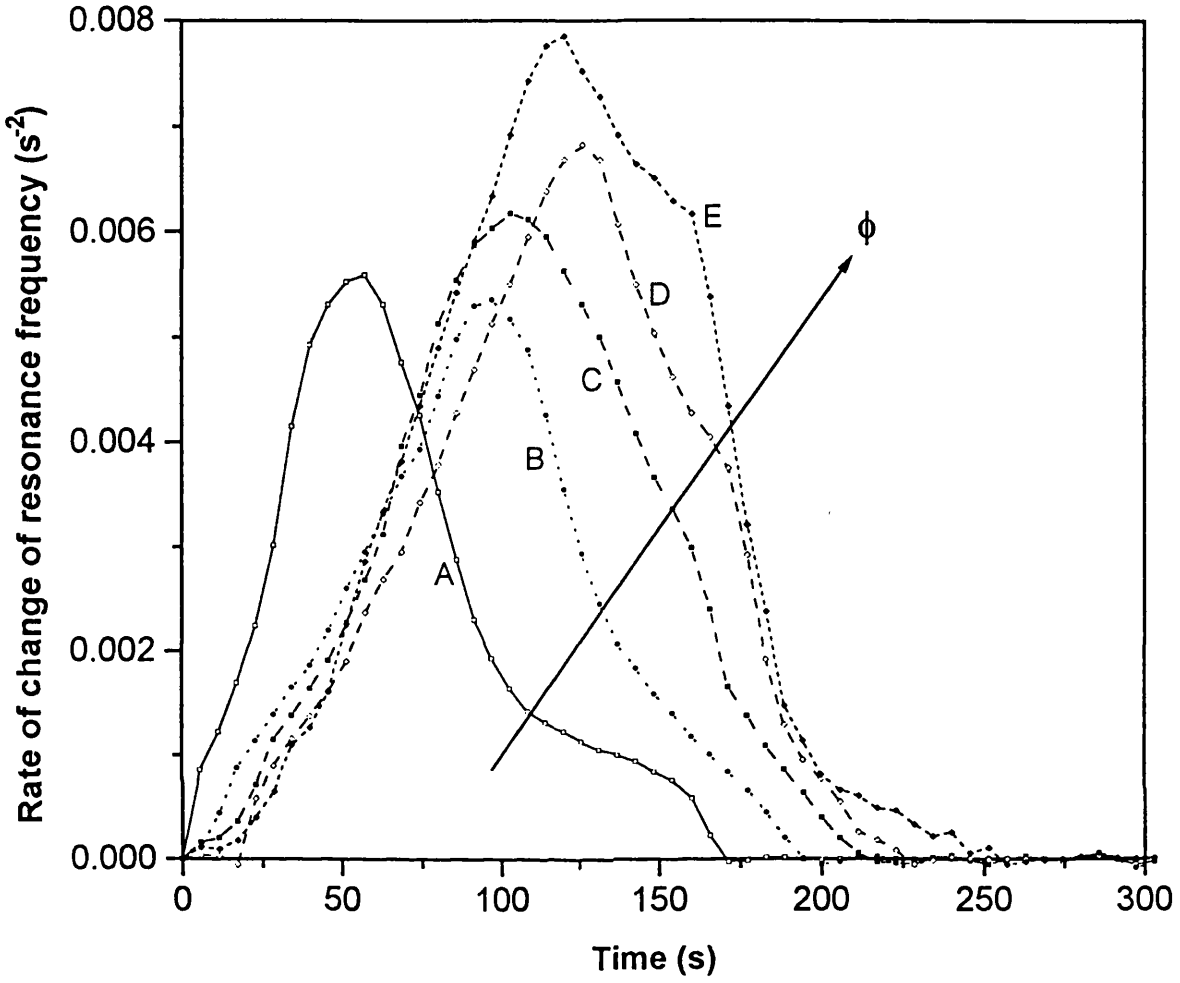

Figure 8.36

The variation of rate of change of resonance frequency with time at reed position 4 (1296 mm from top of settling zone) for polydisperse 100 - 200 μm glass ballotini spheres (density 2550 kgm^{-3}) settling in water @ 17 °C at various initial suspended solids volume concentrations, ϕ: curve A, ϕ = 1.75 %; curve B, ϕ = 2.01 %; curve C, ϕ = 2.35 %; curve D, ϕ = 2.56 % and curve E, ϕ = 2.81 %

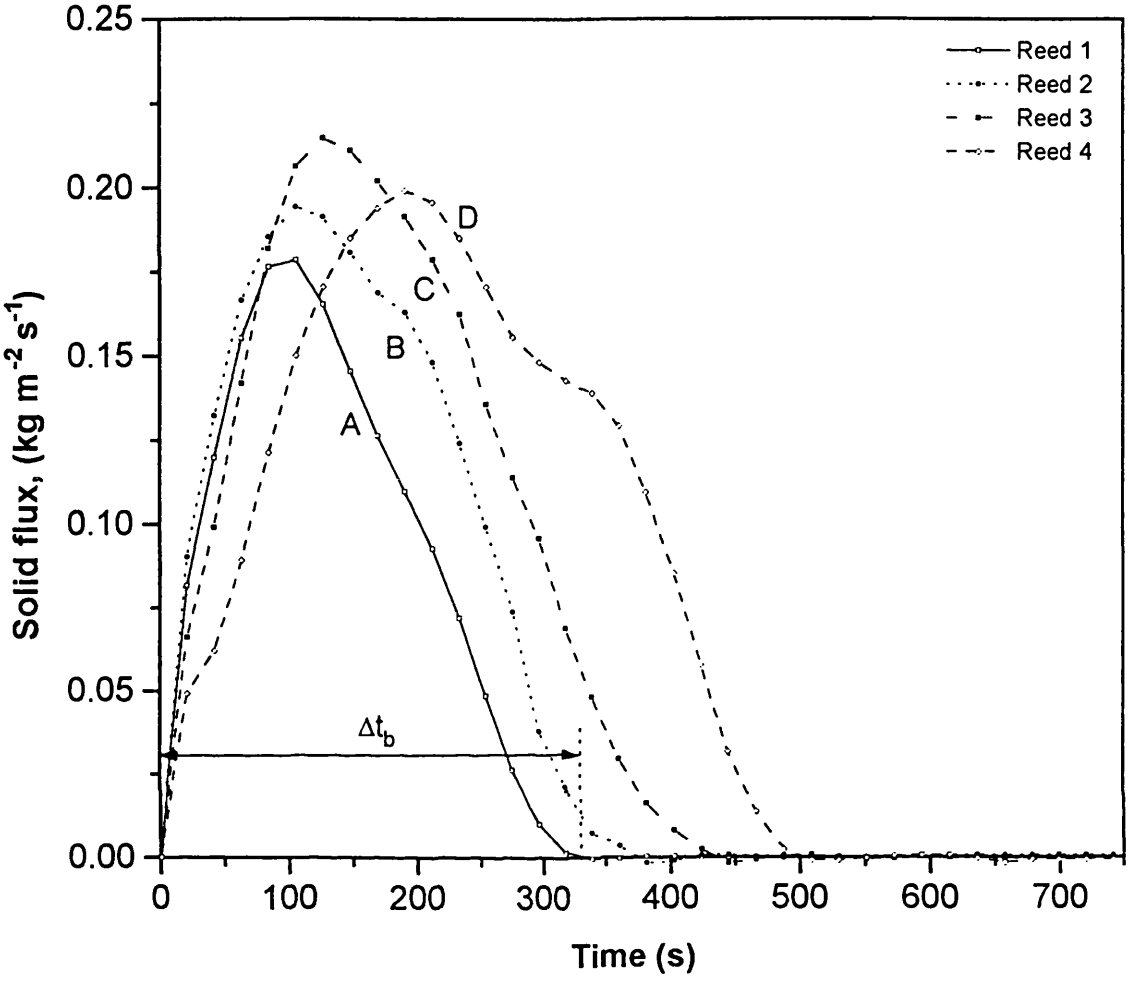

Figure 8.37
The variation of solids flux with time for polydisperse 55 - 100 μm glass ballotini spheres (density 2550 kgm^{-3}, ϕ = 1.75 %) settling in water @ 17 °C at various reed positions as measured from the top of the settling zone: curve A, 699 mm; curve B, 900 mm; curve C, 1096 mm and curve D, 1296 mm

	Area (kgm^{-2})	Measured Solids Throughput (g)	Volume-based Solids Throughput (g)	Percentage Difference (%)
Curve A	31.99	566.2	548.9	3.1
Curve B	42.14	744.7	709.7	4.7
Curve C	50.21	887.2	864.2	2.6
Curve D	58.96	1041.9	1022.0	1.9

is zero and therefore, the solids flux is zero. Interestingly, at any given time during the first few seconds of the sedimentation process, the solids flux profile along the settling tank remains relatively constant. This is superseded by a progressive 'densification' of the two-phase system towards the base of the settling tank until a maximum solids flux corresponding to each reed position is reached. At any given time beyond this peak value, the rate of decrease in the solids flux becomes more rapid towards the top of the settling zone.

Figures 8.38 - 8.41 show the corresponding solids flux data for 55 - 100 μm ballotini systems at the initial solids volume concentrations, ϕ 2.01 - 2.81 % v/v respectively. As before, for the same initial solids concentration, the maximum solids flux increases towards the base of the settling tank (from reed 1 to reed 4). Moreover, an increase in the initial solids concentration results in a corresponding increase in the solids flux detected at a given reed position.

Figures 8.42 - 8.56 show solids flux profiles obtained from reeds 1 - 4 for the polydisperse ballotini size fractions 80 - 115 μm (figures 8.42 - 8.46), 90 - 135 μm (figures 8.47 - 8.51) and 100 - 200 μm (figures 8.52 - 8.56) suspensions. The initial solids volume concentrations, ϕ vary in the range 1.75 - 2.81 % v/v. The trends in the data are similar to those for the 55 - 100 μm size fraction suspensions described above.

8.5 Solids Mass Balance Calculations

The area under each of the solids flux profiles shown in figures 8.37 - 8.41 represents the corresponding mass of solids settling per unit area (kgm^{-2}). It may be calculated by integrating the solids flux curve, Φ using the integration tool of the software Microcal Origin (version 3.5, 1994) between time, t = 0 s (the onset of settling) and the appropriate breakthrough time, Δt_b. By multiplying this result by the cross-sectional area (1.77×10^{-2} m^2) of the settling tank, the experimental solids mass throughput (kg) for each of reeds 1 - 4 can be determined. Mathematically, therefore, the total solids mass throughput can be expressed as:

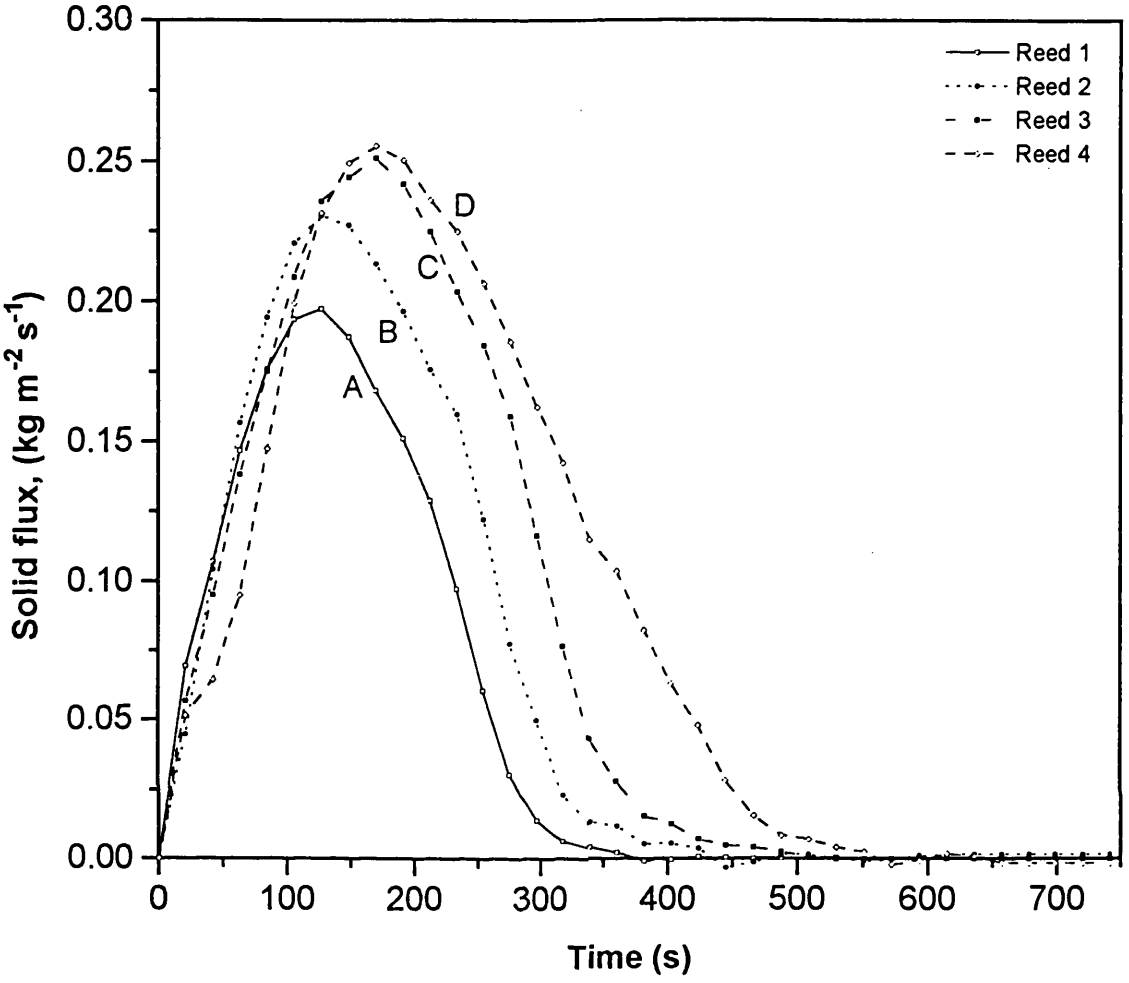

Figure 8.38

The variation of solids flux with time for polydisperse 55 - 100 μm glass ballotini spheres (density 2550 kgm^{-3}, ϕ = 2.01 %) settling in water @ 17 °C at various reed positions as measured from the top of the settling zone: curve A, 699 mm; curve B, 900 mm; curve C, 1096 mm and curve D, 1296 mm

	Area (kgm^{-2})	Measured Solids Throughput (g)	Volume-based Solids Throughput (g)	Percentage Difference (%)
Curve A	36.80	650.3	633.1	2.6
Curve B	47.43	838.1	815.2	2.7
Curve C	57.69	1019.4	992.7	2.6
Curve D	67.13	1186.3	1173.8	1.1

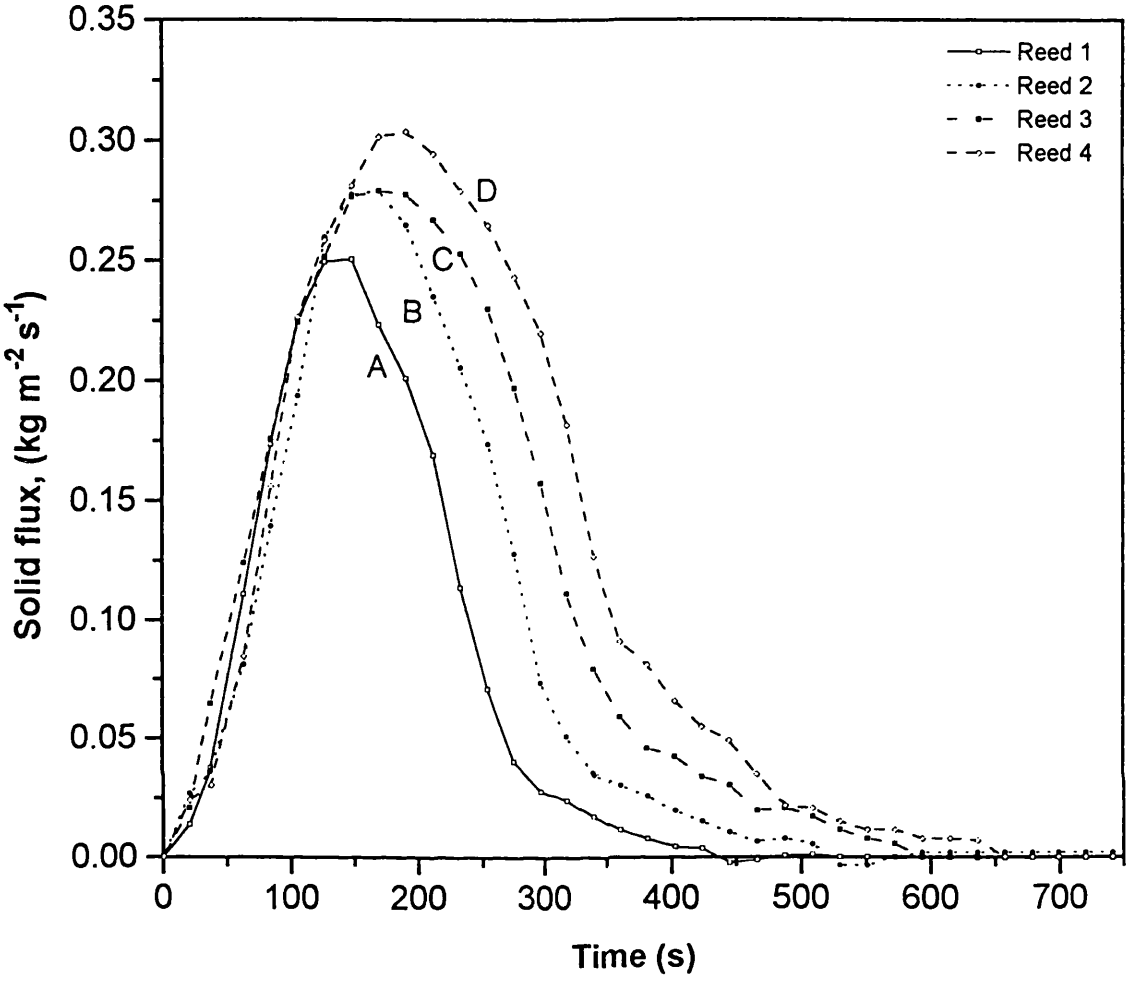

Figure 8.39

The variation of solids flux with time for polydisperse 55 - 100 μm glass ballotini spheres (density 2550 kgm^{-3}, ϕ = 2.35 %) settling in water @ 17 °C at various reed positions as measured from the top of the settling zone: curve A, 699 mm; curve B, 900 mm; curve C, 1096 mm and curve D, 1296 mm

	Area (kgm^{-2})	Measured Solids Throughput (g)	Volume-based Solids Throughput (g)	Percentage Difference (%)
Curve A	42.03	742.8	740.2	0.4
Curve B	54.91	970.4	953.0	1.8
Curve C	69.73	1232.3	1160.6	5.8
Curve D	79.73	1408.9	1372.4	2.6

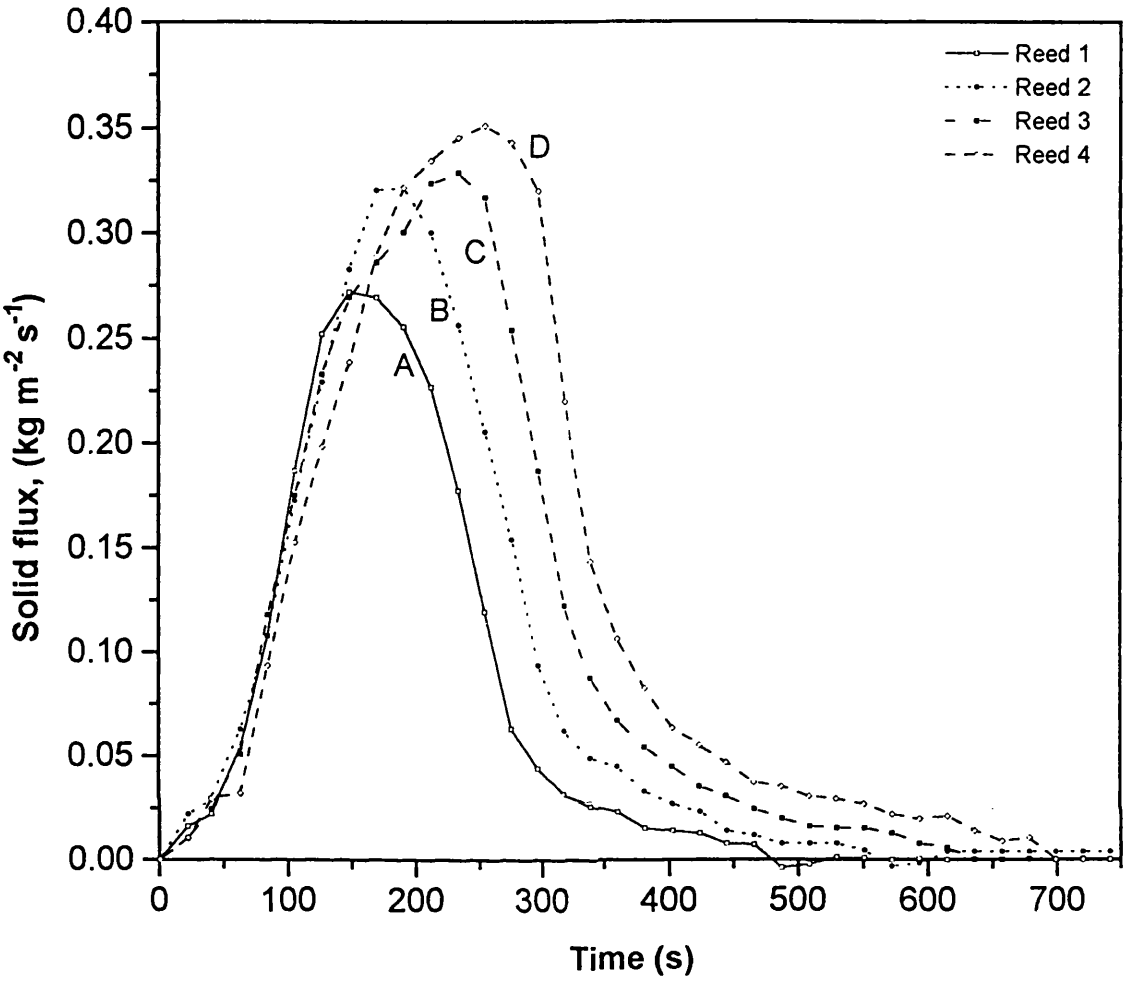

Figure 8.40

The variation of solids flux with time for polydisperse 55 - 100 μm glass ballotini spheres (density 2550 kgm^{-3}, ϕ = 2.56 %) settling in water @ 17 °C at various reed positions as measured from the top of the settling zone: curve A, 699 mm; curve B, 900 mm; curve C, 1096 mm and curve D, 1296 mm

	Area (kgm^{-2})	Measured Solids Throughput (g)	Volume-based Solids Throughput (g)	Percentage Difference (%)
Curve A	46.46	821.1	806.3	1.8
Curve B	60.65	1071.8	1038.2	3.1
Curve C	72.70	1284.7	1264.3	1.6
Curve D	85.35	1508.2	1495.0	0.9

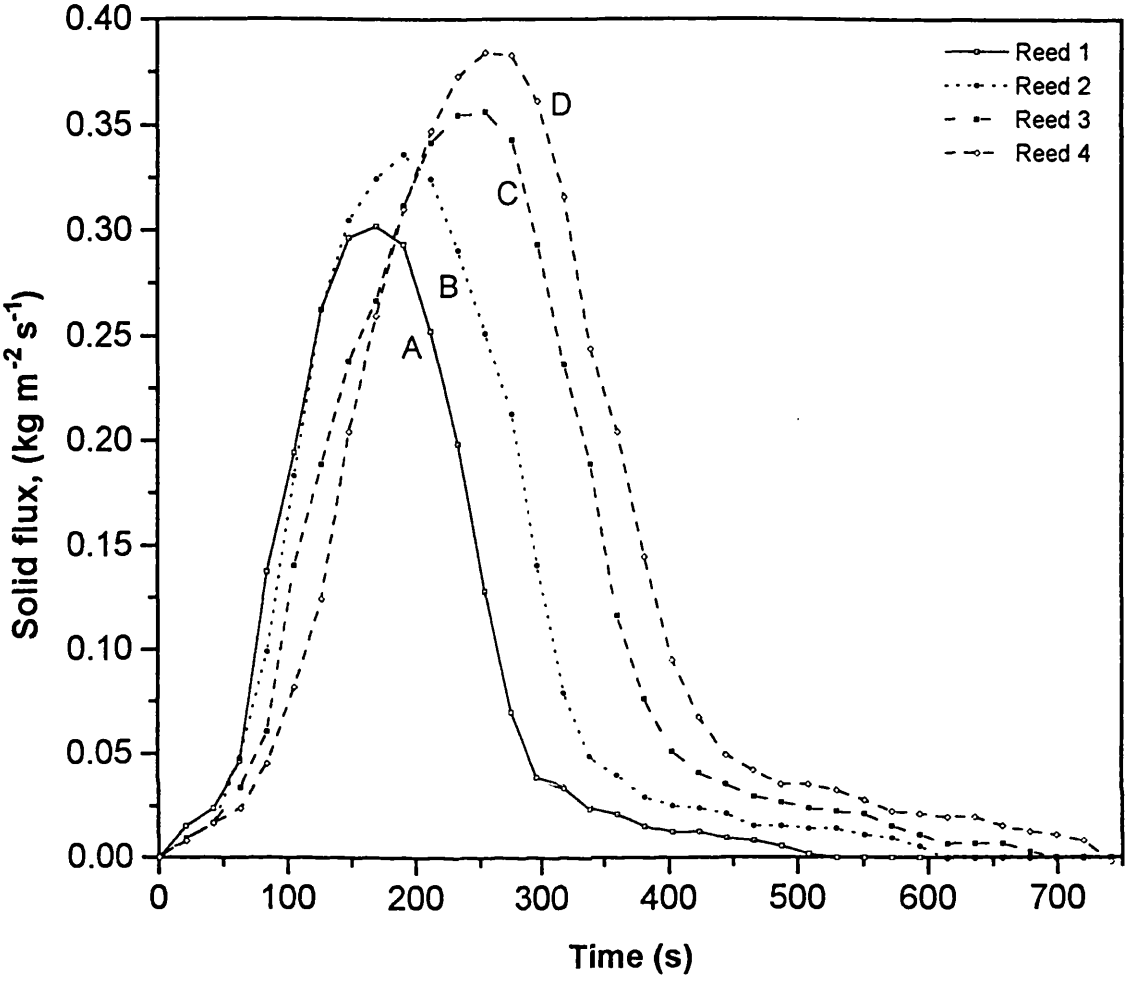

Figure 8.41

The variation of solids flux with time for polydisperse 55 - 100 μm glass ballotini spheres (density 2550 kgm^{-3}, ϕ = 2.81 %) settling in water @ 17 °C at various reed positions as measured from the top of the settling zone: curve A, 699 mm; curve B, 900 mm; curve C, 1096 mm and curve D, 1296 mm

	Area (kgm^{-2})	Measured Solids Throughput (g)	Volume-based Solids Throughput (g)	Percentage Difference (%)
Curve A	50.70	895.9	885.1	1.2
Curve B	66.55	1176.0	1139.6	3.1
Curve C	81.89	1447.1	1387.7	4.1
Curve D	91.94	1624.8	1641.1	1.0

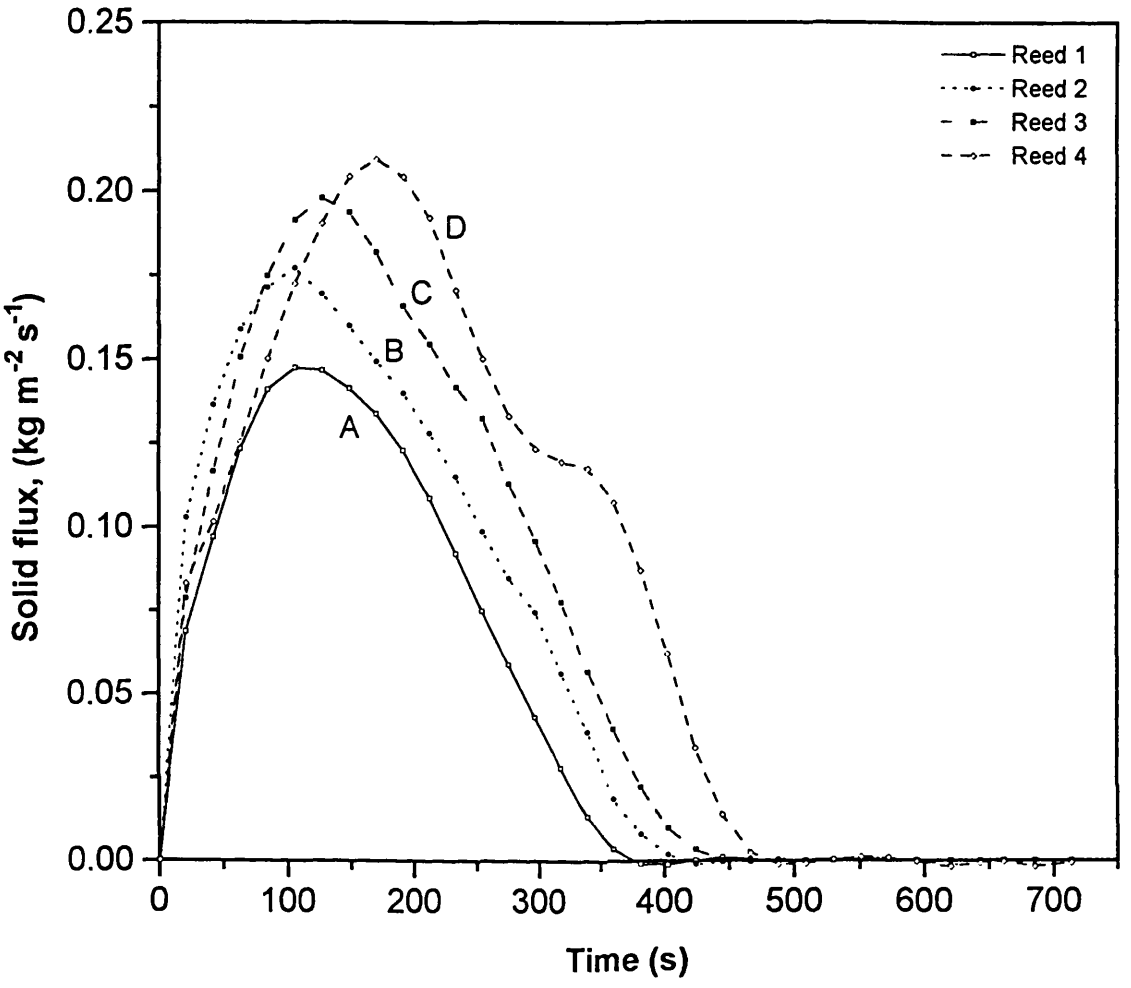

Figure 8.42

The variation of solids flux with time for polydisperse 80 - 115 μm glass ballotini spheres (density 2550 kgm^{-3}, ϕ = 1.75 %) settling in water @ 17 °C at various reed positions as measured from the top of the settling zone: curve A, 699 mm; curve B, 900 mm; curve C, 1096 mm and curve D, 1296 mm

	Area (kgm^{-2})	Measured Solids Throughput (g)	Volume-based Solids Throughput (g)	Percentage Difference (%)
Curve A	32.68	577.5	551.2	4.6
Curve B	42.01	742.4	709.7	4.4
Curve C	48.67	860.0	864.2	0.5
Curve D	58.22	1028.8	1022.0	0.7

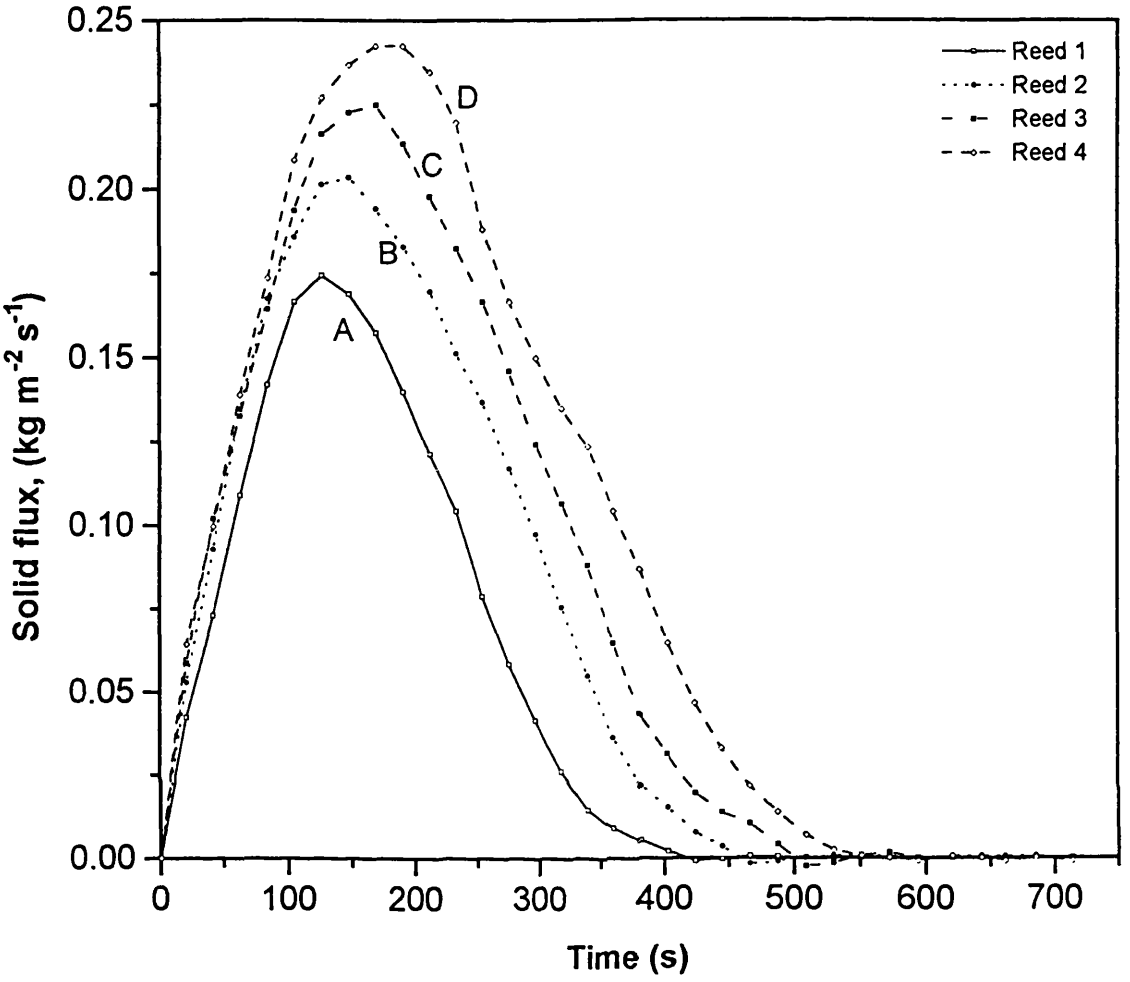

Figure 8.43
The variation of solids flux with time for polydisperse 80 - 115 μm glass ballotini spheres (density 2550 kgm^{-3}, ϕ = 2.01 %) settling in water @ 17 °C at various reed positions as measured from the top of the settling zone: curve A, 699 mm; curve B, 900 mm; curve C, 1096 mm and curve D, 1296 mm

	Area (kgm^{-2})	Measured Solids Throughput (g)	Volume-based Solids Throughput (g)	Percentage Difference (%)
Curve A	34.56	610.7	633.1	3.7
Curve B	48.72	861.0	815.2	5.3
Curve C	57.67	1019.1	992.7	2.6
Curve D	68.39	1208.6	1173.8	2.9

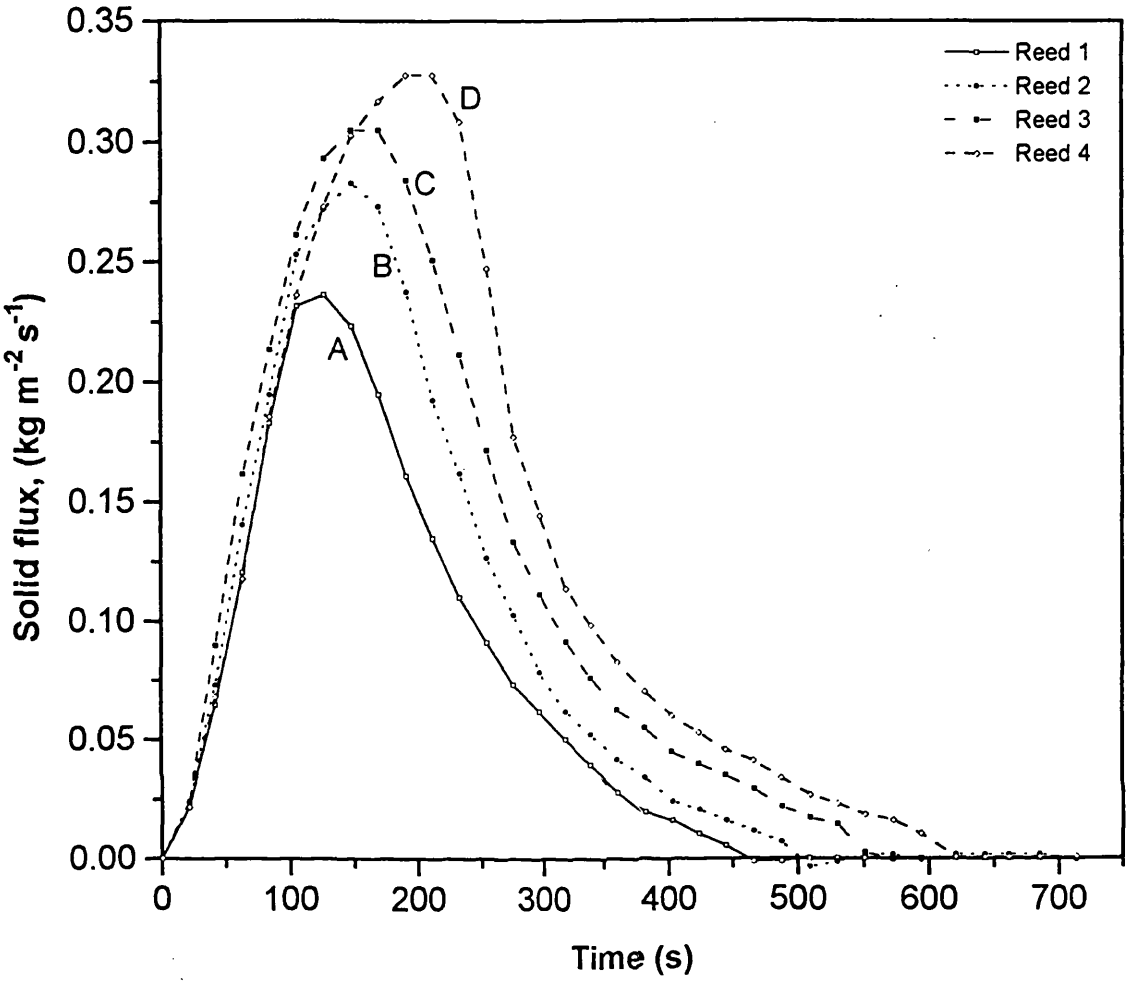

Figure 8.44

The variation of solids flux with time for polydisperse 80 - 115 μm glass ballotini spheres (density 2550 kgm^{-3}, ϕ = 2.35 %) settling in water @ 17 °C at various reed positions as measured from the top of the settling zone: curve A, 699 mm; curve B, 900 mm; curve C, 1096 mm and curve D, 1296 mm

	Area (kgm^{-2})	Measured Solids Throughput (g)	Volume-based Solids Throughput (g)	Percentage Difference (%)
Curve A	43.85	775.0	740.2	4.70
Curve B	56.80	1003.8	953.0	5.33
Curve C	69.89	1235.0	1160.6	6.41
Curve D	79.40	1403.1	1372.4	2.24

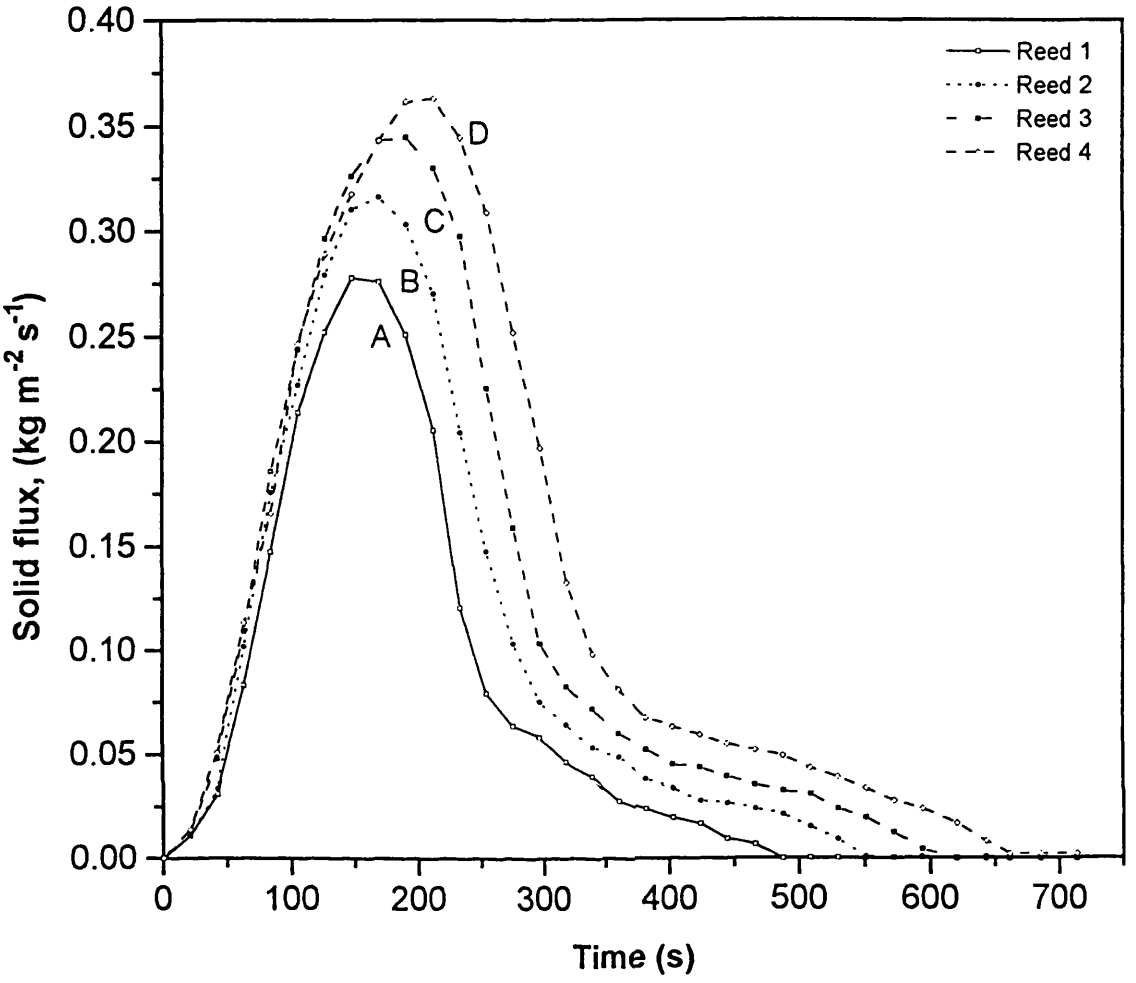

Figure 8.45

The variation of solids flux with time for polydisperse 80 - 115 μm glass ballotini spheres (density 2550 kgm^{-3}, ϕ = 2.56 %) settling in water @ 17 °C at various reed positions as measured from the top of the settling zone: curve A, 699 mm; curve B, 900 mm; curve C, 1096 mm and curve D, 1296 mm

	Area (kgm^{-2})	Measured Solids Throughput (g)	Volume-based Solids Throughput (g)	Percentage Difference (%)
Curve A	47.74	843.7	806.3	4.4
Curve B	61.78	1091.7	1038.2	4.9
Curve C	75.59	1335.9	1264.3	5.4
Curve D	89.51	1581.7	1495.0	5.5

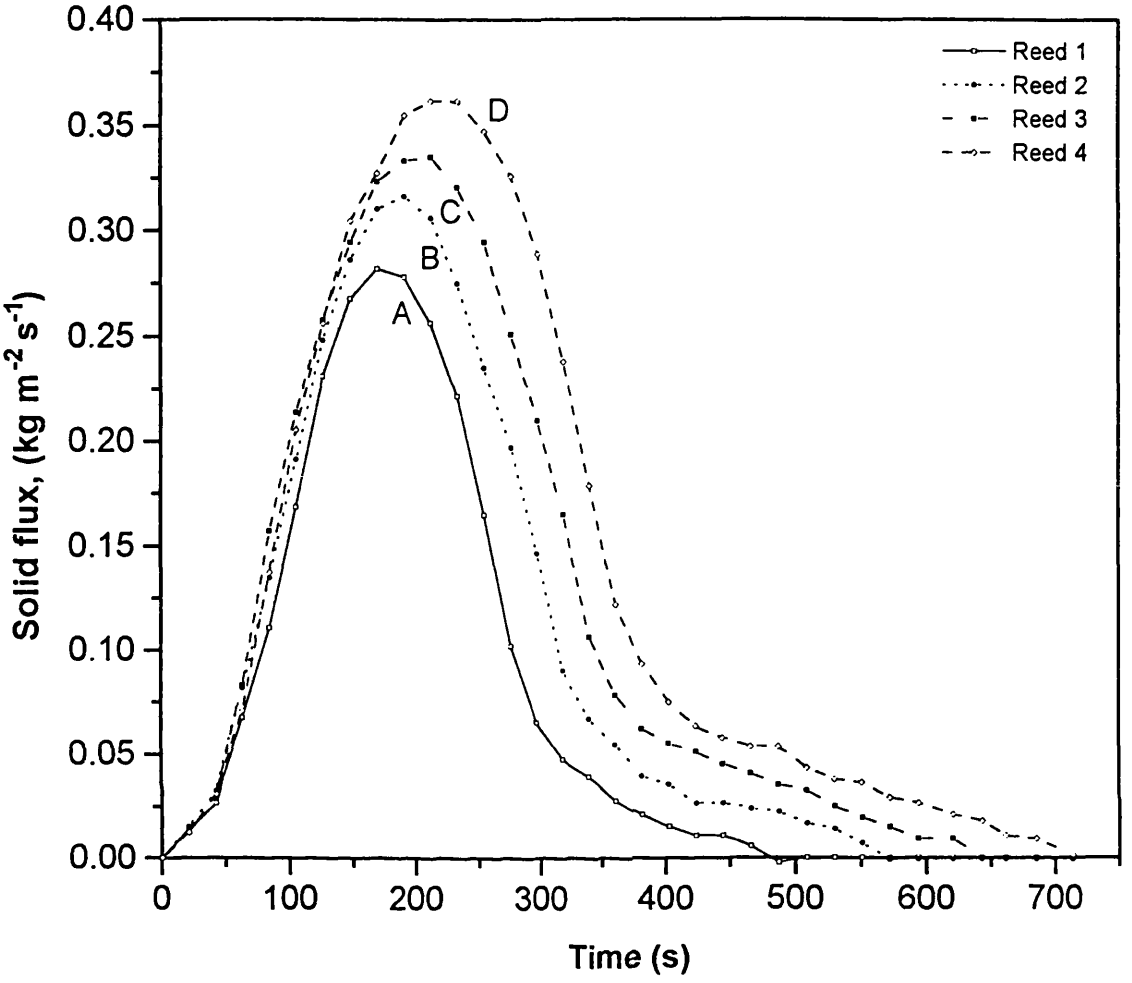

Figure 8.46

The variation of solids flux with time for polydisperse 80 - 115 μm glass ballotini spheres (density 2550 kgm^{-3}, ϕ = 2.81 %) settling in water @ 17 °C at various reed positions as measured from the top of the settling zone: curve A, 699 mm; curve B, 900 mm; curve C, 1096 mm and curve D, 1296 mm

	Area (kgm^{-2})	Measured Solids Throughput (g)	Volume-based Solids Throughput (g)	Percentage Difference (%)
Curve A	51.39	908.1	885.1	2.5
Curve B	67.50	1192.7	1139.6	4.5
Curve C	81.82	1446.0	1387.7	4.0
Curve D	96.59	1706.9	1641.1	3.9

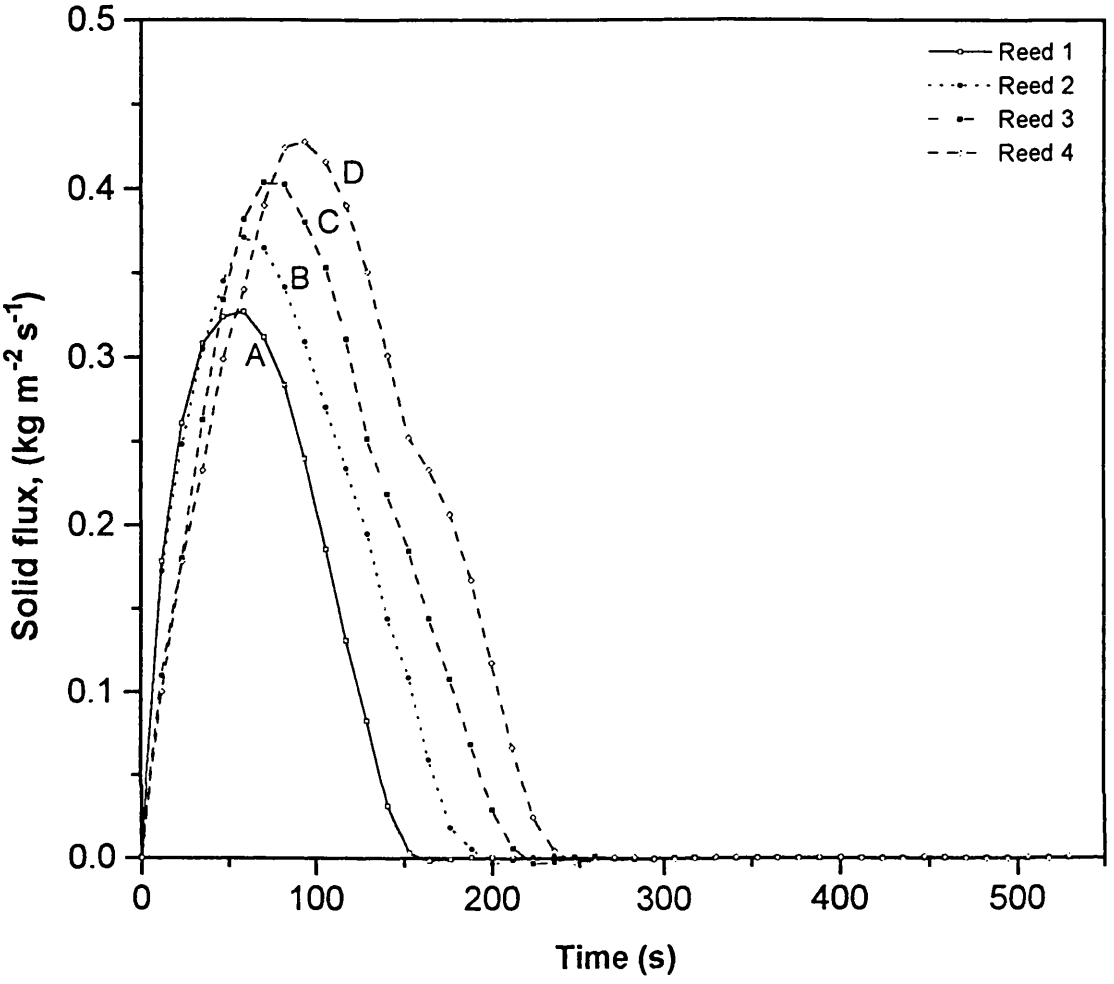

Figure 8.47

The variation of solids flux with time for polydisperse 90 - 135 μm glass ballotini spheres (density 2550 kgm^{-3}, ϕ = 1.75 %) settling in water @ 17 °C at various reed positions as measured from the top of the settling zone: curve A, 699 mm; curve B, 900 mm; curve C, 1096 mm and curve D, 1296 mm

	Area (kgm^{-2})	Measured Solids Throughput (g)	Volume-based Solids Throughput (g)	Percentage Difference (%)
Curve A	31.35	554.0	551.2	0.5
Curve B	41.03	725.1	709.7	2.1
Curve C	48.46	856.4	864.2	0.9
Curve D	57.87	1022.7	1022.0	0.1

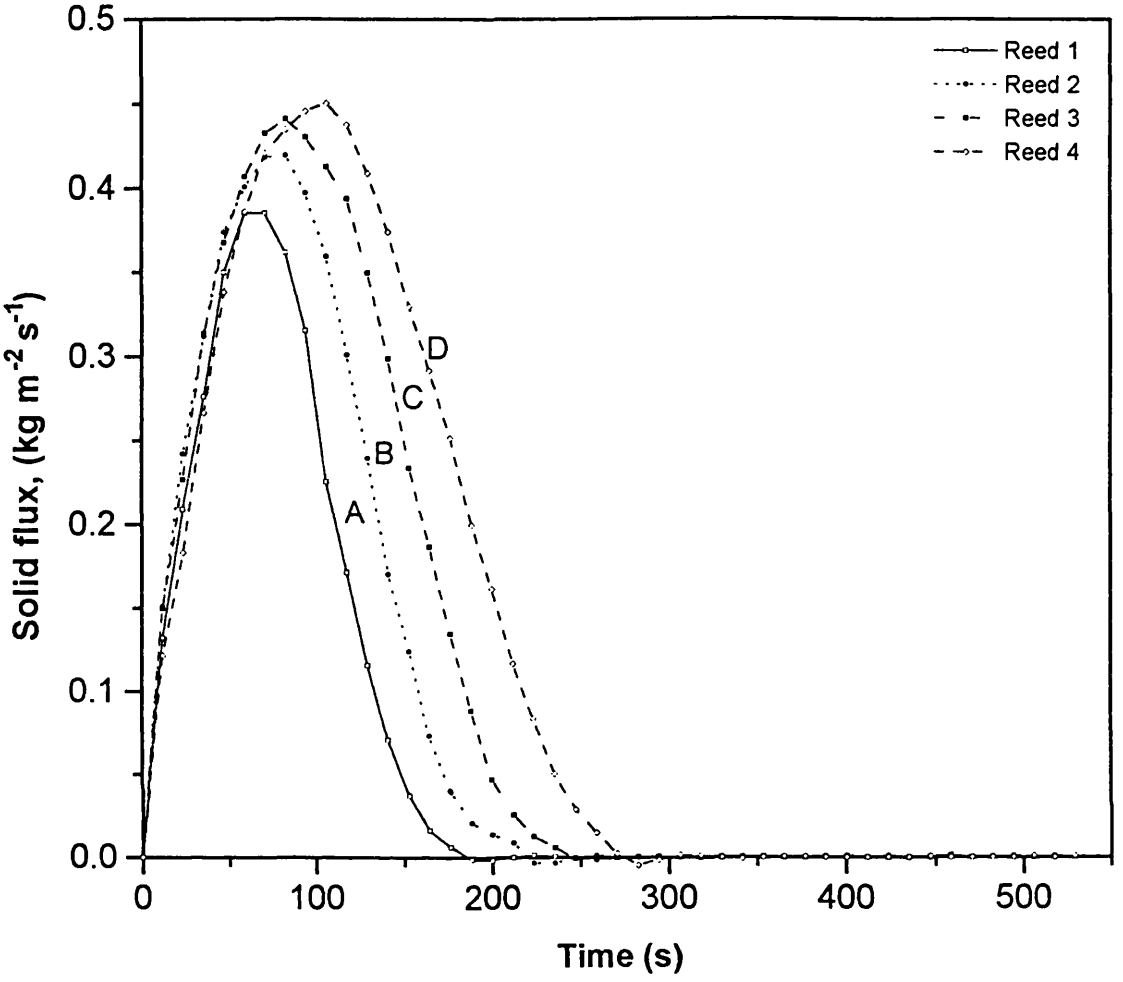

Figure 8.48

The variation of solids flux with time for polydisperse 90 - 135 μm glass ballotini spheres (density 2550 kgm^{-3}, $\phi = 2.01$ %) settling in water @ 17 °C at various reed positions as measured from the top of the settling zone: curve A, 699 mm; curve B, 900 mm; curve C, 1096 mm and curve D, 1296 mm

	Area (kgm^{-2})	Measured Solids Throughput (g)	Volume-based Solids Throughput (g)	Percentage Difference (%)
Curve A	35.92	634.8	633.1	0.3
Curve B	47.74	843.7	815.2	3.4
Curve C	58.23	1029.1	992.7	3.5
Curve D	68.15	1204.4	1173.8	2.5

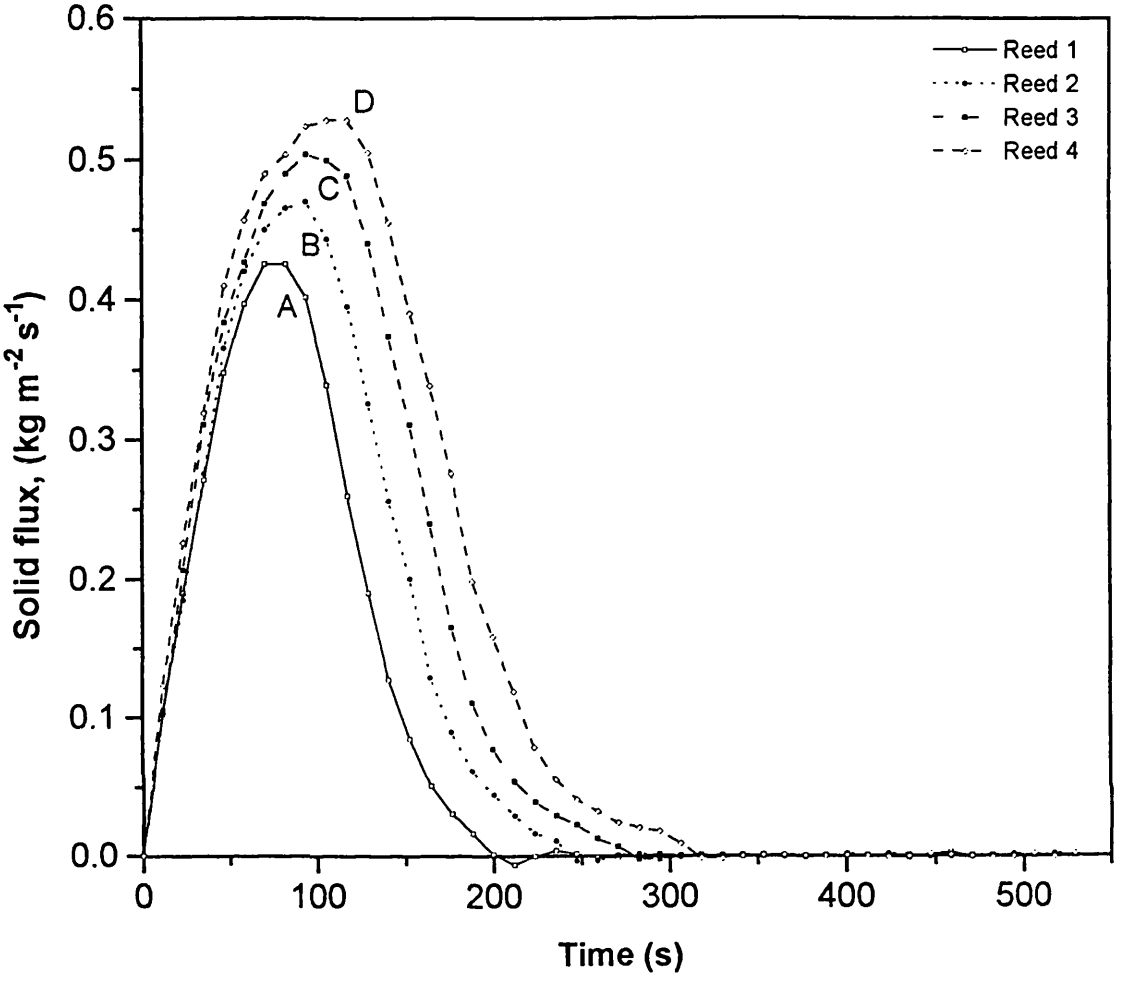

Figure 8.49

The variation of solids flux with time for polydisperse 90 - 135 μm glass ballotini spheres (density 2550 kgm^{-3}, ϕ = 2.35 %) settling in water @ 17 °C at various reed positions as measured from the top of the settling zone: curve A, 699 mm; curve B, 900 mm; curve C, 1096 mm and curve D, 1296 mm

	Area (kgm^{-2})	Measured Solids Throughput (g)	Volume-based Solids Throughput (g)	Percentage Difference (%)
Curve A	43.00	759.9	740.2	2.6
Curve B	55.66	983.5	953.0	3.1
Curve C	67.70	1196.3	1160.6	3.0
Curve D	80.24	1418.0	1372.4	3.2

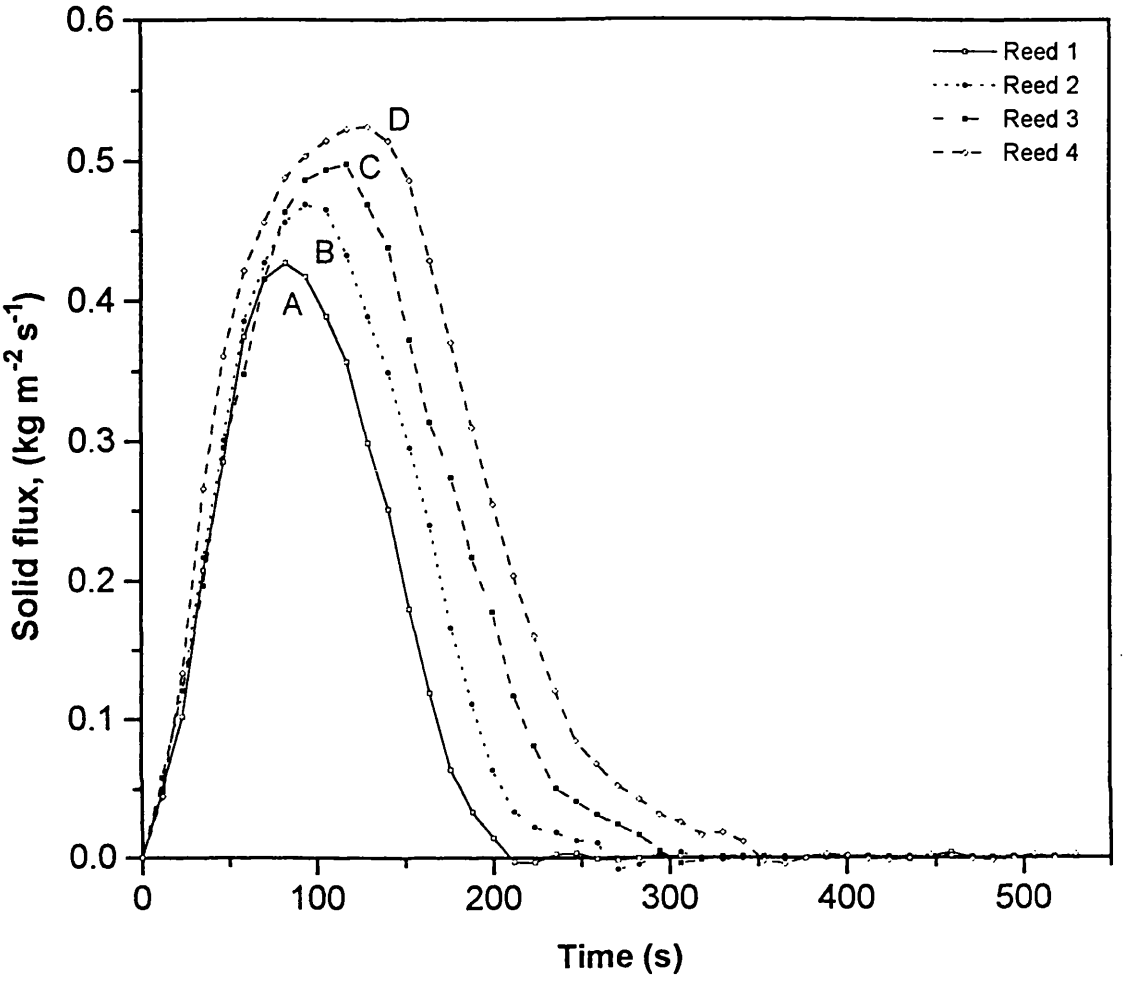

Figure 8.50
The variation of solids flux with time for polydisperse 90 - 135 μm glass ballotini spheres (density 2550 kgm^{-3}, ϕ = 2.56 %) settling in water @ 17 °C at various reed positions as measured from the top of the settling zone: curve A, 699 mm; curve B, 900 mm; curve C, 1096 mm and curve D, 1296 mm

	Area (kgm^{-2})	Measured Solids Throughput (g)	Volume-based Solids Throughput (g)	Percentage Difference (%)
Curve A	46.81	827.2	806.2	2.5
Curve B	59.11	1044.6	1038.2	0.6
Curve C	70.57	1247.0	1264.3	1.4
Curve D	87.36	1543.7	1495.0	3.2

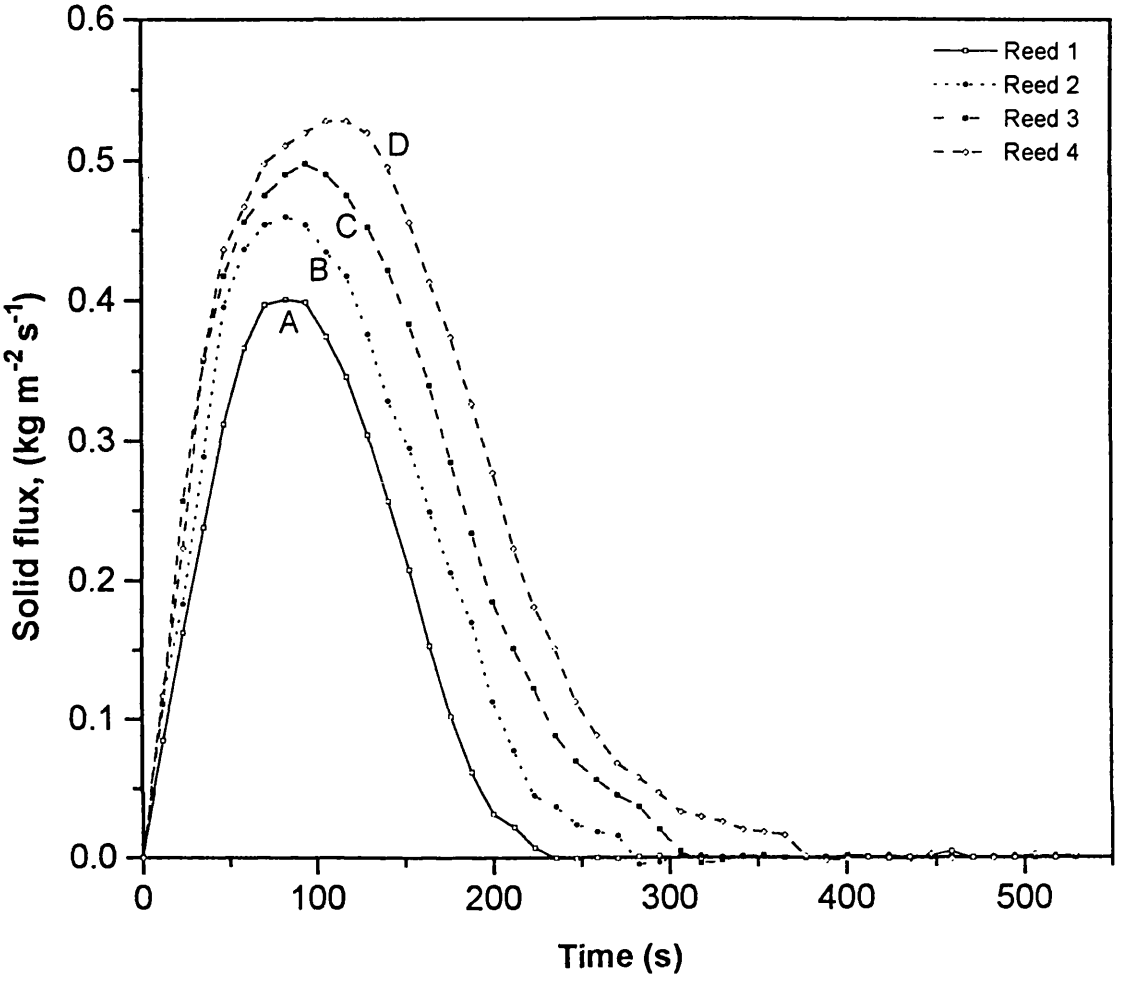

Figure 8.51

The variation of solids flux with time for polydisperse 90 - 135 μm glass ballotini spheres (density 2550 kgm^{-3}, ϕ = 2.81 %) settling in water @ 17 °C at various reed positions as measured from the top of the settling zone: curve A, 699 mm; curve B, 900 mm; curve C, 1096 mm and curve D, 1296 mm

	Area (kgm^{-2})	Measured Solids Throughput (g)	Volume-based Solids Throughput (g)	Percentage Difference (%)
Curve A	49.66	877.6	885.1	0.9
Curve B	65.74	1161.7	1139.6	1.9
Curve C	81.26	1436.0	1387.7	3.4
Curve D	95.45	1686.8	1641.1	2.7

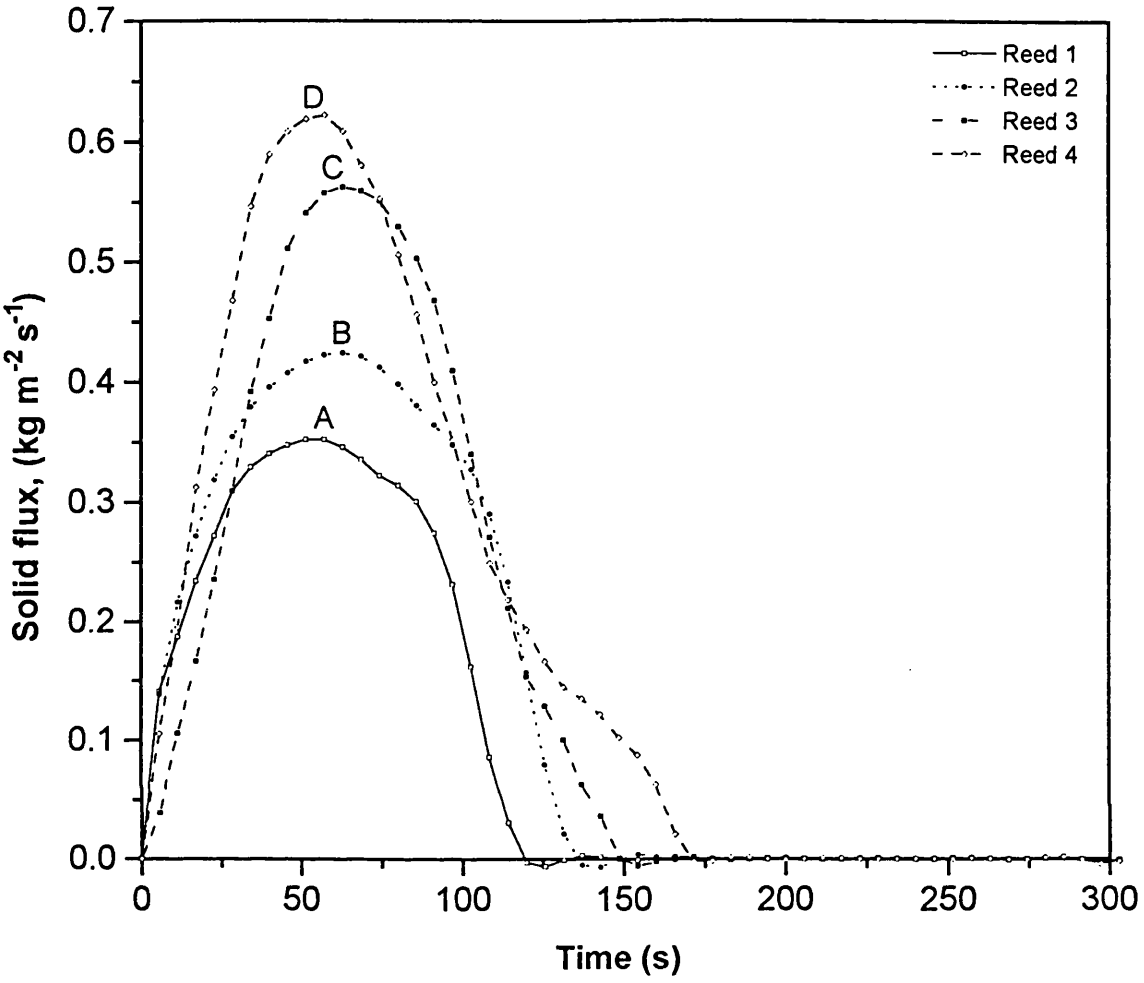

Figure 8.52

The variation of solids flux with time for polydisperse 100 - 200 μm glass ballotini spheres (density 2550 kgm^{-3}, ϕ = 1.75 %) settling in water @ 17 °C at various reed positions as measured from the top of the settling zone: curve A, 699 mm; curve B, 900 mm; curve C, 1096 mm and curve D, 1296 mm

	Area (kgm^{-2})	Measured Solids Throughput (g)	Volume-based Solids Throughput (g)	Percentage Difference (%)
Curve A	30.33	536.0	551.2	2.8
Curve B	41.41	731.8	709.7	3.0
Curve C	47.27	835.3	864.2	3.5
Curve D	56.08	991.0	1022.0	3.1

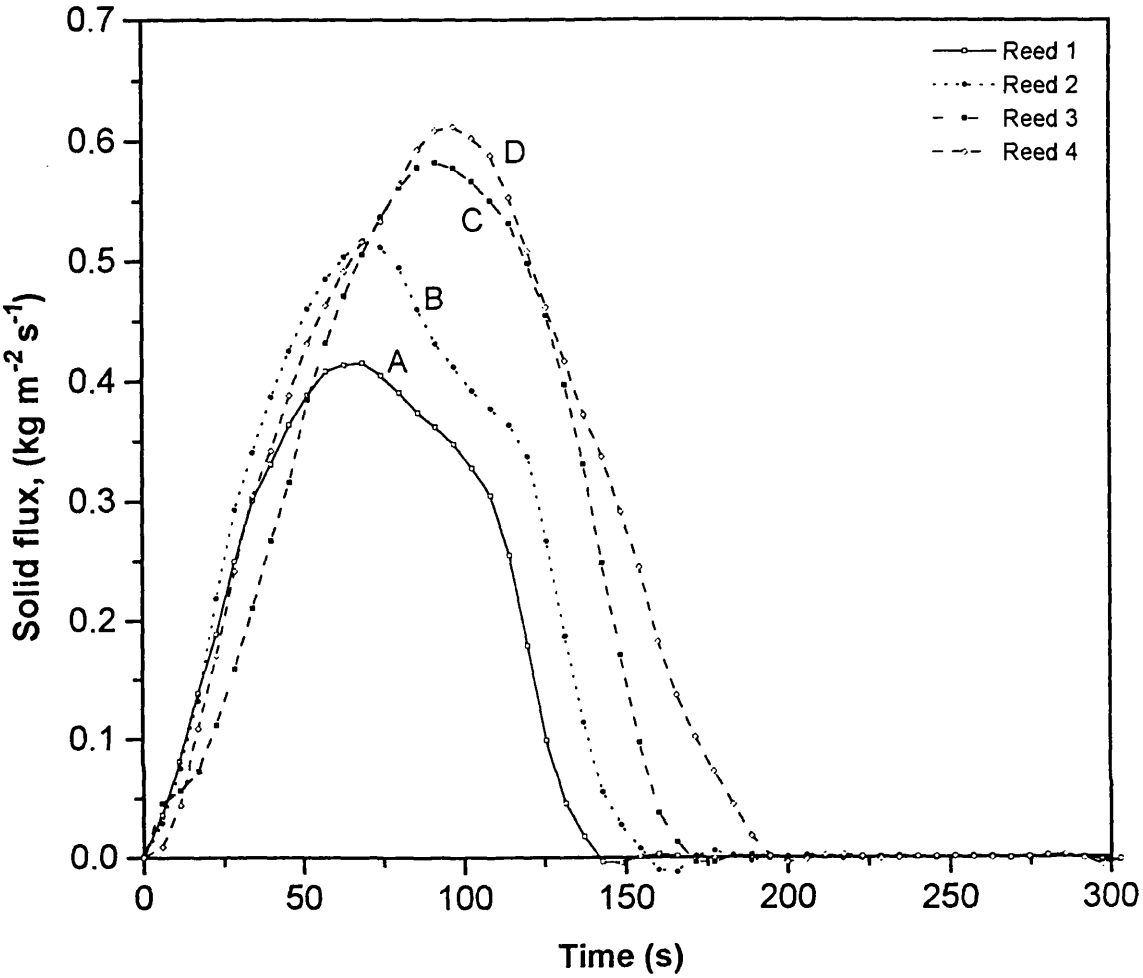

Figure 8.53

The variation of solids flux with time for polydisperse 100 - 200 μm glass ballotini spheres (density 2550 kgm^{-3}, ϕ = 2.01 %) settling in water @ 17 °C at various reed positions as measured from the top of the settling zone: curve A, 699 mm; curve B, 900 mm; curve C, 1096 mm and curve D, 1296 mm

	Area (kgm^{-2})	Measured Solids Throughput (g)	Volume-based Solids Throughput (g)	Percentage Difference (%)
Curve A	37.10	655.6	633.1	3.4
Curve B	48.05	849.1	815.2	4.0
Curve C	56.37	996.2	992.7	0.4
Curve D	65.58	1158.8	1173.8	1.3

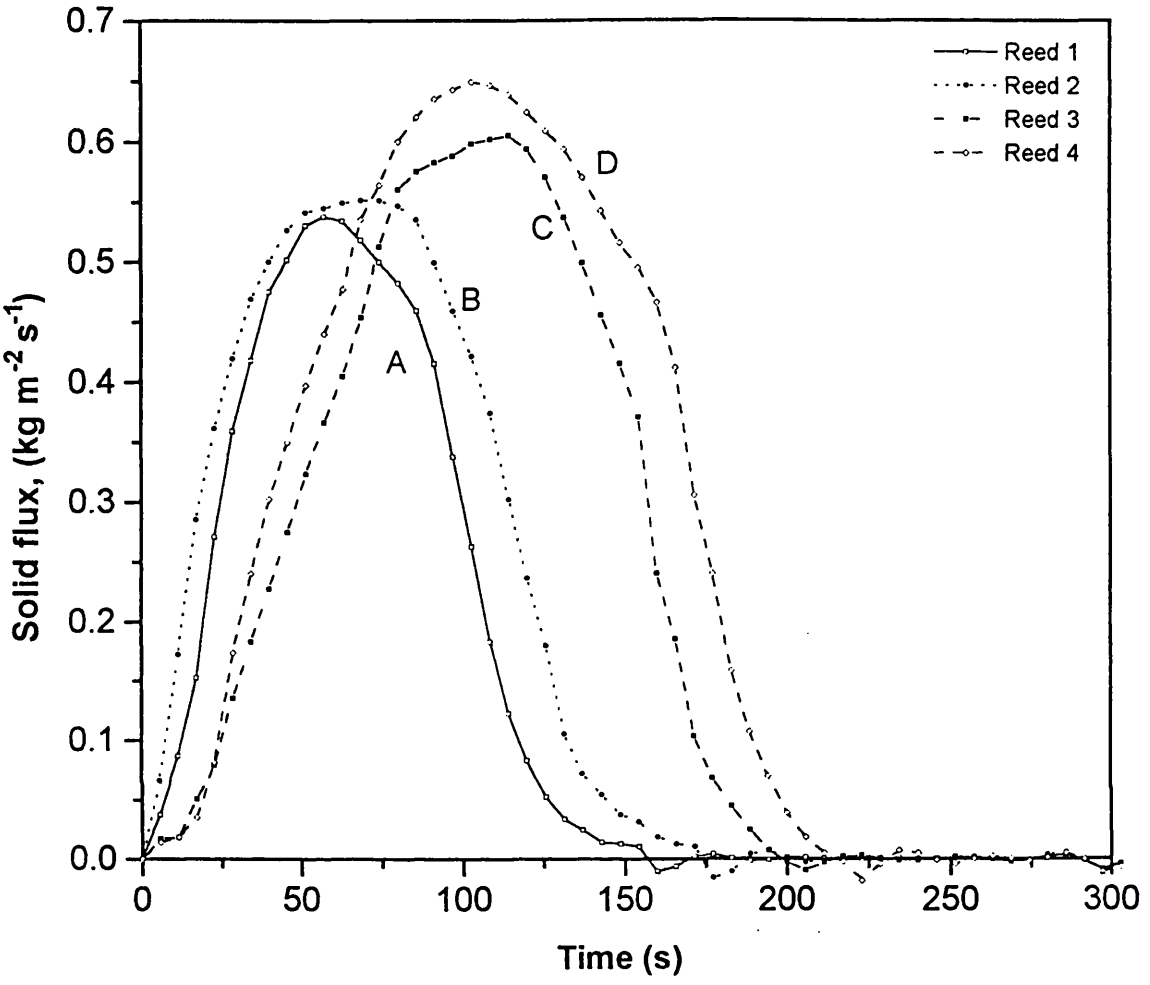

Figure 8.54

The variation of solids flux with time for polydisperse 100 - 200 μm glass ballotini spheres (density 2550 kgm^{-3}, ϕ = 2.35 %) settling in water @ 17 °C at various reed positions as measured from the top of the settling zone: curve A, 699 mm; curve B, 900 mm; curve C, 1096 mm and curve D, 1296 mm

	Area (kgm^{-2})	Measured Solids Throughput (g)	Volume-based Solids Throughput (g)	Percentage Difference (%)
Curve A	43.33	765.7	740.2	3.3
Curve B	55.16	974.8	953.0	2.2
Curve C	65.42	1156.0	1160.6	0.4
Curve D	80.30	1419.0	1372.4	3.3

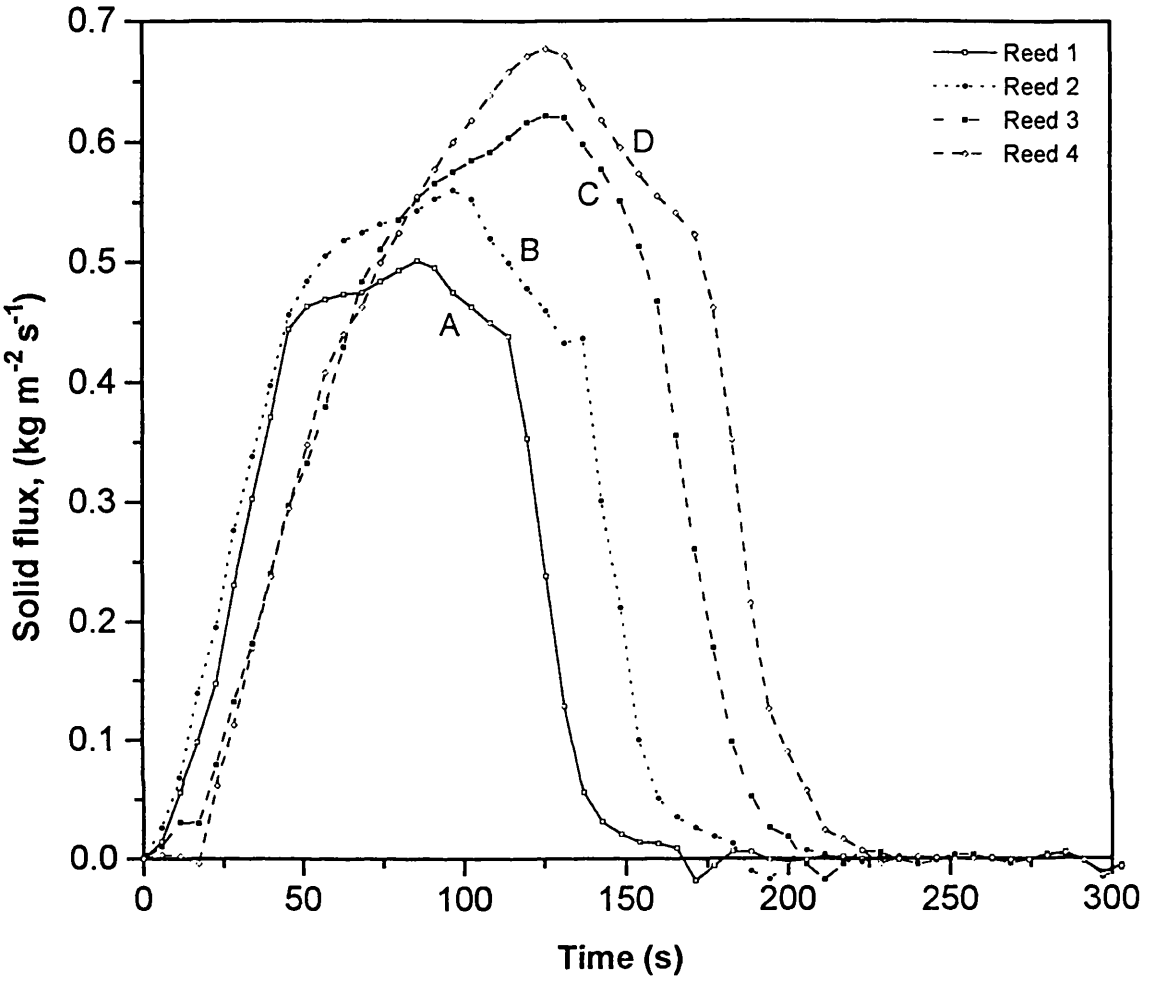

Figure 8.55

The variation of solids flux with time for polydisperse 100 - 200 μm glass ballotini spheres (density 2550 kgm^{-3}, ϕ = 2.56 %) settling in water @ 17 °C at various reed positions as measured from the top of the settling zone: curve A, 699 mm; curve B, 900 mm; curve C, 1096 mm and curve D, 1296 mm

	Area (kgm^{-2})	Measured Solids Throughput (g)	Volume-based Solids Throughput (g)	Percentage Difference (%)
Curve A	48.20	851.7	806.3	5.3
Curve B	63.21	1116.9	1038.2	7.0
Curve C	73.82	1304.5	1264.3	3.1
Curve D	85.13	1504.3	1495.0	0.6

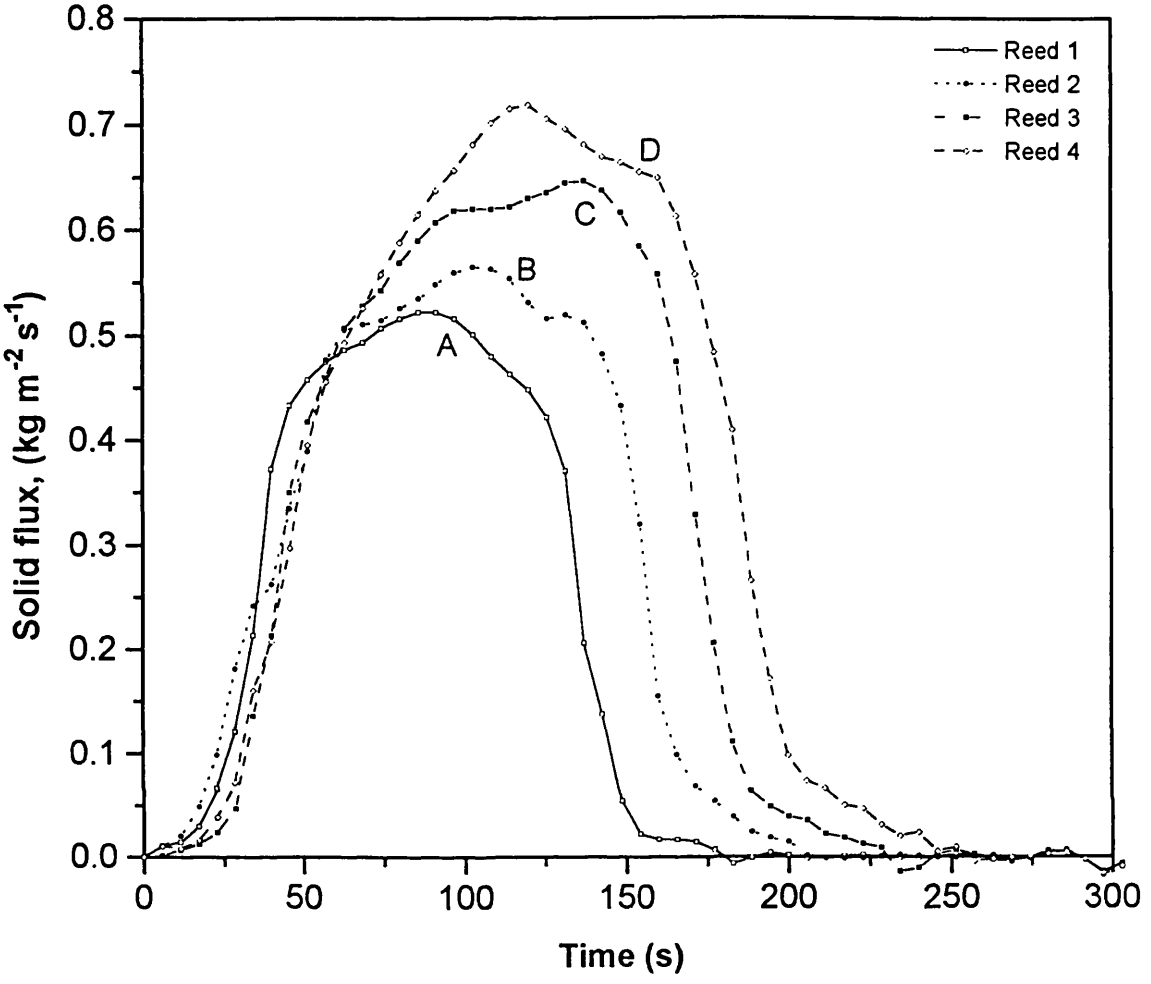

Figure 8.56

The variation of solids flux with time for polydisperse 100 - 200 μm glass ballotini spheres (density 2550 kgm^{-3}, ϕ = 2.81 %) settling in water @ 17 °C at various reed positions as measured from the top of the settling zone: curve A, 699 mm; curve B, 900 mm; curve C, 1096 mm and curve D, 1296 mm

	Area (kgm^{-2})	Measured Solids Throughput (g)	Volume-based Solids Throughput (g)	Percentage Difference (%)
Curve A	52.54	928.4	885.1	4.7
Curve B	66.26	1170.9	1139.6	2.7
Curve C	80.45	1421.7	1387.7	2.4
Curve D	94.47	1669.4	1641.1	1.7

$$Solids\ throughput\,(kg) = \int_{t=0}^{t=\Delta t_b} \Phi\, A\, dt \qquad (8.1)$$

where A is the settling tank cross-sectional area. The same equation may of course be used to determine the solids throughput at any other time, t during the sedimentation process. In such a case the upper limit in equation 8.1 becomes, t.

In practice, direct measurement of the solids throughput is important as it can be used as a useful process parameter in monitoring the degree of separation say in a settling tank or where appropriate, the stability of a two phase suspension.

In order to evaluate the capability of our system in correctly providing such type of data, we compare the measured solids throughputs obtained from the reeds' response to those estimated directly from the solids concentration in a given volume during the entire settling process.

Taking curve A in figure 8.37 relating to the solids flux kinetic data for 55 - 100 μm suspensions as an example, the above procedure gives an integrated area of 32 kgm^{-2} for a breakthrough time of ca. 340 s. The latter refers to the time at which the solids flux curve intersects the abscissa. Multiplying the value of the integral by the settling tank cross-sectional area of 1.77×10^{-2} m^2 yields a measured solids mass throughput of 566.2 g for reed 1. This result can be compared with a volume-based estimate of the solids mass throughput calculated by multiplying the known initial solids concentration (1.75 % v/v; equivalent particle mass per unit volume, 44.63 kgm^{-3}) by the suspension volume above reed 1 (1.23×10^{-2} m^3). This gives a solids mass throughput of 548.9 g representing a percentage difference of only 3.1 % when compared to that measured from the reed response.

The table in figure 8.37 shows data obtained from reeds 2 - 4 for which the maximum difference between experimental and volume-based solids mass throughputs is 4.7 %.

The tables in figures 8.38 - 8.41 show mass balance data at the higher solids concentrations 2.01 % v/v (equivalent particle mass per unit volume, 51.3 kgm^{-3}) to 2.81 % v/v (equivalent particle mass per unit volume, 71.7 kgm^{-3}) for the 55 - 100 μm size fraction. Similarly, the tables in figures 8.42 - 8.46, figures 8.47 - 8.51 and figures 8.52 - 8.56 show mass balance data for the 80 - 115 μm, 90 - 135 μm and 100 - 200 μm size fraction suspensions respectively. As it may be observed, the percentage difference between measured and volume-based estimates of the solids mass throughput is not greater than 7.0 % thus substantiating the viability of the vibrating reed device in providing mass throughput data.

8.6 Comparison of Experimental Data with Theoretical Models

As discussed in chapter 4, in contrast to monodisperse systems, most of the theoretical models developed for predicting the settling velocities of polydisperse systems have been mainly confined to relatively concentrated systems (> 5 % v/v). As such it has been difficult to draw a meaningful comparison between the predictions obtained from these models and the experimental data obtained in this work as these are mainly confined to dilute systems (< 3 % v/v). In such systems, in contrast to concentrated suspensions, differential settling results in diffuse interfaces the settling rates of which are not representative of the bulk behaviour of suspensions. For example, the empirical-hydrodynamic correlation of Masliyah (1979) (equation 4.26) was developed in conjunction with suspensions with solids volume concentrations > 10 % v/v. The hydrodynamic correlation of Smith (1967) (equation 4.29) on the other hand, was developed in conjunction with solids volume concentrations in the range 0.8 - 2.5 % v/v. However, this model consistently underestimates individual particle settling velocities (Patwardhan and Tien, 1985). The empirical-hydrodynamic simulation model of Mirza and Richardson (1979) was developed in conjunction with suspensions with solids volume concentrations in the range 25 - 45 % v/v. Similarly, the more rigorous hydrodynamic simulation model of Williams and Amarasinghe (1989) was developed in conjunction with suspensions with solids volume concentrations in the range 5 - 60 % v/v.

The experimental interface velocity data obtained in conjunction with the nominally monodisperse 200 - 212 μm glass ballotini/water suspensions were shown to accurately represent the average settling rate of the particulate phase (see figure 7.20, chapter 7). Here, these results are compared with those calculated from some of the predictive models for monodisperse systems reviewed in chapter 4. The experimentally determined mean particle size ($\overline{d}_p$ = 206 μm) is used, where appropriate, to determine the particle Reynolds number, Re_p. The average particle terminal settling velocity, $\overline{u}_o$ (26.1 mms^{-1}) on the other hand is determined by dropping individual particles into a 2 m long × 30 cm diameter perspex column filled with water. The terminal velocity is then calculated from the time taken for a particle to fall a distance of 50 cm. This procedure is repeated a total of 30 times in order to obtain a representative average.

Figure 8.57 shows a comparison of experimentally determined settling velocities to those predicted from theoretical models for various initial suspended solids volume concentrations. As it may be observed, the experimental settling velocities are in especially good agreement with those predicted from Richardson and Zaki's (1954) empirical correlation (equation 4.8). Although this correlation was developed in conjunction with solids volume concentrations in the range 10 - 40 % v/v (the hindered settling regime) it can be applied to dilute systems (solids volume concentrations < 5 % v/v) by using an appropriate value for the flow index, n calculated from the known particle Reynolds number, Re_p. The empirical correlation of Garside and Al-Dibouni (1977) (equation 4.10) is also in good accord with experimental measurements. It is noteworthy that this correlation was developed in conjunction with systems with solids volume concentrations as low as 5 % v/v.

In contrast, the hydrodynamic model of Reed and Anderson (1980) (equation 4.13) appears to consistently underestimate settling velocities. This is probably due to overestimation of the influence of hydrodynamic and electrostatic phenomena on the settling behaviour of the particles as previously discussed in chapter 4. The hydrodynamic model of Batchelor (1972) (equation 4.12) which was developed on a similar basis also underestimates particle settling velocities.

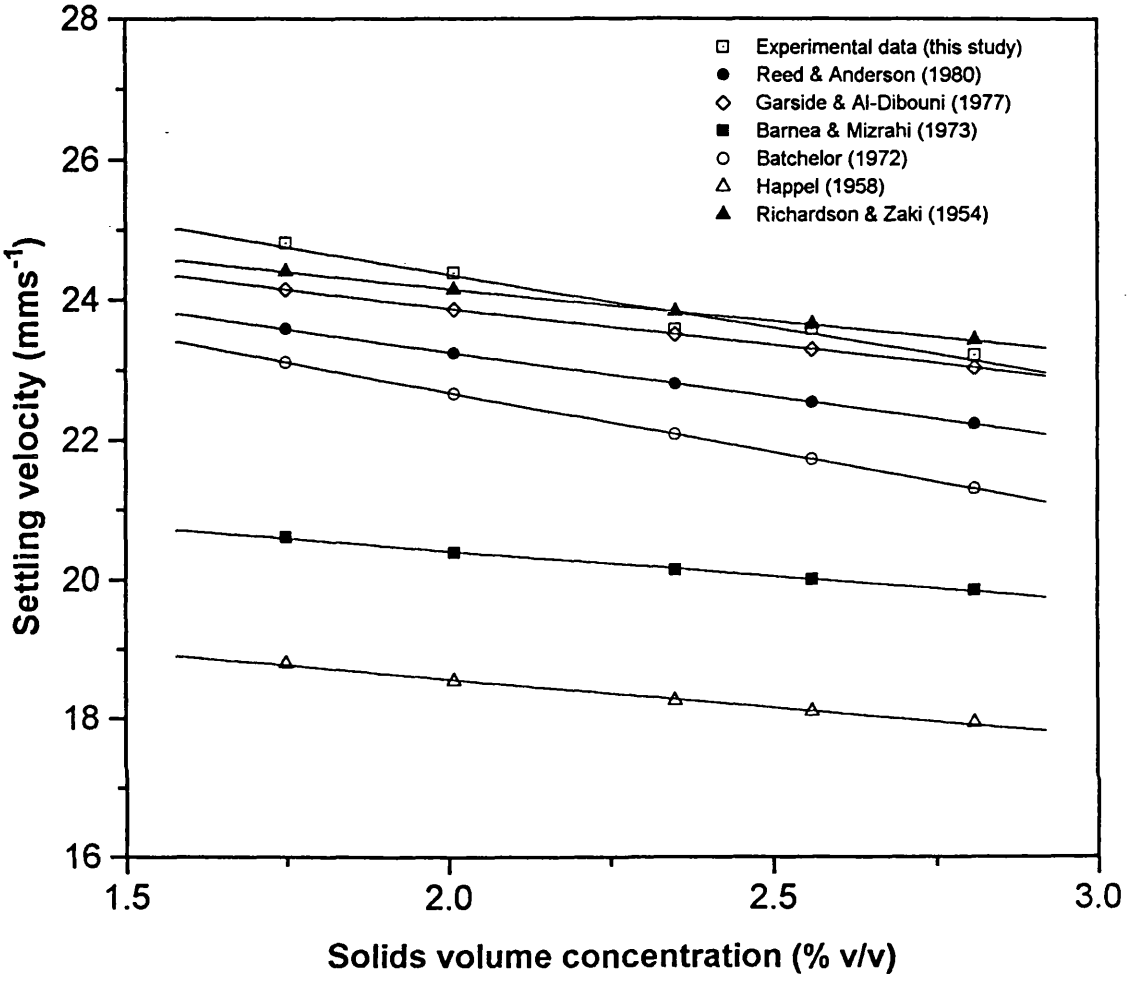

Figure 8.57
A comparison of experimentally determined settling velocities to those predicted from various theoretical models. The data relate to monodisperse 200 - 212 μm glass ballotini spheres (density 2550 kgm^{-3}) settling in water @ 17 °C at initial suspended solids volume concentrations in the range (1.75 - 2.81%).

The data calculated from the hydrodynamic model of Barnea and Mizrahi (1973) (equation 4.11) indicates an even greater underestimation of settling velocities. This is somewhat unexpected since the model is quite rigorous taking into account hydrostatic, momentum transfer and wall effects. A plausible explanation for this trend is that the model only applies to hindered settling. In addition, compared to the models of Richardson and Zaki (1954) and Garside and Al-Dibouni (1977) the correlation of Barnea and Mizrahi (1973) is entirely based on the solids volume concentration and does not take the particle size into account. The hydrodynamic correlation of Happel (1958) (equation 4.30) shows the largest deviation from experimental data. This model is also entirely based on the particle concentration and does not take the particle size into account.

8.6.1 Estimation of Propagation Wave Velocities

As mentioned in section 8.1, the switching off of the circulation pump marks the onset of transition from steady state to unsteady state operation. This results in the propagation of a disturbance wave which travels from the top of the settling zone towards the base of the settling tank. The speed at which this wave travels or the propagation wave velocity can be directly determined from the time taken between the switching off of the pump and that resulting in a change in the resonance frequency.

Figure 8.58 shows the variation of the lag time in the frequency response plotted against reed position relative to the top of the settling zone for different concentrations of 200 - 212 μm glass ballotini/water suspensions.

As it is clear, the data may be fitted to straight lines. The table in figure 8.58 gives the corresponding fitting equations, the appropriate correlation coefficients as well as the propagation wave velocities (the inverse of the slope of each line). Within the ranges tested the propagation wave velocity does not significantly change with solids concentration.

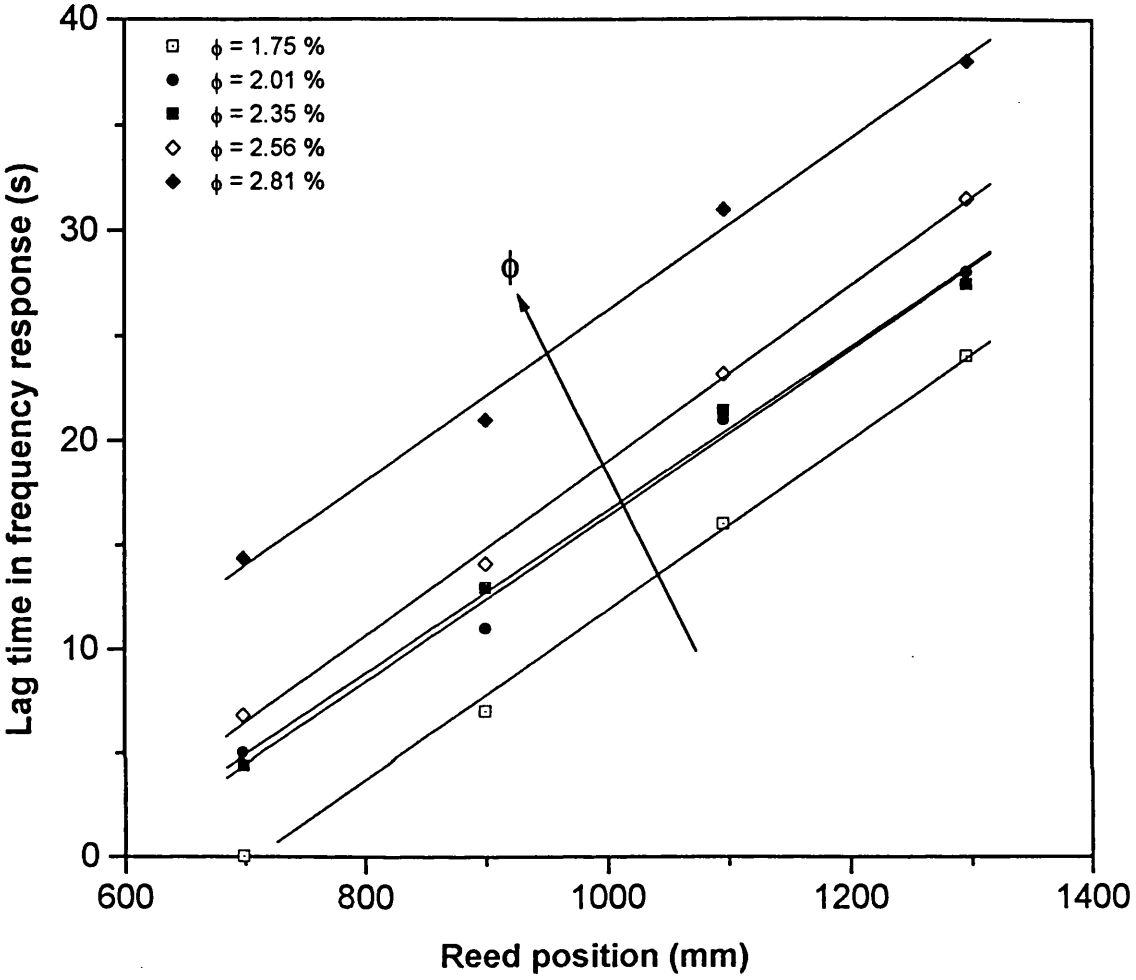

Figure 8.58
The variation of lag time in resonance frequency response with reed position relative to the top of the settling zone for monodisperse 200 - 212 μm glass ballotini spheres (density 2550 kgm^{-3}) settling in water @ 17 °C at various initial suspended solids volume concentrations, ϕ).

ϕ (%)	Fitting equation	Correlation coefficient	Propagation wave velocity (mm/s)
1.75	y = 0.0408x - 28.91	0.9987	24.5
2.01	y = 0.0397x - 23.40	0.9953	25.2
2.35	y = 0.0391x - 22.48	0.9968	25.6
2.56	y = 0.0416x - 22.52	0.9987	24.1
2.81	y = 0.0407x - 14.55	0.9965	24.6

Figures 8.59 - 8.62 show the same data as those in figure 8.58 but in conjunction with different size particles in the range 55 - 100 μm (figure 8.59), 80 - 115 μm (figure 8.60), 90 - 135 μm (figure 8.61) and 100 - 200 μm (figure 8.62). The same trends in the data may be observed. The propagation wave velocities are independent of particulate concentrations. However, there is a clear dependency on the particle size. As it turns out the speed at which the disturbance wave propagates from the top of the settling zone towards the base of the column appears to increase with increase in the mean particle size. Figure 8.63 shows the variation of propagation wave velocity with mean particle size. The data are average values of the propagation wave velocities shown in the tables in figures 8.58 - 8.62.

8.6.2 Interface Velocity Measurements

Figure 8.64 shows the variation of solids breakthrough time, Δt_b, with reed position relative to the top of the settling zone for the polydisperse 55 - 100 μm glass ballotini/water suspensions. As mentioned before, Δt_b corresponds to the time at which the solids flux curve intersects the abscissa. As for the monodisperse suspensions (see figure 7.19, chapter 7), the breakthrough time increases with increase in particle concentration as well as the distance of each reed relative to the top of the settling zone. The linear variation of breakthrough time with reed position is consistent with a constant interface velocity.

The table in figure 8.64 on the other hand, shows the corresponding experimental interface velocities determined by taking the reciprocal of the gradients of the fitted lines A to E. As it is clear, the interface velocity decreases with increase in solids concentration.

Figures 8.65 - 8.67 show the corresponding variations in the breakthrough time with reed position for various concentration ballotini/water suspensions with particles in the size ranges 80 - 115 , 90 - 135 and 100 - 200 μm respectively. As before, the linear variation in the data indicate that the interface velocity remains constant throughout the settling zone and decreases with increase in solids concentration.

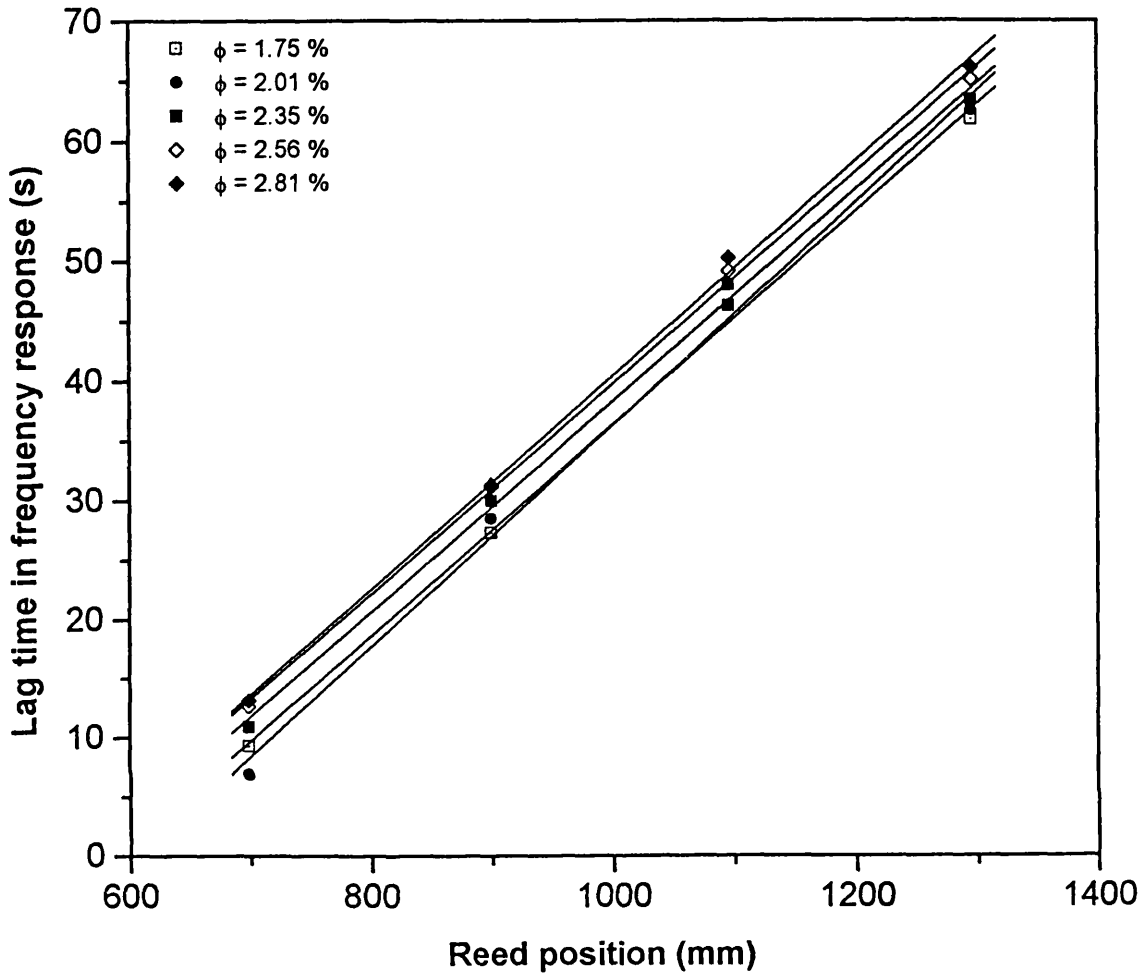

Figure 8.59
The variation of lag time in resonance frequency response with reed position relative to the top of the settling zone for polydisperse 55 - 100 μm glass ballotini spheres (density 2550 kgm^{-3}) settling in water @ 17 °C at various initial suspended solids volume concentrations, ϕ).

ϕ (%)	Fitting equation	Correlation coefficient	Propagation wave velocity (mm/s)
1.75	y = 0.0889x - 52.54	0.9991	11.3
2.01	y = 0.0930x - 56.79	0.9980	10.8
2.35	y = 0.0884x - 50.15	0.9989	11.3
2.56	y = 0.0883x - 48.55	0.9994	11.3
2.81	y = 0.0895x - 49.07	0.9993	11.2

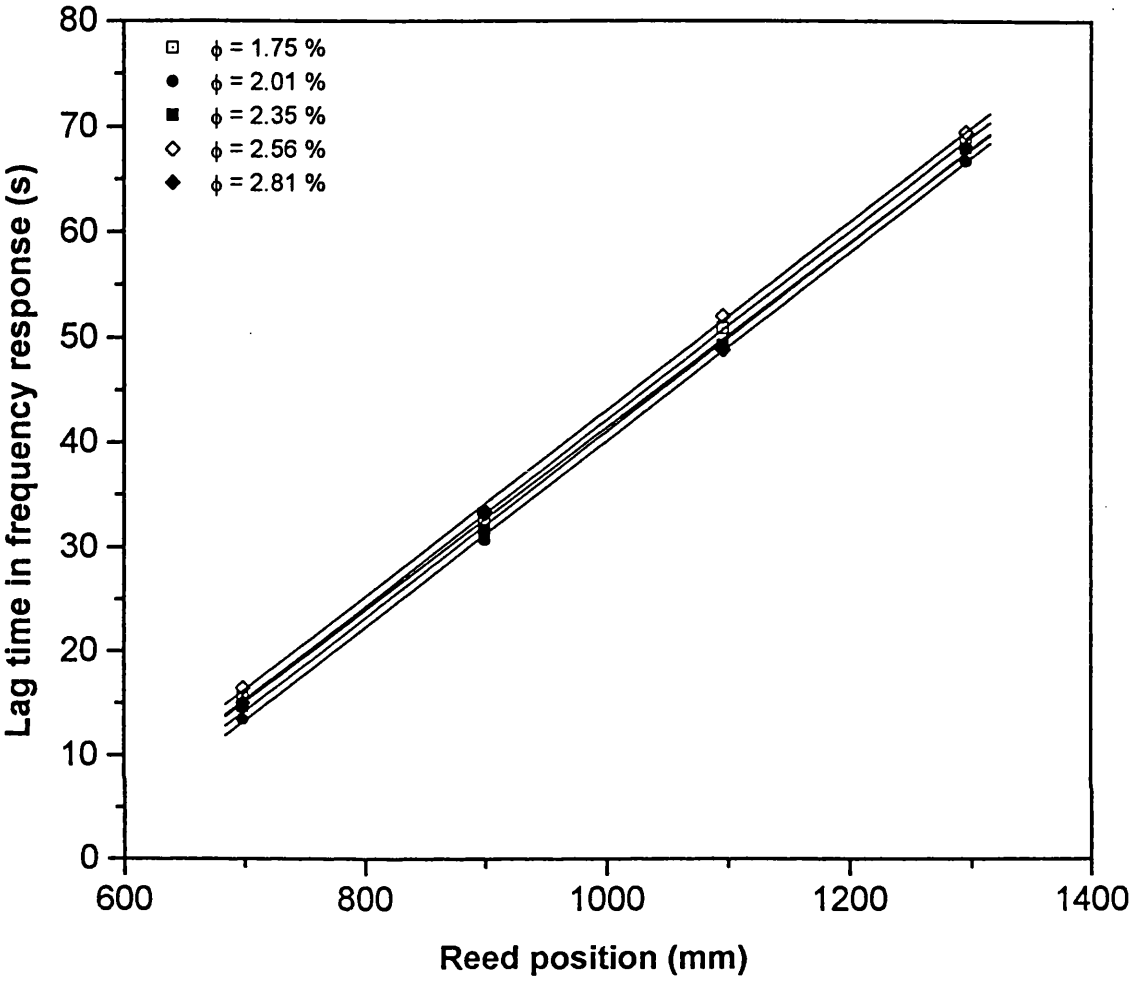

Figure 8.60
The variation of lag time in resonance frequency response with reed position relative to the top of the settling zone for polydisperse 80 - 115 μm glass ballotini spheres (density 2550 kgm^{-3}) settling in water @ 17 °C at various initial suspended solids volume concentrations, ϕ.

ϕ (%)	Fitting equation	Correlation coefficient	Propagation wave velocity (mm/s)
1.75	y = 0.0896x - 47.48	0.9998	11.2
2.01	y = 0.0896x - 49.48	0.9999	11.2
2.35	y = 0.0894x - 48.53	0.9997	11.2
2.56	y = 0.0894x - 46.36	0.9998	11.2
2.81	y = 0.0879x - 46.46	0.9994	11.4

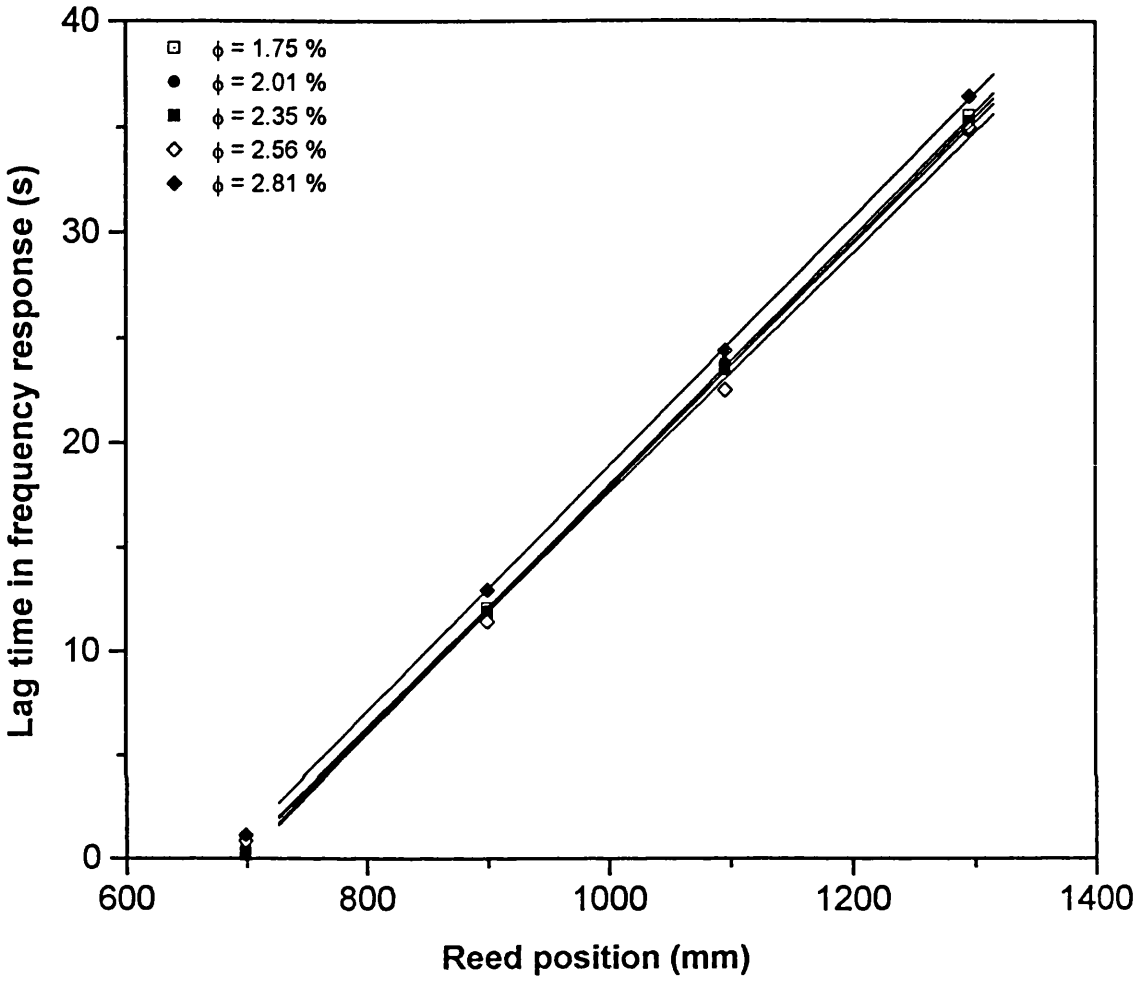

Figure 8.61
The variation of lag time in resonance frequency response with reed position relative to the top of the settling zone for polydisperse 90 - 135 μm glass ballotini spheres (density 2550 kgm^{-3}) settling in water @ 17 °C at various initial suspended solids volume concentrations, ϕ.

ϕ (%)	Fitting equation	Correlation coefficient	Propagation wave velocity (mm/s)
1.75	y = 0.0591x - 41.21	0.9999	16.9
2.01	y = 0.0578x - 39.93	0.9998	17.3
2.35	y = 0.0590x - 41.23	0.9999	17.0
2.56	y = 0.0571x - 39.53	0.9992	17.5
2.81	y = 0.0590x - 40.19	0.9997	17.0

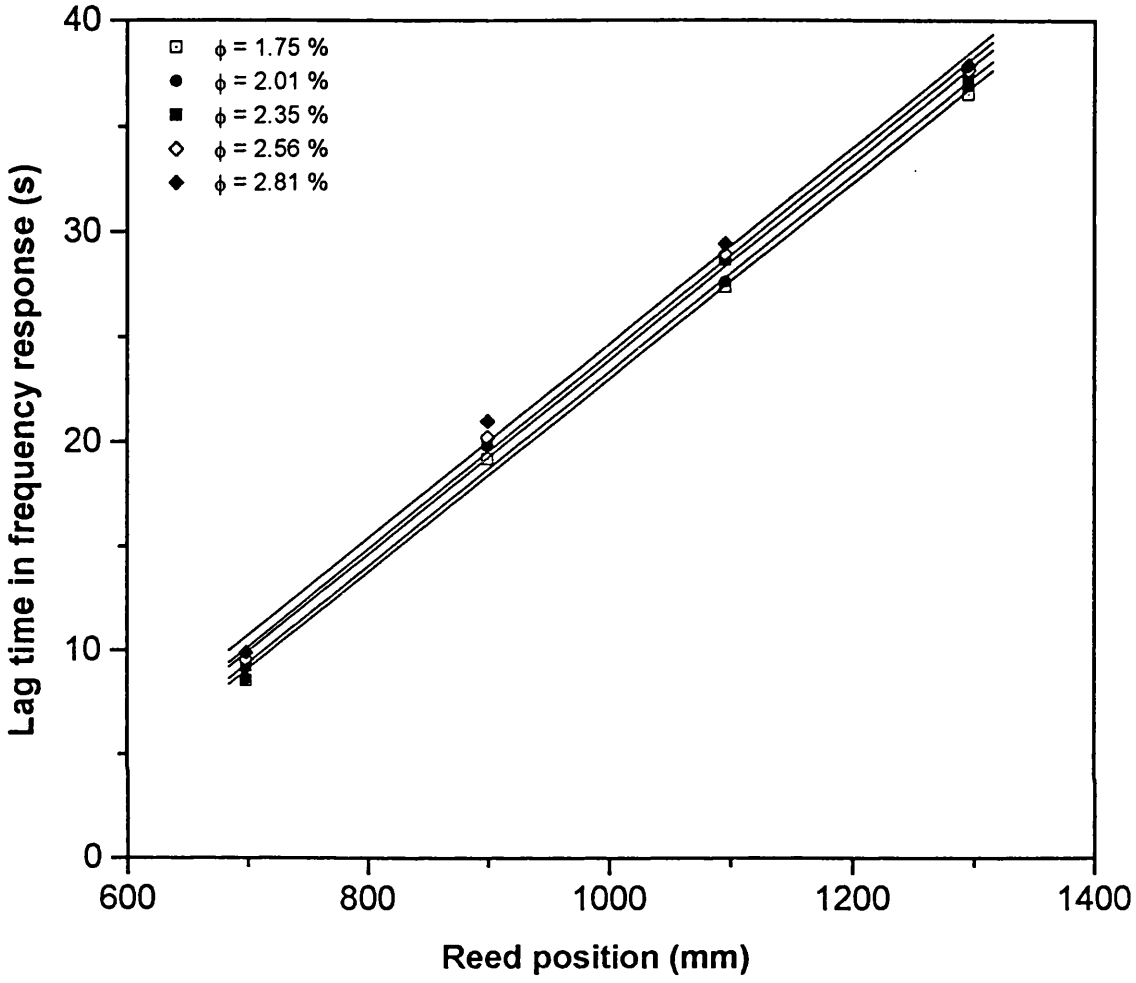

Figure 8.62
The variation of lag time in resonance frequency response with reed position relative to the top of the settling zone for polydisperse 100 - 200 μm glass ballotini spheres (density 2550 kgm^{-3}) settling in water @ 17 °C at various initial suspended solids volume concentrations, ϕ.

ϕ (%)	Fitting equation	Correlation coefficient	Propagation wave velocity (mm/s)
1.75	y = 0.0464x - 23.37	0.9988	21.6
2.01	y = 0.0466x - 23.30	0.9979	21.5
2.35	y = 0.0466x - 22.71	0.9983	21.5
2.56	y = 0.0469x - 22.66	0.9988	21.3
2.81	y = 0.0465x - 21.86	0.9977	21.5

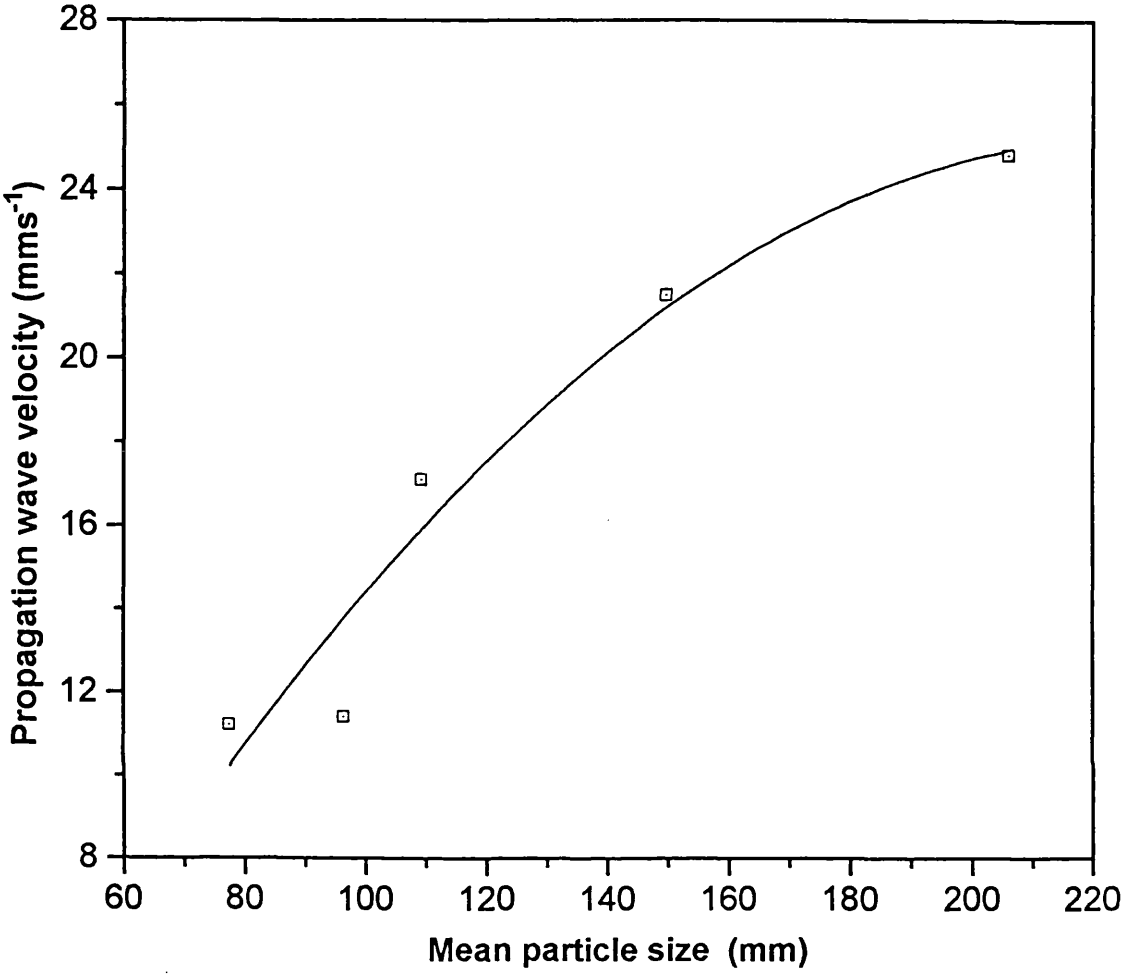

Figure 8.63
The variation of propagation wave velocity with mean particle size for glass ballotini spheres (density 2550 kgm^{-3}) settling in water @ 17 °C.

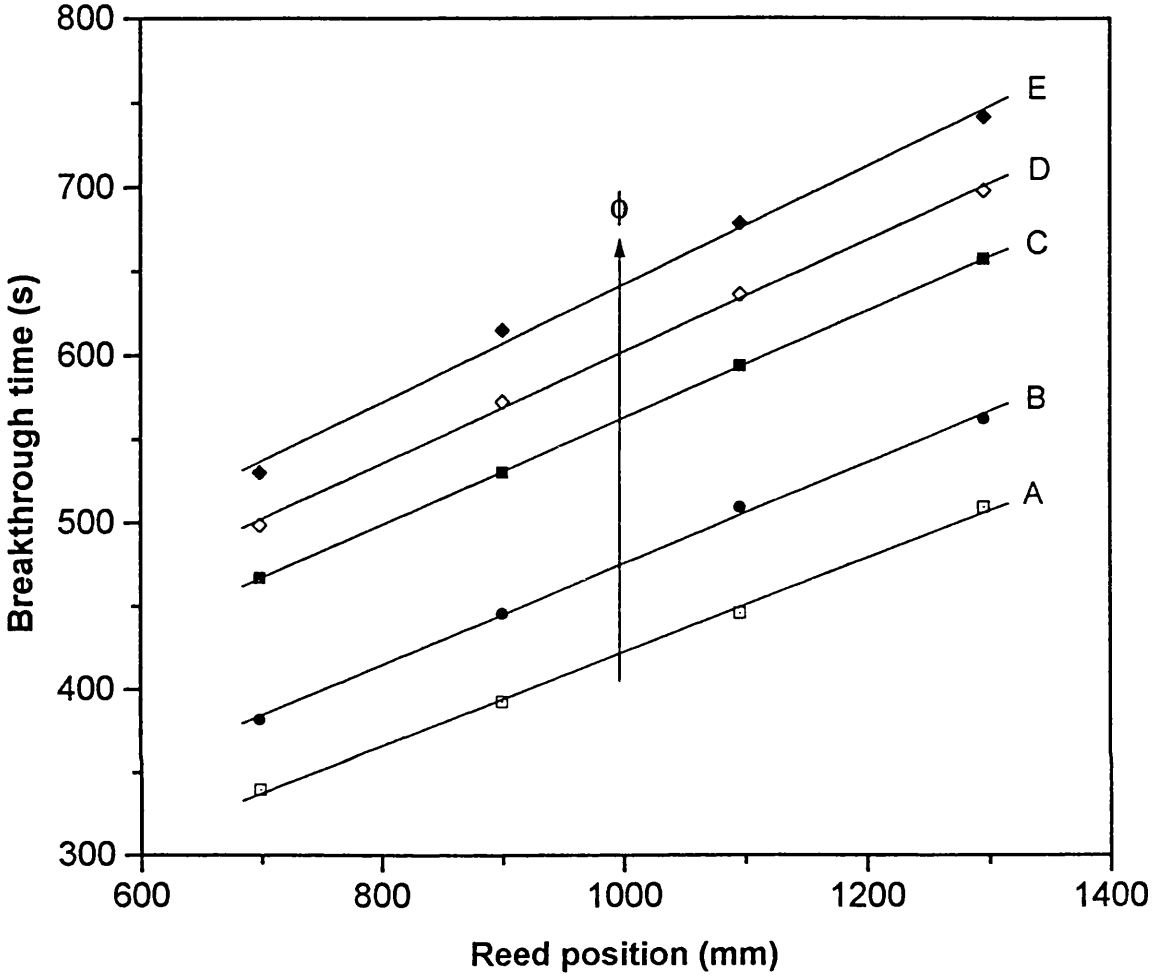

Figure 8.64
The variation of solids breakthrough time with reed position relative to the top of the settling zone for polydisperse 55 - 100 μm glass ballotini spheres (density 2550 kgm^{-3}) settling in water @ 17 °C for various initial suspended solids volume concentrations, ϕ: curve A, ϕ = 1.75 %; curve B, ϕ = 2.01 %; curve C, ϕ = 2.35 %; curve D, ϕ = 2.56 % and curve E, ϕ = 2.81 %

	Fitting equation	Interface velocity (mms^{-1})
Curve A	y = 0.283x + 139.47	3.54
Curve B	y = 0.304x + 171.17	3.29
Curve C	y = 0.319x + 243.22	3.13
Curve D	y = 0.333x + 268.75	3.00
Curve E	y = 0.351x + 290.55	2.85

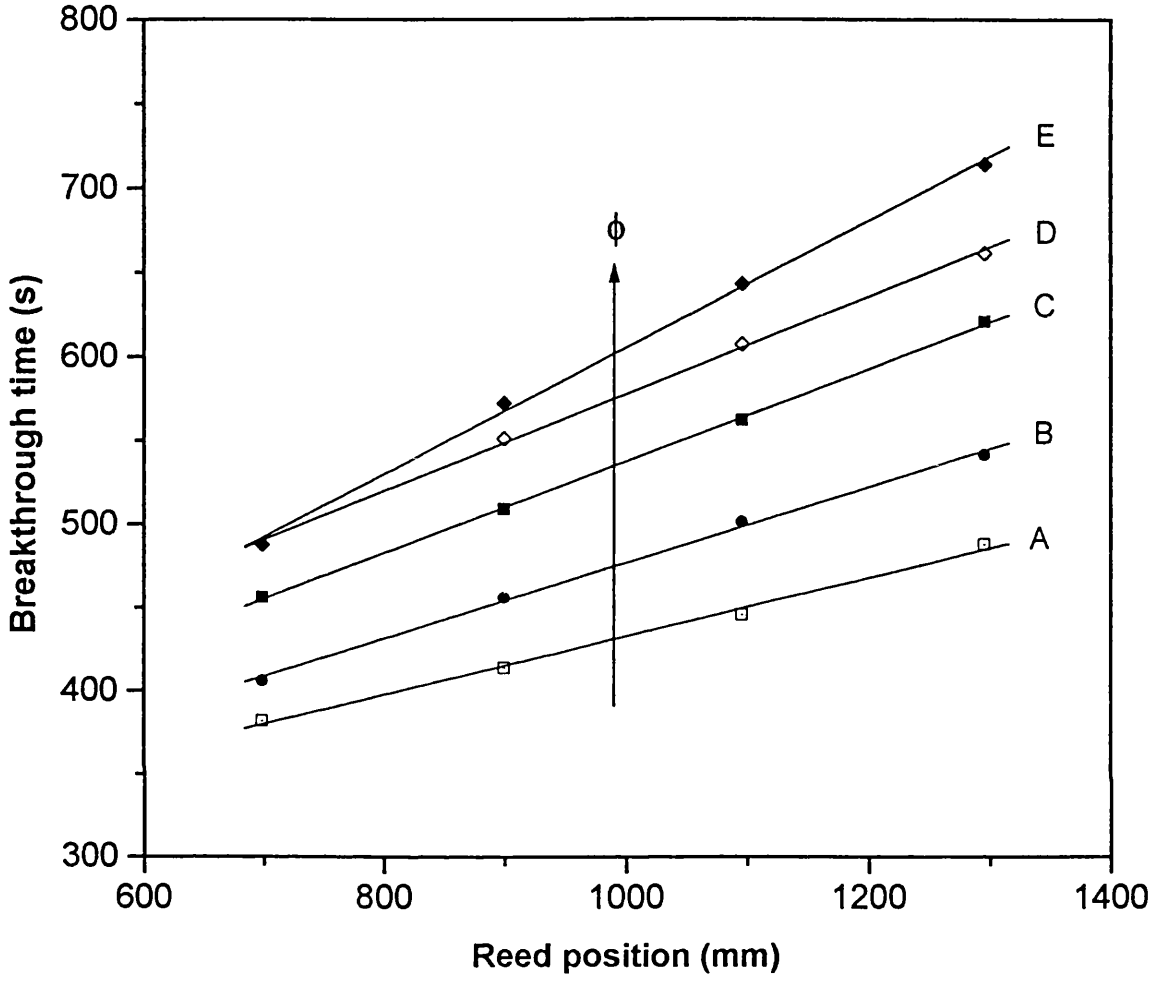

Figure 8.65
The variation of solids breakthrough time with reed position relative to the top of the settling zone for polydisperse 80 - 115 μm glass ballotini spheres (density 2550 kgm^{-3}) settling in water @ 17 °C for various initial suspended solids volume concentrations, ϕ: curve A, ϕ = 1.75 %; curve B, ϕ = 2.01 %; curve C, ϕ = 2.35 %; curve D, ϕ = 2.56 % and curve E, ϕ = 2.81 %

	Fitting equation	Interface velocity (mms^{-1})
Curve A	y = 0.176x + 256.46	5.68
Curve B	y = 0.227x + 249.49	4.41
Curve C	y = 0.275x + 262.55	3.64
Curve D	y = 0.290x + 287.37	3.45
Curve E	y = 0.377x + 227.92	2.65

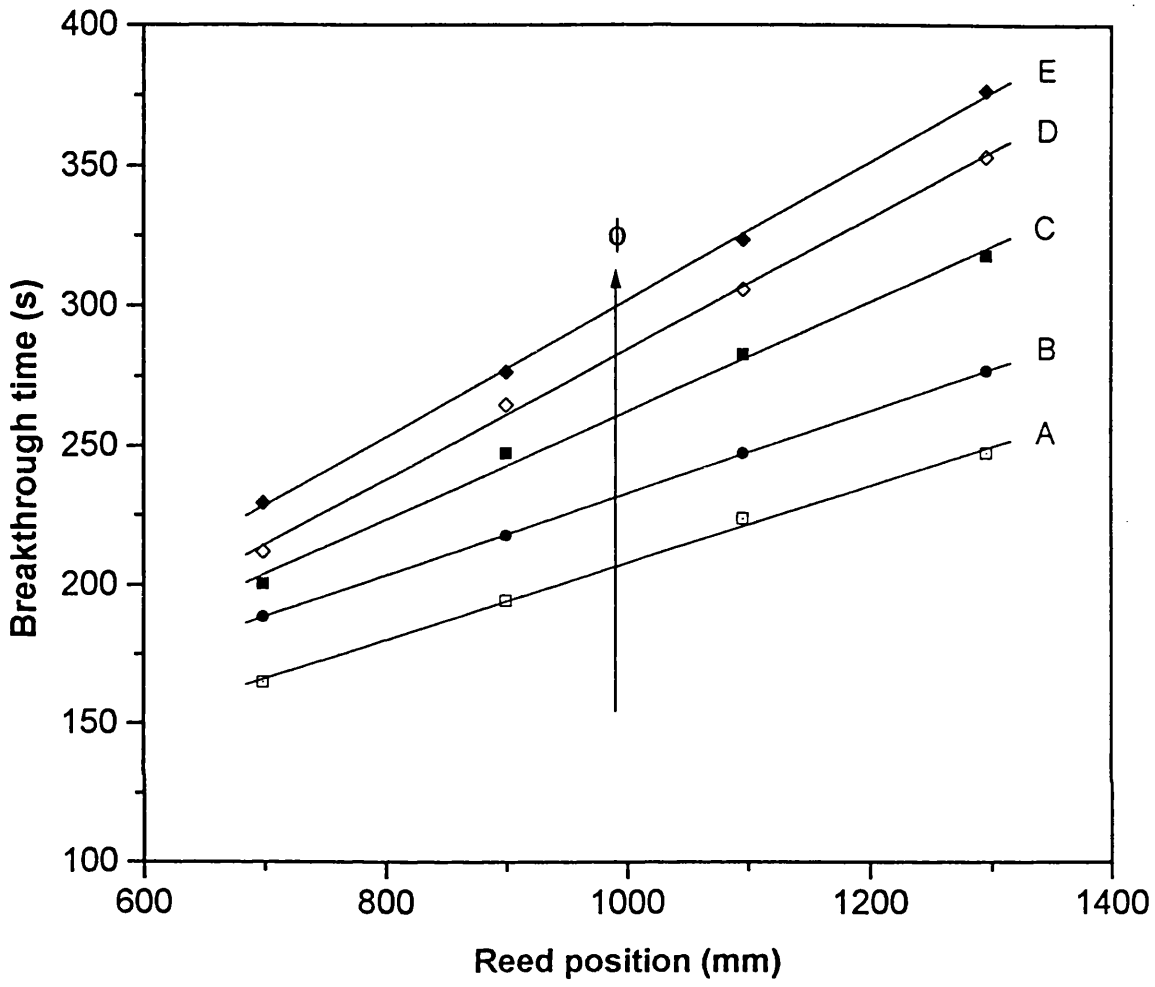

Figure 8.66
The variation of solids breakthrough time with reed position relative to the top of the settling zone for polydisperse 90 - 135 μm glass ballotini spheres (density 2550 kgm^{-3}) settling in water @ 17 °C for various initial suspended solids volume concentrations, ϕ: curve A, ϕ = 1.75 %; curve B, ϕ = 2.01 %; curve C, ϕ = 2.35 %; curve D, ϕ = 2.56 % and curve E, ϕ = 2.81 %

	Fitting equation	Interface velocity (mms^{-1})
Curve A	y = 0.1391x + 68.66	7.19
Curve B	y = 0.1480x + 84.80	6.78
Curve C	y = 0.1954x + 66.91	5.12
Curve D	y = 0.2339x + 50.57	4.28
Curve E	y = 0.2457x + 56.45	4.07

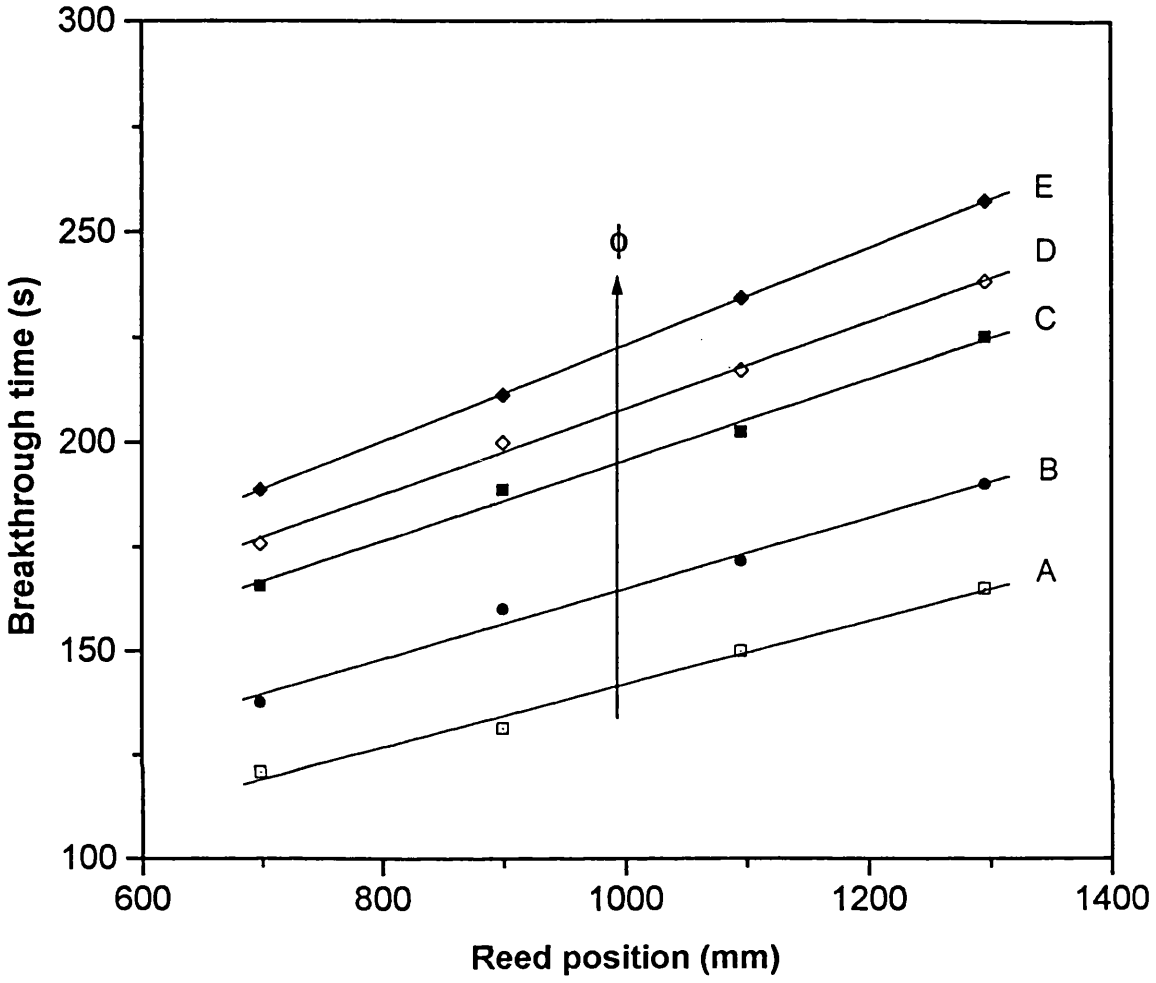

Figure 8.67
The variation of solids breakthrough time with reed position relative to the top of the settling zone for polydisperse 100 - 200 μm glass ballotini spheres (density 2550 kgm^{-3}) settling in water @ 17 °C for various initial suspended solids volume concentrations, ϕ: curve A, ϕ = 1.75 %; curve B, ϕ = 2.01 %; curve C, ϕ = 2.35 %; curve D, ϕ = 2.56 % and curve E, ϕ = 2.81 %

	Fitting equation	Interface velocity (mms^{-1})
Curve A	y = 0.076x + 65.74	13.16
Curve B	y = 0.085x + 80.10	11.79
Curve C	y = 0.097x + 98.71	10.31
Curve D	y = 0.103x + 104.10	9.71
Curve E	y = 0.115x + 108.15	8.70

Figure 8.68 shows the variation of Stokes diameter (equation 4.2) estimated from the measured interface velocities for 55 - 100 μm particles (figure 8.64) plotted against initial particle concentration. It is noteworthy that the data represent the settling behaviour of the smaller particles in the 55 - 100 μm size range indicating that these are most likely to comprise the main proportion of the particles in the diffuse interfaces observed in practice. As the initial solids concentration increases, the estimated Stokes diameter decreases indicating a greater tendency for the particles to segregate resulting in more diffuse interfaces. Interestingly the estimated Stokes diameter corresponding to the lowest solids concentration compares favourably with particle size distribution data presented in chapter 7 (see figure 7.2) for which the first significant species in the population is ca. 65 μm (number frequency ca. 5.6 %).

Figures 8.69 - 8.71 show the corresponding variation of the estimated Stokes diameter versus initial solids concentration for particles in the range 80 - 115, 90 - 135, and 100 - 200 μm receptively. Once again, the data indicate that the suspension-clear liquid interface in all the systems studied mainly comprises the smaller particles in each size range. Also, the effect becomes more pronounced with increase in particle size and concentration. Additionally, the calculated Stokes diameters (particularly those at the lowest particle concentrations) compare favourably with the smallest particles comprising the first significant fraction of each size range as measured independently from the particle size distribution data (see figures 7.3 - 7.5, chapter 7). The corresponding values for the 80 - 115, 90 - 135, and 100 - 200 μm are 84.9, 95.6 and 120 μm respectively.

8.7 Real Systems

8.7.1 Sedimentation of Flocculated Kaolin/Water Suspensions

Figure 8.72 shows the variation of normalised resonance frequency with time for reeds 1 - 4 for a 10 % v/v kaolin/water suspension (density 1207 kgm^{-3}) at 17 °C following the addition of a flocculant (see later). The data are normalised by dividing by the corresponding resonance frequency of each reed in pure water at 17 °C.

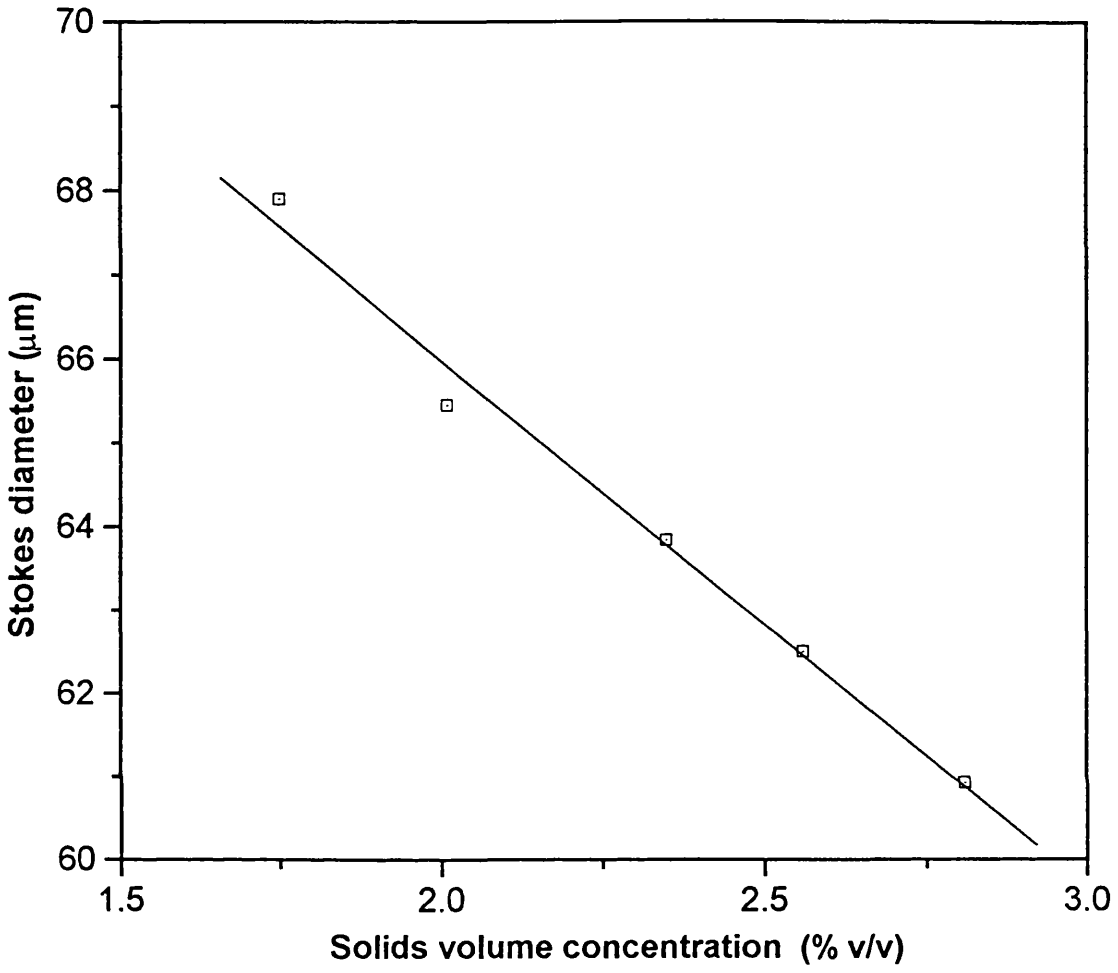

Figure 8.68
The variation of Stokes diameter (estimated from measured interface velocities) with initial solids concentration for 55 - 100 μm glass ballotini particles settling in water @ 17 °C.

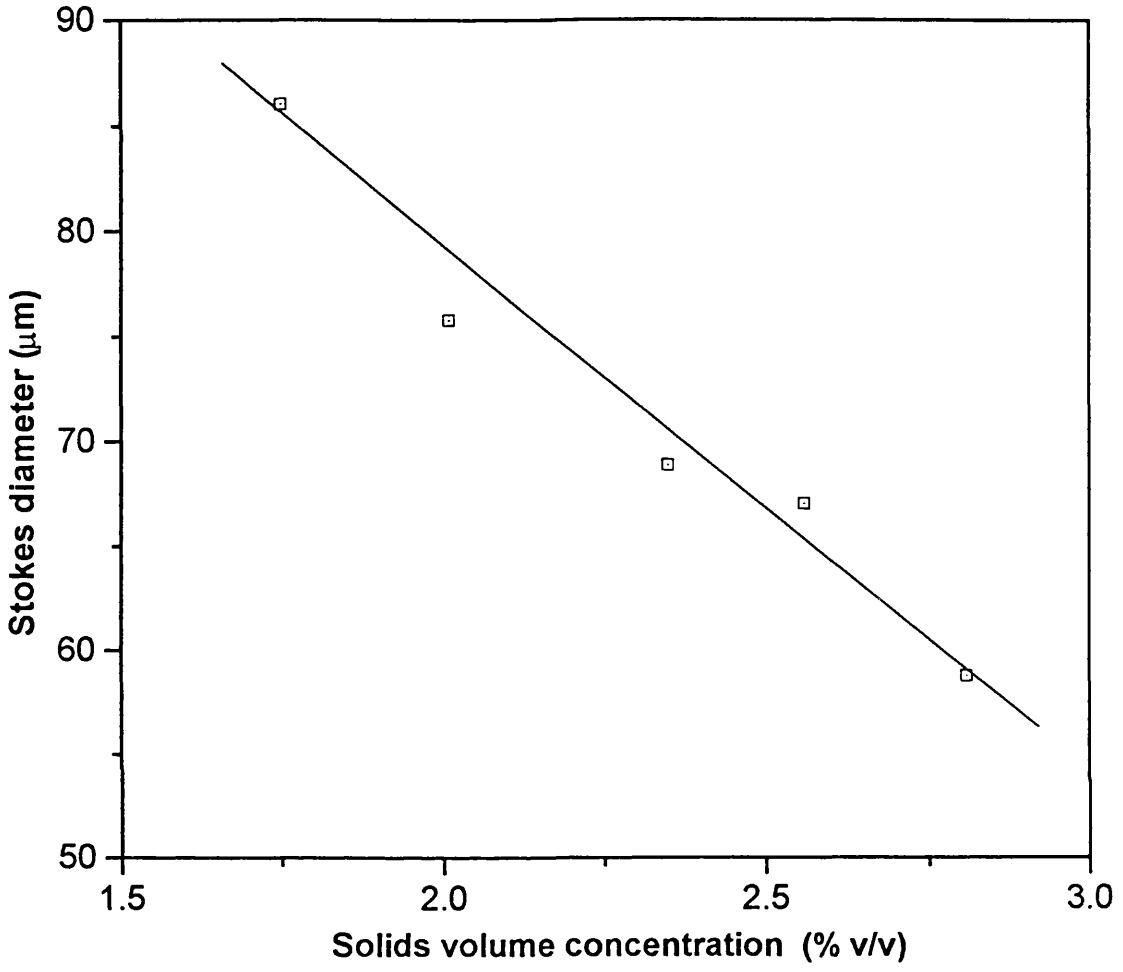

Figure 8.69
The variation of Stokes diameter (estimated from measured interface velocities) with initial solids concentration for 80 - 115 μm glass ballotini particles settling in water @ 17 °C.

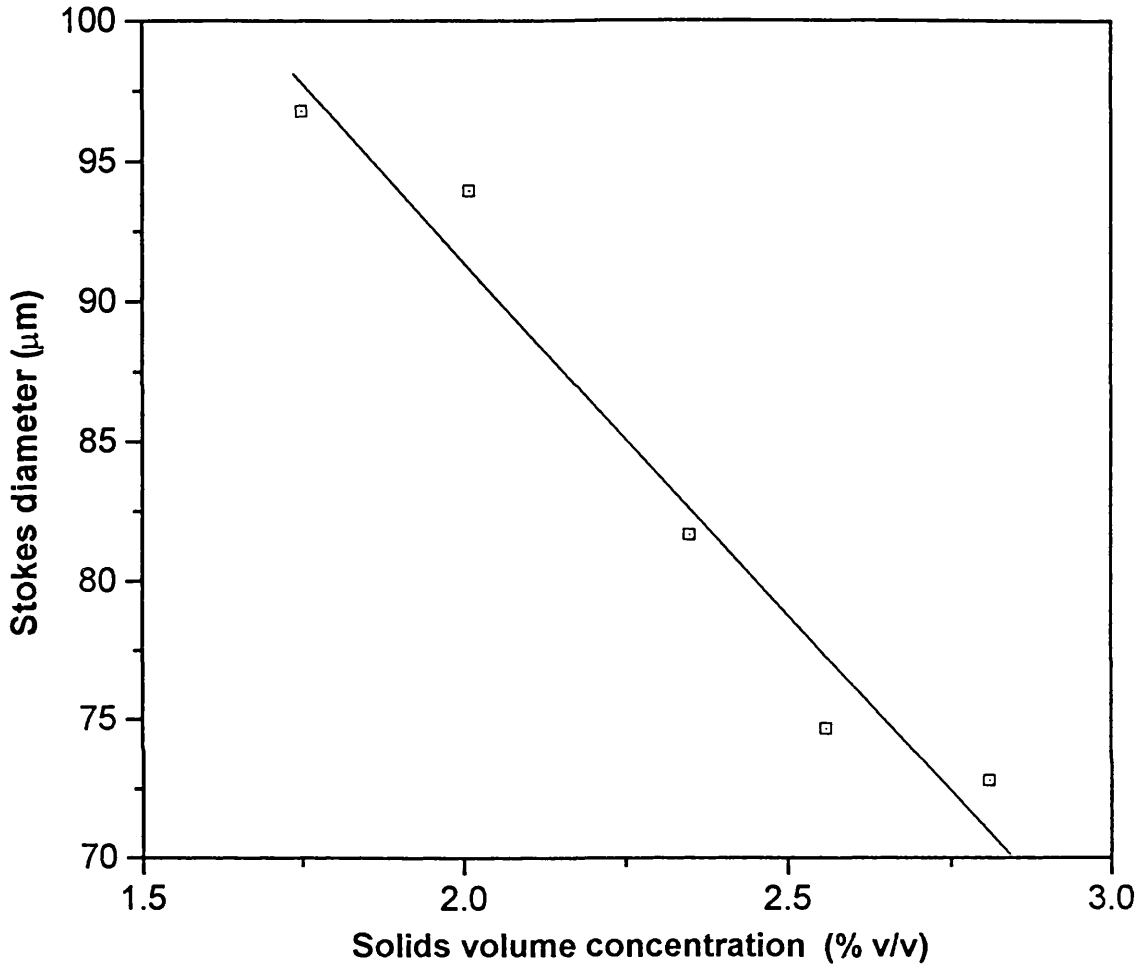

Figure 8.70
The variation of Stokes diameter (estimated from measured interface velocities) with initial solids concentration for 90 - 135 μm glass ballotini particles settling in water @ 17 °C.

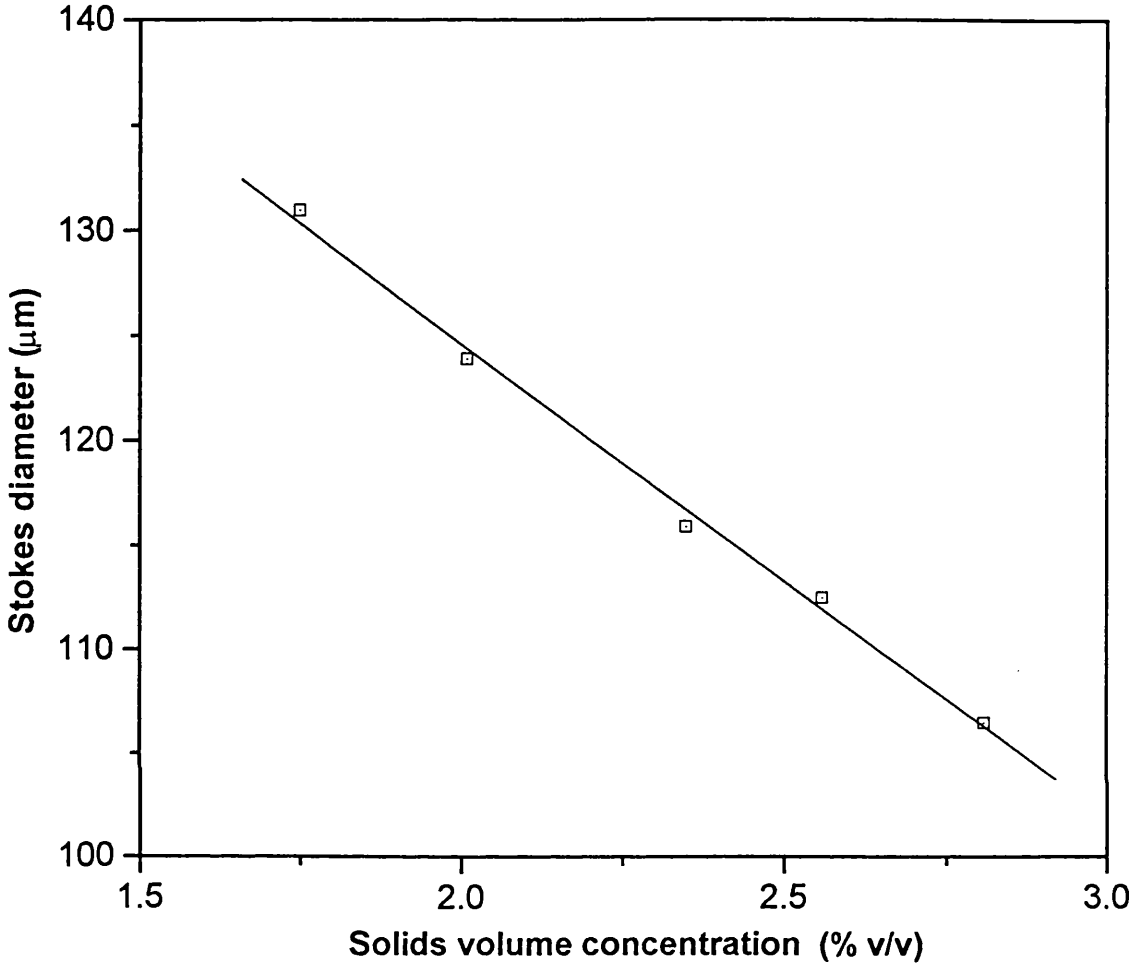

Figure 8.71
The variation of Stokes diameter (estimated from measured interface velocities) with initial solids concentration for 100 -200 μm glass ballotini particles settling in water @ 17 °C.

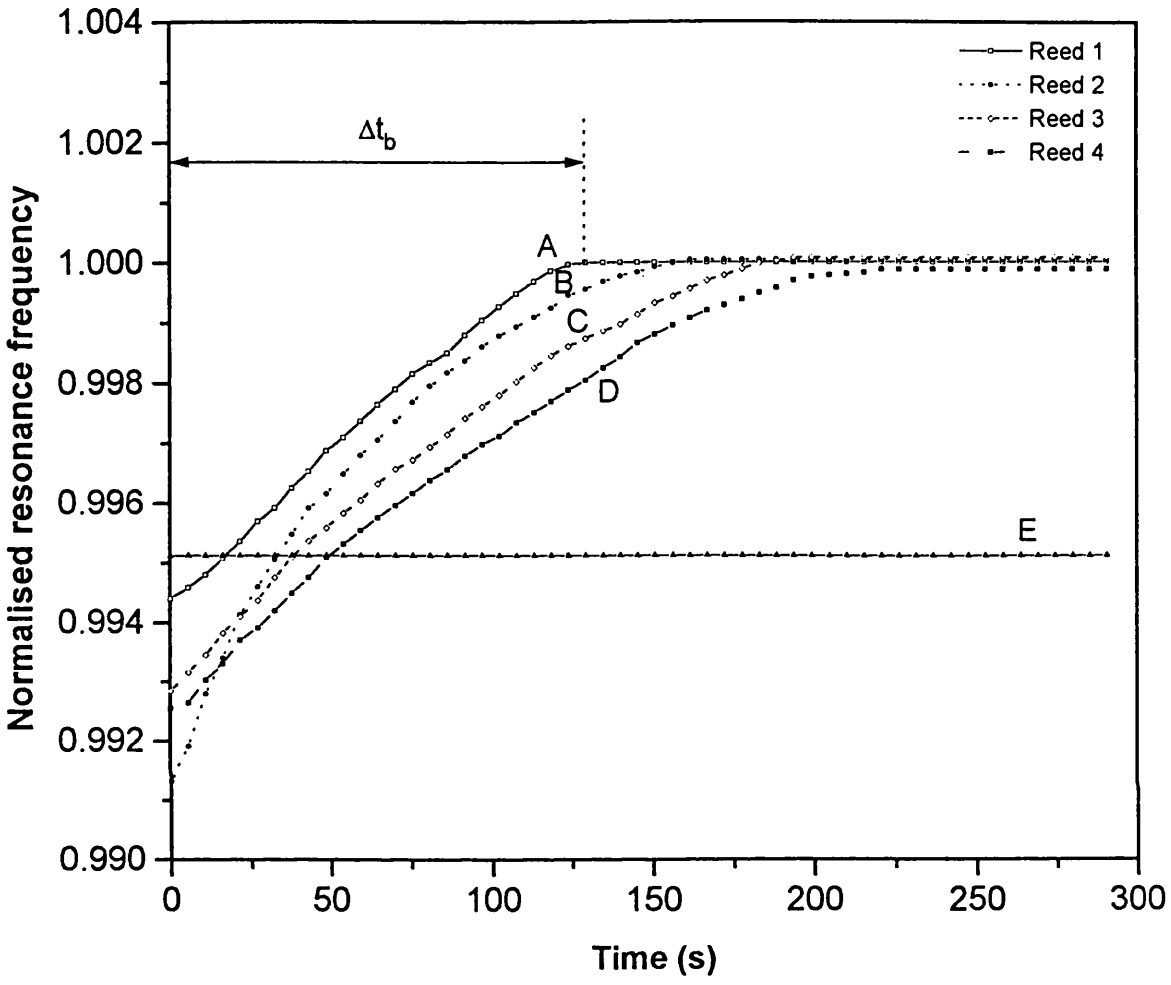

Figure 8.72

The variation of normalised resonance frequency with time for a 10 % v/v kaolin/water suspension (density 1207 kgm^{-3}) @ 17 °C at various reed positions relative to the top of the settling zone: curve A, 699 mm; curve B, 900 mm; curve C, 1096 mm and curve D, 1296 mm. Sedimentation is induced by adding 200 cm^3 of a 5 % wt/wt anionic flocculant (Magnafloc 155) solution to the suspension.

The results for the unflocculated sample (curve E) obtained using reed 1 are also presented. The constant value of the resonance frequency with time for this system is indicative of highly stable behaviour which lasted over a protracted period of time (ca. 20 minutes). Also, no changes in resonance frequency were observed using reeds 2 - 4. These data are not shown here in order to avoid congestion.

The suspension was prepared by slowly adding kaolin (calcined clay, type Metastar 501: 94 % wt/wt 0.1 - 2 μm) supplied by English China Clays Ltd. (Cornwall, UK) to deionised water in a 40 litre plastic bucket. The mixture (28.3 litres) was continuously stirred for ca. 20 minutes in order to achieve uniform dispersion of the clay powder. Sedimentation was artificially induced by the slow addition of 200 cm^3 of a 5 % wt/wt anionic flocculant (Magnafloc 155) supplied by Allied Colloids (Bradford, UK) to the well mixed suspension. The efficient admixture of the flocculant solution was achieved by stirring the suspension very gently for no more than 2 minutes since prolonged mixing tends to result in floc (aggregate) disruption (Gregory, 1991).

The flocculant (Magnafloc 155) is a high molecular weight polyacrylamide supplied as a free flowing granular powder. The 200 cm^3 solution was prepared by:

(i) Weighing 0.5 g of Magnafloc 155 powder into a clean 200 cm^3 bottle

(ii) Adding 3 cm^3 of methanol in order to wet the powder.

(iii) Quickly adding 97 cm^3 of deionised water.

(iv) Covering the bottle and shaking vigorously for ca. 15 s.

(v) Allowing the solution to stand (with occasional shaking) for ca. 2 hours prior to use.

Since clay particles carry a negative surface charge (Brindley, 1958 and Micheals, 1958), the flocculant probably induces aggregation via a depletion mechanism (Sperry,

1984). Thus, since the polymer molecules are also negatively charged, they are not likely to bring about aggregation via adsorption onto the surfaces of neighbouring particles (a mechanism known as bridging) in the manner described by Gregory (1991). Instead, steric (rather than electrostatic) attractive forces between adjacent particles are induced by the depletion of the non-adsorbing polymer from the gaps between particles. This process results in polymer-rich and polymer-free interparticle regions. The associated osmotic pressure difference drives particles towards one another resulting in the formation of flocs (aggregates containing entrapped water). The latter tend to be several orders of magnitude larger (diameters up to 400 μm) than individual particles and therefore, settle at much faster rates (Micheals and Bolger 1962).

In contrast to the model glass ballotini/water suspensions studied so far, the flocculated suspension was not introduced to the settling zone via the recirculating pump due to the associated high shear rates which would have resulted in floc disruption. Instead, the suspension was poured directly into the settling tank following which resonance frequency measurements were taken in the manner described in section 6.4.1, chapter 6.

Returning to figure 8.72, the data shows that the settling process starts immediately since there is no lag in the resonance frequency response. Also, reeds 1 - 4 are exposed to the clear liquid at the end of the settling process.

Figure 8.73 shows the variation of solids breakthrough time, Δt_b, with reed position relative to the top of the settling zone for the 10 % v/v flocculated kaolin/water suspension. The data is extracted from the normalised resonance frequency profiles (curves A to D) shown in figure 8.72. The linear variation in the data is indicative of a constant settling rate. The corresponding suspension-clear liquid interface velocity as calculated from the slope of the fitted line is 6.37 mms^{-1}.

Figure 8.74 on the other hand, shows the variation of interface height (obtained by direct visual observation) with time relative to the bottom of the settling zone.

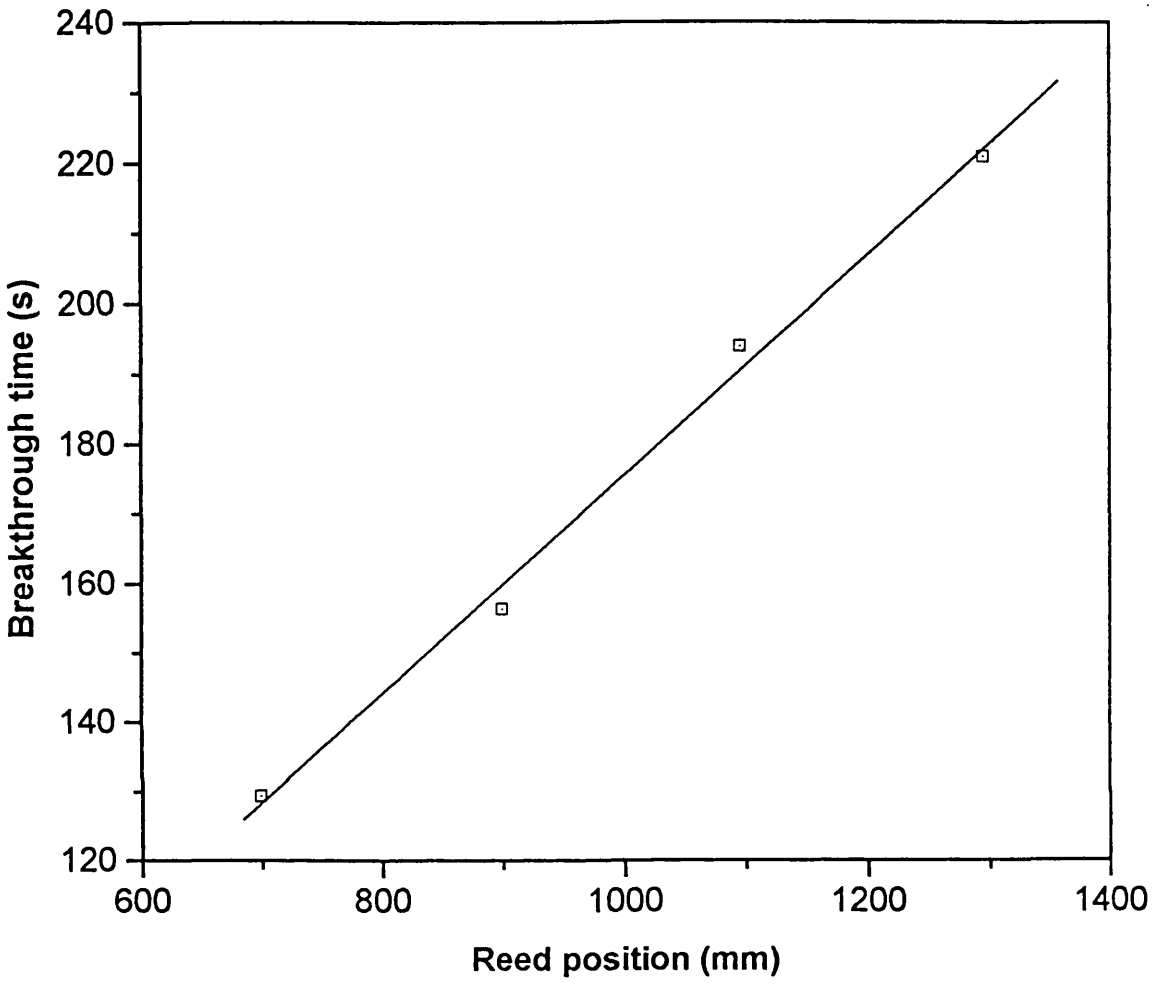

Figure 8.73
The variation of solids breakthrough time with reed position relative to the top of the settling zone for a 10 % v/v flocculated kaolin/water suspension (density, 1080 kgm^{-3}) @ 17 °C.

Fitting equation	Interface velocity (mms^{-1})
y = 0.1570x + 18.48	6.37

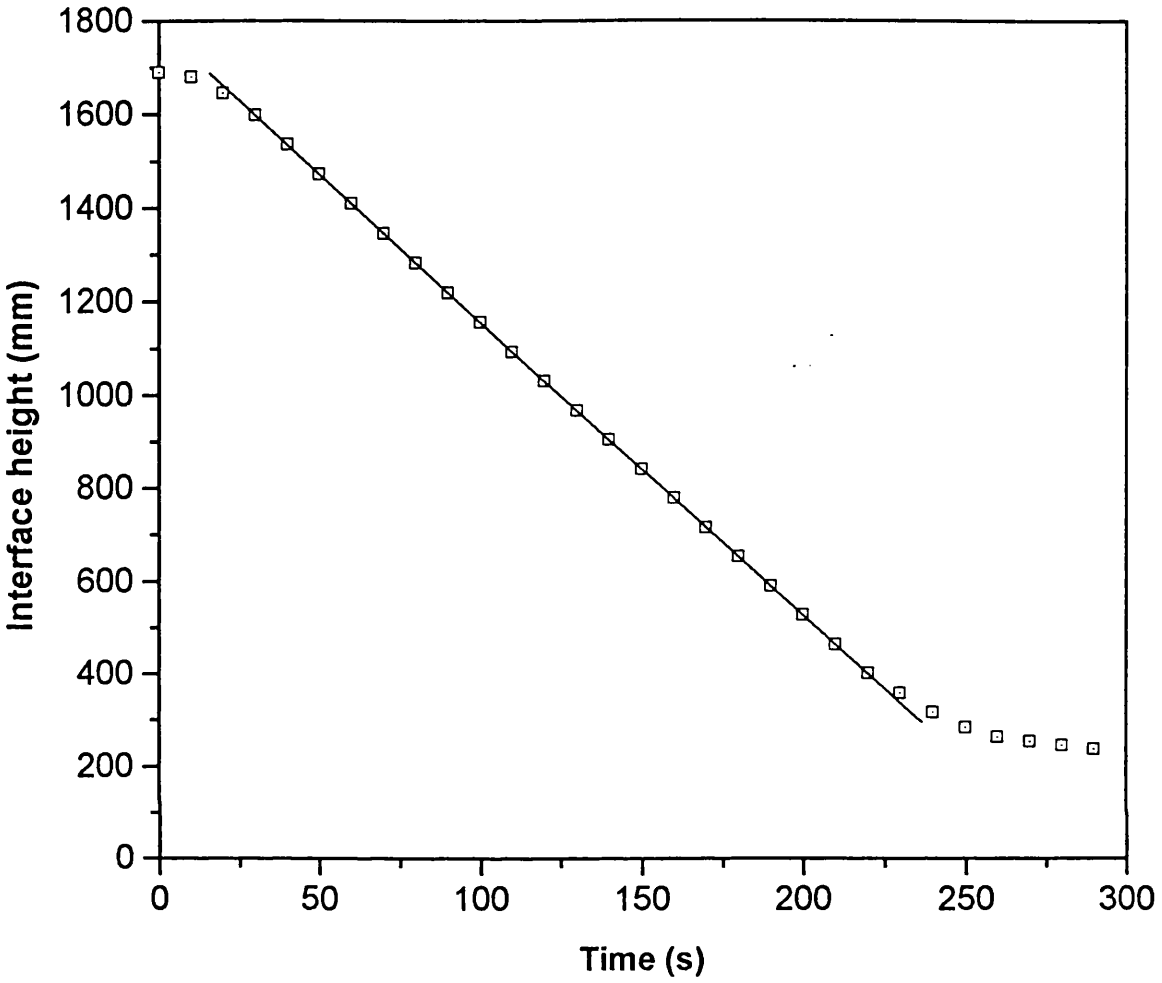

Figure 8.74
The variation of suspension-clear liquid interface height with time as determined by direct visual observation relative to the bottom of the settling zone for a 10 % v/v flocculated kaolin/water suspension (density 1080 kgm^{-3}) @ 17 °C.

Fitting equation	Interface velocity (mms^{-1})
y = -6.30x + 1787.44	6.30

The inferred interface velocity of 6.30 mms^{-1} is in good agreement with the experimentally determined value (cf. 6.37 mms^{-1}).

Figure 8.75 shows the variation of normalised resonance frequency with time for reeds 1 - 4 for a 15 % v/v flocculated kaolin/water suspension (density 1289 kgm^{-3}) at 17 °C. Curves A to C follow trends similar to those for the lower solids concentration system described above. However, in contrast, curve D shows that the resonance frequency for reed 4 (closest to the base of the settling tank) decreases with time indicating an effective increase in the hydrodynamic head. This is because with such a highly concentrated suspension, reed 4 is situated in the sediment which has a higher density than the original suspension. Like before, the plateau marks the end of sedimentation (see later).

Figure 8.76 shows the variation of normalised resonance frequency with time for reeds 1 - 4 for a 20 % v/v flocculated kaolin/water suspension (density 1370 kgm^{-3}) at 17 °C. In this case, the resonance frequencies of reeds 3 (curve C) and reed 4 (curve D) decrease with time indicating an actual densification due to the build up of sediment in their proximity.

At the start of sedimentation, flocs are weak and irregular interconnected structures which experience strong drag forces and therefore exhibit low settling rates (Micheals and Bolger, 1962). This effect becomes more pronounced as the distance down the settling zone increases since the flow path of displaced fluid becomes more tortuous. In addition, the time required for the subsequent coalescence of flocs into more distinct faster settling spherical aggregates increases with distance down the settling zone. This probably explains the initial flat region (i) of curve C. As the settling process proceeds a loosely packed sediment starts to form above reed 3. This increases in depth with time as the sediment-suspension interface rises and corresponds to region (ii) of curve C. During this interval, reed 3 is exposed to an increasingly more dense medium than the original suspension. Accordingly, the resonance frequency decreases with time. At the end of the settling process thin vertical channels start to appear in the sediment. These visibly increase in size with time and the sediment-clear liquid interface begins to

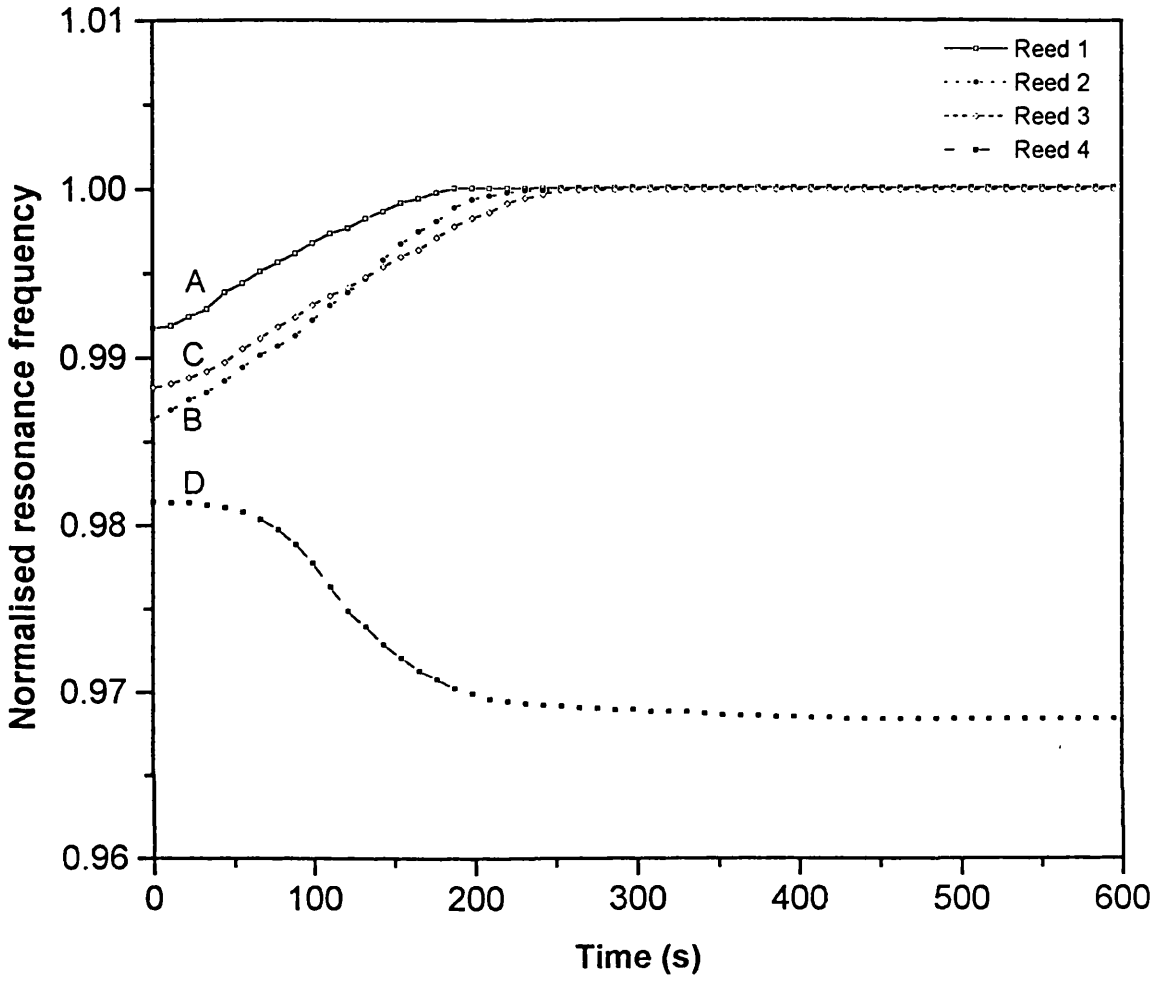

Figure 8.75
The variation of normalised resonance frequency with time for a 15 % v/v kaolin/water suspension (density 1289 kgm^{-3}) @ 17 °C at various reed positions relative to the top of the settling zone: curve A, 699 mm; curve B, 900 mm; curve C, 1096 mm and curve D, 1296 mm. Sedimentation is induced by adding 200 cm^3 of a 5 % wt/wt anionic flocculant (Magnafloc 155) solution to the suspension.

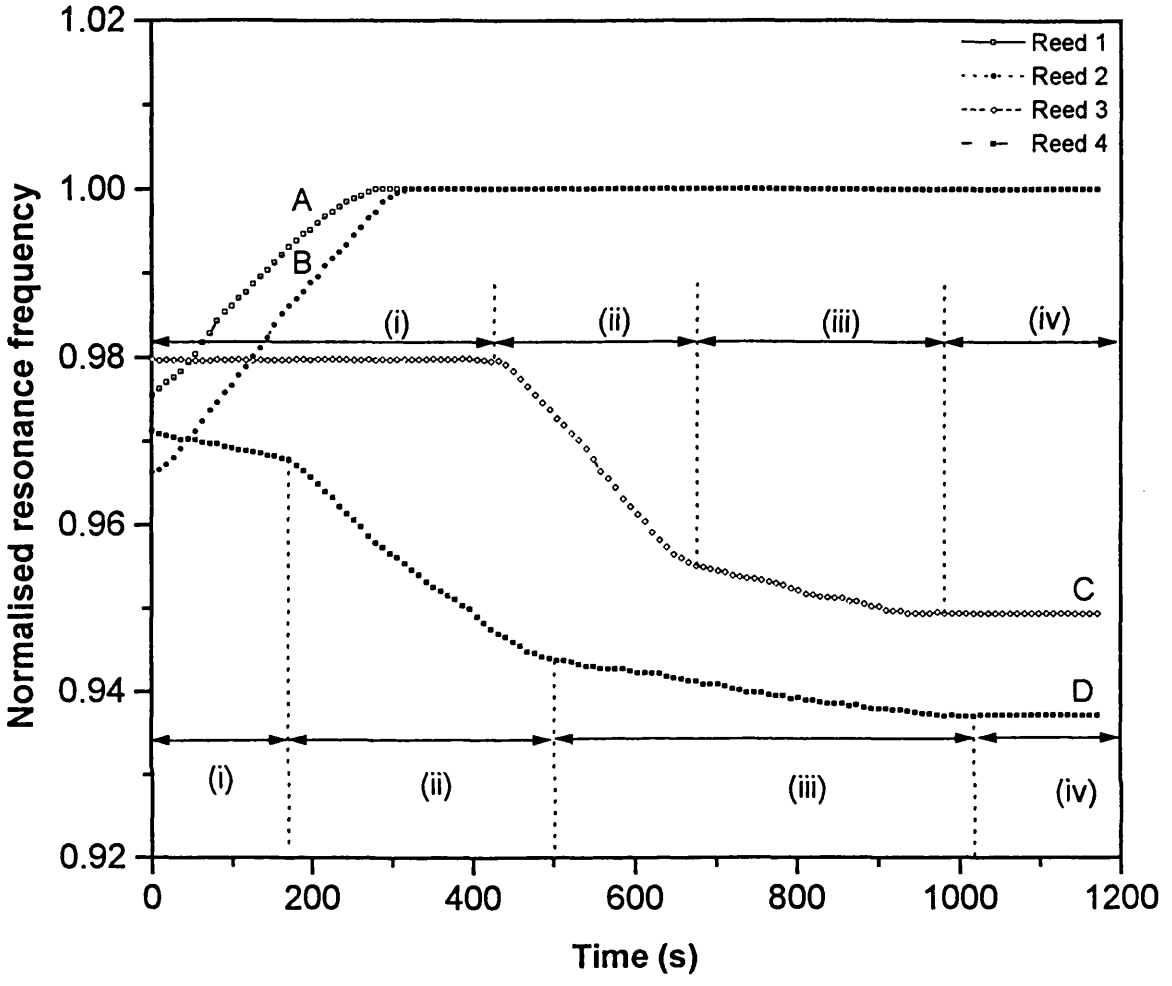

Figure 8.76

The variation of normalised resonance frequency with time for a 20 % v/v kaolin/water suspension (density 1370 kgm^{-3}) @ 17 °C at various reed positions relative to the top of the settling zone: curve A, 699 mm; curve B, 900 mm; curve C, 1096 mm and curve D, 1296 mm. Sedimentation is induced by adding 200 cm^3 of a 5 % wt/wt anionic flocculant (Magnafloc 155) solution to the suspension.

fall as compression and dewatering effects become more prominent. This process corresponds to region (iii) of curve C and is known as sediment consolidation (Auzerais et al., 1990). The latter is characterised by the collapse of flocs and results in a more densely packed sediment. Accordingly, the resonance frequency continues to decrease in this interval. Region (iv) represents the end of sediment consolidation at which time the sediment-suspension interface stops falling.

Curve D shows that the system response obtained in conjunction with reed 4 follows a similar trend. In this case the reed is covered in sediment much earlier (region (ii))since it is situated further down the settling zone. In addition, the duration of the compression and dewatering phase (region (iii)) is much longer due to a larger sediment volume.

On the basis of the above preliminary data it is evident that the multiple vibrating reed system is capable of providing useful information on the settling behaviour of real suspensions.

Considering the 10 % v/v flocculated kaolin/water suspension, the equivalent particle mass per unit volume in the well mixed slurry is ca. 307.4 kgm^{-3}. This is based on the added powder mass of 8.70 kg. The corresponding solids flux estimated by multiplying the particle concentration (307.4 kgm^{-3}) by the interface velocity (6.37 mms^{-1}) is ca. 1.96 $kgm^{-2}s^{-1}$. The latter clearly falls outside the calibrated range of the system (see figures 7.21 - 7.24, chapter 7). Accordingly, frequency measurements for this suspension can not be used to calculate corresponding solids flux profiles in the manner described in section 8.4. Therefore, mass balance calculations similar to those described in section 8.5 are also not possible. The same applies to the 15 and 20 % v/v suspensions since the estimated solids fluxes associated with these systems are even higher (2.85 and 3.66 $kgm^{-2}s^{-1}$) respectively.

It is important to note that the above systems have been tried primarily to demonstrate, qualitatively, the feasibility of operation of the system in real suspensions rather than for the quantitative determination of sedimentation kinetic data.

8.7.2 Two-Phase Liquid/Liquid Emulsions

The feasibility of extending the application of the current measurement technique to monitoring the stability/separation of two-phase liquid/liquid emulsions has been demonstrated in conjunction with oil/water systems. Figure 8.77 shows the variation of normalised resonance frequency with time for reeds 1 - 4 for a 30 % v/v oil (density 915 kgm^{-3}, viscosity 65 cP) and water emulsion at 17 °C. The data are normalised by dividing by the corresponding resonance frequency of each reed in pure oil at 17 °C. The resonance frequencies of reeds 1 - 4 when exposed to pure oil are 58.62, 49.43, 48.14 and 47.15 Hz respectively.

The emulsion (28.3 litres) was prepared by pouring the appropriate volumes of water and oil (sunflower oil) supplied by KTC Ltd. (Wednesbury, UK) into a 40 litre plastic bucket and stirring for ca. 30 minutes in order to ensure adequate dispersion of the two phases. As in the case of the kaolin/water suspensions (see section 8.7.1), the emulsion was poured directly into the settling tank following which resonance frequency measurements were taken.

Considering curve A, for example, a probable explanation (based on direct visual observation) for the trend in the data is as follows: Region (i) represents the initial period in which the two phases are uniformly mixed. Region (ii) on the other hand, corresponds to the first stage of the phase separation process. This is characterised by the slow coalescence of fine oil droplets into larger entities which rise whilst the more dense aqueous phase settles. With time, a critical droplet size is reached following which rapid phase separation occurs. The latter corresponds to region (iii) whilst region (iv) represents complete phase separation. Figures 8.78 and 8.79 show similar data for 40 and 50 % v/v oil/water emulsions respectively. It is noteworthy that in all cases the system resonance frequency increases with time as the heavy phase (water) passes the reeds. This is due to a reduction in the fluid hydrodynamic head.

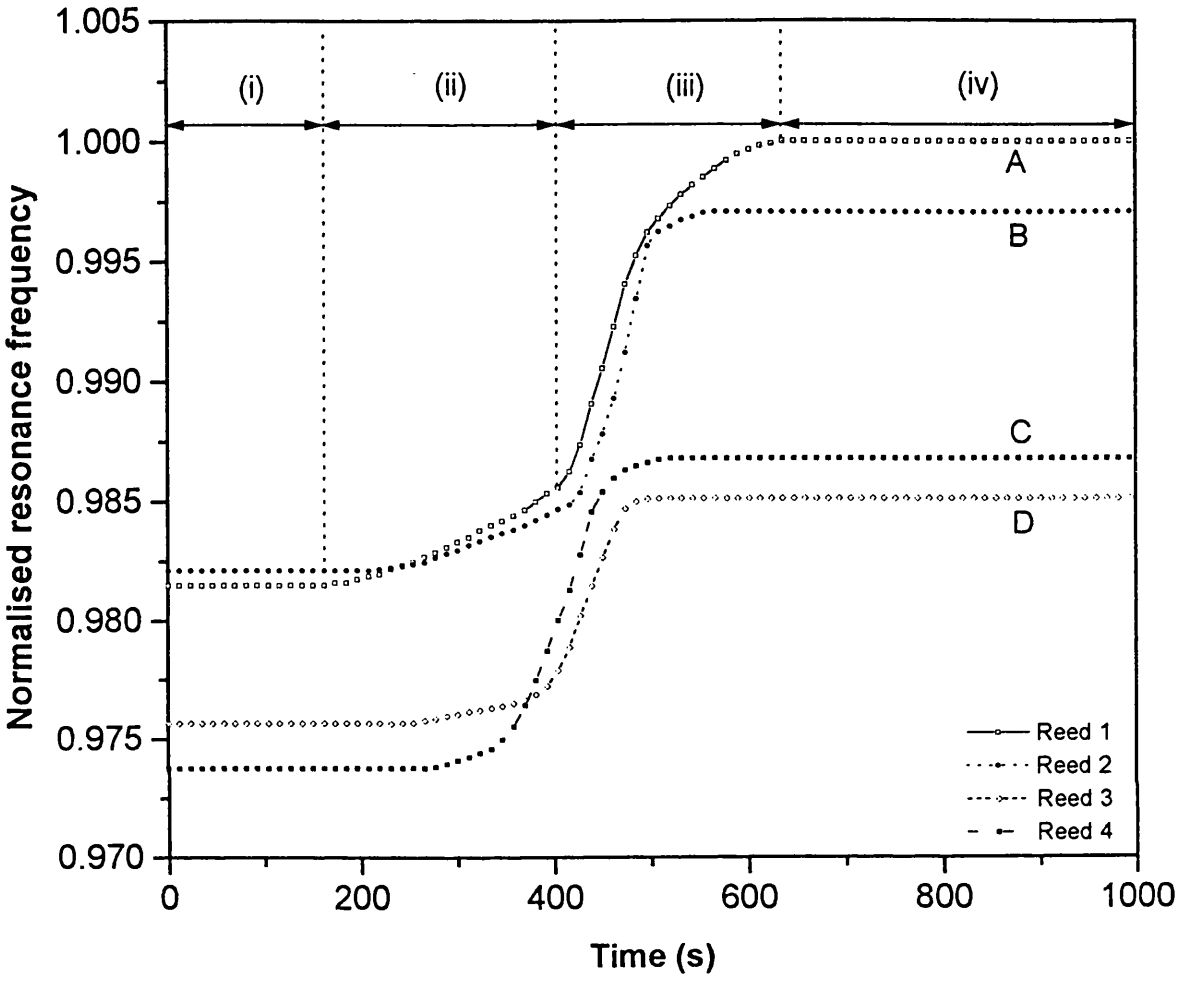

Figure 8.77
The variation of normalised resonance frequency with time for a 30 % v/v oil (density 915 kgm^{-3}, viscosity 65 cP) and water emulsion @ 17 °C at various reed positions relative to the top of the settling zone: curve A, 699 mm; curve B, 900 mm; curve C, 1096 mm and curve D, 1296 mm. The data shows how the two phases separate.

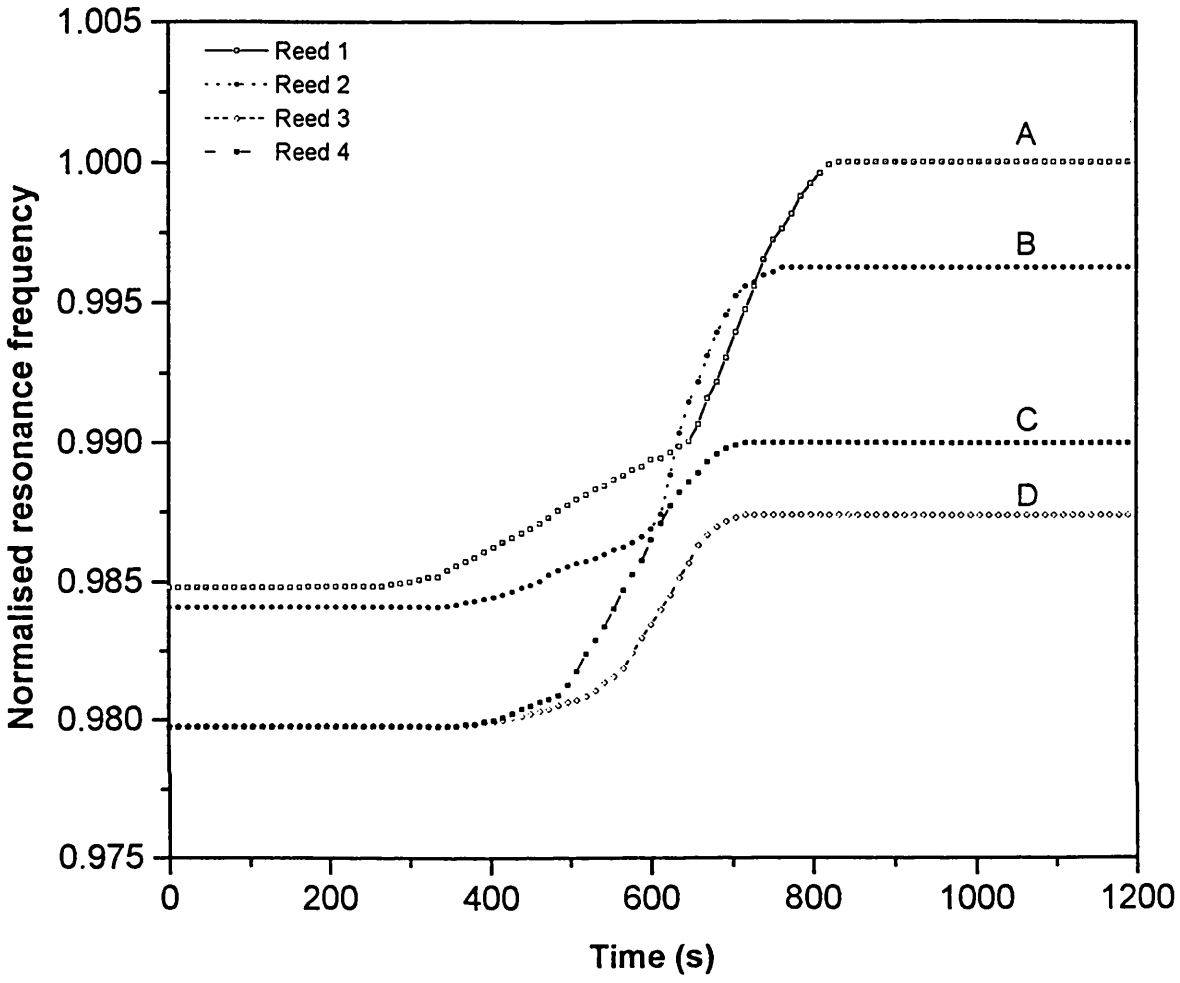

Figure 8.78

The variation of normalised resonance frequency with time for a 40 % v/v oil (density 915 kgm^{-3}, viscosity 65 cP) and water emulsion @ 17 °C at various reed positions relative to the top of the settling zone: curve A, 699 mm; curve B, 900 mm; curve C, 1096 mm and curve D, 1296 mm. The data shows how the two phases separate.

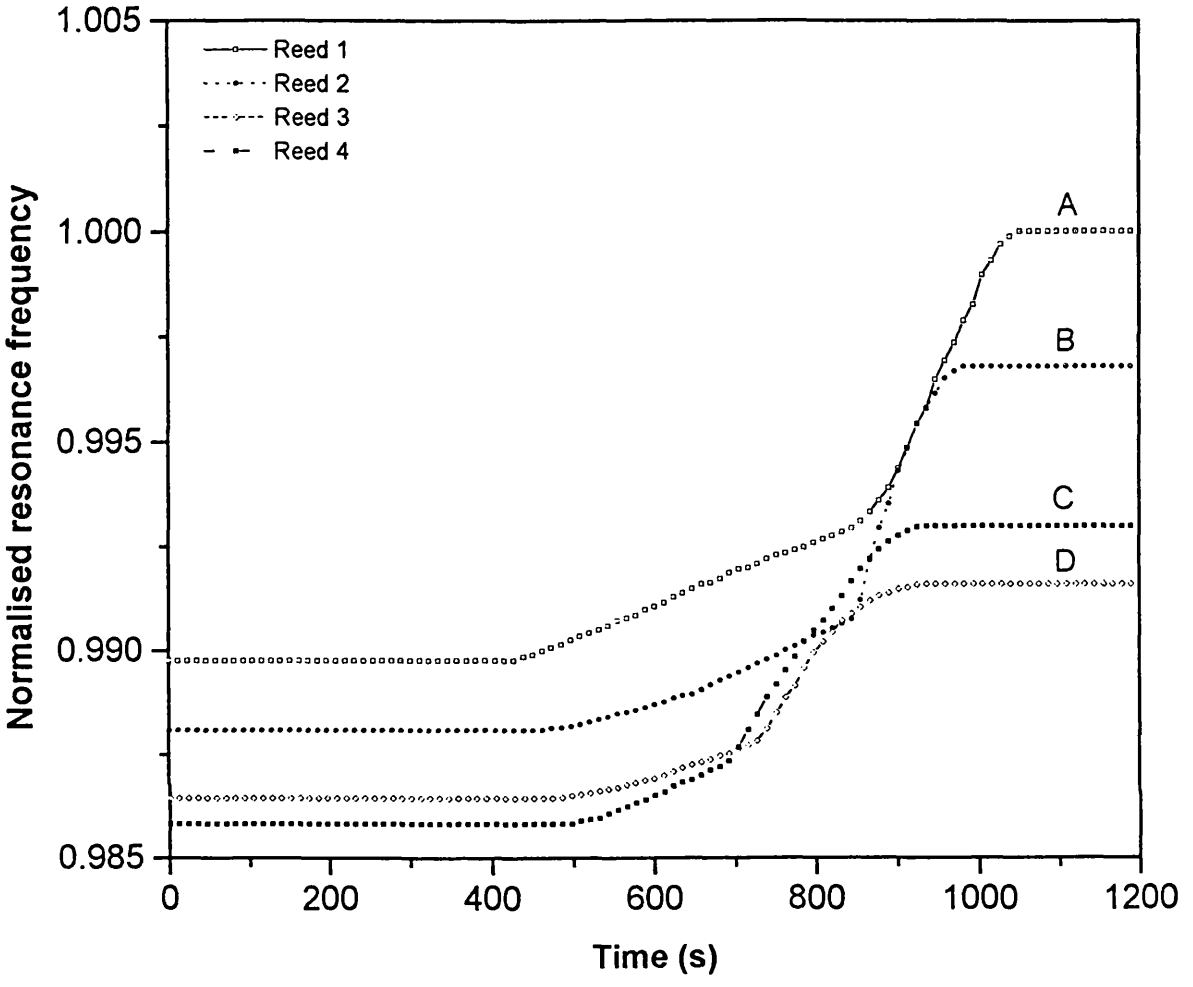

Figure 8.79

The variation of normalised resonance frequency with time for a 50 % v/v oil (density 915 kgm^{-3}, viscosity 65 cP) and water emulsion @ 17 °C at various reed positions relative to the top of the settling zone: curve A, 699 mm; curve B, 900 mm; curve C, 1096 mm and curve D, 1296 mm. The data shows how the two phases separate.

CHAPTER 9

SUMMARY, CONCLUSIONS AND FURTHER WORK

9.0 Summary

This thesis describes the design and development of a multiple vibrating reed analyser for the routine on-line measurement of particle settling velocities and the solids flux (mass settling per unit area per unit time) during sedimentation. The device comprises a stainless steel rod pinned at an intermediate point along its length. One end (the 'remote side') is exposed to the settling suspension whilst the other (the 'drive side') is driven into transverse vibration at resonance by an alternating current electromagnet. With length ratios of the drive to the remote spans of the reed of less than 0.4, the resonance frequency of the reed becomes predominantly sensitive to changes occurring on the remote side only (Mahgerefteh et al., 1990).

The principle of operation of the device is simple and relies on the fact that the resonance of a stiff reed performing simple harmonic motion in a fluid medium is directly related to the fluid hydrodynamic head. In the case of a settling suspension, the fluid bulk density and hence the hydrodynamic head decreases with time as solids settle out of suspension. Particle settling velocities and solids flux profiles may in turn be easily obtained by continuous monitoring of the resonance frequencies of a number of reeds positioned at set levels along a settling tank.

The primary incentive for this work has been the lack of a robust and model-independent technique for the characterisation of the settling behaviour of suspensions. The current system addresses this issue as it allows for the acquisition of in-situ measurements without the need for calibration to specific dispersions.

A critical review of traditional approaches for the analysis of settling suspensions as well as the design of practical sedimentation equipment was presented in chapter 2.

The theory of fluid-particle and particle-particle hydrodynamic interactions in two-phase solid/liquid media was reviewed in chapter 3 since this governs the theoretical modelling of sedimentation which was in turn discussed in chapter 4.

Chapter 5 dealt with a literature review of the main design features of some of the most commonly used methods for sedimentation analysis. The chapter is concluded by highlighting the fact that the majority of such techniques require calibration to specific dispersions. Most are not capable of continuous on-line operation.

The main body of experimental work on the design, development and application of the sedimentation analyser was presented in chapters 6 to 8.

In chapter 6, the design and development of the vibrating reed sedimentation analyser including the main features of the ancillary electronic drive and data acquisition systems were described. The first stage of this task involved the design of a bench-top unit utilising a single reed. This unit was used in conjunction with theoretical modelling (Mahgerefteh and Al-Khoory, 1991(a)) as a tool for determining the optimal design and operational characteristics for the multiple reed analyser. This led to the design of a system with a mass resolution of ca. $\pm$ 4.85 $\times$ 10^{-4} g. The chapter concluded by describing the main design features of the multiple reed system and the associated sedimentation rig.

The results of a series of experiments elucidating the performance characteristics of the multiple reed system were presented in chapter 7. In the main, these demonstrated the effects of the reed amplitude of vibration, the suspension bulk viscosity as well as its temperature on the system's response. This work and the results of further studies formed the basis for establishing the feasibility and reliability of the vibrating reed system in providing particle settling velocities and solids flux profiles. The methods and equipment used to prepare and characterise test samples as well as the manner in which test suspensions were prepared and monitored were also discussed.

The main body of experimental data was presented in chapter 8. The chapter dealt with the utilisation of the system calibration plots presented in chapter 7 to characterise the settling behaviour of various polydisperse glass ballotini (density 2550 kgm^{-3})/water suspensions. This was achieved by taking the first derivative of resonance frequency versus time profiles. The resulting rate of change of resonance frequency data was then used in conjunction with the system calibration plots to produce solids flux ($kgm^{-2}s^{-1}$) versus time profiles the accuracy of which was validated by direct mass balance. The latter involved determining the area under each solids flux profile (kgm^{-2}) and multiplying by the cross-sectional area of the settling tank to obtain the experimental solids mass throughput (kg). Such data was then compared with the corresponding volume-based estimate of the solids mass throughput calculated from the known initial solids concentration (kgm^{-3}) and the suspension volume above each reed.

Chapter 8 also discussed the comparison of experimental settling velocity measurements with data generated from some of the predictive models presented in chapter 4. However, this analysis was limited to the monodisperse 200 - 212 μm glass ballotini/water suspensions for which the correlations are appropriate. The reliability of measurements obtained in conjunction with the various polydisperse suspensions on the other hand, was deduced from the aforementioned direct mass balance approach rather than by comparison with theoretical models. This was primarily due to a lack of reliable models capable of simulating the behaviour of very dilute (solids concentrations < 5 % v/v) polydisperse suspensions.

During the course of carrying out studies using the solid/liquid systems, we observed a finite time delay (δt) between the onset of sedimentation and that resulting in a change in the reed resonance frequency. Our results were highly indicative of a disturbance wave which travelled from the top of the settling zone to the bottom of the sedimentation tank. By measuring δt with respect to the position of each reed we were able to predict the speed of propagation of this wave and hence the time lapsed for the entire column to traverse from steady to unsteady state operation. Interestingly, our results showed that the propagation wave velocity was independent of the solids concentration but increased with the mean particle size.

The chapter concluded by presenting data on the sedimentation of different concentration flocculated kaolin/water slurries which demonstrated the feasibility of operation of the device in conjunction with an industrially relevant suspension. Preliminary data demonstrating the application of the device for monitoring the stability of two-phase liquid/liquid emulsions such as an oil/water mixture was also presented.

9.1 Conclusions

The important conclusions based on the results presented in chapters 7 and 8 are:

- For all the dilute (solids concentrations 1.75 - 2.81 % v/v) ballotini (density 2550 kgm^{-3})/water suspensions investigated the system resonance frequency is independent of the bulk viscosity and temperature. Therefore, the system resonance frequency response is directly related to the fluid bulk density and hence the fluid hydrodynamic head which changes with time as particles settle.

- For the nominally monodisperse 200 - 212 μm ballotini/water suspensions, experimental interface velocities inferred from reed breakthrough times, are in excellent agreement (typically within ca. 0.1 %) with corresponding measurements obtained from direct visual observation of the suspension-clear liquid interface. The data are also in good accord with those predicted from the empirical correlations of Richardson and Zaki (1954) (ca. 1.3 % difference) and Garside and Al-Dibouni (1977) (ca. 2.7 % difference). This is probably due to the use of an appropriate value for the flow index, n calculated from the known particle Reynolds number, Re_p. However, the majority of the other predictive correlations reviewed appear to seriously underestimate (by up to 24 %) particle settling velocities. This is probably because the hindered settling function for such models does not take the particle size into account and is entirely based on the suspension voidage.

- In the case of the polydisperse ballotini/water test suspensions, experimental interface velocities correspond to Stokes particle sizes comparable (typically within

ca. 6 %) to the smallest significant particle size in the respective distributions. As the initial solids concentration increases the estimated Stokes diameter decreases indicating a greater tendency for the particles to segregate thus resulting in more diffuse interfaces.

- For all the polydisperse ballotini/water suspensions tested, the experimental solids throughput (kg) inferred from the area under the solids flux curves is comparable (typically within ca. 3 %) to the volume-based solids throughput calculated from the known initial solids concentration (kgm^{-3}) and the suspension volume above each reed. Therefore, the system is viable for providing solids mass throughput data.

- The resonance frequency of each reed is independent of particle size and decreases in a linear manner with increase in solids volume concentration and hence the system bulk density.

9.2 Further Work

9.2.1 Monitoring of Colloidal Stability and Dispersion Structure

The capability of the system in monitoring the behaviour of concentrated kaolin/water suspensions under unstable flocculation conditions as well as oil/water emulsions is promising. This is because such systems are representative of the mixed-colloidal-non-colloidal dispersions typically handled in a wide range of chemical processes (Williams and Simons, 1992) for the production of materials such as paints, pharmaceuticals and foodstuffs (particularly diary products) and in the solid/liquid dispersions encountered during crystallisation, mineral processing and waste water treatment. Data obtained using the reed analyser in conjunction with carefully designed experiments can be useful in elucidating how such systems respond under different shear forces. This information is vital for process design of chemical reactors and the subsequent downstream processing, storage and transportation of products. For instance, in the case of liquid/liquid emulsions, low shear forces lead to separation of the constituent phases (see section 8.8.2, chapter 8) via coalescence of the dispersed phase whilst a

degree of stability is attained under high shear conditions. Therefore, the control of this type of shear-dependent behaviour during the processing of emulsions is critical. We believe that a device based on the current measurement technique could be used as a highly efficient tool for the on-line monitoring and control of colloidal stability and dispersion structure.

In recent years considerable effort has been spent on the reproducible production of high strength ceramics formed from sub-micron powders. One route towards this that is receiving attention is known as the "colloidal processing" method (Williams et al., 1991) where a dispersion of precursor powders is densified to an appropriate consistency and then molded via "slip casting" into what is known as a "green body". The structure of the green body depends, in part, on the underlying colloid science. For instance, the dispersions are often stabilised using polymer additives to prevent aggregation which could lead to large voids and defects in the green body upon consolidation. It is envisaged that by monitoring the stability of such dispersions directly and on-line, advances can be made in the modelling of such processes leading to production optimisation. In essence, the current technique could be used to infer the state of the dispersion structure in relation to initial particle concentration as well as the electrical potential.

9.2.2 Concentrated Systems: De-coupling the Effects of Bulk Density and Viscosity

In this study, the performance characteristics of the multiple reeds have so far been evaluated in conjunction with dilute (solid volume concentrations < 5 %) ballotini/water suspensions in which the effect of viscosity on the resonance frequency is negligible. However, in the case of concentrated suspensions, the resonance frequency is likely to be influenced by both density and viscosity. Accordingly, the accurate interpretation of kinetic data for such systems will require the de-coupling of the effects of these two parameters on the reed's response.

An important part of such a study would involve the development of appropriate mathematical models primarily based on Navier-Stokes equations for simulating the

interaction of the fluid environment with the system's signal (Retsina et al., 1986, 1987). In essence, this approach would entail treating the suspension as a pseudo-continuum with average properties such as density and viscosity. It is expected that the amplitude of vibration will be largely governed by the system viscosity.

NOMENCLATURE

CHAPTER 2:

G_w	Working solid flux (Equation 2.1), kg m^{-2} s^{-1}
u_s	Suspension settling velocity, m s^{-1}
C_T	Concentration of solids in settling vessel, kg m^{-3}
C_u	Concentration of solids in underflow product, kg m^{-3}

CHAPTER 3:

F_D	Drag force, N
C_D	Drag coefficient
u_ϕ	Particle velocity relative to fluid, m s^{-1}
d_p	Particle diameter, m
Re	Reynolds number
F_g	Gravitational force, N
u_o	Stokes' terminal velocity for a single particle settling in an unbounded fluid, m s^{-1}
g	Acceleration due to gravity (9.81), m s^{-2}
d_p'	Projected area diameter for a non-spherical particle, m
A_p	Projected area for a non-spherical particle, m^2
k'	Heywood's volume shape factor for irregular particles
u_o'	Heywood's terminal velocity for irregular particles, ms^{-1}
K_p	Empirical particle volume shape factor
k_e	Empirical volume shape factor for a given particle geometry
l_p	Particle length in plane of greatest stability, m
b_p	Particle breadth in plane of greatest stability, m
t_p	Particle thickness in plane of greatest stability, m

u_t	Stokes' terminal velocity for a single particle settling in a bounded fluid, m s^{-1}
D	Diameter of settling vessel, m
C_{Dt}	Drag coefficient for a single particle settling in a bounded fluid (Equation 3.25)
C_{Dt}^*	Drag coefficient for multiple particles settling in a bounded fluid (Equation 3.25)
u_t^*	Stokes' terminal velocity for multiple particles settling in a bounded fluid (Equation 3.26), m s^{-1}
$g(\varepsilon)$	Voidage function
F_{Dt}	Drag force acting on a single particle (Equation 3.27), N
Re_t	Reynolds number for a particle settling at its terminal velocity in a bounded fluid
Re_o	Reynolds number for a particle settling at its terminal velocity in an unbounded fluid
k	Empirical constant in Equations 3.27, 3.28 and 3.36
C_{Do}	Drag coefficient for a single particle settling in an unbounded fluid (Equation 3.28)
Re_o'	Modified Reynolds number in Equation 3.31 and 3.32
K_v	Fluid consistency factor, Pa s
n	Flow index calculated from the particle Reynolds number

Greek Letters

ρ_f	Fluid density, kg m^{-3}
ρ_s	Particle density, kg m^{-3}
μ_f	Fluid viscosity, Pa s
ε	Suspension voidage or porosity
μ_a	Apparent fluid viscosity, Pa s
ϕ_s	Solids volume fraction

CHAPTER 4:

u_s	Suspension settling velocity, m s^{-1}
u_o	Stokes' terminal velocity for a single particle settling in an unbounded fluid, m s^{-1}
$f(\phi_s)$	Hindered settling function
K	Empirical constant in Equation 4.3
k	Empirical constant in Equation 4.4
Q	Vand's interaction constant
Re_p	Particle Reynolds number
K_1	Stoke's shape factor
K_2	Ratio of drag coefficient of a particle to drag coefficient of an equivalent sphere
K_{10}	Limiting value of Stoke's shape factor
C_{Ds}	Drag coefficient for a single particle settling in Newton's regime
d_v	Particle equivalent sphere diameter, m
A, B, C, D	Coefficients in Equation 4.16
$F(\varepsilon)$	Voidage function in Equations 4.26 and 4.27
F_1, F_2, F_3	Coefficients in Equation 4.29
u_i	Settling velocity of i^{th} size fraction in a suspension, m s^{-1}
$u_{\phi i}$	Relative velocity of i^{th} size fraction in a suspension, m s^{-1}

Greek letters

ζ	Zeta potential, V
ρ_p	Particle density, kg m^{-3}
ρ_m	Supension or Mixture density, kg m^{-3}
μ_s	Suspension viscosity, Pa s
ϕ_s	Solids volume fraction
ε	Suspension voidage or porosity

ϕ	Particle sphericity
v	Particle settling velocity in Equation 4.24, m s^{-1}
ϕ_i	Solid volume fraction of i^{th} size fraction in a suspension
ε_i	Suspension voidage or Porosity of i^{th} size fraction in a suspension
ρ_{pi}	Particle density of i^{th} size fraction in a suspension, kg m^{-3}

CHAPTER 5

p_o	Percentage of particles with settling velocities $\leq v_o$
v_o	Critical settling velocity corresponding to particles leaving a sedimentation column, m s^{-1}
v_s	Particle settling velocity in Equation 5.1, m s^{-1}
Z_x	Complex impedance of suspending fluid, Ω
L_x	Inductance of suspending fluid, H
R_x	Resistance of suspending fluid, Ω
C_x	Capacitance of suspending fluid, F
C_m	Measured capacitance of suspending fluid, F
G_x	Conductance of suspending fluid, Ω^{-1}

Greek letters

τ_c	Duration of charge pulse for electrical transducer, s

CHAPTER 6

y	Transverse deflection of a vibrating beam, m
x	Distance along the beam, m
t	Time, s
a	Cross-sectional area of the beam, m^2
E	Young's modulus of elasticity, N m^{-2}

I	Area moment of inertia of the cross-section about the neutral axis of the beam, m^4
Y(x)	Function defining beam shape for the normal mode of vibration
F(t)	Function describing the motion of the beam during simple harmonic motion
A, B, C, D	Arbitrary constants in Equation 6.6

Greek letters

ρ	Density of the beam, kg m^{-3}
α,β	Arbitrary constants in Equation 6.3
ω	Angular frequency, rad s^{-1}

CHAPTER 7

$f(x, \mu, \sigma)$	Normal distribution function describing proportion of particles of different sizes in a given sample
x	Particle size, m
Δt_b	Solids breakthrough time, s

Greek letters

μ	Arithmetic mean of the particle size distribution, m
σ	Standard deviation of the particle size distribution

CHAPTER 8

$\overline{d}_p$	Mean particle size, m
A	Settling tank cross-sectional area, m^2
t	Time, s

Greek letters

ϕ	Initial suspension solids volume concentration, % v/v
Φ	Solids flux in Equation 8.1, kg m^{-2} s^{-1}
Δt_b	Solids breakthrough time, s

Al-Khoory H., The design and development of a vibrating reed transducer for process monitoring and particle characterisation, PhD thesis, Department of Chemical Engineering, University College London, (1992).

Allen T., Particle size measurement., 4th edition, Chapman and Hall, London, (1990).

Al-Naffa M. A. and Selim S.M., Sedimentation of monodisperse and bidisperse hard sphere colloidal suspensions., AICheE J., 38, (1992), 1618.

Amarasinghe B.M.W.P.K., Ph.D Thesis, University of Manchester Institute of Science and Technology, (1990).

Amarasinghe W.P.K., M.Sc. Thesis, University of Manchester Institute of Science and Technology, (1987).

Arai Y., "Methods of particle size measurement", in Chemistry of powder production, Powder technology series, Chapman and Hall, London, (1996).

Auzerais F.M., Jackson R., Russel W.B. and Murphy W.F., The transient settling of stable and flocculated dispersions., J. Fluid Mech., 221, (1990), 613-639.

Bak P., The Devil's Staircase, Physics Today, 39, 12, (1986), 39-45.

Balachandran W. and Beck M.S., Solids-concentration measurement and flow measurement of slurries and sludges using ultrasonic sensors with random data analysis, Part I: Solids-concentration measurement, Trans. Inst. Meas. Control, 2, 4, (1980), 181-197.

Barnea E. and Mizrahi J., A generalised approach to the fluid dynamics of particulate systems. Part I: General correlation for fluidization and sedimentation in solid multi-particle systems., Chem. Eng. Sci., 5, (1973), 171-189.

Barnes H.A. and Holbrook S.A., High concentration suspensions: preparation and properties, in "Processing of solid-liquid suspensions", Shamlou P.A. (Editor), Butterworth-Heinemann (1993).

Batchelor G.K., Brownian diffusion of particles with hydrodynamic interactions., J. Fluid Mech., 131, (1976), 155-175.

Batchelor G.K., Sedimentation in a dilute dispersion of spheres., J. Fluid Mech., 52, (1972), 245-268.

Batchelor G.K. and Wen C.S., Sedimentation in a dilute polydisperse system of interacting spheres, Part II, Numerical results., J. Fluid Mechanics, 124, (1982), 495-528.

Beards C.F., Engineering vibration analysis with application to control systems., published by Edward Arnold, (1995).

Beards C.F., Vibrations and Control Systems., Ellis Horwood series in Mechanical Engineering, published by Ellis Horwood Ltd., (1988).

Bishop R.E.D. and Johnson D.C., Mechanics of vibration., Cambridge University Press, London, (1960).

Blasquez G., Pons P. and Boukabache A., Capabilities and limits of silicon pressure sensors., Sensors and Actuators., 17, (1989), 387-403.

Bonnet J.C. and Tavlarides L.L., Ultrasonic technique for dispersed-phase holdup measurements, Ind. Eng. Chem. Res., 26, 1, (1987), 811-814.

Boycott A.E., Sedimentation of blood corpuscles., Nature, 104, (1920), 532.

Brindley G.W., "Ceramic fabrication processes", Chapter 1, Kingery W.D. (Ed.), Wiley, New York, (1958).

Briscoe B.J. and Mahgerefteh H. Continuous gas density measurement at high pressures and temperatures: Development of a novel technique. The Chemical Engineer, No. 412, 1985, 28-30.

Briscoe B.J. and Mahgerefteh H., A novel technique for the quantitative measurement of gaseous uptake in organic polymers at high pressure. J Phys. E: Sci. Instrum., 17, (1984), 483-487.

Briscoe B.J., Liatsis D. and Mahgerefteh H., An analysis of the behaviour of a composite vibrating beam. J. Phys. E: Sci.Instrum., 19, (1987), 1039-40.

Bruggeman D.A.G., Berechnung verschiedener physikalisscher konstanten von heterogenen substanzen., Annalen der Physik, 24, (1935), 636-679.

BS 1796: Part: 1, Test sieving: Methods using test sieves of woven wire cloth and perforated metal plates, BSI, (1989).

Bukhari K.M. and Lahey R.T., An experimental study of 2-D phase separation phenomena, Int. J. Multiphase flow, 13, (1987), 387-402.

Burgers J.M., On the influence of the concentration of a suspension upon the sedimentation velocity., Proc. K. Ned. Akad. Wetensch., 44, (1941), 1045-1051, 1177-1184.

Burgers J.M., On the influence of the concentration of a suspension upon the sedimentation velocity., Proc. K. Ned. Akad. Wetensch., 45, (1942), 9-16, 1269-128.

Cimmino A. and Davis T.J., A simple optical transducer for the measurement of small vibration amplitudes, J. Phys. E: Sci. Instrum., 18, (1985), 947-948.

Clift R., Grace J.R. and Weber M.E., Bubbles, drops and particles., Academic Press, (London), 1978.

Coe H.S. and Clevenger G.H., Capacities of slime settling tanks., Trans. AIME, 55, (1916), 356-384.

Concha F. and Almendra E.R., Settling velocities of particulate systems.I. Settling velocities of individual spherical particles. Int. J. Mineral Process., 5, (1979a), 349-367.

Concha F. and Almendra E.R., Settling velocities of particulate systems.II. Settling velocities of suspensions of spherical particles. Int. J. Mineral Process., 6, (1979b), 31-41.

Dallavalle J.M., "Micrometric",2nd Edition. Pitman (London), (1948).

Davis R.H. and Acrivos A., Sedimentation of non-colloidal particles at low Reynolds numbers., Ann. Rev. Fluid Mech., 17, (1985), 91-118.

Davis R.H. and Birdsell K.H., Hindered settling of semi-dilute mono-disperse and poly-disperse suspensions., AIChE J., 34, (1988), 123-129.

Davis R.H. and Hassen, M.A., Spreading of the interface at the top of a slightly poly-disperse sedimenting suspension., J. Fluid Mechanics, 196, (1988), 107-134.

Dick R.I., Gravity thickening of sewage sludges., Wat. Pollut. Control, 71, (1972), 368.

Di Felice R., A relationship for the wall effect on the settling velocity of a sphere at any flow regime., Int. J. Multiphase Flow, 22, 1, (1996a), 515-525.

Di Felice R., The particle in a tube analogy for a multi-particle suspension., Int. J. Multiphase Flow, 22, 3, (1996b), 527-533.

Duncombe C.G. and Withrow J.R., The Kelly tube and the sedimentation of Portland cement., J. Phy. Chem., 36, (1932), 31-51.

Einstein A., Eine neue bestimmung der molekuldimensionen, Ann. Phys., 19, (1906), 289-306.

Famularo J.and Happel J., Sedimentation of dilute suspensions in creeping motion., AIChE J., 11, (1965), 981.

Fidleris V. and Whitmore R.L., Experimental determination of the wall effect for spheres falling axially in cylindrical vessels., Brit. J. Appl. Phys., 12, (1961), 490-494.

Fitch E.B., Sedimentation of flocculent suspensions - state of the art. AIChE J., 25, (1979), 913-930.

Francis A.W., Wall effect in falling ball method for viscosity., Physics, 4, (1933), 403.

French A.P., Vibrations and Waves, M.I.T introductory physics series, published by Nelson, (1970).

Gadala-Maria F.A., The reology of concentrated suspensions., PhD thesis, Stanford University, California, (1979).

Ganser G.H., A rational approach to drag prediction of spherical and non-spherical particles, Powder Technology, 77, (1993), 143-152.

Garside J. and Al-Dibouni M.R., Velocity-voidage relationship for fluidization and sedimentation in solid-liquid systems., Ind. Eng. Chem. Process des. Dev., 16, (1977), 206-214.

Genthe W.K., in Wendt R.E (Ed.), Symp. on flow: Its measurement and control in science and industry., Vol.1, Instrument soc. America, NC, (1974), 849.

Glendinning A.B. and Russel W.B., A pairwise additive description of sedimentation and diffusion in concentrated suspensions of spheres., J. Colloid Interface Sci., 89, (1982), 124-143.

Gregory J., Effect of dosing and mixing conditions on flocculation by polymers. In "Advances in Measurement and Control of Colloidal Processes", Williams R.A. and de Jaeger N.C. (Eds.). Butterworth-Heinemann (London), (1991).

Haberman W.L. and Sayre R.M., David Taylor model basin report No. 1143 U.S. Navy Dept. Washington D.C. (1958).

Haider A. and Levenspiel O., Drag coefficient and terminal velocity of spherical and nonspherical particles, Powder Technology, 58, (1989), 63-70.

Hall T. and Hyde R.A., Water treatment process and practices., WRc, Swindon, Chapters 8-10, (1992).

Happel J., Viscous flow in multi-particle systems: slow motion of fluids relative to bed of spherical particles., AIChE J., 4, (1958), 197-201.

Hawksley P.G.W, The effect of concentration on the settling of suspensions and flow through porous media, Inst. of Phys. symposium, 36, (1950), 114.

Hayakawa R., Kanda H., Sakamoto M. and Wada Y., New apparatus for measuring the complex dielectric constant of a highly conductive material, Japanese Journal of Applied Physics, 14, 12, (1975), 2039-2052.

Heywood H., Calculation of particle terminal velocities., J. Imp. Coll. Chem. Eng. Soc., 4, (1948), 17-29.

Hibberd D.J., Howe A.M., Mackie A.R., Purdy P.W., Robins M.M. in Dickenson E.(Ed.), Food, Emulsions and Foams, Roy. Soc. Chem. Spec. Publ., 58, (1987), 219.

Hin-Sum Law et al., Gravity separation of bidisperse suspensions: light and heavy particle species. Chem. Engng Sci., 42, 7, (1987), 1527-38.

Howe A.M. and Robins M.M., Determination of gravitational separation in dispersions from concentration profiles., Colloids and surfaces, 43, 1, (1990), 83-94.

Huang S., Green R.G., Plaskowski A. and Beck M.S., A high frequency stray-immune capacitance transducer based on the charge transfer principle, IEEE Transactions on instrumentation and measurement, Volume 37, No.3, (1988), 368-373.

Huang S.M., Stott S.L., Green R.G. and Beck M.S., Electronic transducers for industrial measurement of low value capacities, J. Phys. E: Sci. Instrum., 21, (1988), 242-250.

Huckel E., The theory of concentrated aqueous solutions of strong electrolytes., Phys. Z, 26, (1924), 93-147.

Ikeda K. and Isozaki K., A precision densimeter which compensates for liquid viscosity, IEEE Trans. Instrum. Meas. IM-35, 4, (1986), 624-629.

Iordache O. and Corbu S., A stochastic approach to sedimentation., Chem. Eng. Sci., 41, (1986), 2589-2593.

Iwaoka M. and Ishii T., Experimental wall correction factors of single solid spheres in circular cylinders., J. Chem. Engng Japan, 12, (1979), 239-242.

Jones E.B., Mechanical measurements, in Jones' Instrument technology (Noltingk B.E. editor), Volume 1, 4th edition, published by Butterworths (1985).

Kaye B.H. and Boardman R.P., Cluster formation in dilute suspensions. In "Interactions between fluids and particles", Institution of Chemical Engineers (London), (1962) , 17-21.

Kearsey H.A. and Gill L.E., A study of the sedimentation of flocculated thoria slurries using a gamma-ray technique, Trans. Inst. Chem. Eng., 41, (1963), 296-306.

Khodaverdian A., Added mass effects in Two-phase liquid-solid media., PhD thesis, Department of Chemical Engineering, University College London, (1994).

Kolmogoroff A.N., A refinement of previous hypotheses concerning the local structure of turbulence in a viscous incompressible fluid at high Reynolds number., J. Fluid Mech., 13, Part I, (1962), 82-85.

Kynch G.J., A theory of sedimentation., Trans. Faraday soc., 48, (1952), 166-176.

Lali A.M., Khare A.S., Joshi J.B., and Nigam K.D.P, Behaviour of solid particles in viscous non-newtonian solutions: Settling velocity, wall effects and bed expansion in solid-liquid fluidized beds., Powder Technology, 57, (1989), 39-50.

Langdon R.M., "Liquid level sensing device", UK Patent 1595194 (1977).

Lappel C.E. and Shepherd C.B, Calculation of particle trajectories., Ind. Engng Chem., 32, (1940), 605-617.

Leighton D. and Acrivos A., Viscous resuspension., Chem. Engng. Sci., 41, (1986), 1377-1384.

Leighton D. and Acrivos A., The shear-induced migration of particles in concentrated suspensions., J. Fluid Mechanics, 181, (1987), 415-439.

Leith D., Drag on nonspherical objects., Aerosol Science and Technology, 6, (1987), 153-161.

Lockett M.J. and Al-Habbooby H.M., Relative particle velocities in two-species settling., Powder Technology, 10, (1974), 67-71.

Mahgerefteh H.and Khodaverdian A., Added mass effects in two-phase solid/liquid media, Trans.I.Ch.E: Research and Development, 79(A2), (1996), 272-280.

Mahgerefteh H., Al-Khoory H.F. and Khodaverdian A., A novel thermogravimetric analyser, Thermochemica Acta, 237, (1994), 175-185.

Mahgerefteh H.and Al-Khoory H.F., Predictive criteria for the optimisation of a vibrating reed transducer. Trans. Inst. Meas. Cont., 13, (1991a), 48-56.

Mahgerefteh H. and Al-Khoory H.F. The design, development and optimisation of a robust transducer for process monitoring., Proc. of the 12th IMEKO World congress, Measurement and Control, Beijing, China, (1991b), 126-139.

Mahgerefteh H., Al-Khoory H.F. and Khodaverdian A., The design and development of a novel transducer for the monitoring of process parameters under aggressive environments. Chem. Eng. Comm., 92, (1990), 49-63.

Mahgerefteh H. and Khodaverdian A., A novel transducer for the on-line measurement of flow of viscous fluids., The Chemical Engineer, (1989).

Mahgerefteh H., Briscoe B.J. and Liatsis D., Large amplitude vibrating resonant device for process monitoring. Proc. 11th World congress, Instrumentation for the 21st century, Houston Texas, (1988), 619-42.

Masliyah J.H., Hindered settling in multi-species particle systems, Chem. Engng Sci., 34, (1979), 1166-1168.

Massey B.S., Mechanics of fluids., 6th edition, Van Nostrand Co., London, (1989).

Matusik, F.J. and Scarna P.C., Latest instrument makes on-line control of slurries possible., Control Eng., 28, (1981), 116.

Meredith R.E. and Tobias C.W., Advances in Electrochemistry and Electrochemical Engineering, Volume 2, Interscience, New York, (1962).

Merta H. and Ziolo J., On the method of thickener area calculation based on the data of batch settling tests., Chem. Engng. Sci., 41, (1986), 1918-1920.

Micheals A.S. and Bolger J.C., Settling rates and sediment volumes of flocculated kaolin suspensions., I & EC Fundamentals, 1, (1962), 24-33.

Micheals A.S., "Ceramic fabrication processes", Chapter 2, Kingery W.D. (Ed.), Wiley, New York, (1958).

Mirza S. and Richardson J.F., Sedimentation of suspensions of particles of two or more sizes., Chem. Eng. Sci., 34, (1979), 447-454.

Miskin I., Elliott L., Ingham D.B. and Hammond P.S., Steady suspension flows into two-dimensional horizontal and inclined channels., Int. J. Multiphase Flow, 22, 6, (1996), 1223-1246.

Montgomery J.M., Water treatment principles and design, John Wiley & Sons, New York, Chapter 7, (1985).

Munroe H.S., The English versus the Continental system of jigging-is close sizing advantageous?, Trans. Am. Inst. Min. Engrs., 17, (1988), 637-659.

Myers D.F. and Saville D.A., Dielectric spectroscopy of colloidal suspensions, part I: The dielectric spectrometer, J.Colloid Interface Sci., 131, (1989a), 448-460.

Myers D.F. and Saville D.A., Dielectric spectroscopy of colloidal suspensions, part II: Comparison between experiment and theory, J.Colloid Interface Sci., 131, (1989), 460-470.

Nakamura H., Husimi Y. and Wada A., Time domain measurement of dielectric spectra of aqueous polyelectrolyte solutions at low frequencies, Journal of Applied Physics, 52, 4, (1981), 3053-3061.

Napier-Munn T.J., Reeves T.J. and Hansen J.O., in 2nd Samancor symposium on dense medium separation, Perth, Samancor Ltd., Johannesburg, (1985).

Nasr-el-din H., Shook C.A., and Colwell J., Determination of solids concentrations in slurries., Hydrotransport, 10, (1987), 191.

Newton I., Principia. Lib. II, Prop. XXXIX, Theor. XXXI. Cambridge University Press, Cambridge, (1687).

Noltingk G.E., Electrical and Radiation measurements., Butterworths (London), (1987).

Patwardhan V.S., and Tien C., Sedimentation and liquid fluidization of solid particles of different sizes and densities, Chem. Eng. Sci., 40, (1985), 1051-1060.

Perry R.H. and Chilton C.H., Chemical engineers' handbook., 5th edition, MaGraw-Hill, (1973).

Peter H.S., Transducers in measurement and control., 3rd Edition, Adam Hilger Ltd, Bristol, (1985).

Pettyjohn E.S. and Christiansen E.B., Effect of particle shape on free-settling rates of isometric particles., Chemical Engineering Progress, 44, (1948), 157-172.

Phillips R.J., Armstrong R.C., Brown R.A., Graham A.L. and Abbott J.R., A constitutive equation for concentrated suspensions that accounts for shear-induced particle migration., Phys. Fluids A, 4, (1992), 30-40.

Priess U., A high resolution temperature sensor., Qualite Rev. Prat. Controle Ind., 22, (1983), 76.

Raffle J.F., Pressure variation within concentrated settling suspensions., J. Phys. D: Appl. Phys., 9, (1976), 1239-1252.

Reed C.C. and Anderson J.L., Hindered settling of a suspension at low Reynolds number., AIChE J., 26, (1980), 816-827.

Retsina, T., Richardson, S.M. and Wakeham, W. A. The theory of a vibrating-rod densimeter., Applied Sci Research, 43, (1986), 127.

Retsina, T., Richardson, S. M. and Wakeham, W.A., The theory of a vibrating-rod viscometer., Applied Sci. Research, 43, (1987), 325.

Richardson J.F. and Zaki W.N., Sedimentation and fluidization: Part I, Trans. Instn. Chemical. Engrs, 32, (1954), 35-53.

Robinson C.S., Some factors influencing sedimentation, Ind. Eng. Chem., 18, (1926), 869.

Roy P.K. and Ganesan N., Studies on the dynamic behaviour of a cantilever beam with variying thickness., Journal of sound and vibration, 177(1), (1994), 1-13.

Rumpf H., Representing the characteristics of particle assemblies., in "Particle technology", Powder technology series, Chapman and Hall, (1990), 13-27.

Russel, W.B., Saville, D.A. and Schowalter, W.R., Colloidal Dispersions, Cambridge University Press, Cambridge (1989).

Seely S., Electron tube circuits, McGraw-Hill, New York, USA(1958).

Selim T.N., Kothari A.C. and Turian R.M., Sedimentation of multisized particles in concentrated suspensions., AICheE J., 29, (1983), 1029-38.

Shaflinger U., Influence of nonuniform particle size on settling beneath downward facing walls., Int. J. Multiphase Flow, 11, (1985), 783-796.

Shaflinger U., Acrivos A. and Zhang K., Viscous resuspension of a sediment within a laminar and stratified flow., Int. J. Multiphase Flow, 16, (1990), 567-578.

Shannon P.T., Dehaas R.D., Stroupe E.P. and Tory E.M., Batch and Continuous thickening: Prediction of batch settling behaviour from intial rate data with results for rigid spheres., Ind. Eng. Chem. Fundam., 3, (1964), 250-260.

Shannon P.T. and Tory E.M., The analysis of continuous thickening., Trans. AIME, 235, (1966), 375-382.

Shi T.M., Simons S.J.R., Dickin F.J. and Williams R.A., Electrical sensing of dispersion behaviour, Colloids and Surfaces A: Physicochemical and Engineering Aspects, 77, (1993), 9-27.

Shih Y.T., Gidaspow D. and Wasan D.T., Hydrodynamics of sedimentation of multisized particles., Powder technology, 50, (1987), 201-215.

Simon S.W., Gregory J.N. and Robert H., Measuring thickness of metal/lubricant interfacial regions with ac impedance spectroscopy., J. Colloid Interface Sci., 132, (1989), 243-249.

Simons S.J.R. and Williams R.A., Particle size measurement using non-invasive dielectric sensors, Powder Technology, 73, (1992), 85-90.

Simons S.J.R., The development of non-invasive sensors for monitoring concentrated sedimenting suspensions., PhD thesis, Department of Chemical Engineering, University of Manchester Institute of Science and Technology., (1991).

Smith T.N., The differential sedimentation of particles of various species., Trans. Inst. Chem. Eng., 45, (1967), T311-T313.

Smits J.G., Tilmans H.A.C., Hoen K., Mulder M., Van Vuuren J. and Boom G., Resonant diaphram pressure measurement system with ZnO on Si excitation., Sensors and Actuators, 4, (1983), 565.

Smoluchowski M. von, Contribution a la theorie de l'endosmose electrique et de quelques phenomenes correlatifs., Bulletin International de l'accademie des sciences de cracorie, 8, (1903), 182-200.

Sperry P., Morphology and mechanism in latex flocculated by volume restriction., J. Colloid Interface Sci., 99, (1984), 97-108.

Steinour H.H., Rate of sedimentation of non-flocculated suspensions of uniform spheres., Ind. Eng. Chem., 39, 7, (1944), 618-624 & 840-901.

Stern O., The theory of the electric double layer., Z. Elektrochem., 30, (1924), 508.

Stokes G.G., On the effect of internal friction of fluids on the motion of pendulums, Trans. Cam. Phil. Soc., 9, (1851), 8.

Tadros, Th. F., "Separation of suspensions and prevention of formation of dilatent sediments", in Solid-Liquid Dispersions, Academic Press, London, (1992), 225-274.

Talmage W.P. and Fitch E.B., Determining thickener unit areas., Ind. Chem. Eng., 47, (1955), 38-41.

Tebbutt T.H.Y., Principles of water quality control, 4th Edition, Pergamon Press, Oxford, Chapter 11, (1992).

Tebbutt T.H.Y., Primary sedimentation of wastewater., J. Wat. Pollut. Control Fedn., 51, (1979), 2858.

Thompson T.L. and Clark N.N., A holistic approach to particle drag prediction, Powder Technology, 67, (1991), 57-66.

Timoshenko S., Vibration problems in Engineering., Constable, London, (1937).

Tory E.M. and Pickard D.K., A three parameter Markov model for sedimentation., Can. J. Chem. Eng., 55, (1977), 655-665.

Tory E.M., Kamel M.T. and Chan Man Fong C.F., Sedimentation is container-size dependent., Powder technology, 73, (1992), 219-238.

Urick R.J., A sound velocity method for determining the compressibility of finely divided substances., J. Appl. Phys., 18, (1947), 983-987.

Vand V., Viscosity of solutions and suspensions: Part I., J. Phys. Coll. Chem., 52, (1948), 277-299.

Wadell H., Some new sedimentation formulas., Physics, 5, (1934), 281-291.

Wakeman R.J. and Holdich R.G., Theoretical and Experimental modelling of solids and liquid pressures in batch sedimentation., Proc. World Filt. Congress III, Dawington, U.S.A., Upland Press, Croydon, (1989), 346-353.

Wedlock D.J., Fabris I.J. and Grimsey J., Sedimentation in poly-dispersed particulate suspensions., Colloids and surfaces, 43, 1, (1990), 67-81.

Weiland R.H. and McPherson R.R., Accelerated settling by addition of bouyant particles., Ind. Eng. Chem. Fundam., 18, (1979), 45-49.

Whitmore R.L., The sedimentation of suspensions of spheres., Brit. J. Appl. Phys., 6, (1955), 239-245.

Williams R.A. and Simons S.J.R., Handling Colloidal materials, in Colloid and Surface Engineering: Applications in the process industries (Williams R.A. Ed.), Butterworth-Heinemann (Oxford), (1992), 55-111.

Williams R.A., Amarasinghe W.P.K., Simons S.J.R and Xie C.G., Sedimentation behaviour of complex poly-disperse suspensions., Powder technology, 65, (1991), 411-432.

Williams R.A., Xie C.G., Bragg R. and Amarasinghe W.P.K., Experimental techniques for monitoring sedimentation in optically opaque suspensions., Colloids and surfaces, 43, (1990), 1-32.

Williams R.A. and Amarasinghe W.P.K., Measurement and simulation of sedimentation behaviour of concentrated polydisperse suspensions., Trans. Instn Min. Metall. (Sec. C: Min. Process. Extr. Metall.), 98, (1989), C68-C82.

Wright P., The impact of the EC Urban Waste Water Treatment Directive., JIWEM, 6, (1992).

Xie C.G., Huang S.M., Stott A.L., Plaskowski A. and Beck M.S., in Zhang H.X.(Ed.), Proc. Int. Conf. Meas. and control granular materials, Shenyang, China, Shenyang Int. Conf. centre Sci. Tecnol., (1988), 81-89.

Xie C.G., Williams R.A., Simons S.J.R., Beck M.S. and Bragg R., A novel sedimentation analyser, Meas. Sci. Tech., 1, (1990), 1216-1227.

Young R.A., Meril J.T., Clarke T.L. and Proni J.R., Acoustic profiling of suspended sediments in the marine bottom boundary layer., Geophys. Res.Lett., 9, 3, (1982), 175-178.

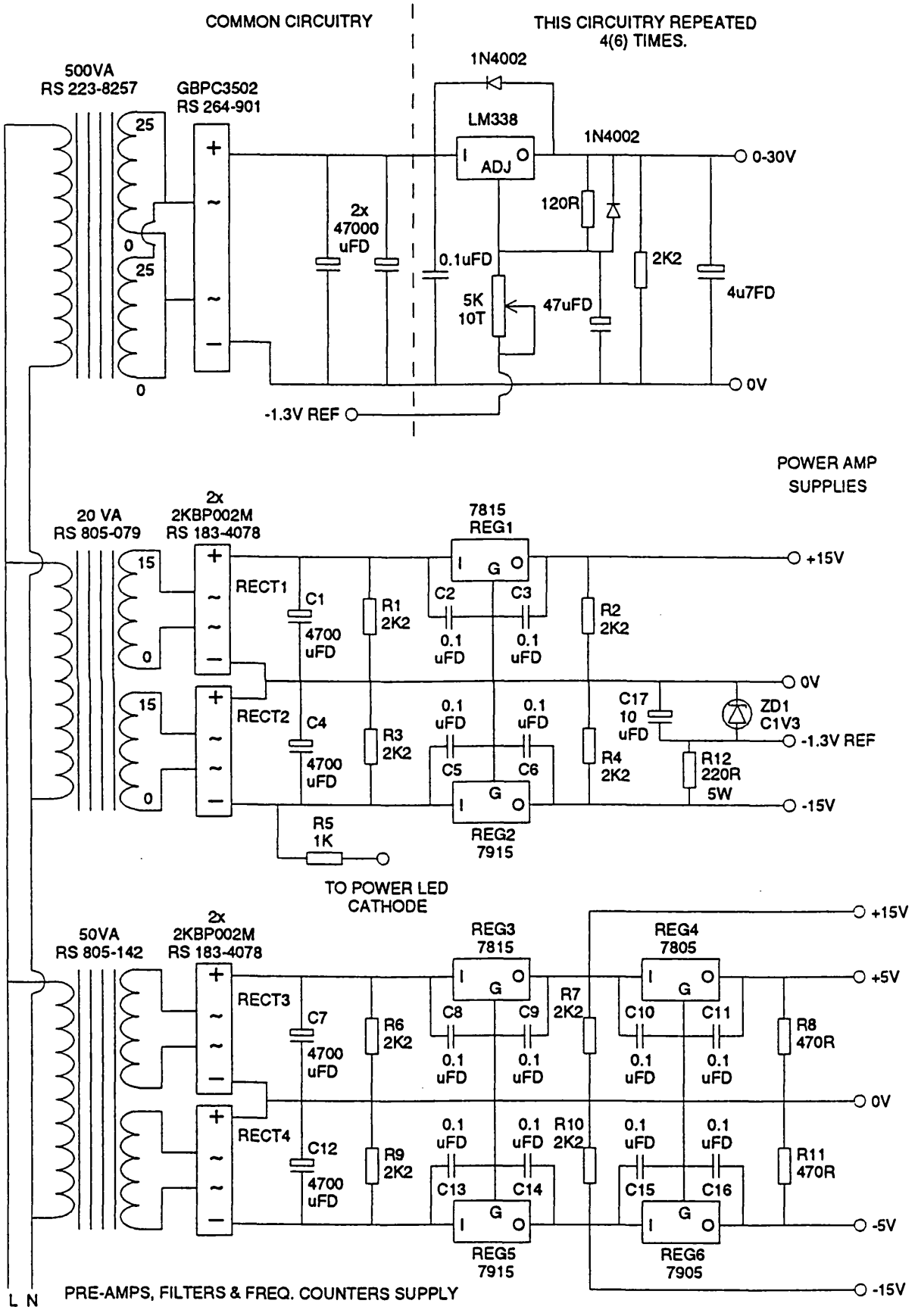

Figure I Electronic circuit diagram showing the system power regulators.

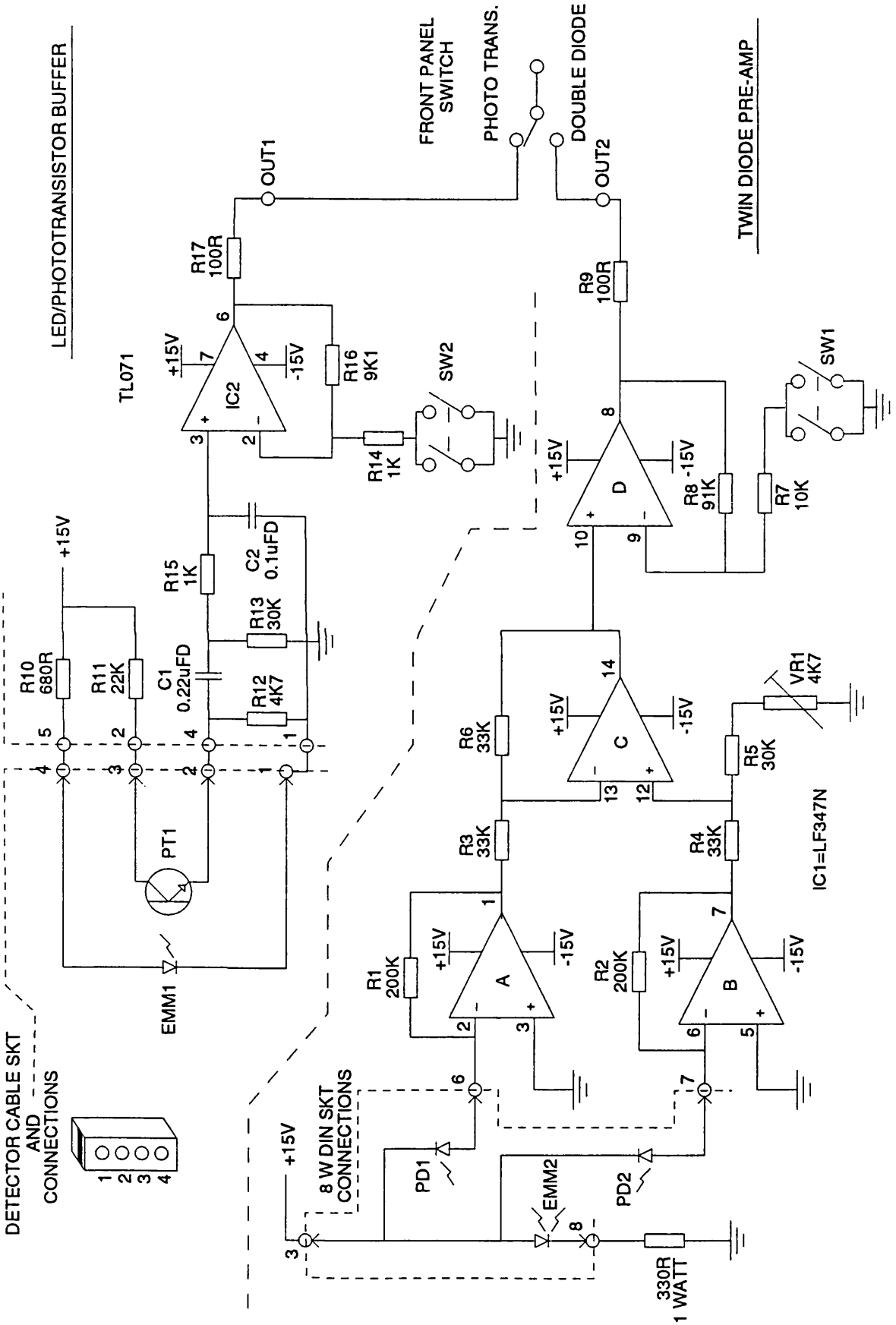

Figure II Electronic circuit diagram showing the photo-transistor detectors used to monitor the system response.

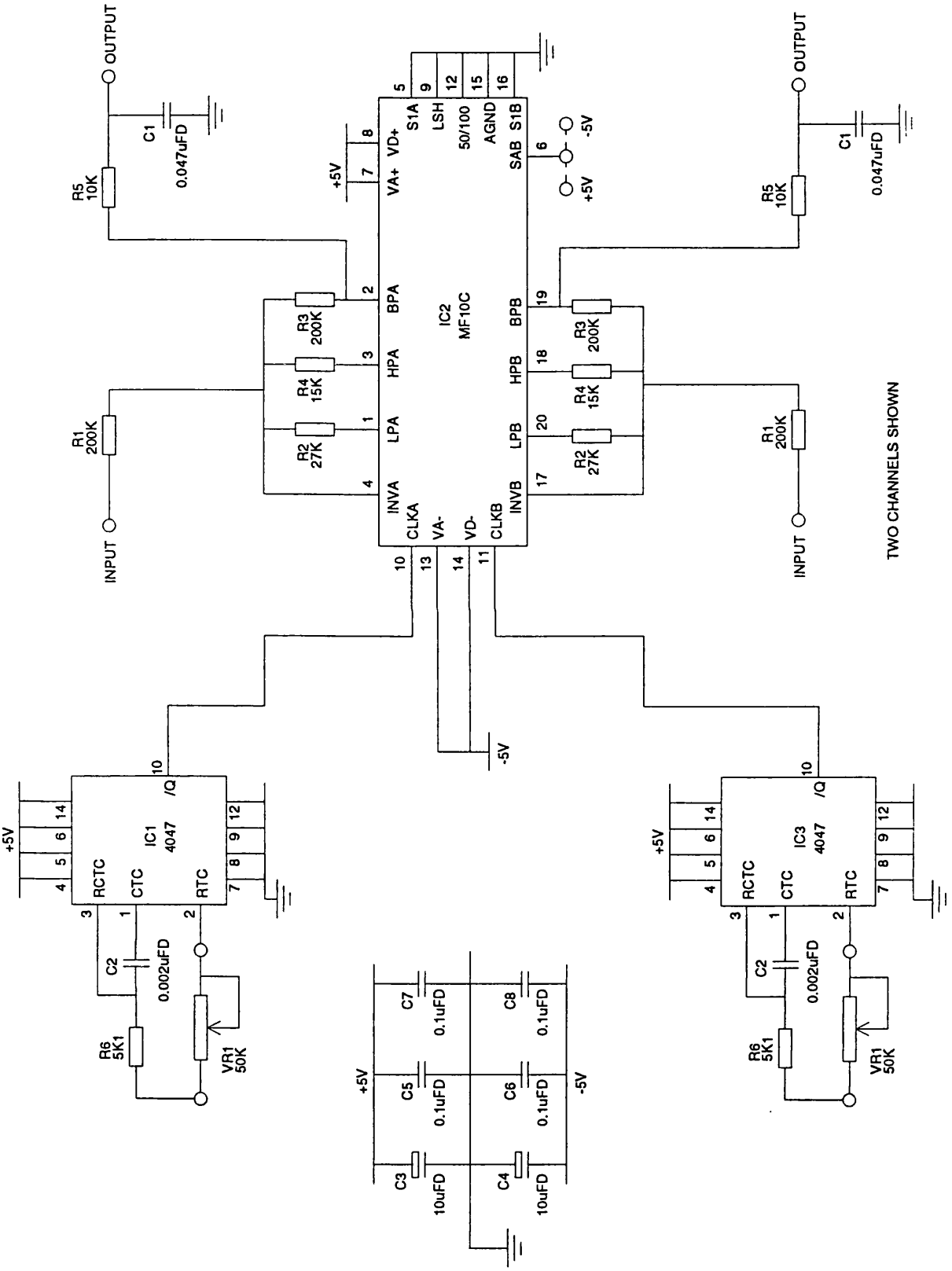

Figure III Electronic circuit diagram showing the variable bandpass filter used to select the system resonance frequency.

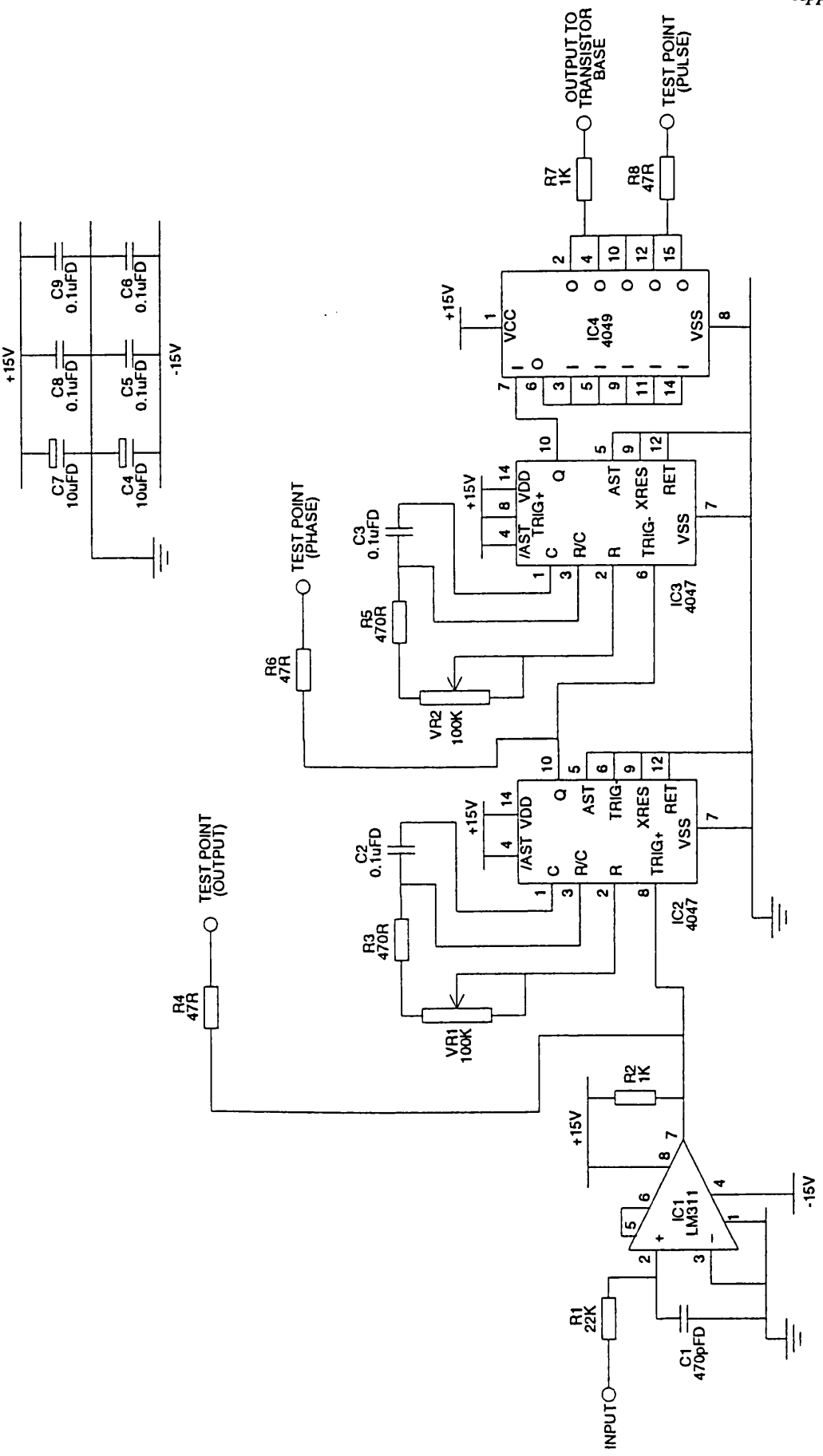

Figure IV Electronic circuit diagram showing the system pulse power amplifier.

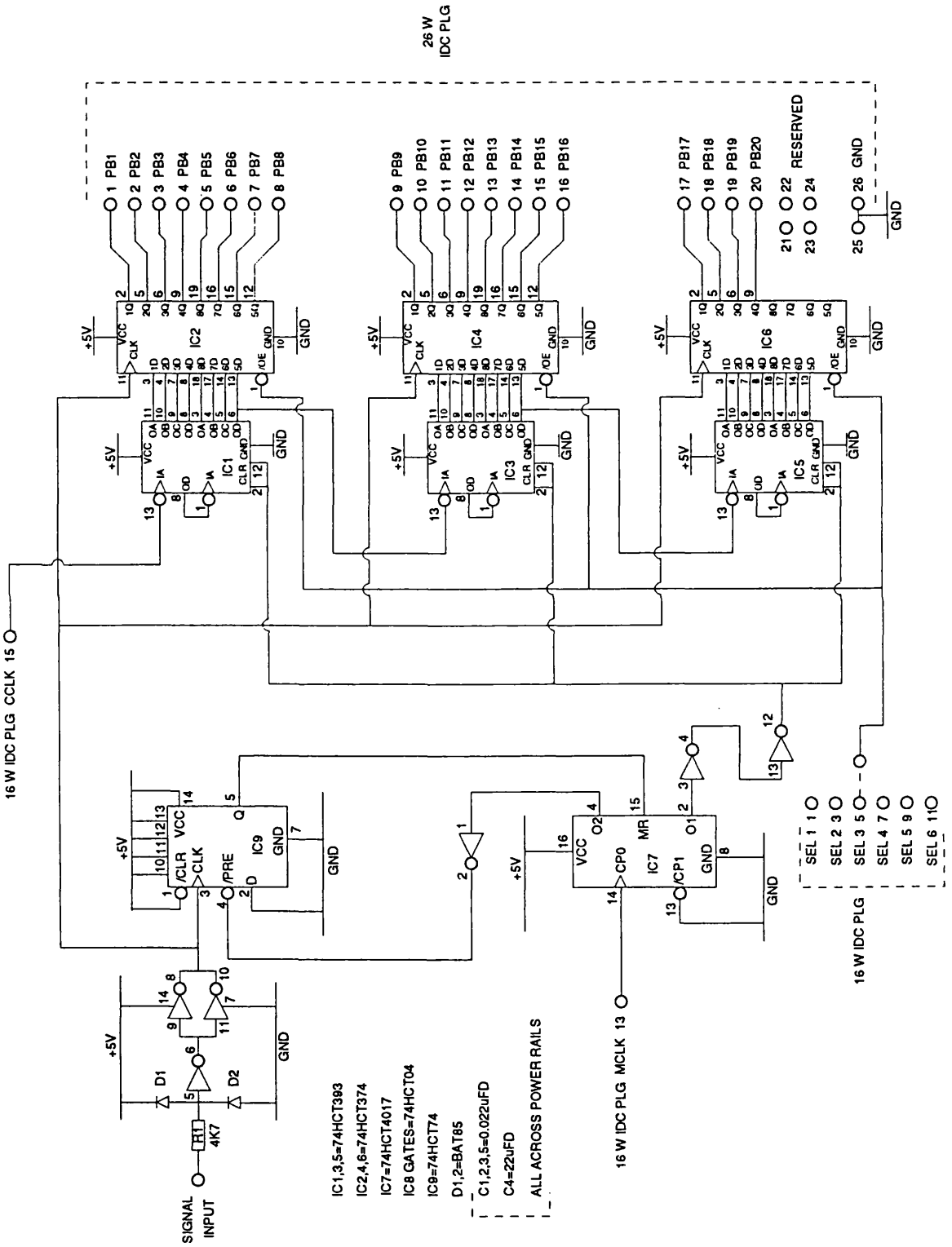

Figure V Electronic circuit for regulating the system frquency. The diagram also shows the associated data logging circuitry.

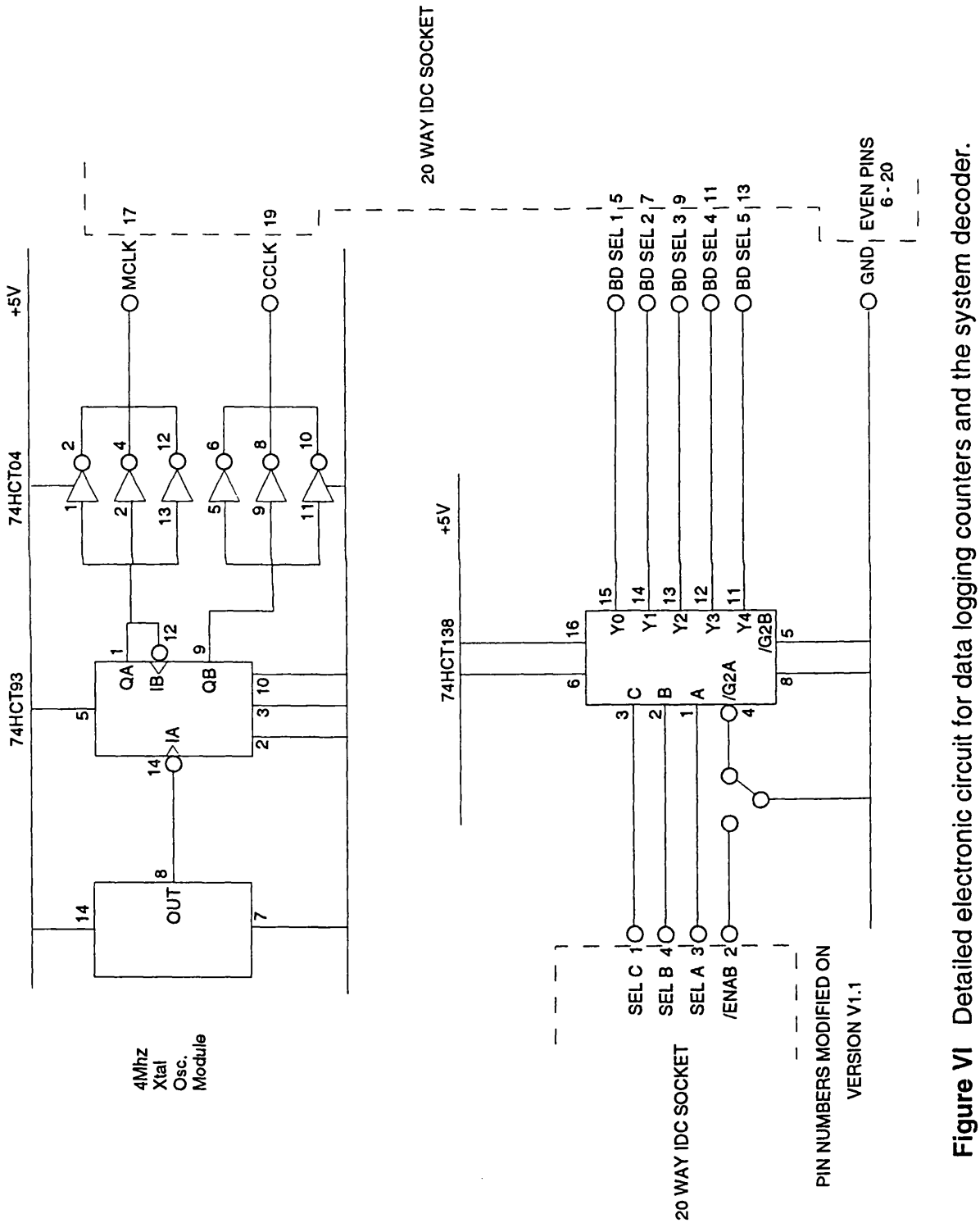

Figure VI Detailed electronic circuit for data logging counters and the system decoder.

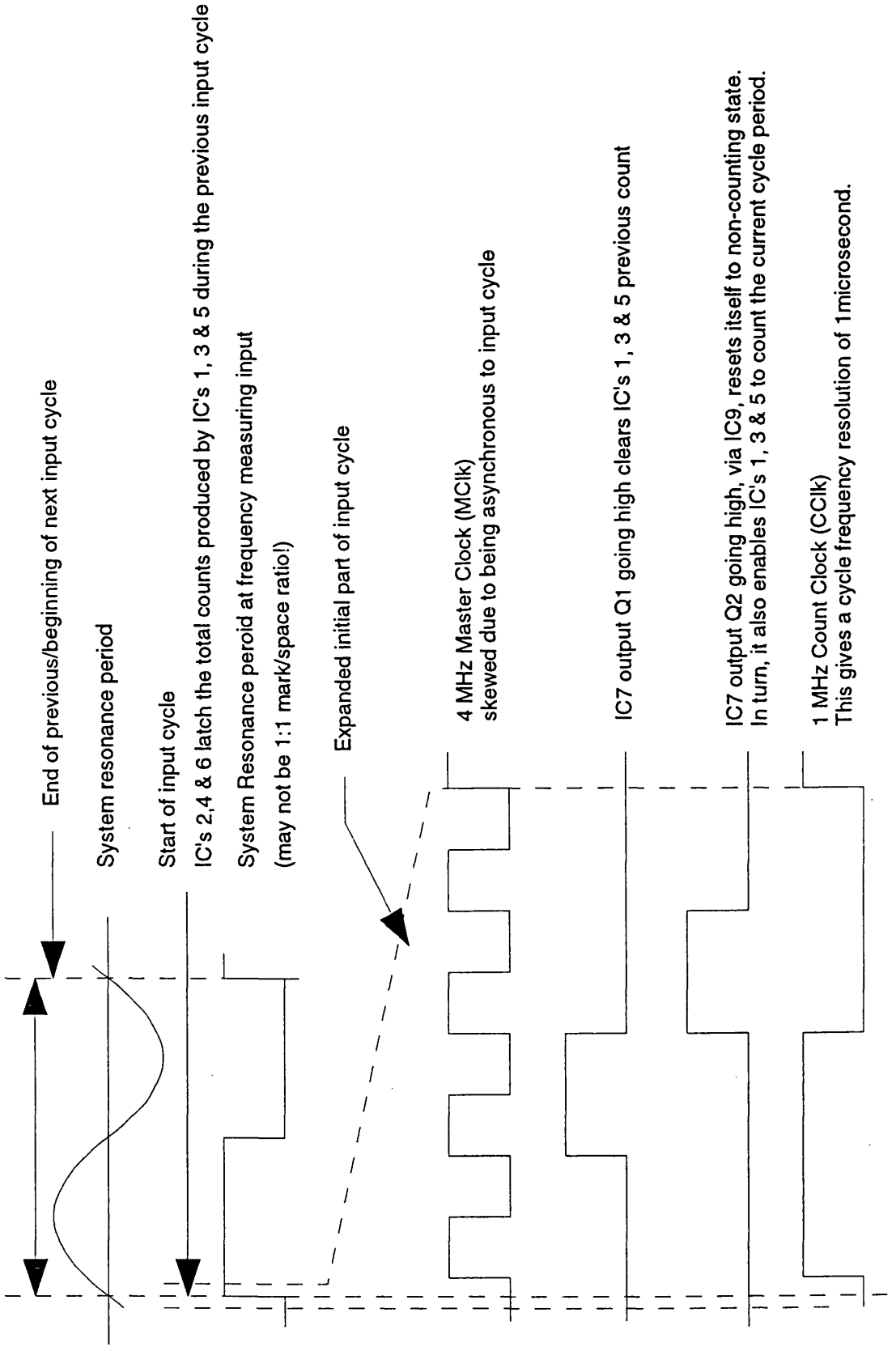

Figure VII A schematic illustration of the electronic counter working principle.

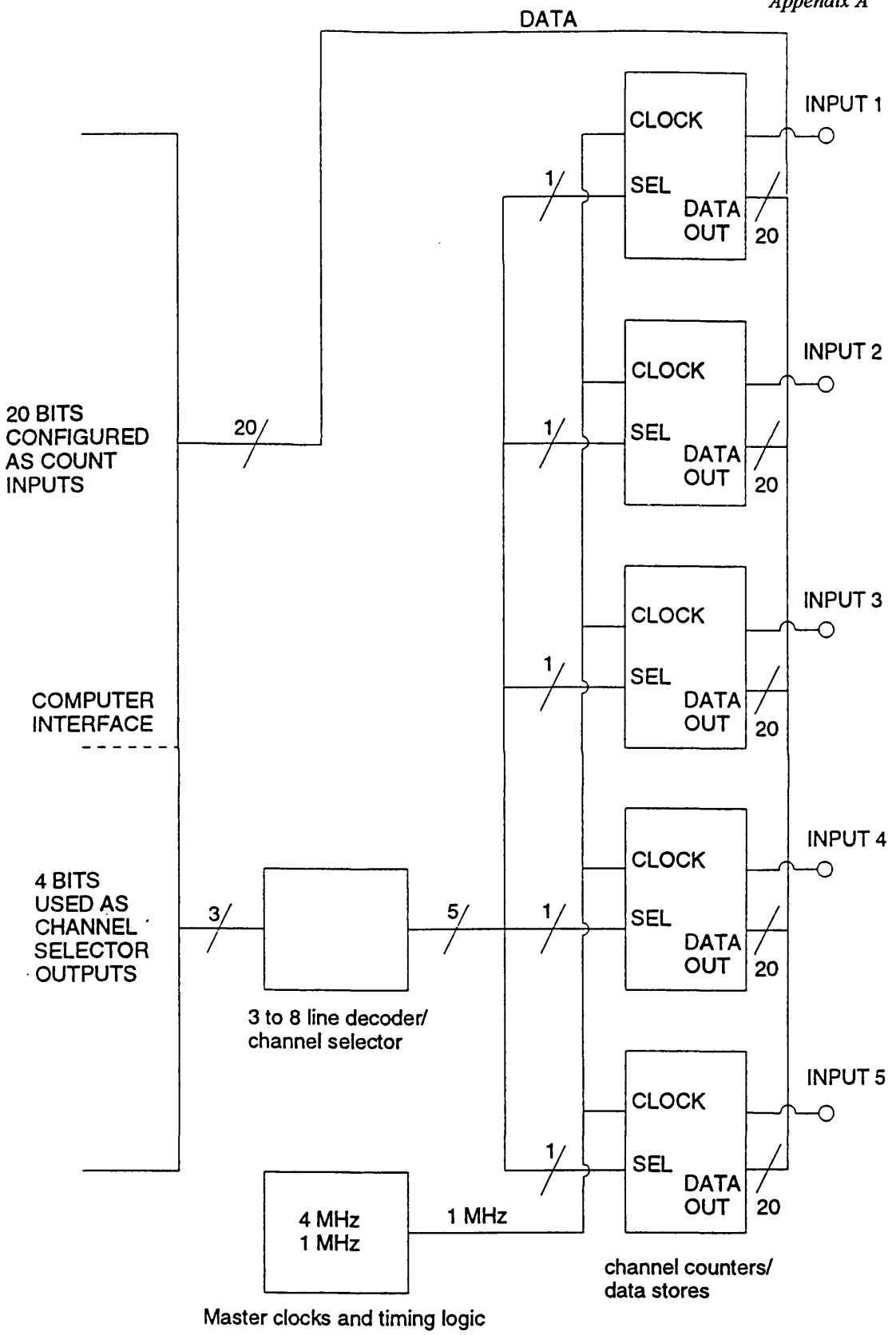

Figure VIII A schematic layout of the computerised data logging system.

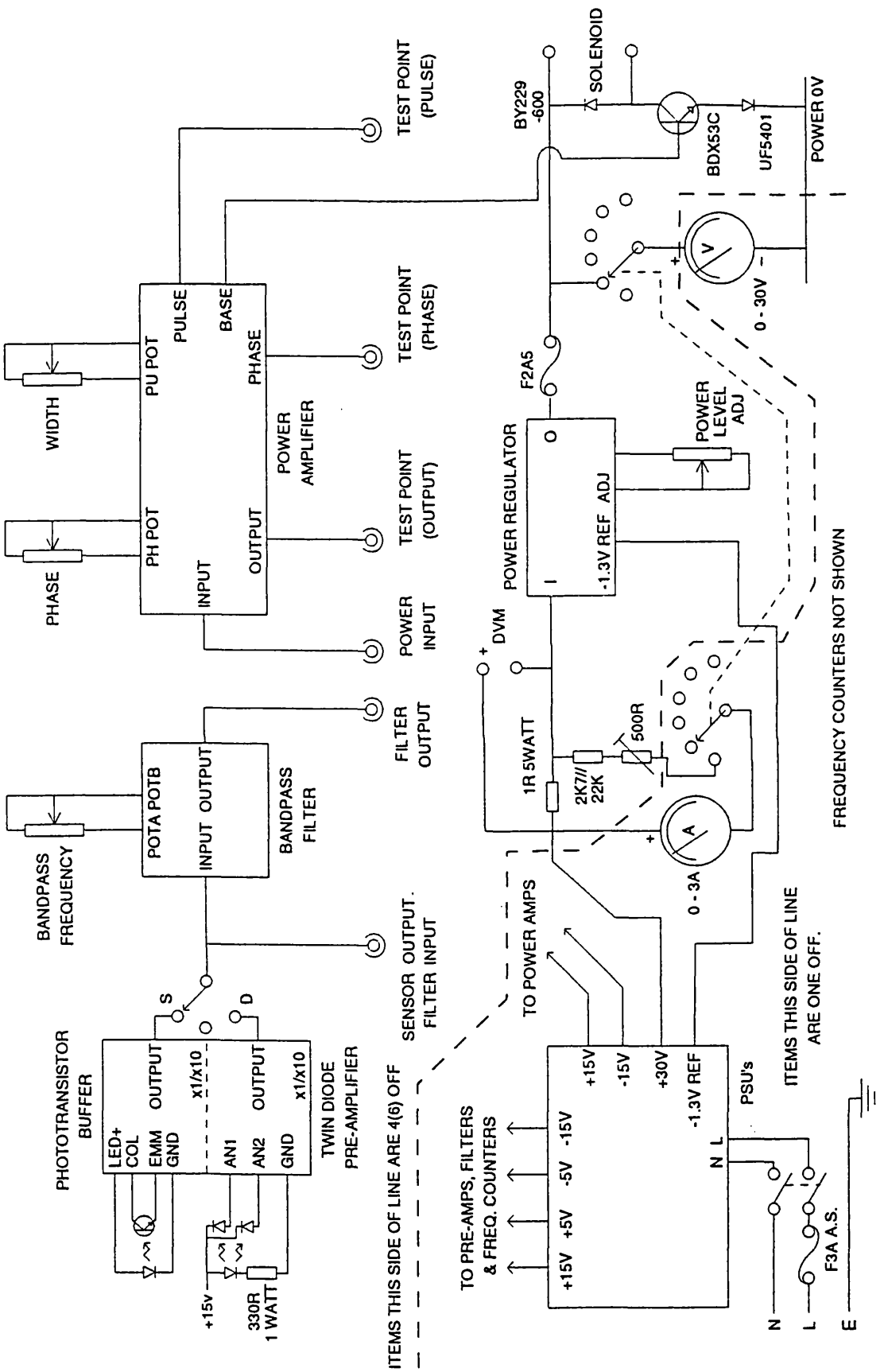

Figure IX A detailed layout of the multiple reed electronic drive and detection system.

```
'FREQUENCY MEASUREMENT PROGRAM

CONST baseadd = &H300          ' card base address
CONST clock = 1000000          ' master clock frequency (1MHz)

CLS

DIM freq(4)

filename$ = "C:\excel\data\datalog\rawdata.xls"
OPEN filename$ FOR OUTPUT AS #1

DO
FOR channel = 0 TO 4

' set ports A, B & lower C as input and upper port C as output
OUT baseadd + 11, 147

' select frequency input channel
OUT baseadd + 10, channel * 16



 porta = INP(baseadd + 8)     ' get port A count
 portb = INP(baseadd + 9)     ' get port B count
 portc = INP(baseadd + 10)    ' get port C count

 ' extract lower 4 bits of port C
 portc = portc MOD 16


 ' display results on screen
 PRINT "Input Channel ="; channel;
 PRINT "      Porta = ";
 PRINT USING "###.##"; parta;
 PRINT "      Portb = ";
 PRINT USING "##.##"; partb;
 PRINT "      Portc = ";
 PRINT USING "#.#"; partc;

 freq(channel) = clock / (portc * 65536 + portb * 256 + porta + .0000001)

 FOR delay = 0 TO 50: NEXT delay

NEXT channel

 'print result to userfile
 PRINT #1, freq(4), freq(1), freq(2), freq(3)

 'keep taking readings until a key is pressed
LOOP UNTIL INKEY$ <> ""

CLOSE #1
```

Appendix B

Typical chemical composition and important physical properties for glass ballotini

The samples used in this study have the following chemical composition:

SiO_2	67 %
Na_2O	10 %
K_2O	7 %
BaO	6 %
CaO	5 %
B_2O_3	2 %
Al_2O_3	1 %
MgO	1 %
PbO	< 0.01 %

The density of test samples has been measured using a specific gravity bottle and found to be 2550 kg $m^{-3} \pm 1 \times 10^{-5}$ kg. physical properties include:

Linear Coefficient of Expansion (between 0 °C and 300 °C, per °C)	8×10^{-6}
Refractive Index	1.51
Specific Heat (between 20 °C and 100 °C, Cal/g °C)	0.27
Hardness (based on Moh's scale)	7
Modulus of Elasticity (kP/mm^2)	6500
Maximum Working Temperature (°C)	350
Compressive Strength (N @ 3 mm diameter)	1770
Dielectric Constant (at 1 Mc and 20 °C)	7.2
Percentage of Beads with Air Inclusion (%)	< 0.3